

INFORMATION TO USERS

This manuscript has been reproduced from the microfilm master. UMI films the text directly from the original or copy submitted. Thus, some thesis and dissertation copies are in typewriter face, while others may be from any type of computer printer.

The quality of this reproduction is dependent upon the quality of the copy submitted. Broken or indistinct print, colored or poor quality illustrations and photographs, print bleedthrough, substandard margins, and improper alignment can adversely affect reproduction.

In the unlikely event that the author did not send UMI a complete manuscript and there are missing pages, these will be noted. Also, if unauthorized copyright material had to be removed, a note will indicate the deletion.

Oversize materials (e.g., maps, drawings, charts) are reproduced by sectioning the original, beginning at the upper left-hand corner and continuing from left to right in equal sections with small overlaps. Each original is also photographed in one exposure and is included in reduced form at the back of the book.

Photographs included in the original manuscript have been reproduced xerographically in this copy. Higher quality 6" x 9" black and white photographic prints are available for any photographs or illustrations appearing in this copy for an additional charge. Contact UMI directly to order.

UMI

A Bell & Howell Information Company
300 North Zeeb Road, Ann Arbor MI 48106-1346 USA
313/761-4700 800/521-0600



**NATURAL CONVECTION HEAT TRANSFER IN HEAT EXCHANGERS
WITH VERTICAL HELICAL COILS**

by

HESSAM TAHERIAN

A Thesis Submitted to the
Faculty of Engineering
in Partial Fulfillment of the Requirements
for the Degree of

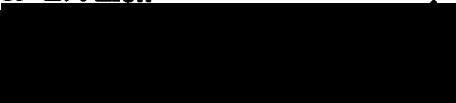
DOCTOR OF PHILOSOPHY

Major Subject: Mechanical Engineering

APPROVED:



Dr. Peter L. Allen



Dr. V. Ismet Ugursal



Dr. Lino R. Correia



Dr. Simon Furbo

DALHOUSIE UNIVERSITY DALTECH

Halifax, Nova Scotia, Canada

1998



National Library
of Canada

Bibliothèque nationale
du Canada

Acquisitions and
Bibliographic Services

Acquisitions et
services bibliographiques

395 Wellington Street
Ottawa ON K1A 0N4
Canada

395, rue Wellington
Ottawa ON K1A 0N4
Canada

Your file Votre référence

Our file Notre référence

The author has granted a non-exclusive licence allowing the National Library of Canada to reproduce, loan, distribute or sell copies of this thesis in microform, paper or electronic formats.

L'auteur a accordé une licence non exclusive permettant à la Bibliothèque nationale du Canada de reproduire, prêter, distribuer ou vendre des copies de cette thèse sous la forme de microfiche/film, de reproduction sur papier ou sur format électronique.

The author retains ownership of the copyright in this thesis. Neither the thesis nor substantial extracts from it may be printed or otherwise reproduced without the author's permission.

L'auteur conserve la propriété du droit d'auteur qui protège cette thèse. Ni la thèse ni des extraits substantiels de celle-ci ne doivent être imprimés ou autrement reproduits sans son autorisation.

0-612-31535-5

Canada

DALHOUSIE UNIVERSITY DALTECH LIBRARY

“AUTHORITY TO DISTRIBUTE MANUSCRIPT THESIS”

TITLE:

Natural Convection Heat Transfer in Heat Exchangers with
Vertical Helical Coils

The above library may make available or authorize another library to make available
individual photo/microfilm copies of this thesis without restrictions.

Name of Author: Hessam Taherian

Signature:  _____

Date: Feb., 13, 1998

DEDICATION

This thesis is dedicated to:

My father, Mr. Abbas Taherian

My mother, Mrs. Nasrin Taherian

and,

My wife, Mrs. Sahar Hajitaheri

TABLE OF CONTENTS

	Page
LIST OF TABLES	viii
LIST OF FIGURES	ix
NOMENCLATURE	xiv
ACKNOWLEDGEMENTS	xviii
ABSTRACT	xix
CHAPTER 1: INTRODUCTION	1
1.1. BACKGROUND	1
1.2. APPLICATIONS	2
1.3. MOTIVATION	3
1.4. OBJECTIVE	3
1.5. MODELING	4
CHAPTER 2: SUMMARY OF LITERATURE	6
2.1. SOLAR DOMESTIC WATER HEATING SYSTEMS	6
2.2. NATURAL CONVECTION HEAT EXCHANGERS	7
2.3. HELICAL COILS IN NATURAL CONVECTION	11
2.4. HORIZONTAL CYLINDERS	15
2.5. VERTICAL CYLINDERS	18
2.6. HORIZONTAL ROD BUNDLES (BANK OF TUBES)	19
2.7. VERTICAL ROD BUNDLES	24
2.8. VERTICAL ANNULI	26
2.9. VERTICAL CIRCULAR DUCTS	29
2.10. COMBINED NATURAL AND FORCED CONVECTION	30
2.11. HEAT AND FLUID FLOW INSIDE COILED PIPES	30
2.12. SCALE ANALYSIS	39
CHAPTER 3: THEORETICAL BACKGROUND	41
3.1. TUBE-SIDE FLUID FLOW AND HEAT TRANSFER	41
3.1.1. GEOMETRY OF A HELICAL COIL	41
3.1.2. FLOW INSIDE A VERTICAL HELICAL COIL	42

3.1.3. HEAT TRANSFER INSIDE A HELICAL COIL	45
3.2. SHELL-SIDE FLUID FLOW AND HEAT TRANSFER	47
3.2.1. SHELL-SIDE FLUID FLOW	47
3.2.2. SHELL-SIDE HEAT TRANSFER	49
3.2.2.1. DIMENSIONAL ANALYSIS	49
3.2.2.2. ADDITIONAL PARAMETERS	51
3.2.2.3. SCALE ANALYSIS	55
3.3. PHYSICAL PROPERTY EVALUATION	56
3.4. EXPERIMENTAL UNCERTAINTY ANALYSIS	56
3.5. SUMMARY	57
CHAPTER 4: EXPERIMENTAL SETUP AND PROCEDURE	58
4.1. EXPERIMENTAL APPARATUS	58
4.1.1. GLYCOL RESERVOIR	58
4.1.2. GLYCOL PUMP	58
4.1.3. HEATER	58
4.1.4. THE SHELL-AND-COIL HEAT EXCHANGER	59
4.1.5. FLOW METERS	64
4.1.6. THERMOCOUPLES	66
4.1.7. PRESSURE TRANSDUCER	67
4.1.8. WATER STORAGE TANK	68
4.1.9. DATA ACQUISITION SYSTEM	69
4.1.10. PIPING	69
4.2. EXPERIMENTAL PROCEDURE	73
4.3. PROCESSING THE DATA	77
CHAPTER 5: RESULTS AND DISCUSSION - I	78
5.1. TEMPERATURE DISTRIBUTION	78
5.1.1. SINGLE COILS	78
5.1.1.1. THE EFFECT OF COIL HEIGHT	87
5.1.2. MULTIPLE COILS	91
5.2. LOGARITHMIC MEAN TEMPERATURE DIFFERENCE	94
5.3. MODIFIED EFFECTIVENESS	98
5.3.1. EFFECTIVENESS-NTU RELATION	103

5.4.	WATER FLOW RATE	106
5.5.	HEAT TRANSFER COEFFICIENTS	111
5.5.1.	TUBE-SIDE HEAT TRANSFER COEFFICIENT	111
5.5.1.1.	EFFECT OF TUBE DIAMETER	112
5.5.1.2.	EFFECT OF COIL DIAMETER	115
5.5.1.3.	EFFECT OF COIL PITCH	116
5.5.1.4.	EFFECT OF SURFACE AREA	117
5.5.2.	PRESSURE DROP IN COILS	118
5.5.3.	FLOW DISTRIBUTION IN MULTIPLE COILS	122
5.5.4.	SHELL-SIDE HEAT TRANSFER COEFFICIENT	124
5.5.4.1.	SINGLE COILS	124
5.5.4.1.1.	EFFECT OF COIL SURFACE AREA	124
5.5.4.1.2.	EFFECT OF COIL LENGTH	126
5.5.4.1.3.	EFFECT OF TUBE OUTSIDE DIAMETER	127
5.5.4.1.4.	EFFECT OF COIL DIAMETER	129
5.5.4.1.5.	EFFECT OF COIL PITCH	133
5.5.4.1.6.	EFFECT OF HEAT RATE	136
5.5.4.1.7.	EFFECT OF GLYCOL FLOW RATE	136
5.5.4.1.8.	EFFECT OF SHELL DIAMETER	138
5.5.4.1.9.	EFFECT OF SHELL HEIGHT	139
5.5.4.2.	MULTIPLE COILS	140
5.5.4.2.1.	DOUBLE COILS	141
5.5.4.2.2.	TRIPLE COILS	148
5.6.	THE STANTON NUMBER	153
5.7.	OVERALL HEAT TRANSFER COEFFICIENT	156
5.8.	REGIME OF FLOW	159
CHAPTER 6:	RESULTS AND DISCUSSION - II	161
6.1.	NUSSELT NUMBER CORRELATIONS	161
CHAPTER 7:	APPLICATIONS	176
7.1.	OPTIMUM CONFIGURATION	176
7.1.1.	TUBE DIAMETER	176
7.1.2.	SHELL DIAMETER	177

7.1.3. COIL DIAMETER	177
7.1.4. SHELL HEIGHT	178
7.1.5. COIL PITCH	178
7.1.6. RECOMMENDED CONFIGURATION	178
7.2. DESIGN PROCEDURE	179
7.2.1. DESIGN	180
7.2.2. RATING	183
7.3. THE EFFECT OF THE AUXILIARY PARTS	187
CHAPTER 8: CONCLUSIONS	188
8.1. SUMMARY	188
8.2. CONCLUSIONS	188
8.3. RECOMMENDATIONS FOR FUTURE WORK	191
REFERENCES	193
APPENDIX A: PHYSICAL PROPERTIES OF GLYCOL	203
APPENDIX B: COMPUTER CODE	207
APPENDIX C: SAMPLE HEAT TRANSFER DATA	217
APPENDIX D: GOVERNING EQUATIONS	218

LIST OF TABLES

TABLE	DESCRIPTION	PAGE
2.1	Exponent m in equation 2.16	14
3.1	Tube-side Nusselt number	46
3.2	Conditions for table 3.1	46
3.3	Experimental uncertainties of important parameters	57
4.1	Coil specifications	63
5.1	Percentage of distortion of the tubes cross section	114
7.1	Specifications for the proposed heat exchanger	179
7.2	Results of the design procedure for the NCHE	183
7.3	Typical results of the proposed rating procedure	186
C.1	Typical heat transfer data	217

LIST OF FIGURES

FIGURE	DESCRIPTION	PAGE
1.1	A SDHW system with two loops	2
2.1	Solar fraction versus flow rate for a system with no heat exchanger ...	7
3.1	Geometry of a helical coil	42
3.2	Secondary flow inside a circular cross-section coil	43
3.3	Hydraulic drag coefficients for in-line tube bundles	48
4.1	Physical dimensions of the three shells used in the experiments	60
4.2	Three heat exchanger shells used in the experiments	61
4.3	Top cap of the 77 mm ID heat exchanger	62
4.4	Coils #1, #2 and #22	64
4.5	Glycol flow meter calibration curves	65
4.6	Pressure transducer calibration curve	68
4.7	Water piping	71
4.8	Experimental apparatus	72
4.9	Shell-and-coil NCHE	74
4.10	An assembled shell-and-coil heat exchanger	75
5.1(a)	Axial temperature distribution for coils in a 77 mm ID shell, coil #1 ..	80
5.1(b)	Axial temperature distribution for coils in a 77 mm ID shell, coil #12	80
5.1(c)	Axial temperature distribution for coils in a 77 mm ID shell, coil # 15	80
5.2	Axial coil surface temperature distribution of coil #12 for various R_m	81
5.3	Axial temperature distribution of coil #12 for $R_m=0.38$	81
5.4(a)	Axial temperature distribution for coils in a 77 mm diameter shell, coil #6	82
5.4(b)	Axial temperature distribution for coils in a 77 mm diameter shell, coil #10	82
5.4(c)	Axial temperature distribution for coils in a 77 mm diameter shell, coil #13	82
5.5(a)	Axial temperature distribution for coils in a 77 mm diameter shell, coil #16	84
5.5(b)	Axial temperature distribution for coils in a 77 mm diameter shell, coil #18	84

5.5(c)	Axial temperature distribution for coils in a 77 mm diameter shell, coil #21	84
5.6	Axial coil surface temperature distribution of coil #16 for various R_m	85
5.7	Centerline temperature profile of the exchanger for fixed heat rate and mass flow rate ratio	86
5.8	Effect of the heat rate on the axial temperature distribution for coil #6	87
5.9(a)	Axial temperature profiles for coil #23 in the 762 mm long shell, $R_m=1.81$	88
5.9(b)	Axial temperature profiles for coil #23 in the 762 mm long shell, $R_m=2.32$	88
5.9(c)	Axial temperature profiles for coil #23 in the 762 mm long shell, $R_m=2.78$	88
5.10(a)	Axial temperature profiles for coil #24 in the 762 mm long shell, $R_m=1.66$	89
5.10(b)	Axial temperature profiles for coil #24 in the 762 mm long shell, $R_m=2.18$	89
5.10(c)	Axial temperature profiles for coil #24 in the 762 mm long shell, $R_m=2.74$	89
5.11(a)	Axial temperature profiles for coil #25 in the 762 mm long shell, $R_m=1.74$	90
5.11(b)	Axial temperature profiles for coil #25 in the 762 mm long shell, $R_m=2.32$	90
5.11(c)	Axial temperature profiles for coil #25 in the 762 mm long shell, $R_m=2.75$	90
5.12(a)	Recirculation, larger diameter coils.....	91
5.12(b)	Recirculation, smaller diameter coils	91
5.13(a)	Axial temperature profiles of the coil surface for triple coil tests in the shorter heat exchanger, $R_m=1.8$	92
5.13(b)	Axial temperature profiles of the coil surface for triple coil tests in the shorter heat exchanger, $R_m=3.35$	92
5.14(a)	Effect of the mass flow rate ratio on axial temperature profiles for multiple coils, Coil surface temperature	93
5.14(b)	Effect of the mass flow rate ratio on axial temperature profiles	

	for multiple coils, Water temperature on the centerline	93
5.15(a)	Variations of logarithmic mean temperature difference, coil #1	95
5.15(b)	Variations of logarithmic mean temperature difference, coil #9	95
5.15(c)	Variations of logarithmic mean temperature difference, coil #15	95
5.16	Variations of LMTD for triple coil tests, coils #1, 2, 22	96
5.17(a)	Variations of logarithmic mean temperature difference for the long exchanger, coil #23	97
5.17(b)	Variations of logarithmic mean temperature difference for the long exchanger, coil #24	97
5.17(c)	Variations of logarithmic mean temperature difference for the long exchanger, coil #25	97
5.18	Modified effectiveness for all the test configurations	99
5.19	Plot of the modified effectiveness on a logarithmic scale	100
5.20	Modified effectiveness of the coil #21	101
5.21	Comparison of the effectiveness data with standard heat exchanger configurations	104
5.22	The effectiveness-NTU data compared with the counter-flow concentric tube heat exchanger for different values of C_r	105
5.23	Water mass flow rate for all configurations	107
5.24	Water flow rate versus heat transfer rate	108
5.25	Comparison of water flow rate data versus heat transfer rate.....	110
5.26	Tube-side Nusselt number versus the Dean number	112
5.27	Helical coil number compared to the Dean number	116
5.28	Measured friction factor for coils	119
5.29	Friction factor from equation 3.5	121
5.30	Onset of figure 5.29	121
5.31	Distribution of flow in double coils	122
5.32	Distribution of flow in triple coils for $H=762$ mm	123
5.33	Shell-side heat transfer coefficient of all single coils for $q \geq 900$ W ...	125
5.34	Effect of coil length on the shell-side heat transfer coefficient of single coils with various tube diameters, for $q \geq 900$ W	126
5.35	Shell-side heat transfer coefficient versus the heat rate for various tube diameters	128
5.36	Variations of dimensionless spacing with respect to coil diameter	129

5.37	Nusselt number data for single coils as a function of modified dimensionless flow space for $960 W \leq q \leq 1280 W$	130
5.38	Relationship between cross-sectional flow area and coil diameter for single coils	131
5.39	h_o versus heat flux for various coil pitch.....	134
5.40	Variations of the shell-side heat transfer coefficient with heat flux	136
5.41(a)	Shell-side heat transfer coefficient versus the glycol mass flow rate, coil #3	137
5.41(b)	Shell-side heat transfer coefficient versus the glycol mass flow rate, coil #6	137
5.41(c)	Shell-side heat transfer coefficient versus the glycol mass flow rate, coil #9	137
5.41(d)	Shell-side heat transfer coefficient versus the glycol mass flow rate, coil #17	137
5.42	Effect of shell diameter on the Nusselt number	138
5.43	Effect of shell height on the Nusselt number	139
5.44	Shell-side heat transfer coefficients of double and single coil heat exchangers	141
5.45	Distribution of the total heat rate between the two coils in all double coil configurations	142
5.46(a)	Individual h_o values in double-coil configurations, coil #1, #2	143
5.46(b)	Individual h_o values in double-coil configurations, coil #23, #24	143
5.47(a)	Individual h_o values in double-coil configurations, coil #23, #25	144
5.47(b)	Individual h_o values in double-coil configurations, coil #24, #25	144
5.48	Performance of coil #23 in single and double-coil configurations	145
5.49	Performance of coil #24 in single and double-coil configurations	146
5.50	Performance of coil #25 in single and double-coil configurations	146
5.51	Performance of coil #23 in single, double and triple coil configurations	148
5.52	Performance of coil #24 in single, double and triple coil configurations	149
5.53	Performance of coil #25 in single, double and triple coil configurations	150
5.54	Glycol outlet temperatures for triple coil configuration	152

5.55	Stanton number as a function of $Ra_{D_{hx}}$ for single coils	154
5.56	Variation of the Stanton number with the coil surface area	155
5.57	Variation of the overall heat transfer coefficient with the heat rate	156
5.58	Variation of the overall heat transfer coefficient with the total coil surface area	157
5.59	Percentage deviation of h_o calculated by two methods	159
5.60	Flow regime for the current experiments according to the mixed convection regimes plot of Metais and Eckert (1964)	160
6.1	Nusselt number based on tube diameter for all single coils	161
6.2	Nusselt number based on tube diameter compared with those for a single horizontal cylinder	162
6.3	Nusselt number versus Reynolds number based on tube diameter ...	163
6.4	Nusselt number versus Rayleigh number based on total coil length ..	164
6.5	Comparison of Nu_L vs. Ra_L plots with those of Ali (1994) and Ajele (1995)	165
6.6	Nusselt number versus modified Rayleigh number based on shell height	166
6.7	Nu_H data compared with those by Ajele (1995)	167
6.8	Nusselt number based on the heat exchanger hydraulic diameter	168
6.9	$Nu_{D_{hx}}$ versus modified Rayleigh number based on D_{hx}	169
6.10	$Nu_{D_{hx}}$ versus $Ra_{D_{hx}}^*$ compared with Ajele's (1995) correlation	170
6.11	Nusselt number versus Rayleigh number based on the heat rate for all configurations	172
6.12	Comparisonn of $Nu_{D_{hx}}$ vs. Rayleigh number based on the heat rate .	173
6.13	Nusselt number versus Rayleigh number based on total coil length and heat rate	174
7.1	Flowchart of the NCHE design procedure	182
7.2	Flow chart of the NCHE rating procedure	185
A.1	Specific heat of 40/60 propylene glycol	203
A.2	Thermal conductivity of 40/60 propylene glycol	204
A.3	Dynamic viscosity of 40/60 propylene glycol	205
A.4	Density of 40/60 propylene glycol	206

NOMENCLATURE

A	Surface area of coil
A_c	Collector area
$A_{c,f}$	Heat exchanger cross sectional area of flow, $\frac{\pi(D_s^2 - D_{eq}^2)}{4}$
A_p	Wetted surface area of heat exchanger, $\pi(D_{t,o}L + D_sH)$
C_r	Heat capacity ratio, $\frac{(\dot{m}c_p)_{min}}{(\dot{m}c_p)_{max}}$
D	Diameter
D_c	Coil mean diameter
De	Dean number, $Re\sqrt{\frac{d}{D_c}}$
D_{eq}	Equivalent diameter of multiple coils, $\left(\sum_{j=1}^N (D_{c,o}^2 - D_{c,i}^2)_j\right)^{1/2}$
D_{hx}	Heat exchanger hydraulic diameter, $\frac{4A_{c,f}H}{A_p}$
D_s	Shell inner diameter
$D_{t,o}$	Tube outer diameter
Eu	Euler number, $Eu = \frac{2\Delta P}{\rho u_0^2 n}$
F	Flow number, $\frac{\dot{m}_g c_{p,g} D_{t,o}}{2k_w A}$
F'	Collector plate efficiency factor
Gr	Grashof number, $\frac{g\beta\Delta TD^3}{\nu^2}$
Gz	Graetz number, $(D/x)RePr$
H	Effective height of heat exchanger
He	Helical coil number, $De\left[1 + \left(\frac{P}{2\pi R}\right)^2\right]^{-1/2}$

L	Total coil length
LMTD	Logarithmic mean temperature difference
M_w	Dimensionless water mass flow rate, $\frac{\dot{m}_w}{\dot{m}_g} \left(\frac{L}{H} \right)^2$
N	Number of coils
NCHE	Natural convection heat exchanger
NTU	Number of transfer units, $\frac{UA}{(\dot{m}c_p)_{\min}}$
Nu_{Dt}	Nusselt number based on the tube outside diameter, $\frac{h_o D_{t,o}}{k_w}$
Nu_i	Nusselt number inside tube, $\frac{h_i d}{k_s}$
Nu_{Dhx}	Nusselt number based on heat exchanger hydraulic diameter
P	Pressure, dimensionless coil pitch, $\frac{p}{D_{t,o}}$
Pr	Prandtl number, $\frac{\nu}{\alpha}$
R	Radius
R_m	Mass flow rate ratio, $\frac{\dot{m}_g}{\dot{m}_w}$
R_{opt}	Optimum heat capacity ratio, $\left(\frac{\dot{m}_c c_{p,c}}{\dot{m}_t c_{p,t}} \right)_{opt}$
Ra_{Dhx}	Rayleigh number based on D_{hx} , $\frac{g\beta(T_{m,w} - T_{\infty})(D_{hx})^3}{\nu\alpha}$
Ra_{Dhx}^*	Modified Rayleigh number based on D_{hx} , $Ra_{Dhx} \frac{H}{L}$
Ra_{Dt}	Rayleigh number based on tube diameter
Ra_H^*	Modified Rayleigh number based on the exchanger height, $Ra_H (H/L)^{1.5}$
$Ra_{q,Dhx}$	Heat-rate Rayleigh number based on D_{hx}
$Ra_{q,L}$	Heat-rate Rayleigh number based on coil length
$Ra_{q,R}$	Heat-rate Rayleigh number based on R, $\frac{g\beta q'' R^5}{\nu H k \alpha}$
Re	Reynolds number, $\frac{uD}{\nu}$

Ri	Richardson number, $\frac{Gr}{Re^2}$
S	Dimensionless spacing, $\frac{D_s - D_c}{D_s}$
S'	Dimensionless flow space, $\frac{D_s - D_{eq}}{D_{eq}}$
SDHW	Solar domestic hot water
St	Stanton number, $\frac{h_o A_{c,f}}{\dot{m}_w c_{p,w}}$
T	Temperature
U	Overall heat transfer coefficient
U_L	Collector heat loss coefficient
W	Enclosure width
c_p	Specific heat
d	Tube inside diameter
f	Fricion factor
g	Gravitational acceleration
h	Heat transfer coefficient
k	Thermal conductivity
\dot{m}	Mass flow rate
n	Number of tube rows in a tube bank, number of coil turns
p	Coil pitch
q	heat transfer rate
q''	Heat rate per unit area
u	Mean flow velocity
u_o	Mean velocity in the minimum intertube spacing

Greek symbols

α	Thermal diffusivity
β	Coefficient of volumetric thermal expansion

ε	Heat exchanger effectiveness, $\frac{(\dot{m}c_p)_h(T_{h,i} - T_{h,o})}{(\dot{m}c_p)_{\min}(T_{h,i} - T_{c,i})}$
ε'	Modified effectiveness, $\frac{T_{h,i} - T_{h,o}}{T_{h,i} - T_{c,i}}$
Γ	Dimensionless heat rate, $\left(\frac{q\rho^2 L^4}{\dot{m}_g^2 \mu H}\right)^{0.1}$
μ	Dynamic viscosity
ν	Kinematic viscosity
ρ	Mass density

Subscripts

c	Coil, Collector, Cold stream
crit.	Critical
D	Diameter
D _{hx}	Heat exchanger hydraulic diameter
D _t	Tube outer diameter
g	Glycol
h	Hot stream
hyd	Hydraulic
i	Inside
L	Length
long.	Longitudinal
m	Mean
o	Outside
q	based on heat rate
t	Tube, Tank
trans.	Transverse
w	Water
W	Enclosure width
x	Heat exchanger

ACKNOWLEDGEMENTS

I would like to offer my deepest gratitude to my thesis supervisor, Dr. Peter Allen. His thorough understanding of the subject paved the road for me to accomplish a goal in my life. I greatly benefited from the discussions we had throughout the period of my study and thesis preparation.

Many thanks to the other members of the guiding committee, Dr. V. Ismet Ugursal and Dr. Lino Correia for their valuable comments.

A note of thanks to Mr. Felix Roma for assisting me in manufacturing some of the equipments I used in my research.

The generosity of the Iranian nation who granted me the opportunity to complete my studies abroad is highly appreciated. Without their financial support I would not be able to achieve this goal. Also the administrative efforts of the representative of the Iranian Ministry of Culture and Higher Education in Canada, Dr. Reza Hosseini is acknowledged.

I am also grateful for the funding provided by the Canadian government for carrying on this research.

ABSTRACT

Natural convection heat transfer was studied in shell-and-coil heat exchangers. One or more helical coils were installed in a cylindrical shell to form a natural convection shell-and-coil heat exchanger. A heated aqueous solution of 40% propylene glycol was pumped through the coils. Water from a storage tank circulated naturally on the shell side of the heat exchanger. The helical coils were made of copper tubes of 4.76, 6.35, 7.94 and 9.52 mm outer diameter. Coil outer diameter was varied from 35.7 to 74.5 mm and coil pitch from 1.00 to 5.96 tube diameters. Two shell diameters of 51 and 77 mm were tested and the shell height was either 382 or 762 mm. Experiments were conducted for glycol mass flow rates from 0.00185 to 0.0343 kg/s and heat transfer rates from 160 to 2300 W.

The effects of tube diameter, coil diameter, coil pitch, shell diameter and shell height on the shell-side heat transfer coefficient were studied. Axial temperature profiles in the heat exchangers were analyzed. The shell-side heat transfer coefficient decreased with increasing coil surface area. The optimum dimensionless pitch for the coils was found to be in the range, $1.25 \leq P \leq 1.80$. Tube diameter had little influence on the shell-side heat transfer coefficient. Increasing the height of the heat exchanger slightly increased the shell-side heat transfer coefficient. The heat exchanger hydraulic diameter was the most appropriate characteristic length for the $Nu-Ra$ correlations. The Nusselt number was correlated well with the modified Rayleigh number based on the heat exchanger hydraulic diameter by $Nu_{D_{hx}} = 0.182 Ra_{D_{hx}}^{*0.394}$ for $2 \times 10^3 \leq Ra_{D_{hx}}^* \leq 2 \times 10^7$. The Nusselt number was also correlated well with the heat-rate Rayleigh number based on the heat exchanger hydraulic diameter by, $Nu_{D_{hx}} = 0.139 Ra_{q,D_{hx}}^{0.293}$ for $6 \times 10^4 \leq Ra_{q,D_{hx}} \leq 2 \times 10^{10}$. The UA product (the overall heat transfer coefficient multiplied by the heat transfer area) of the heat exchangers was not directly proportional to the coil surface area, but varied as $UA \propto A^{0.67}$. The largest coil in the triple-coil configurations had heat transfer coefficients 46% less than the values for the single-coil configuration. Suggestions were made to improve the performance of the heat exchangers. The optimum configuration for the shell-and-coil natural convection heat exchanger was discussed. Design and rating procedures were proposed for the heat exchangers.

CHAPTER 1

INTRODUCTION

1.1 Background

A natural convection heat exchanger (NCHE) is a heat exchanger in which the dominant mode of heat transfer in one or both flows is natural convection, as opposed to the traditional heat exchangers with forced-convection domination on both sides. The field of natural convection heat exchangers is relatively new. This concept only limits the mode of heat transfer in the heat exchanger, while various geometries can be employed. At first the traditional shell-and-tube heat exchangers were adapted to be used as natural convection heat exchangers. Parent (1988), Richmond and Hollands (1989), Parent *et al.* (1990), reported works on shell-and-tube natural convection heat exchangers when the buoyancy driven flow occurred inside the tubes. Van Rossum (1990) studied double pipe heat exchangers with twisted tapes inserted in the inner tube and buoyancy driven flow inside the tubes. Experiments on shell-and-tube NCHEs were reported by Srinivasan and Christensen (1994) for the case where the buoyancy driven flow occurs in the shell. Srinivasan and Christensen also studied NCHEs with fluted tubes instead of smooth circular ones. Recently, NCHEs with multiple helical coils in a cylindrical shell were introduced by White *et al.* (1990). In this configuration, natural convection occurs in the shell-side flow. White *et al.* (1990) found that the new shell-and-coil heat exchanger outperformed a concentric tube heat exchanger by 100% and increased the solar domestic hot water system performance by 20%. In addition, the cost of manufacturing was found to be less. Since then, shell-and-coil natural convection heat exchangers have been studied by Allen and Ajele (1993), (1994a), (1994b), Bergelt *et al.* (1993), Fraser *et al.* (1995), Ajele (1995), Avina (1995) and Taherian and Allen (1997a), (1997b).

A shell-and-coil natural convection heat exchanger consists of a cylindrical shell with one or more helical coils placed inside it. The flow inside the coils is forced by a pump while buoyancy forces are the cause of flow within the heat exchanger shell.

1.2 Applications

NCHEs have been used mainly in solar domestic hot water (SDHW) systems. However, their use in heat recovery systems for space heating has also been reported [Srinivasan and Christensen (1994)]. In SDHW systems operating in cold climates, the risk of freezing precludes the use of tap water in the collector loop. Instead, an antifreeze solution, such as propylene glycol, must be used. As a consequence, a secondary loop is needed to transfer the heat from the glycol loop to the storage tank, and a heat exchanger is required as a means of this heat transfer. The loop containing the collector is called the heat delivery loop and the one with the storage tank is called the heat storage loop.

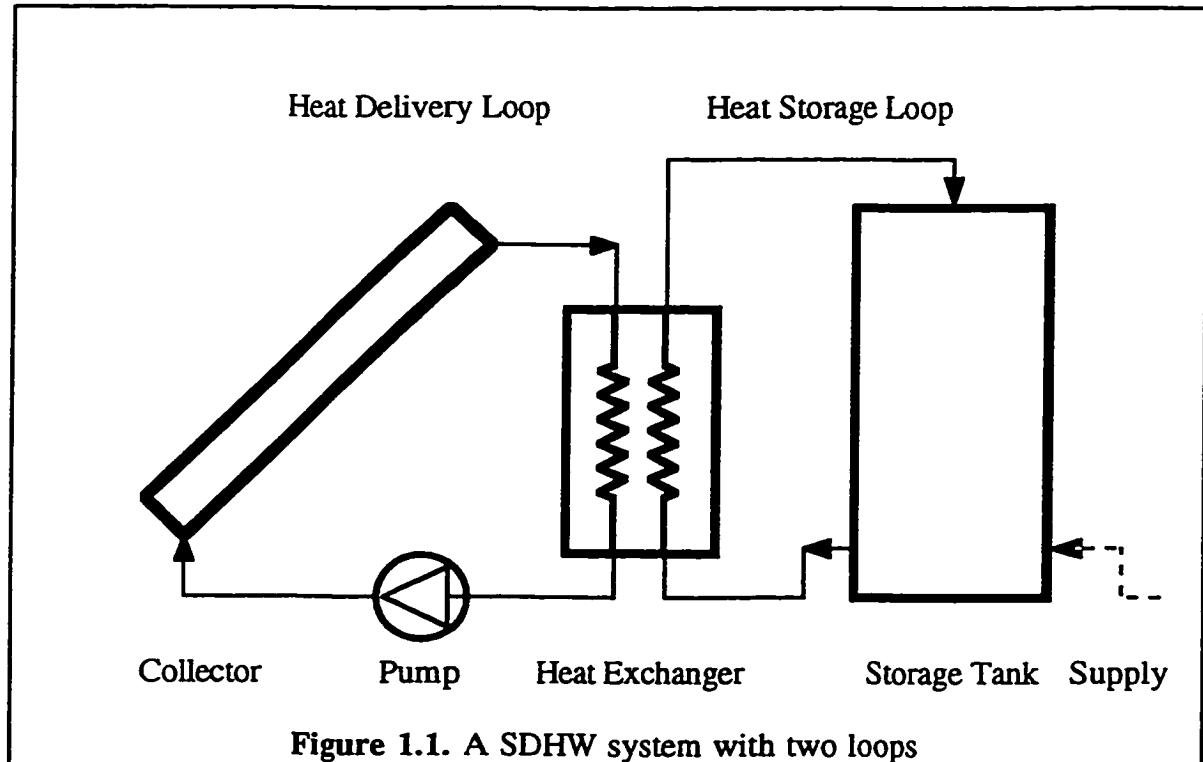


Figure 1.1. A SDHW system with two loops

Normally one pump is needed for each loop. However, by employing a NCHE in the SDHW system, the flow in the storage loop can be driven by buoyancy forces resulting from the temperature difference between the heat exchanger and the storage tank. The great

advantage of this system is that the pump in the storage loop is no longer required. Figure 1.1 is a schematic diagram of a double loop SDHW system with a NCHE and no pump in the storage loop. Use of natural circulation complies well with the requirement of low flow velocities in the storage loop. The thermal stratification in the storage tank is less likely to be disturbed and therefore the performance of the SDHW system will be improved. Moreover, one less pump has been used which means less dependence on electricity from the network. If the pump in the collector loop were to be driven by the electricity generated by a photovoltaic module, the whole system could be taken off the electrical grid, meaning more rural applications for the SDHW system [Allen and MacLeod (1994)].

By no means is the application of shell-and-coil NCHEs restricted to SDHW systems. They can be employed in any heat exchange application which requires compactness due to lack of space, low flows on one side of the exchanger, flexibility in configuration and ease of manufacture.

1.3. Motivation

Due to the fact that the subject of NCHEs is very young, there is limited information available. The published data is limited to a handful of journal and conference papers. This scarcity of data was the motivation for the current thesis. In fact, this thesis is a continuation of the work started by White *et al.* (1990) and then developed further by Ajele (1995).

1.4. Objective

Prior to the work of Ajele (1995), no data was available for the natural convection heat transfer coefficient from vertical helical coils to be employed in designing natural convection shell-and-coil heat exchangers. In order to design a shell-and-coil NCHE the relationship between the UA product (the overall heat transfer coefficient of the heat exchanger multiplied by the heat transfer area) and the terminal temperatures of the heat exchanger must be known. This relationship is usually presented in the form of ϵ - NTU equations or graphs (ϵ is the heat exchanger effectiveness and NTU is the number of

transfer units). For the traditional heat exchangers, the ε - NTU relations are readily available. The same relationships for the case of natural convection on one side, must be known. This can be referred to as a macroscopic study of the heat exchanger.

In order for heat exchanger design to be optimized, a thorough understanding of the heat exchanger performance is needed. In other words, the variations of the natural convection heat transfer coefficient with respect to thermal, hydraulic and geometrical parameters must be understood. This can be referred to as a microscopic study of the exchanger. The objective of this thesis is to provide a microscopic look at the performance of the heat exchanger by evaluating the shell-side heat transfer coefficient for various configurations. Ajele (1995) presented the general Nusselt number correlations for a shell-and-coil NCHE. However, the work needed to be developed further especially to clarify the effects of the tube diameter, shell diameter, shell height and coil pitch. Also the search for an optimum configuration needed to be conducted.

1.5. Modeling

Two general approaches can be followed in order to solve a physical problem. These two approaches are mathematical and physical modeling. The problem of modeling of a shell-and-coil NCHE is no exception. A mathematical model is the result of the theoretical approach to the problem. Usually the model is presented in the form of a set of equations. In case of natural convection heat transfer, the equations are partial differential equations for mass, momentum and energy conservation where the latter two are coupled. Equations D.1 to D.4 of Appendix D are the general governing equations for natural convection problems. A mathematical model can be solved either analytically or numerically. Due to the complex nature of the equations, an analytical solution is out-of-reach at this time. A numerical solution is not as far-fetched at first glance. However, there are some difficulties in applying it to the current problem. One major difficulty is the three-dimensionality of the problem which makes the model tedious and time consuming. A great deal of difficulties arise from the indeterminate nature of the boundary conditions. Inside the heat exchanger, the steady-state temperatures are only defined by the interaction between the hot and cold streams. Similarly, the inlet and outlet water temperatures are influenced by the temperature profile inside the storage tank. As a

result, the boundary conditions for the model if defined independently, would be quite unrealistic and therefore of no use.

For a numerical model to be worthwhile, the heat exchanger model must be solved together with a model for the forced convective flow inside the coils and also a model for the flow and heat transfer inside the storage tank. The effects of the piping should be included in the model as well. In summary, developing such a model would be very complex and time consuming. Considering the fact that the basic governing equations are based on the theories and hypotheses which are yet to be proved, the result of such a model would still not be fully reliable.

The approach adapted for the current thesis was the physical modeling approach. It may not be the simplest approach but it certainly is the most reliable one regarding the explained nature of the problem. Full-scale shell-and-coil heat exchangers were constructed with several different configurations and experiments were carried out under various conditions.

CHAPTER 2

SUMMARY OF LITERATURE

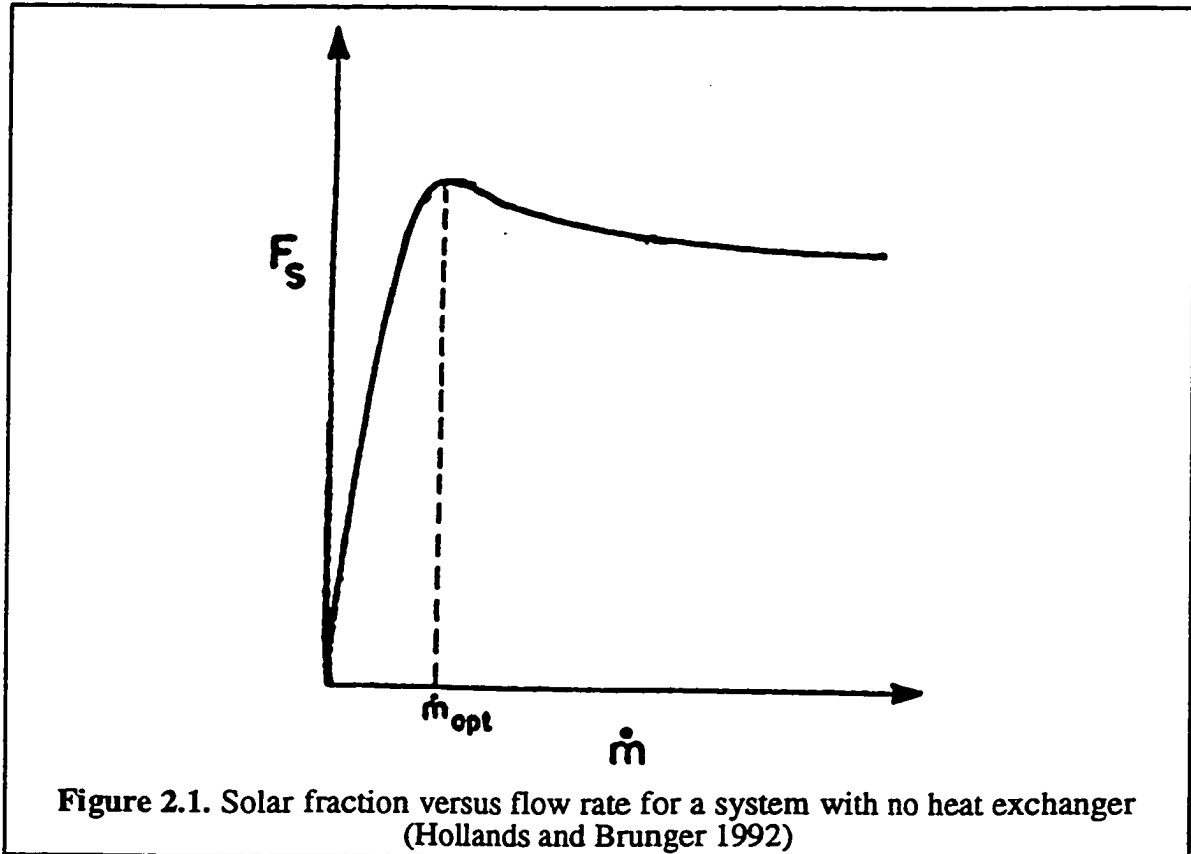
2.1. Solar domestic water heating systems

The primary application of the shell-and-coil natural convection heat exchanger is in SDHW systems. Therefore a review of the literature on SDHW systems with heat exchangers would be beneficial.

Hollands and Lightstone (1989) published a review of low-flow stratified-tank solar water heating systems. A typical flow rate for low-flow systems is stated to be 0.002 kg/s per square meter of collector area. Low-flow systems have several advantages over conventional high-flow systems. These advantages are: less piping and plumbing costs, elimination of the storage loop pump due to use of natural circulation, lower collector costs, and better tank stratification. Maintaining good stratification in the tank can improve performance by as much as 38% compared to fully mixed tanks [Hollands and Lightstone (1989)].

Hollands and Brunger (1992) investigated the existence of an optimum flow rate in solar water heating systems with a counter flow exchanger. After numerical and analytical simulations, Hollands and Brunger (1992) concluded that optimum flow rates do exist for such systems, provided the heat exchanger overall conductance $(UA)_x$ is fixed. It was established that the curve of the solar fraction (fraction of required energy that is provided by solar collectors) versus the mass flow rate for a system without a heat exchanger has a peak (figure 2.1). The optimum flow rate for the collector loop is at the peak solar fraction (F_p). Determining the optimum storage loop flow rate of systems with heat exchangers requires simulation of systems of various collector areas without exchangers. The optimum heat capacity ratio is then given by equation 2.1 (subscript 't' refers to the tank loop and A_c is the collector area).

$$R_{opt} = \frac{\dot{m}_c c_{p,c}}{\dot{m}_t c_{p,t}} = 1 + \frac{F' U_L A_C}{(UA)_x} \quad 2.1$$



2.2. Natural convection heat exchangers

Natural convection heat exchangers (NCHE) have recently been employed in SDHW systems installed in cold climates. The conventional shell-and-tube heat exchanger was the first configuration adapted for this purpose.

Richmond and Hollands (1989) reported a finite volume numerical solution to open cavity natural convection heat exchangers. The heat exchanger was assumed to consist of

several vertical tubes in a body of fluid. Natural circulation took place inside the tubes, while the regime outside the tubes was forced convection. A new dimensionless parameter, the flow number was introduced as the ratio of the energy in the hot stream to the ability of the cold stream to absorb it. It was believed that at low flow rates, the fluid is preheated by axial conduction before it enters the cavity. Therefore, in the numerical model a fictitious inlet plenum was introduced to account for the axial conduction. The results were presented in the form of graphs of the Nusselt number, dimensionless mass flow rate and effectiveness, versus the modified Rayleigh number.

Parent *et al.* (1990) tested two natural convection heat exchangers to assess two different models. The heat exchangers they tested and the numerical model they used, were similar to that described by Richmond and Hollands (1989). At high values of hot fluid inlet temperature, the numerical model under-predicted the experimental results. This under-prediction was attributed to recirculation in the heat exchanger. The second model was called the forced-convection-based (FCB) model, because h_i was found using standard laminar forced convection relations. The method is based on trial and error, and starts with a guess for the natural circulation mass flow rate, and at the end yields the value of the pressure difference on the tube side. The FCB model prediction was not reliable at higher temperature differences.

Van Rossum (1990) conducted experimental studies on natural convection double-pipe heat exchangers with or without twisted tape inserts inside the tubes. The focus of Van Rossum's study was on the Nusselt number for natural convection inside the tubes. Two concentric tube heat exchangers were constructed. One of the heat exchangers consisted of a 25 mm diameter shell and a 19 mm diameter copper tube. The second heat exchanger had a shell of 13 mm diameter and a 10 mm tube. The buoyancy-driven fluid flowed inside the inner tube. For a vertical circular tube with no tape insert, equation 2.2 was found to correlate the data for $2.6 \times 10^4 < Ra < 4.5 \times 10^5$ and $2.75 < Pr < 6.6$.

$$Nu_D = 0.408 Ra_D^{0.341} Pr^{-0.368} \quad 2.2$$

The average Nusselt number increased by 20 to 40% when flat tapes were inserted in the tube. A twist ratio was defined to measure the degree of tape twist as the length per

360° rotation divided by the tape width. Tapes with a twist ratio of about 7 increased the Nusselt number by 40 to 50%.

Bergelt *et al.* (1993) studied the optimum hydraulic resistance for natural convection SDHW systems heat exchanger loops. The model developed by Fraser, Hollands and Brunger (1995) was utilized in the study, and the experiments were performed on a shell-and-coil heat exchanger. The optimum hydraulic resistance of the rest of the loop was found to be nearly the same as the hydraulic resistance of the heat exchanger. The optimum collector flow rate was close to 0.025 kg/s, for a collector area of 5.2 m². They also compared the NCHE loop with one having a fixed forced flow, and found that by using natural circulation, there is a slight improvement in performance.

Srinivasan and Christensen (1994) studied the performance of NCHEs as space-conditioning devices. Two designs were considered in their study. One was a plain shell-and-tube heat exchanger consisting of 72 stainless steel, 25.4 mm OD tubes, 6.1 m long, in a steel shell. 35 m² of heat transfer area was produced by this design. The second design was comprised of 204 fluted aluminum 9.53 mm OD tubes, 2.13 m long in a 356 mm diameter plastic shell. Forced and natural convection Nusselt numbers, from existing literature, were combined in equation 2.3, to obtain the tube side Nusselt number.

$$Nu_C = [Nu_F^6 + Nu_N^6]^{1/6} \quad 2.3$$

In equation 2.3 the subscripts C, F and N stand for combined, forced and natural convection, respectively. For the shell-side heat transfer coefficient, the authors argue that there exists a forced laminar convection component due to natural circulation, and natural convection is also present. The presence of natural convection is believed to be by reason of the Richardson number being well above unity. Equation 2.4 was used to predict the forced convection component.

$$Nu_F = 0.033Re^{0.8}Pr^{0.33} \quad 2.4$$

Equation 2.5 was proposed for the natural convection component of heat transfer in the range, $1.32 \times 10^9 \leq Ra_q \leq 1.23 \times 10^{10}$.

$$Nu_N = 0.04Ra_q^{0.26}$$

2.5

The Nusselt number for combined forced and natural convection heat transfer was found using equation 2.3 as proposed by El-Genk *et al.* (1990). This model was then used to predict the heat transfer parameters during the tests in a flooded mine and also a lake, in both the cooling and heating modes. The model correlated the cooling mode data within $\pm 20\%$. The heating mode data was not predicted well with the model. This was attributed to some preexisting upward flow, which apparently worked against the natural circulation current.

Fraser *et al.* (1995), presented an empirical model for natural convection heat exchangers in SDHW systems. The model requires plots of effectiveness and pressure drop versus the water flow rate obtained by performing tests on the exchanger in question. The proposed model can be summarized as follows. The pressure drop in connecting pipes is calculated using standard hydraulic equations. The pressure drop in the exchanger was determined experimentally. Inside the tank, the shear component of the pressure drop is assumed zero, and the buoyant component is calculated knowing the temperature distribution. For a specified glycol inlet temperature, the water outlet temperature and flow rate can be calculated by equating the sum of pressure differences in each section of the loop to zero. The heat balance inside the exchanger must also be utilized. Validation tests in transition state were also performed and the model was found to predict the parameters with sufficient accuracy.

Avina (1995) presented two models for the thermal performance of a NCHE in a SDHW system. One model was based on the method proposed by Fraser *et al.* (1995). In the second model, which was called the detailed model, the empirical equations for heat transfer from an array of tubes found in the literature, were used to predict the Nusselt number for the shell-and-coil NCHE. Based on the detailed model and taking into account economic factors, Avina obtained an optimal shell-and-coil heat exchanger configuration. The coil tube diameter and also the gap between the two coils were found to be less influential, whereas, the height of the heat exchanger and the number of the coils had more impact on the heat exchanger performance. Avina suggested that the optimum heat exchanger should contain two coils made of 6.35 mm tube, having inner diameters of 25.4

and 44.5 mm and a height of 450 mm. The shell diameter and the coil pitch should be 102 mm and 8.9 mm, respectively.

2.3. Helical coils in natural convection

Little literature is available on the subject of helical coils in natural convection heat transfer. This section is a review of the relevant literature.

Heat transfer from a heating helical coil immersed in a jet-stirred vessel was the subject of the study by Hsu and Shih (1984). The study does not cover natural convection heat transfer, but it contains some results beneficial to the current subject. Tube diameters of 6.35, 12.7, and 19.05 mm, coil diameters ranging from 115 to 216 mm, and four coil pitches of 1.5, 2, 2.5 and 3 tube diameters were tested. The container was of 315 mm diameter and 450 mm height. A general correlation for Nusselt number as a function of the Reynolds number based on the jet nozzle diameter was presented. The Nusselt number was found to be insensitive to changes in the coil diameter as well as pitch, however, it decreased slightly as the tube diameter increased.

Ali (1994), investigated natural convection from vertical helical coils to water. Brass, helically coiled tubes were tested in a tank filled with water. Two tube diameters of 8 and 12 mm OD, with five coil diameters and five different pitches were tested. Coils consisted of either 5 or 10 turns and pitches of 1.5 to 4 tube diameters. The heat transfer coefficient was calculated using the overall heat transfer coefficient, U , and applying equation 2.6 (Rogers and Mayhew 1964) to find h_i .

$$Nu = 0.023Re^{0.85}Pr^{0.4}(d_i/D)^{0.1} \quad 2.6$$

Ali based the Rayleigh number for natural convection on the temperature difference between the mean water temperature inside the tube, and the mean water temperature in the tank. Two correlations were presented using L as the characteristic length. There is a dramatic change in the exponents of the Rayleigh number for the two tube diameters

investigated. For the 12 mm OD tube, equation 2.7 was given for $3 \times 10^{12} \leq Ra_L \leq 8 \times 10^{14}$.

$$Nu_L = 0.685(Ra_L)^{0.295} \quad 2.7$$

and for the 8 mm OD tube, Ali presents equation 2.8 for $6 \times 10^{11} < Ra_L < 1 \times 10^{14}$.

$$Nu_L = 0.00044(Ra_L)^{0.516} \quad 2.8$$

The above correlations show that, for $D_{i,o}=12$ mm, h_o , decreases as the coil length increases and this trend is reversed for $D_{i,o}=8$ mm. This behavior was left unexplained. Ali also correlated the data for $D_{i,o}=12$ mm, and found out that h_o is almost insensitive to coil height.

$$Nu_H = 0.257(Ra_H)^{0.323} \quad 6 \times 10^8 \leq Ra_H \leq 3 \times 10^{11} \quad 2.9$$

However, for $D_{i,o}=8$ mm, Ali presented two correlations. For $D_c/D_{i,o}=19.957$ and $2 \times 10^8 \leq Ra_H \leq 5 \times 10^{10}$ equation 2.10 was proposed.

$$Nu_H = 0.016(Ra_H)^{0.433} \quad 2.10$$

Equation 2.11 was proposed for $D_c/d_o=9.914$ and $3.5 \times 10^8 \leq Ra_H \leq 7 \times 10^{10}$.

$$Nu_H = 0.0023(Ra_H)^{0.494} \quad 2.11$$

Equations 2.10 and 2.11 indicate a dependence of the heat transfer coefficient on the coil height. The degree of this dependence varied. Ali also included the number of coil turns in other correlations and concluded that, for the 12 mm OD tube, the number of coil turns, N , does not affect the heat transfer coefficient, yet h_o increases abruptly as N increases for the 8 mm OD tube.

The research closest to the current thesis is the work of Ajele (1995). Ajele tested vertical helical coils in a cylindrical shell of 100 mm ID and a height of 400 mm. The coils were made of 6.35 mm OD copper tube. The coil pitch was fixed at an average of 2 tube diameters. Eleven combinations of one to four coils were tested. Coil diameters varied from 26.8 to 88.7 mm. Ajele found that the dimensionless flow space was an influential parameter on the shell-side Nusselt number. Consequently, Ajele proposed equations 2.12 and 2.13 for $S' < 1.5$ and $S' > 1.5$ respectively.

$$Nu_{Dhx} = 0.53 \frac{Ra_{Dhx}^*{}^{0.33}}{S'} \quad (S' < 1.5) \quad 2.12$$

$$Nu_{Dhx} = 0.48 \frac{Ra_{Dhx}^*{}^{0.38}}{S'} \quad (S' > 1.5) \quad 2.13$$

The range of the modified Rayleigh number for equations 2.12 and 2.13 is $1.2 \times 10^5 < \frac{Ra_{Dhx}^*}{S'^4} < 4 \times 10^5$.

Ajele also correlated the data for single coils using the modified Rayleigh number based on the shell height. Equations 2.14 and 2.15 are the correlations for $S' < 1.5$ and $S' > 1.5$ respectively.

$$Nu_H = 5.40 \frac{Ra_H^*{}^{0.25}}{S'} \quad 3 \times 10^7 < Ra_H^* < 2 \times 10^8 \quad 2.14$$

$$Nu_H = 1.91 \frac{Ra_H^*{}^{0.33}}{S'} \quad 2 \times 10^8 < Ra_H^* < 2 \times 10^9 \quad 2.15$$

When multiple-coil configurations were added to the single coil data, the flow number was found to play an important role. What Ajele referred to as the general correlation is in fact a series of correlations for various S' , F and Ra_{Dhx}^* ranges. For

$S' < 1.5$, $0.4 < F < 30$ and $1.2 \times 10^5 < \frac{Ra_{Dhx}^*}{S'^4} < 4 \times 10^5$, equation 2.16 correlated the experimental data.

$$Nu_{Dhx} = 0.53 \frac{[F^{(N-1)/3} Ra_{Dhx}^*]^{0.33}}{S'^m} \quad 2.16$$

The exponent m is a function of the number of coils N and is given in table 2.1.

Table 2.1. Exponent m in equation 2.16

N	1	2	3	4
m	1	1/3	-1/5	0

For $S' > 1.5$, equation 2.13 is valid for the multiple-coil configurations as well. A second set of equations was presented for $S' < 1.5$ and two ranges of the flow number.

Equation 2.16 was valid for $F < 1$. For $F > 1$, $S' < 1.5$ and $1.2 \times 10^5 < \frac{Ra_{Dhx}^*}{S'^4} < 4 \times 10^5$, equation 2.17 was proposed.

$$Nu_{Dhx} = 0.50 \frac{Ra_{Dhx}^{*0.33}}{S'^m} \quad 2.17$$

For the optimum shell-and-coil NCHE, Ajele suggested that $0.4 < S' < 0.7$. Regarding the configurations that Ajele tested, the above requirement was met by the triple-coil configurations.

Natural convection heat transfer from helicoidal pipes to air, was the subject of a recent study by Xin and Ebdian (1996). Three helical coils were tested with tube diameters of 25.4, 12.7 and 12.7 mm. Coil diameters were, 259, 127 and 127 mm respectively, and the pitches were, 62.5, 28.2 and 76.0 mm. The coils had either 5 or 10 turns. The local coefficients of heat transfer to air were calculated taking into account the radiation loss to ambient. The authors argued that despite some similarities, natural convection heat transfer

from a vertical helical coil is different from a vertical array of horizontal cylinders in two ways. First, the curvature and helix angle may disturb the temperature and flow fields around the tube relative to a vertical array of horizontal cylinders. Second, the inside flow along the axis of the coil is similar to confined space natural convection, instead of free space natural convection, especially for small coil-to-tube diameter ratios and long coil height. In their study, the heat transfer from the first turn was found to be the same as for a single horizontal cylinder. Local Nusselt numbers were calculated for horizontal, as well as vertical coils. For the first two coils, equation 2.18 was presented for the average overall Nusselt number of the vertical coil.

$$Nu = 0.290Ra^{0.293} \quad 2.18$$

The range of the Rayleigh number based on the tube diameter was, $4 \times 10^3 \leq Ra \leq 1 \times 10^5$. The regime is said to be laminar in this range. The third coil ($P=6$) did not obey the above equation. No explanations were offered for this unique behavior. A different correlation was given for the helical coil in the horizontal orientation.

2.4. Horizontal cylinders

Due to some similarities, natural convection heat transfer from a single horizontal cylinder is a reference for validating the results of the current thesis. Data for single horizontal cylinder provides a rough estimate of what the Nusselt number should be for natural convection from helical coils.

Churchill and Chu (1975) presented an empirical correlation (equation 2.19) for a wide range of Rayleigh number ($10^{-6} < Ra < 10^{13}$) in natural convection heat transfer from a horizontal cylinder.

$$Nu = \left[0.60 + 0.387 \left(\frac{Ra}{[1 + (0.559 / Pr)^{9/16}]^{16/9}} \right)^{1/6} \right]^2 \quad 2.19$$

Equation 2.19 is recommended for both constant heat flux and constant surface temperature cases. Churchill and Chu based their equation on the finding that for very low Rayleigh numbers the Nusselt number approaches a significant finite value, which was stated to be 0.36. It is suggested that simple power-law expressions are inadequate when applied to a wide range of Rayleigh number and should no longer be used for that purpose.

Raithby and Hollands (1976) stated that there exist large discrepancies between experiment and analysis in predicting the heat transfer by free convection from the external surfaces of bodies of various contours. Two reasons were given for these discrepancies. One is due to the fact that the boundary layers become thick at low Rayleigh numbers. This makes the boundary layer equations inaccurate in predicting the physical phenomenon. The second reason is turbulence on part of the surface at high Rayleigh numbers is usually ignored. Raithby and Hollands showed that thin-layer solutions do not predict well the average heat transfer performance of circular and elliptic horizontal cylinders. Thin-layer solutions refer to those methods in which the y -conduction term in the energy equation can be approximated by $k(\partial^2 T/\partial y^2)$. The modified solution agreed well with available experimental data. Equation 2.20 was proposed for $Pr > 2$, considering the flow to be turbulent everywhere along the surface of the cylinder.

$$Nu = 0.1Ra^{0.33}Pr^{0.084} \quad 2.20$$

Equation 2.20 can be used for both the flat plate and the horizontal cylinder, as well as all elliptic surfaces between the two extreme cases. After modification for both turbulent and thick layer effects the following equation was proposed.

$$Nu = \frac{1.64}{\ln(1 + 2.64Ra_{q,B}^{-0.2})} + 0.22Ra_{q,B}^{0.25} \quad 2.21$$

The first term in equation 2.21 is the thick-layer modification term and the second term is the result of turbulence consideration with the subscript 'B' referring to the ellipse major axis.

Fand *et al.* (1977) studied natural convection heat transfer from a horizontal cylinder to air, water and silicone oils. The test section was a 11.57 mm diameter, electrically heated titanium cylinder, 25.4 mm in length. The study was carried out to account for property variation with temperature. Three $Nu-Ra$ relations were proposed and evaluated, all of them suggesting that such relations must include Pr^m , explicitly (the exponent 'm' must be evaluated experimentally). The three correlations differ in the way fluid properties are calculated. The authors also concluded that the Nusselt number is a function of another dimensionless parameter, in addition to Ra and Pr , and suggest that this dimensionless parameter is a function of viscous dissipation. For the range $2.5 \times 10^2 \leq Ra_{Dt} \leq 1.8 \times 10^7$ and where the fluid properties are evaluated at the mean film temperature, equation 2.22 is applicable.

$$Nu_{Dt} = 0.474 Ra_{Dt}^{0.25} Pr^{0.047} \quad 2.22$$

Sparrow and Pfeil (1984) studied the effect of vertical shrouding surfaces on natural convection heat transfer from a horizontal cylinder to air. The cylinder outer diameter was 37.9 mm and it was 757 mm long. The cylinder was shrouded with two vertical walls having heights equal to 5, 10 and 20 cylinder diameters. The spacing between the walls (S) was varied from 1.5 to 10 cylinder diameters. The experiments were also carried out with no walls. For the unshrouded cylinder, equation 2.23 was proposed.

$$Nu_{Dt} = 0.605 Ra_{Dt}^{0.225} \quad 2 \times 10^4 \leq Ra_{Dt} \leq 2 \times 10^5 \quad 2.23$$

Values for the multiplier and the exponent of correlations of this form were presented in a table for various configurations. Heat transfer enhancement as high as 40% compared with the unshrouded cylinders were reported. For fixed channel heights, the enhancement increased with decreasing spacing. There was no significant enhancement for $S/D \geq 10$. At a fixed S/D , an increase in the channel height increased the cylinder Nusselt number. The extent of the increase was highly sensitive to S/D . For small spacings there was an enhancement between 11 to 40% when the height was increased, whereas at large spacings, the shroud height increase had little significance.

Karim *et al.* (1986) studied the effect of vertical confining adiabatic walls, on natural convection from a horizontal cylinder to air. Two cylinders of 25.4 and 38.1 mm OD having the same length of 660 mm comprised the test section. The cylinder was placed between two vertical walls with a varying distance from each other. The wall spacing was varied from 1.5 to 12 cylinder diameters, and the tests were also carried out with no confining walls. The wall height to cylinder diameter ratio (H/D) was 64 and 96 for the larger and smaller cylinders, respectively. Equations of the form $Nu_{Dt} = CRa_{Dt}^m$ were used to correlate the data. Values of C and m as a function of wall spacing to cylinder diameter ratio (W/D) were arranged in a table. For $W/D=12$, equation 2.24 was suggested.

$$Nu_{Dt} = 0.32 Ra_{Dt}^{0.29} \quad 2.24$$

The authors presented equation 2.25 as an empirical correlation for the entire range of W/D and $2 \times 10^3 \leq Ra_{Dt} \leq 3 \times 10^5$.

$$Nu_{Dt} = \{0.481 + 0.172 \exp[-0.258(W/D)]\} Ra_{Dt}^{0.25} \quad 2.25$$

The heat transfer from the cylinder was enhanced by the confinement and the magnitude of the enhancement decreased with increasing wall spacing. For the range of Rayleigh number studied, no optimal W/D was obtained for maximum heat transfer.

A numerical study of transient natural convection from horizontal cylinders was reported by Wang *et al.* (1991). The formation of a plume was described in detail. Recirculation was observed.

The results of Clemes *et al.* (1994) for horizontal circular cylinders (50 mm ID and 510 mm nominal length) were in agreement with those by Kuehn and Goldstein (1976) and Raithby and Hollands (1985).

Recently, Morgan (1997) published an extensive review of the literature on natural convection heat transfer from a horizontal isothermal cylinder to air. Morgan tabulated the average values of Nusselt number of all the literature for decade intervals of Rayleigh number.

2.5. Vertical cylinders

Fujii *et al.* (1970), studied natural convection heat transfer, from a heated vertical cylinder to water and two types of oil. Their experiments covered a wide range of Prandtl numbers from 2.4 to 2600. The test section consisted of a 82.0 mm OD brass cylinder, 1 m long. Since the diameter of the cylinder was considerably larger than the thickness of the boundary layer, the local Nusselt number data was found to be in good agreement with the equations for natural convection from vertical flat plates. For the range, $10^{10} \leq Ra_L$, equation 2.26 correlated all the data with reasonable accuracy.

$$Nu_L = 0.017Ra_L^{0.4}(v_\infty/v_0)^{0.21} \quad 2.26$$

In the equation 2.26, the subscripts ∞ and 0 indicate the fluid property at the ambient and cylinder wall temperatures, respectively. Fujii *et al.* also reported boundary layer visualization by the “mirage method”. It is an optical method based on differences in refractive indices in the flow field, and was introduced for the first time by the authors.

2.6. Horizontal rod bundles (bank of tubes)

A vertical helical coil has some geometrical similarities to an array of horizontal cylinders. Unlike the case of natural convection from helical coils, there is an abundance of literature on natural convection from array of cylinders. This provides a source of comparison for the current data, especially in addressing the optimum coil pitch which is equivalent to the center-to-center distance of an array of cylinders.

Lieberman and Gebhart (1969) investigated natural convection from an array of heated wires. The wires had a diameter of 0.127 mm and a nominal length of 184 mm. The minimum spacing was 37.5 wire diameters. Increasing the wire spacing in the vertical direction increased the average Nusselt number of the array up to the point of 112 wire diameters thereafter, the Nusselt number started to decline.

A vertical array of horizontal cylinders in natural convection to air, was studied by Marsters (1972). The apparatus consisted of an array of 3, 5, or 9 stainless steel tubes of 6.35 mm outer diameter. The tubes were 585 mm long, and the minimum spacing was 2 tube diameters. An emissivity of 0.3 was used to account for radiation heat transfer. The Grashof number based on the tube diameter varied from 750 to 2000. Marsters suggested that the tube diameter should not be used as the characteristic length. Rather, the position of the cylinder in the array should be used. Based on this characteristic length, Marsters claimed that the tubes undergo some sort of transition at Grashof numbers of the order of 10^6 - 10^7 . Marsters also mentioned that the case can no longer be considered as natural convection since the upper cylinders experience a flow velocity induced by the lower cylinders. This certainly applies to the current problem also.

Apparatus similar to Marsters (1972) was used by Marsters and Paulus (1972) to study the effect of confining walls on heat transfer from a vertical array of horizontal cylinders. The tube spacing was fixed at 6 tube diameters. Wall spacing was varied from 4 to 40 tube diameters. Marsters and Paulus found that the average temperature in the array increases with decreasing wall spacing, and the effect of wall is almost negligible when the spacing is $40D_c$. Closely-spaced walls enhanced heat transfer from the lowest cylinders, but had the opposite effect for cylinders further up the array. The average heat transfer coefficient decreased by 10% as the wall spacing was reduced from 40 to 4 tube diameters. With the walls spaced at $10D_c$, the plume did not fill the channel completely.

Tillman (1976) studied the influence of tube spacing on natural convection heat transfer from a bundle of heated horizontal tubes to air. The test section consisted of 14 cartridge heaters, 12.7 mm in diameter and having a 76.2 mm active length, arranged in staggered configuration. Tillman also tested the tubes in a square configuration, in which case 16 tubes were employed. The tests were carried out for tube spacings from 1/8 to 2 tube diameters. A hydraulic diameter similar to that defined by Kays and London (1984) was used to take into account the effect of tube spacing. Thermal properties were evaluated at the film temperature. Equations 2.27 and 2.28 correlated the data in the range, $50 \leq Ra_{Dh} \leq 5 \times 10^6$, for staggered and square arrays respectively.

$$Nu_{Dh} = 0.057 Ra_{Dh}^{0.5} \quad (\text{staggered array}) \quad 2.27$$

$$Nu_{Dh} = 0.067 Ra_{Dh}^{0.5} \quad (\text{square array}) \quad 2.28$$

The data for the square array with the spacing equal to 2 tube diameters did not correlate well with the equation 2.28.

A pair of horizontal cylinders located parallel to each other in a vertical plane was tested by Sparrow and Niethammer (1981). The effects of center-to-center distance of the cylinders and also the effect of a temperature imbalance between the two cylinders were investigated. The operating conditions encompassed upper-cylinder Rayleigh numbers between 2×10^4 and 2×10^5 and separation distances ranging from two to nine times the cylinder diameter. Prandtl number was constant at 0.7. The cylinder diameter was 37.87 mm and its length was 762 mm. The authors argued that, when the buoyancy-induced fluid flow from one of the cylinders washes others in the array, the impinged cylinders can no longer be assigned heat transfer coefficients from the available data bank for the single cylinder. First, the fact that the fluid arriving at the upper cylinder is in motion (due to the buoyancy created by the lower cylinder) means that the upper cylinder is situated in a forced convection flow. Consequently, on this account, the presence of the lower cylinder should enhance the heat transfer coefficient at the upper cylinder relative to that for the single cylinder. On the other hand, the heat transfer at the lower cylinder raises the temperature of the fluid which arrives at the upper cylinder to a value that is higher than that of the ambient fluid. Thus, with respect to the upper cylinder, the lower cylinder acts as a preheater. This preheating effect tends to decrease the heat transfer coefficient of the upper cylinder compared with that which would exist if the lower cylinder were absent. Therefore, the relative strengths of these effects vary with the vertical separation between the cylinders, both for laminar and turbulent plumes. In either case, the preheating effect should diminish as the separation distance increases. With regard to the fluid flow, which is induced by the lower cylinder and impinges on the upper cylinder, the velocity of impingement increases with increasing separation distance when the plume is laminar but is independent of the separation distance when the plume becomes turbulent. With small separation, the Nusselt number increases sharply with increasing separation. With a further increase in separation, the Nusselt number increase becomes more and more gradual, with the ultimate attainment of a maximum. The degree of enhancement or degradation of the

heat transfer from the upper cylinder is strongly dependent on the cylinder-to-cylinder separation. For the smaller separations, degradation is generally the rule, while at larger separations, enhancement predominates.

Farouk and Guceri (1983) studied natural convection from single and double rows of infinite number of horizontal cylinders numerically. Transverse spacings of 2 to 6 cylinder diameters, and longitudinal spacing of 4 cylinder diameters were considered. The Prandtl number of the fluid was assumed to be 0.721. While, only the laminar flow situation was considered for double rows of cylinders, for single row of cylinders both laminar and turbulent regimes were taken into account. The authors concluded that the heat transfer characteristics were strongly dependent on cylinder spacings as well as the Rayleigh number.

Tokura *et al.* (1983) conducted experimental studies of natural convection from a vertical array to air. Copper tubes having 28.5 mm diameter and 600 mm length constituted the test section. For five-cylinder array, it was found that when the tube spacing decreases to less than 3 tube diameters, the Nusselt number of the individual cylinders starts to decrease to a value less than that of a single cylinder. The average Nusselt number of the array also decreased considerably as the tube spacing decreased to the same value. The authors also investigated the effect of the distance between the walls, when the array of cylinders was placed between two parallel plates. It was found that, for five-cylinder array, decreasing the wall-to-wall distance to less than 5 tube diameters will decrease the Nusselt number. This decrease is more profound for cylinder spacing of 2 tube diameters. In general, it was found that the tube spacing is more influential on the Nusselt number, than the wall-to-wall distance.

Sparrow and Vemuri (1985) studied combined natural convection and radiation heat transfer from pin fin arrays to air. Several horizontal aluminum cylinders of 6.35 mm diameter were attached to a square baseplate, 76.2 mm wide. The effect of the cylinder length and the number of cylinders were studied. An array having between 30 and 40 pin fins was suggested to be optimal. This corresponds to a pitch value of 1.9 to 2.5 tube diameters.

Sadeghipour and Asheghi (1994) investigated natural convection from arrays of horizontal cylinders to air at low Rayleigh numbers. Cylinders of 6.6 mm diameter and 66.4 cm length were used as the test section. It was found that heat transfer from the arrays cannot be improved by increasing the center-to-center distance to more than 15 tube diameters. A generalized correlation, for the average Nusselt number of the array was presented in the form of equation 2.29 for $500 \leq Ra \leq 700$, $3.5 \leq P \leq 27.5$ and $2 \leq N \leq 8$.

$$\overline{Nu} = Ra^{0.25} [0.823 + \exp(-1.5P^{0.05N})] \quad 2.29$$

Bejan *et al.* (1995) conducted theoretical, numerical and experimental studies on the optimal spacing between horizontal cylinders in a fixed volume cooled by natural convection. A theoretical argument was presented to prove the existence of an optimal cylinder-to-cylinder spacing for maximum heat transfer. It was concluded that the optimal spacing is almost insensitive to changes in cylinder diameter. The result of the numerical study was presented in form of a correlation, which after some manipulation will result in equation 2.30.

$$P_{opt} = 2.35 \left(\frac{H}{D} \right)^{1/3} Ra_D^{-1/4} + 1.09 \quad 2.30$$

Experiments were also carried out to confirm the results of the numerical model. It was found that the optimal spacing was insensitive to whether the array was uniform flux or isothermal. The predictions of the model were in good agreement with the experiments.

Keyhani and Dalton (1996) studied natural convection heat transfer in horizontal rod-bundle enclosures. Electric cartridge heaters with a diameter of 9.42 mm and 585 mm active length comprised the test section. Horizontal arrays of 3×3 , 5×5 and 7×7 were tested. The pitch value was fixed at 1.35 tube diameters. Pressurized air or helium from 1 to 7 atm was used as working fluid. The results were corrected for radiation and a $Nu-Ra$ correlation based on heat flux and enclosure width was presented for $10^7 \leq Ra_w^* \leq 10^{10}$.

$$Nu_w = 0.0441 Ra_w^{*0.316} (Nd/W)^{0.450} \quad 2.31$$

In addition, correlations in form of $C(Ra_w^*)^m$ were presented for each rod bundle. The flow regime was opined to have three regions: a conduction dominated region, a conduction-convection region and finally a convection dominated region.

2.7. Vertical rod bundles

Two rod bundles of 3×3 and 5×5 , of vertical orientation, in a cylindrical shell were studied under natural convection by Keyhani *et al.* (1985). The tests were conducted with air, helium and water as the heat transfer fluid. The results were corrected for radiation. The 3×3 rod bundle consisted of nine 6.35 mm diameter cartridge heaters with an effective heated length of 876 mm. The 5×5 rod bundle was comprised of twenty-five 19.1 mm diameter cartridge heaters with effective heated lengths of 1.765 m. The outer cylinder had a 82.5 mm ID. Nusselt number correlations for individual cylinders, as well as the overall Nusselt number were presented for two flow regimes. The characteristic length for the correlations was the shell diameter, D_s . For the 3×3 rod bundle, in the range, $1.2 \times 10^5 \leq Ra_D \leq 4.5 \times 10^7$, and air or helium as the heat transfer fluid equation 2.32 was presented.

$$Nu_D = 0.072 Ra_D^{0.332} \quad (\text{air, helium}) \quad 2.32$$

Equation 2.33 was suggested for the 5×5 rod bundle in the range, $1.48 \times 10^6 \leq Ra_D \leq 1.06 \times 10^9$.

$$Nu_D = 0.095 Ra_D^{0.323} \quad (\text{air, helium}) \quad 2.33$$

The heat transfer coefficients of individual cylinders were varied for different cylinders, for air and helium. However, for water the heat transfer coefficient of all the cylinders were the same. Equation 2.34 correlated the data of the overall Nusselt number in the range, $6.5 \times 10^6 \leq Ra_{Ds} \leq 1.4 \times 10^8$.

$$Nu_{Ds} = 0.151Ra_{Ds}^{0.274} \quad (\text{water}) \quad 2.34$$

Flow visualization in the 3×3 rod bundle indicated that there exists a low speed downward flow between the rods.

Kim and El-Genk (1989) and El-Genk *et al.* (1990) studied mixed convection heat transfer from triangularly arranged rod bundles to water. The test section consisted of seven electrically heated cylinders in a vertical hexagonal Plexiglas shroud. In the natural circulation experiments, the Reynolds number varied from 260 to 2000 and the corresponding Rayleigh numbers based on q ranged from 8×10^6 to 2.5×10^8 . The Prandtl number ranged from 3 to 8.5. The spacing between the heated rods had no effect on the heat transfer rate with natural circulation and the values of Nusselt number were correlated by equation 2.35, for the mentioned range of Ra_q .

$$Nu = 0.272Ra_q^{0.25} \quad 2.35$$

In equation 2.35, the Nusselt number is defined as, $Nu = \frac{q''D_{eh}}{k_w(T_w - T_b)}$, where D_{eh} is the heated equivalent diameter defined as, $4 \times$ cross-sectional flow area divided by heated perimeter, T_b is the mean bulk temperature of water and T_w is the mean wall temperature of the heated section. When the Richardson number is less than unity, forced convection is believed to be dominant, while for Ri greater than unity, mixed convection exists. In such situations, the combined Nusselt number should be evaluated using equation 2.36.

$$Nu_C = [Nu_F^3 + Nu_N^3]^{1/3} \quad 2.36$$

Recently, El-Genk *et al.* (1993) extended their previous experiments to square arrayed vertical rod bundles in natural, mixed and forced convection regimes. For natural convection, equation 2.37 was presented for rod bundles having pitch of 1.25 in the range $6 \times 10^5 \leq Ra_q \leq 9 \times 10^7$ and 1.38 in the range $3 \times 10^6 \leq Ra_q \leq 2 \times 10^8$.

$$Nu = 0.057 Ra_q^{0.35} \quad 2.37$$

In equation 2.37 the Nusselt and Rayleigh numbers are based on the heated equivalent diameter.

2.8. Vertical annuli

Keyhani *et al.* (1983) reported experiments on natural convection in a vertical annular enclosure with constant heat flux on the inner wall and constant temperature on the outer wall. The annular enclosure was comprised of a 19.1 mm diameter inner cylinder and a 82.6 mm ID outer cylinder. The effective heated length of the inner cylinder was 876 mm. Air and helium were used as the fluid medium. Nusselt number correlations corrected for radiative heat transfer were presented as equations 2.38 and 2.39.

$$Nu_l = 1.37 Ra_{q,l}^{0.072} \quad 2.6 \times 10^3 \leq Ra_{q,l} \leq 1.8 \times 10^4 \quad 2.38$$

$$Nu_l = 0.253 Ra_{q,l}^{0.244} \quad 1.8 \times 10^4 \leq Ra_{q,l} \leq 4.21 \times 10^7 \quad 2.39$$

In equations 2.38 and 2.39, l is a length scale and is defined as $l=r_o-r_i$, with r_o and r_i as outer and inner cylinder radii, respectively. Nusselt number correlations with respect to the conventional definition of the Rayleigh number were also presented. Two distinct heat transfer regimes were detected. They were referred to as the conduction and the boundary layer regime.

El-Genk and Rao (1989), reported experiments on heat transfer in vertical annuli with water at low-velocity forced flow, as well as natural and mixed flow regimes. The tests were conducted on vertical annuli of inner to outer diameter ratios of 1.17 and 2.0. The latter consisted of a heated stainless steel tube, 12.7 mm OD, 900 mm long, as the inner cylinder, and an insulated Plexiglas tube, 25.4 mm ID as the outer cylinder. Correlations of Nu and Ra_q were presented for the laminar and turbulent natural convection regimes. The regime was treated as fully turbulent for $Ra_q > 8 \times 10^6$. Equations 2.40 and

2.41 were suggested for correlating the data of laminar and turbulent natural convection regimes, respectively.

$$Nu = 0.625 \left(\frac{Ra_q}{X} \right)^{0.2} \quad 4 \times 10^4 < Ra_q < 6 \times 10^6 \quad 2.40$$

$$Nu = 0.077 Ra_q^{0.285} \quad 10^7 \leq Ra_q \leq 3 \times 10^9 \quad 2.41$$

In equation 2.40, X is the ratio of the axial distance from the bottom of the annuli to the annulus hydraulic diameter.

Khan and Kumar (1989) conducted a numerical study of natural convection in vertical annuli having constant heat flux on the inner wall and cooled on the outer wall. The effects of aspect ratio and diameter ratio on heat transfer were studied. Nusselt number correlations in terms of Rayleigh number, diameter ratio and aspect ratio were presented. The effects of both the aspect and diameter ratio were found to be insignificant for values greater than 5, and equation 2.42 was proposed for predicting the Nusselt number in these cases. The diameter of the inner wall was the characteristic length for equation 2.42.

$$Nu = 0.455 Ra^{0.202} \quad 2.42$$

El-Genk and Rao (1990) used the apparatus of El-Genk and Rao (1989) to study the effects of buoyancy-induced instability on heat transfer in vertical annuli. Dye-injection and temperature-trace techniques were utilized to determine the location of the onset of flow instability in vertical annuli. At low Gr_q , a stable laminar flow prevailed and the local Nu values increased slightly with Gr_q . For $Gr_q > 8 \times 10^5$, corresponding to the onset of instability, Nu increased rapidly as Gr_q increased. The Nu values for unstable flows were as much as three times higher than those for stable laminar flows at the same inlet Reynolds number (Re_{in}) but at lower Gr_q . In order to correlate the Nu data, the average of local Nusselt numbers were obtained. Equation 2.43 correlated the turbulent data well.

$$Nu = 0.088 Ra_q^{0.33} Re_{in}^{-0.12} \quad 2.43$$

Equation 2.43 is valid for $Gr_q < 5 \times 10^7$. The reverse dependence of Nu on the Reynolds number was attributed to the nature of turbulent flow.

Rao and El-Genk (1990) carried a numerical analysis of the same problem as El-Genk and Rao (1990). The prediction of the location of incipient instability was reported to be in agreement with the experiments by El-Genk and Rao (1990).

El-Shaarawi and Al-Nimr (1990) presented analytical solutions to fully developed laminar natural convection in open-ended vertical concentric annuli. Local Nusselt number equations were obtained for four types of boundary conditions.

Rogers and Yao (1990) studied the effect of mixed convection instability on heat transfer in a vertical annulus. The Navier-Stokes and energy equations in terms of annular-cylindrical coordinates were solved with the boundary condition of constant heat flux at the inner wall and adiabatic outer wall. Rogers and Yao found that the assumption of parallel flow can not be used in those situations. Also hydrodynamic instabilities increased the Nusselt number greatly compared to those predicted by the parallel flow assumption. Equation 2.44 was presented for the data in the region between the linear instability limit, where flow remains stable and Ra equal to 600.

$$Nu = 1.02Ra^{0.28} \quad 2.44$$

The difference between the outer and the inner radius of the annulus ($r_o - r_i$) was the characteristic length in equation 2.44.

A numerical analysis of natural convective flow of air in a vertical annulus with longitudinal fins was reported by Kumar (1997). The inner wall was maintained at a constant temperature and the outer wall at a constant but lower temperature. The effects of various parameters on the heat transfer and fluid flow results were discussed. The Nusselt number for the inner cylinder was found to increase as the radius ratio (r_o/r_i) increased. Also it was found that the aspect ratio of the annulus does not influence the Nusselt number value significantly.

2.9. Vertical circular ducts

Scheele and Hanratty (1962) conducted experiments to investigate the effect of natural convection on stability of flow in a vertical pipe. Experiments were conducted with a 18.3 m vertical length of a 20 mm ID copper pipe. Surface thermal conditions of constant heat flux and constant temperature were tested. Transition was detected by measuring the temperature fluctuations at the outlet of the heat transfer section. It was stated that for water, heating or cooling can cause transition to an unsteady flow at Reynolds numbers much lower than are usually associated with transition to turbulence for isothermal flow in pipes. The dimensionless group Gr/Re was found to be appropriate for determining transition to turbulence. The effect of density variation with temperature was found to increase the flow velocity near the wall causing a flattening of the velocity profile in the center of the pipe. At Gr/Re greater than 32.94 the profiles had a dimple at the pipe center and the point of maximum velocity moved radially to the tube wall as the ratio of heat flux to flow rate increased. For Gr/Re greater than 319.1 reversal of flow at the center of the pipe was detected. It was concluded that the stability of a particular flow depends primarily on the shape of the velocity profile and only secondarily on the value of Re .

Kemeny and Somers (1962) reported experiments on combined free and forced convection inside vertical circular tubes. Water and transformer oil were used in the experiments. Measurement of temperature fluctuations were reported. Friction factor and Nusselt number data were collected and plotted against Graetz number and Rayleigh number. Equation 2.45 was presented as a result of the plots of a modified friction factor versus the Rayleigh number.

$$Gz = 0.02Ra^{0.77} \quad 2.45$$

Dyer (1975) studied the development of laminar natural-convective flow in a vertical uniform heat flux duct. In addition to the numerical study, experiments had also been performed with air as the fluid medium. Three circular ducts of 1.22 m long and inside diameters of 19.1, 25.4 and 46.7 mm respectively were examined. Inlet boundary conditions were found to have a negligible effect on the results in all cases. For small

Rayleigh numbers, the Nusselt number was a function of Ra and Pr . However, for large Rayleigh numbers, the Nusselt number was a function of only the Rayleigh number. The theoretical and experimental results were found to be in agreement with equation 2.46 for $Ra_{q,R} > 500$.

$$Nu = 0.67 Ra_{q,R}^{0.2} \quad 2.46$$

2.10. Combined natural and forced convection

The reason behind studying cases of combined forced and natural convection is to determine the boundaries between pure natural and pure forced convection flow regimes. Metais and Eckert (1964) presented plots of $Re - Ra D/L$ based on tube diameter, in order to establish the limit between natural and forced convection regimes. Eshghy (1964) presented Nusselt number relations obtained analytically, for the effect of forced flow on natural convection flows along vertical flat plates. Brown and Gauvin (1965) tried to determine the boundaries between the two regimes of flow inside vertical circular tubes.

Churchill (1977) proposed a set of equations accompanied by tabulated variables to account for the combined effect of free and forced convection in different geometries. As a general rule, Churchill suggested applying equations in form of $Nu^3 = Nu_F^3 + Nu_N^3$ to find the combined regime Nusselt number. Subscripts F and N refer to forced and natural components respectively.

2.11. Heat and fluid flow inside coiled pipes

In their study of heat transfer in tube coils with laminar flow, Seban and McLaughlin (1963) presented an average Nusselt number correlation which was mentioned to be in good agreement with the data from the smaller coil, but the agreement was not nearly as good for the larger coil. Smaller and larger coils had a diameter of 12.5 and 765 mm respectively and were made of 7.37 mm tube. On the contrary, for turbulent flow, the suggested correlation was in relatively good agreement with the larger coil data, but the

equation poorly correlated the data from the smaller coil. This contrariety was left unexplained.

Rogers and Mayhew (1964) concentrated their attention on heat transfer and pressure loss in helically coiled tubes with turbulent flow. Three coils having mean diameters of 10.2, 12.5 and 190 mm, were made of 9.45 mm ID copper tubes. The coils were heated by steam at slightly above atmospheric pressure. Rogers and Mayhew's experiments on isothermal pressure loss confirmed the validity of the available equations of friction coefficient. For the case of heating, use of a Prandtl number correction factor equal to $[Pr_f/Pr_w]^{-0.33}$ in the isothermal equations was recommended. The heat transfer data resulted in the empirical equation 2.47, for $10^4 \leq Re \leq 10^5$ which was considered turbulent.

$$Nu = 0.023Re^{0.85}(d/D)^{0.1}Pr^{0.4} \quad 2.47$$

All fluid properties must be calculated at bulk temperature in equation 2.47.

Mori and Nakayama (1965) carried out a theoretical study of fully developed laminar flow and heat transfer in a curved pipe. Experiments were also conducted on air passing inside a 35.6 mm ID brass pipe having one coil turn of 1.42 m diameter. Nusselt number equations were presented as a function of Dean number and the thermal to velocity boundary layer thickness ratio. For a Prandtl number of 18 (glycol @ 50°C), the first approximate solution results in equation 2.48 for the Nusselt number of a curved pipe.

$$Nu = 2.33De^{0.5} \quad 2.48$$

Measurements of velocity and temperature profiles were claimed to be in agreement with the theoretical results.

Srinivasan *et al.* (1970) experimented on various coils to determine friction factors. The helical coils were made of 12.5 mm ID tube having various coil diameters in the range 92 to 1282 mm. Four coil pitches of 2.5, 3.3, 6.6 and 13.2 tube diameters were tested. Graphs of friction factor with respect to the Dean number were produced. All the graphs

showed breakpoints which was interpreted as the critical Reynolds number value. Equation 2.49 was found to best describe this critical value.

$$Re_{crit.} = 2100[1 + 12(d/D_{c,m})^{0.5}] \quad 2.49$$

Equation 2.49 gives the value of 2100 for the limiting case of a straight tube. For the laminar region where $30 < De < 300$, the friction factor can be calculated from equation 2.50.

$$f = 26.8De^{-0.725} \left(\frac{d}{D_c} \right)^{0.5} \quad 2.50$$

For the transition region where $300 < De < De_{crit.}$, equation 2.51 was suggested.

$$f = 7.2De^{-0.5} \left(\frac{d}{D_c} \right)^{0.5} \quad 2.51$$

For the turbulent region which is marked by $De_{crit.} < De < 14000$, the data was correlated by equation 2.52.

$$f = 0.336De^{-0.2} \left(\frac{d}{D_c} \right)^{0.2} \quad 2.52$$

For $De < 30$ it is recommended to use the friction factor correlation for the straight tube. Srinivasan *et al.* (1970) showed that the friction factors for helical coils can be expressed by a new dimensionless number, for which no name was proposed. This new dimensionless parameter is equal to $Re(D/d)^{0.5}$.

Fully developed laminar flow in helically coiled tubes was studied numerically by Truesdell and Adler (1970). The secondary flow was described as follows. Near the tube center the axial velocity is greatest, causing centrifugal forces to act most strongly. Fluid is thrown outward and replaced by recirculating fluid which flows inward along the walls. In laminar and turbulent flow two strong symmetrical pattern are normally established.

Truesdell and Adler also mentioned that secondary flow stabilizes laminar flow since transition Reynolds numbers of 6000 to 8000 were reported. In this study the helically coiled tube was treated as a torus for simplicity. The effect of the tube-to-coil diameter ratio on flow rate was studied. Truesdell and Adler also considered elliptic tubes. It was found that in elliptical tubes with their major axis perpendicular to helix radius, the secondary flow intensity is less.

Dravid *et al.* (1971) conducted analytical, numerical and experimental studies on the effect of secondary fluid motion on laminar flow heat transfer in helically coiled tubes. For the experiments, a copper tube of 7.37 mm ID was wound into a helical coil of 137 mm mean diameter. The axial temperature or heat flux profiles showed large amplitude oscillations which decayed and damped out in the fully developed region. The secondary flow was opined to be the cause of this phenomenon. From the point of view of design, Dravid *et al.* suggested that it is good practice to use a correlation based on the asymptotic heat transfer coefficient for any length of the coiled tube. Since the region of very high heat transfer coefficients is very short, such a design would be only slightly conservative. Based on this argument, equation 2.53 was suggested for $50 < De < 2000$ and $5 < Pr < 175$.

$$Nu = [0.76 + 0.65De^{0.5}]Pr^{0.175} \quad 2.53$$

It was also concluded that near the tube inlet, a coiled tube offers little advantage over a straight tube.

Akiyama and Cheng (1971) used the boundary vorticity method in their numerical study of laminar forced convective heat transfer in curved pipes. The emphasis was put on the local angular distribution of friction factor. The value of the local Nusselt number was much higher on the outer wall than the inner wall and this trend was intensified as the Dean number increased. For the average Nusselt number a correlation in form of an inverse polynomial with respect to $(De^2Pr)^{0.25}$ was presented. For $(De^2Pr)^{0.25} > 20$ the correlation can be represented by equation 2.54 below.

$$Nu = 0.8De^{0.5}Pr^{0.25} \quad 2.54$$

Patankar *et al.* (1974) employed finite difference numerical schemes to predict laminar flow and heat transfer in helically coiled pipes. Their work also considered the issue of developing entry flow, both hydrodynamic and thermal. Only large curvature ratios ($R/a \geq 15$) were considered. Velocity profiles obtained by the numerical solution were in good agreement with those by Mori and Nakayama (1965) for fully developed flow. Curves of developing axial velocity were presented and compared with those of others. The prediction of fully developed temperature profiles, for the condition of axially uniform heat flux, showed significant difference to those by Mori and Nakayama (1965) in the outside half of the tube cross section. Patankar *et al.* suggested that the temperature profiles of Mori and Nakayama (1965) might be in error. As for the thermal entrance region they discovered that the wall temperature exhibits cyclic oscillations which are damped out as the flow becomes fully developed.

Janssen and Hoogendoorn (1978) conducted experiments on helically coiled tubes in order to study laminar convective heat transfer. One coil made of 5 mm diameter stainless steel tube having a coil diameter of 500 mm, and three coils made of 11 mm diameter tube with coil diameters of 12, 42 and 620 mm constituted the test coils. The wall of the tubes were used as an electrical resistance to maintain a uniform wall heat flux and the mean fluid temperature profile was assumed linear. Although experiments were carried out for both boundary conditions of uniform wall temperature and heat flux, the type of the boundary condition was found to have minimal effect on the results. Equations 2.55, 2.56 and 2.57 were presented for different ranges of the Dean number.

$$Nu = 1.7De^{0.33}Pr^{0.17} \quad De < 20 \quad 2.55$$

$$Nu = 0.9Re^{0.33}Pr^{0.17} \quad 20 < De < 100 \quad 2.56$$

$$Nu = 0.7Re^{0.43}Pr^{0.17}(d/D)^{0.07} \quad 100 < De < 830 \quad 2.57$$

It was found that only for $De < 20$ can the Nusselt number be correlated with the Dean number. For $De > 20$, the Reynolds number was the dimensionless parameter of

preference. Also the tube to coil diameter ratio showed only very small effect on Nu for $De > 100$ and negligible effect for $De < 100$.

Mishra and Gupta (1979) conducted an experimental study of momentum transfer in curved pipes. Flexible tubes of 6.2, 7.8, 11.65, 17.35 and 19.05 mm ID were used to make coils of various diameters and pitches. The following observations were made. The friction factor decreased with an increase in coil pitch. The friction factor for turbulent flow through the largest coil diameter fell very near to the Blasius equation for straight pipes while a considerable increase in resistance with the decrease in coil diameter was observed. The coil-to-straight tube friction factor ratio for laminar flow is a function of the Dean number only. Also the pitch was found to have negligible effect on pressure drop if the pitch is less than the diameter of the coil. In turbulent flow, the action of centrifugal force is dampened by the dominating inertia force where excessive mixing of fluid particles reduces the effect of the secondary flow. Equations 2.58 and 2.59 were presented for the friction factor of coiled tubes in laminar and turbulent flows, respectively.

$$f_c = \frac{64}{Re} [1 + 0.033(\log_{10} De)^4] \quad 1 < De < 3000 \quad 2.58$$

$$f_c = 0.316 Re^{-0.25} + 0.03 \left(\frac{d}{D} \right)^{0.5} \quad 4500 < Re < 10^5 \quad 2.59$$

Manlapaz and Churchill (1980) re-correlated the available data on friction factor associated with fully developed isothermal flow of Newtonian fluids in helically coiled pipes. For transition, Manlapaz and Churchill recommended the simple equation 2.60 which is quoted from White.

$$f_{transition} = 0.036 \quad 2.60$$

Equation 2.61 was found to best describe the available data for a wide range of the Dean number.

$$\frac{f}{f_s} = \left\{ \left[1 - \frac{0.18}{[1 + (35/De)^2]^{0.5}} \right]^m + \left(1 + \frac{d}{3D_c} \right)^2 \frac{De}{88.33} \right\}^{0.5} \quad 2.61$$

In equation 2.61 $m=2$ for $De < 20$, $m=1$ for $20 < De < 40$ and $m=0$ for $De > 40$. In order to include the effect of coil pitch, Manlapaz and Churchill recommended replacing the Dean number with the helical number. They also conducted numerical study of their own and reported agreement with available data.

Manlapaz and Churchill (1981) also worked on fully developed laminar forced convection in a helical coil. By reviewing and employing previously published work of other authors, Manlapaz and Churchill developed new correlations. For the case of axially uniform heat flux with peripherally uniform wall temperature which is known as H1 boundary condition, equation 2.62 was proposed.

$$Nu = \left[\left(\frac{48}{11} + \frac{51/11}{\left(1 + \frac{1342}{PrHe^2} \right)} \right)^3 + 1.816 \left(\frac{He}{1 + \frac{1.15}{Pr}} \right)^{3/2} \right]^{1/3} \quad 2.62$$

Equation 2.62 should not be used for $He > 2000$. Manlapaz and Churchill indicated that the helical coil number had been used to cover the data from large pitch coils even though for intermediate pitches the Dean number would produce acceptable results. They noted that the prediction for a Prandtl number of 0.7 by equation 2.62 was high and that for $Pr=0.1$ somewhat low for intermediate values of the Dean number. Manlapaz and Churchill observed three different regimes. For low values of De the creeping secondary motion produced an increased Nusselt number over that of a straight tube which was proportional to $De^4 Pr^2$. For large values of De the Nusselt number was proportional to $(DePr)^{1/2}$ for $Pr \rightarrow 0$ and to $De^{1/2}$ for $Pr \rightarrow \infty$. Between the two mentioned regimes a quasi-constant state for the Nusselt number was observed.

Gnielinski (1986) reviewed many empirical correlations for the pressure drop in helically coiled tubes published prior to 1986. Based on the comparison of those

correlations and data, Gnielinski reached the conclusion that for the laminar regime, the correlation by Mishra and Gupta (1979), equation 2.58, is preferred over the others. The reason was that equation 2.58 predicts the data well and at the same time is less complicated than the others. For turbulent flow, equation 2.59 by Mishra and Gupta (1979) was suggested as the most suitable. When the fluid is heated, Gnielinski suggested that equations 2.58 and 2.59 be multiplied by a correction factor defined in equation 2.63.

$$K = \left(\frac{\mu_w}{\mu_b} \right)^{0.27} \quad 2.63$$

In equation 2.63, μ_w and μ_b refer to the fluid dynamic viscosity measured at tube wall temperature and bulk mean temperature of the fluid, respectively.

Topakoglu and Ebadian (1987) presented an analytical study of viscous laminar flow in a curved pipe of elliptical cross section. The geometry of the problem is somewhat different from the practical case. In their study the smaller axis of the ellipse was considered parallel to the coil axis. However, in practice the situation is reversed and therefore direct application of the results to the current case is not straightforward. The result of the study showed that for a fixed value of the Reynolds number and at fixed curvature, the rate of flow reduction decreases as well. This is because a smaller flatness ratio means a smaller secondary flow, which also means a smaller rate of flow reduction. The rate of flow reduction is defined as the change of flow rate in a curved pipe of elliptic cross section, relative to that of a straight pipe having the same cross section and the same pressure gradient.

A theoretical and experimental study on laminar heat transfer in a helically coiled tube was carried out by Futagami and Aoyama (1988). Equation 2.64 together with equations 2.65 and 2.66 were proposed to represent the data.

$$\frac{Nu}{Nu_0} = 1 + \left[\left(\frac{Nu_c}{Nu_0} - 1 \right)^4 + \left(\frac{Nu_b}{Nu_0} - 1 \right)^4 \right]^{1/4} \quad 2.64$$

$$\left(\frac{Nu_c}{Nu_o}\right)^6 = 1 + [0.195(DePr^{0.54} \cos\alpha)^{0.5}]^6 \quad 2.65$$

$$\left(\frac{Nu_b}{Nu_o}\right)^{4.5} = 1 + [0.19(ReRaPr \cos\alpha)^{0.2}]^{4.5} \quad 2.66$$

In equations 2.64, 2.65 and 2.66, subscripts *b* and *c* correspond respectively to the case where the buoyancy or centrifugal force acts alone, while Nu_o is that of a straight tube. α is the inclination angle of the tube axis. Equation 2.67 was suggested as the criteria for determining the boundary between the centrifugal-force domination and the region where both centrifugal and buoyant forces are important.

$$De \cdot \cos\alpha \cdot Pr^{0.58} = 1.055(Re \cdot Ra \cdot Pr)^{0.421} \quad 2.67$$

In terms of the coil pitch and for the case of constant wall heat flux, equation 2.67 can be rewritten in the form of equation 2.68.

$$Nu_i = 4.36 \left\{ 1 + \left[0.195 \left(DePr^{0.54} \sqrt{\frac{1}{1 + (p_c/\pi D_{c,m})^2}} \right)^{0.5} \right]^6 \right\}^{1/6} \quad 2.68$$

Futagami and Aoyama also performed experiments on heat transfer inside a helical coil having only one turn. The coil was made of 9.9 mm ID copper tube with a perfectly circular cross section. Coil diameter was 1 m and the inclination angle was 0.12 rad which corresponds to a coil pitch of 41.4 tube diameters. The experimental results agreed with the numerical predictions within 30%.

Ali's (1989) experimental study of the pressure drop performance of coiled tubes confirmed the correlations presented by Srinivasan *et al.* (1970) for helical coils. Helical coil tests were performed on a coil made of 6.2 mm ID tube with a coil mean diameter of 30.64 cm. The coil had a pitch of 50 mm.

Experimental observations of flow instability in a helical coil were reported by Webster and Humphrey (1993). The helical coil under test consisted of a 38.1 mm ID tube coiled to a diameter of 693 mm, measured from the center of the tube. The coil had 5.25 turns with a helix angle of 3.4 degree. A Laser-Doppler Velocimeter (LDV) was used to measure the components of flow velocity at 3 different location along tube radius. Webster and Humphrey observed the first appearance of unsteadiness at $Re=5060$ and marked the flow regime as fully turbulent beyond $Re=7590$. This was concluded based on a significant increase in rms value of flow velocity between $Re=6330$ and $Re=7590$. Earlier, through pressure drop and friction factor measurements, the characteristic of fully turbulent flow was estimated as $Re=8000$.

A numerical study of laminar forced convection in a helical coil was reported by Yang *et al.* (1995). The authors claimed that in most of the previous studies of this subject, the attention had not been focused on the effects of the coil pitch, and in fact toroidal pipes had been the subject of study rather than helicoidal pipe. In their study, Yang, Dong and Ebadian, assumed that the flow was fully developed, fluid properties are constant and the effects of free convection was negligible. As for the friction coefficient, it was found that the coil pitch has almost no effect. The distribution of the local Nusselt number along the circumference of the coil was displayed in detail. The average Nusselt number increased as the Dean number increased. For a constant De , an increase in the coil pitch was found to slightly decrease the Nusselt number. The rate of decline in Nu with the increase in pitch was shown to be much higher for $Pr \geq 5$.

2.12. Scale analysis

George and Capp (1979) introduced a scaling analysis for natural convection turbulent boundary layer next to heated vertical surfaces. Two main regions were considered to exist in the flow near a vertical wall. They were called the inner and outer layers. The inner layer was also divided into a conductive and a thermo-viscous sublayer and the buffer region between them. A buoyant sublayer was also assumed to exist at the outer part of the inner sublayer. The need for different length scales for momentum and temperature equations lead to definition of a new length scale η for the near-wall region.

This was done to retain the viscosity and conduction terms in the process of simplifying the equations. As a result, the two inner layers can be classified as first a viscous and conduction dominant sublayer and then a sublayer where only conduction is dominant. It was shown that in the inner layer the total heat flux across the layer is independent of distance from the wall. The buoyant sublayer was defined as a region far enough from the wall so that the viscous and conduction effects are negligible and yet close enough to the wall that the mean convection effects are not important. In this layer the local Nusselt number was found to be expressed by equations 2.69 and 2.70.

$$Nu_x = f_1(Pr)(Ra_{q,x}Pr)^{1/4} \quad 2.69$$

$$Nu_x = f_2(Pr)(Ra_xPr)^{1/3} \quad 2.70$$

With regards to the boundary condition at the wall, it was stated that the distance required for the flow to become fully turbulent is longer for constant heat flux wall than the constant temperature wall.

CHAPTER 3

THEORETICAL BACKGROUND

The main objective of this thesis is to study the shell-side heat transfer and fluid flow. However, this goal would not be realized without consideration of the heat transfer and fluid dynamics inside the coils. Since, physical modeling was adopted as the method of analysis of the subject, only a brief review of the important parameters will be presented in this chapter.

3.1. Tube-side fluid flow and heat transfer

Knowledge of the tube-side fluid dynamics is used to determine the glycol-loop pressure drop and flow rate. These two parameters are the main factors in selection of a collector-loop pump for SDHW systems. They also affect the electrical power requirement of the pump. Therefore the effects of tube inside diameter, tube length, coil diameter, coil pitch and glycol temperature on the tube-side friction coefficient must be known. The heat transfer coefficient on the inside is also of great importance. It is a contributing factor to the overall heat transfer coefficient of the heat exchanger.

3.1.1. Geometry of a helical coil

Although in some literature (Shah and Joshi (1987)) it was referred to as a horizontal coil (since the tubes in each turn are approximately horizontal), the coil in figure 3.1 will be called a vertical helical coil throughout this thesis. This was found more appropriate since the axis of the helix is vertical. The coil pitch is the distance between two consecutive coil turns measured from the centerlines. The radius of curvature of a toroid, R , is defined as the mean coil radius. However, in case of a helical coil, the effective radius of curvature, R_c , is influenced by the coil pitch p (equation 3.1).

$$R_c = R \left[1 + \left(\frac{p}{2\pi R} \right)^2 \right]$$

3.1

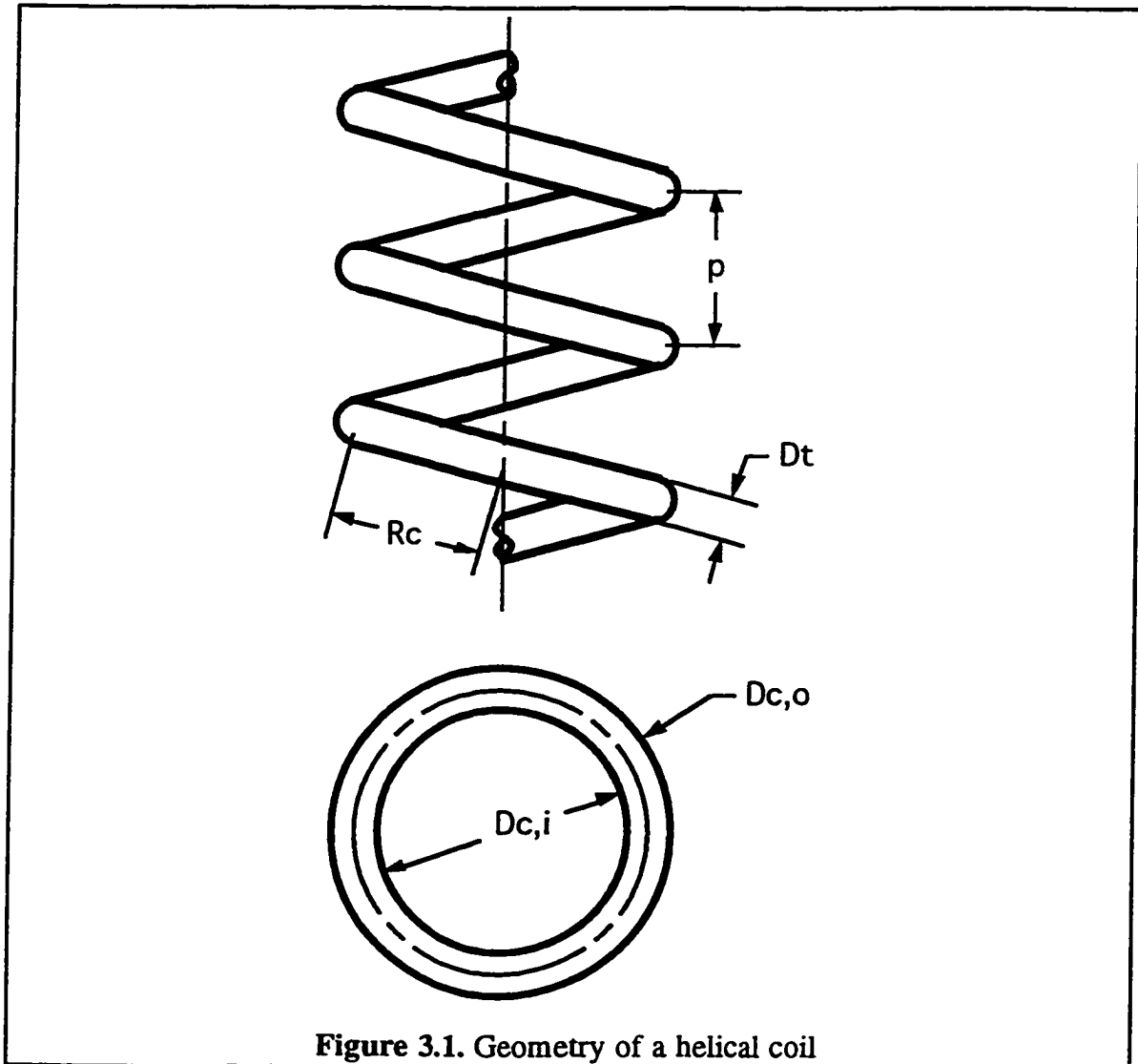


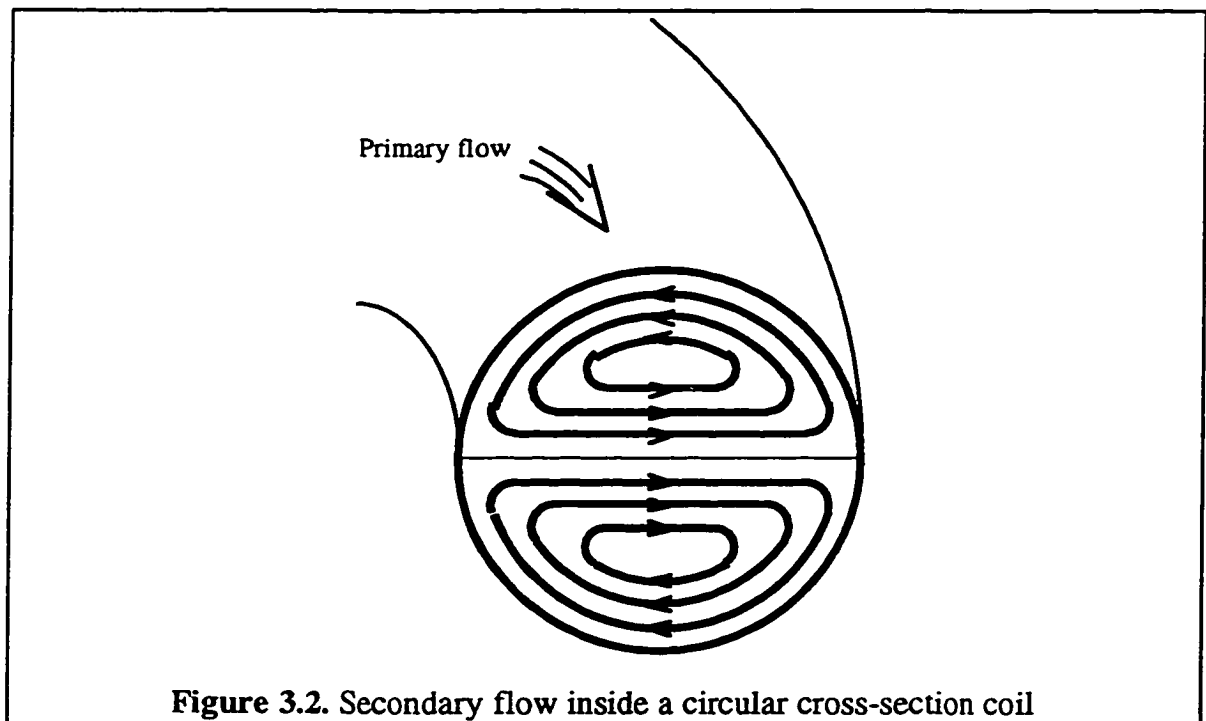
Figure 3.1. Geometry of a helical coil

3.1.2. Flow inside a vertical helical coil

In a helical coil, a centrifugal force is experienced by the fluid as a result of the circular motion due to the coil turns. This centrifugal force imposes a secondary flow

perpendicular to the tube axis. Figure 3.2 shows a sketch of the secondary fluid motion. The buoyancy effects are neglected.

One effect of the secondary flow is the alteration of the velocity profile both in horizontal and vertical planes. In the horizontal plane the peak of the velocity moves towards the tube outer wall (Mori and Nakayama (1965)) Also the secondary flow significantly influences the friction coefficient of the flow. Therefore, the friction factors for straight tubes can not be used for helical coils. The coil pitch is commonly believed to have no effect on friction coefficient (Mishra and Gupta (1979) and Manlapaz and Churchill (1980)).



Many correlations have been proposed for the friction coefficient of a coiled tube in the literature and are summarized in chapter 2. First, a review of the important parameters is necessary. The governing parameter for most fluid flow problems is of course the Reynolds number. The Dean number, which can be treated as the Reynolds number for curved tubes, is the most influential dimensionless parameter. It is defined in equation 3.2.

$$De = Re_i \left(\frac{d}{D_c} \right)^{1/2} \quad 3.2$$

Reynolds number will be calculated from equation 3.3 knowing glycol mass flow rate and considering the fact that the cross section of the tubes will usually be distorted to an elliptical shape from its original circular form. The distortion happens during the process of winding the coils. As a result the hydraulic diameter of tube must be used in equation 3.3.

$$Re_i = \frac{d_h u_i}{\nu_g} \quad 3.3$$

In order to include the effect of the coil pitch, Manlapaz and Churchill (1980) suggested using the coil radius of curvature. By applying equation 3.1 to the definition of the Dean number, the helical coil number will be defined as in equation 3.4.

$$He = De \left[1 + \left(\frac{p}{2\pi R} \right)^2 \right]^{-1/2} \quad 3.4$$

Alternative forms of the dimensionless number similar to that of the Dean number have also been used by some authors (Srinivasan *et al.* (1970)) for the turbulent regime. Also in some cases it has been preferred to treat Re and d/D_c as two separate dimensionless numbers (Rogers and Mayhew (1964)).

The friction factor correlation of choice in this thesis is the one proposed by Srinivasan *et al.* (1970) as in equations 2.50 to 2.52. This set of equations was recommended by Shah and Joshi (1987) who performed an extensive review of the available literature prior to 1987. Shah and Joshi rewrote the laminar and transitional parts of the equations in the matrix format of equation-3.5.

$$f_c = \frac{64}{Re} \begin{cases} 1 & \text{for } De < 30 \\ 0.419De^{0.275} & \text{for } 30 < De < 300 \\ 0.1125De^{0.5} & \text{for } De > 300 \end{cases} \quad 3.5$$

Equation 3.5 offers the advantage of simplicity and at the same time is as accurate as the more complicated equation by Manlapaz and Churchill (1980).

In a helical coil, transition to turbulence occurs rather gradually. For the criteria of turbulence, equation 3.6 will be used.

$$Re_{crit} = 2100 \left[1 + 12 \left(\frac{d}{D_c} \right)^{0.5} \right] \quad 3.6$$

Equation 3.6 is taken from Srinivasan *et al.* (1970) and it covers the limiting case of a straight tube which leads to a Re_{crit} value of 2100 as the coil radius of curvature approaches infinity.

3.1.3. Heat transfer inside a helical coil

The heat transfer coefficient, h , is the most important parameter in any convection problem. Its definition originates from Newton's law of cooling. It is also known that the heat transfer coefficient, unlike thermal conductivity, is not a material property and it depends on fluid condition and geometry when passing over a surface. The Nusselt number is the dimensionless form of the heat transfer coefficient. The tube-side heat transfer coefficient will be used to find the value of the shell-side heat transfer coefficient in an alternative way which will be described later in this chapter. Since the study of the tube-side heat transfer is not included in this thesis, the use of available Nusselt number correlations was considered sufficient. However, finding the most preferred correlation is not quite trivial. As can be seen in table 3.1, significant disagreement exists among theoretical and experimental correlations.

Table 3. 1. Tube-side Nusselt number

Author(s)	Nu
Mori and Nakayama (1965) I (Theoretical)	31.3
Mori and Nakayama (1965) II (Theoretical)	37.9
Dravid <i>et al.</i> (1971) (Experimental)	15.7
Janssen and Hoogendoorn (eq. 2.57) (1978) (Experimental)	14.4
Manlapaz and Churchill (1981) (Experimental)	16.8
Futagami and Aoyama (1988) (Theoretical)	24.8
Yang <i>et al.</i> (1995) (Theoretical, Extrapolated)	20.7

Table 3. 2. Conditions for table 3.1

De	Re	Pr	d	D_c
180	505	18	6.35 mm	50 mm

Table 3.2 shows the condition at which the Nusselt number was calculated. Among the correlations in table 3.1, the theoretical ones yield noticeably higher values. Even among these the agreement is not satisfactory. In contrast, the empirical correlations agree with each other to a reasonable degree. The empirical correlation of Manlapaz and Churchill (1981) has been accepted more widely in the literature and will be adopted as the preferred Nusselt number correlation henceforth. Equation 2.62 is often reported in form of the two equations 3.7 and 3.8 (The Prandtl number is evaluated at the average glycol temperature).

$$Nu_i = \left[\left(4.364 + \frac{4.636}{x_3} \right)^3 + 1.816 \left(\frac{De}{x_4} \right)^{1.5} \right]^{0.333} \quad 3.7$$

where x_3 and x_4 are defined as,

$$x_3 = \left(1 + \frac{1342}{De^2 Pr} \right)^2, \quad x_4 = 1 + \frac{1.15}{Pr} \quad 3.8$$

In their comparative study of data from different literature with equation 3.7, Shah and Joshi (1987) detected a fairly good agreement. Once Nu_i was calculated from equation 3.7, the tube-side heat transfer coefficient can be calculated from equation 3.9.

$$h_i = \frac{Nu_i k_g}{d_h} \quad 3.9$$

3.2. Shell-side fluid flow and heat transfer

This section will review the equations and definitions for analyzing the results of the experiments on the shell-side fluid flow and heat transfer in a natural convection shell-and-coil heat exchanger.

3.2.1. Shell-side fluid flow

The flow of fluid inside a cylindrical shell in the presence of one or more helical coils has attracted little attention. However, the flow can be considered similar to that over an aligned bank of tubes. The pressure drop over a bundle can be expressed in dimensionless form by

$$Eu = f(Re, P_{trans.}, P_{long.}) \quad 3.10$$

Where $P_{trans.}$ and $P_{long.}$ are transverse and longitudinal dimensionless pitches respectively (Zukauskas (1987)). The Euler number is defined on a per tube row basis as

$$Eu = \frac{2\Delta P}{\rho u_0^2 n} \quad 3.11$$

In equation 3.11 n is the row number and u_0 is the mean velocity in the minimum inter-tube spacing. Figure 3.3 is a chart of the hydraulic drag coefficient of in-line tube bundles for $n > 9$. Eu values determined from figure 3.3 have an uncertainty within $\pm 10\%$ (Zukauskas (1987)).

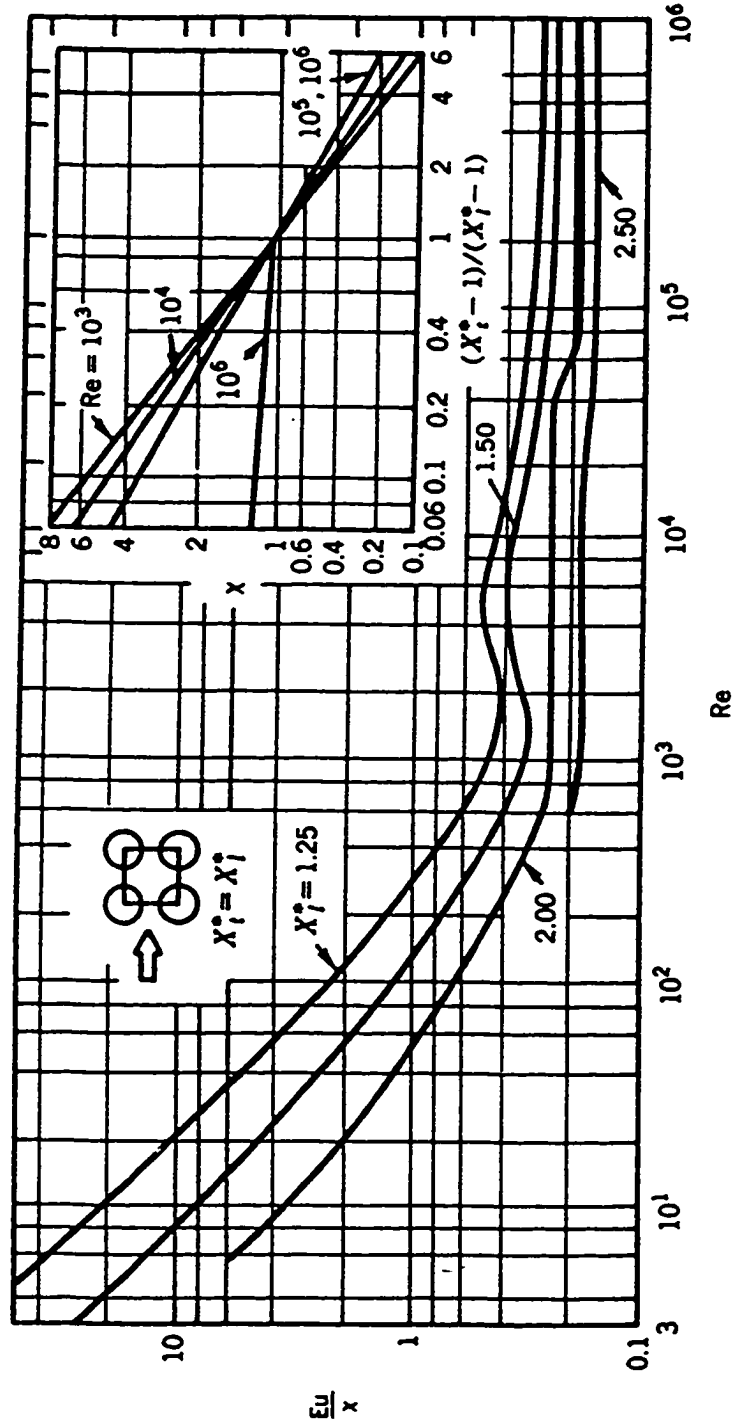


Figure 3.3. Hydraulic drag coefficients for in-line tube bundles (Zukauskas 1987)

Figure 3.3 can be used to estimate the pressure drop over multiple helical coils in a cylindrical shell. The effect of liquid heating can be accounted for by multiplying the value of Eu from the chart, by $(\mu_s/\mu)^p$. μ_s is the dynamic viscosity of the fluid at tube surface temperature and the exponent p is given by equation 3.12 for liquid heating,

$$p = -0.0018Re + 0.28 \quad Re \leq 10^3 \quad 3.12$$

for $Re > 10^3$, $p=0$.

3.2.2. Shell-side heat transfer

Dimensional analysis and scaling analysis are methods that are often used to provide a platform on which further theoretical or experimental studies can be performed. In order to perform a dimensional analysis, a general knowledge of the parameters involved in that particular physical phenomenon is sufficient. Additional information regarding the relationship between some of the parameters will lead the dimensional analysis process towards a more useful path.

However, scale analysis asks for more detailed information about the phenomenon. Often assumptions must be made and hypotheses must be drawn that require a good understanding of the problem. In return, scale analysis will provide more insight compared to dimensional analysis.

3.2.2.1. Dimensional analysis

Dimensionless groups or numbers are widely used in different branches of science, including heat transfer, because of various advantages they offer. The main advantage comes from the requirement that all mathematical equations which describe certain physical phenomena must be dimensionally homogeneous. It means that the equation must be true regardless of the system of units being used. Another benefit is in the lesser number of graphs required to convey the concept of a physical phenomenon. Multiple functional relationships can also be deduced from a single dimensionless correlation.

Ajele (1995) presented a dimensional analysis procedure for the shell-side of the heat exchanger. The same procedure can easily be applied to the current case. Equation 3.13 is the simplified result of Ajele's procedure.

$$Nu_{Dt} = f(Ra_{Dt}, Pr, F, S, P, n) \quad 3.13$$

Among parameters in equation 3.13, Prandtl number, Pr , dimensionless pitch, P , and the number of coil turns, n , are already familiar. In deriving equation 3.13, the geometry was treated as a single coil inside a cylindrical enclosure. Although Nu and Ra in this equation are based on tube diameter, equation 3.13 can be generalized by using a characteristic length instead of tube diameter.

The Nusselt number and Rayleigh number are also well known dimensionless parameters. Flow number, F , and dimensionless flow space, S , however must be defined here. The flow number was first introduced by Richmond and Hollands (1989) and defined as the amount of energy available in the hot stream relative to the ability of the cold stream to absorb it (equation 3.14). This definition is true when the drop in the glycol temperature across the heat exchanger is of the same order of magnitude as the temperature drop in water at a radial distance of roughly one tube radius from the tube wall.

$$F = \frac{\dot{m}_g c_{p,g} D_{t,o}}{2k_w A} \quad 3.14$$

The dimensionless spacing, S , is defined by Ajele (1995) as in equation 3.15 in order to facilitate the study of coil diameter effects.

$$S = \frac{D_s - D_c}{D_c} \quad 3.15$$

The value of S is an indication of the relative diameter of the shell compared to the coil enclosed by it. Equation 3.15 can only be useful where there is only a single coil inside the shell. Multiple coil cases require different parameters to include the geometry of all the coils. The equivalent diameter, D_{eq} , as in the case of concentric annuli, can be used as a measure of the combined diameter of all coils. The outcome of D_{eq} as defined in

equation 3.16 is to combine all the coils together and produce an imaginary solid ring with its cross sectional area equal to the sum of the cross sectional area of all the coils.

$$D_{eq} = \left(\sum_{j=1}^N (D_{c,o}^2 - D_{c,i}^2)_j \right)^{1/2} \quad 3.16$$

The definition of equivalent diameter facilitates the definition of a modified S for the case of multiple coils. This improved parameter is called dimensionless flow space and is defined as in equation 3.17.

$$S' = \frac{D_s - D_{eq}}{D_{eq}} \quad 3.17$$

Although the definition of S' is not a direct result of dimensional analysis, this parameter has proved helpful in the study of shell-and-coil heat exchangers (Ajele 1995). In this thesis, the dimensionless flow space, S' , will be used for all situations of single and multiple coils.

It will be shown later that the dimensional analysis does not reveal all the necessary tools for analyzing the results of the experiments and other parameters must be defined. The necessity of these new parameters indicates the absence of a complete theory in describing the physical phenomenon.

3.2.2.2. Additional parameters

Dimensional analysis suggests the tube diameter as the characteristic length in Nusselt and Rayleigh numbers. However it is obvious that the complex geometry of multiple helical coils of different pitch and diameter inside cylindrical shells of varying height and diameter can not be characterized by the parameter $D_{t,o}$. A more appropriate parameter is needed. The heat exchanger hydraulic diameter, D_{hx} , is such a parameter. The definition of D_{hx} as in equation 3.18 was proposed by Kays and London (1984) and employed by others (Tillman 1976, Ajele 1995).

$$D_{hx} = \frac{4A_{c,f}H}{A_p} \quad 3.18$$

$A_{c,f}$ is the cross sectional flow area of the heat exchanger and A_p is wetted surface area on the shell side somewhat analogous to the wetted perimeter of a non-circular tube. A_p is the sum of the total outside surface area of the coils and the inner surface area of the shell.

More dimensionless heat transfer parameters, based on D_{hx} , can be introduced. The Nusselt and Rayleigh numbers are defined in equations 3.19 and 3.20 respectively.

$$Nu_{D_{hx}} = \frac{h_o(D_{hx})}{k_w} \quad 3.19$$

$$Ra_{D_{hx}} = \frac{g\beta(T_{m,w} - T_\infty)(D_{hx})^3}{\nu\alpha} \quad 3.20$$

In equation 3.20 the temperature difference term is defined in a different way. For natural convection problems near a wall, usually the ΔT term is defined as the temperature difference between the bulk of the fluid and the adjacent wall. The ΔT -term must represent the driving potential of the flow in any case. It is acceptable that the driving force for the current problem is the mean temperature excess of water inside the heat exchanger ($T_{m,w}$) compared to the water temperature at the inlet to the heat exchanger (T_∞). Therefore this temperature difference is used for the ΔT -term in equation 3.20 above.

In constant heat flux problems an alternative definition of the Rayleigh number is used. In these problems, since the heat flux is given, the Rayleigh number is based on the heat flux. A new definition of the Rayleigh number is given in equation 3.21 based on the above facts.

$$Ra_{q,Dhx} = \frac{g\beta q''(D_{hx})^4}{k\nu\alpha} \quad 3.21$$

This definition will be seen to be of great significance in presentation of data in this thesis. In equation 3.21 the physical properties are evaluated at the mean water temperature in the heat exchanger.

Another important parameter is the modified Rayleigh number proposed by Ajele (1995) as in equation 3.22.

$$Ra_{Dhx}^* = Ra_{Dhx} \frac{H}{L} \quad 3.22$$

This parameter is defined taking into account the effect of coil surface area in relation with the shell inner surface area.

The heat transfer rate is calculated from equation 3.23 using either of water or glycol information.

$$q = (\dot{m}c_p)_g \Delta T_g = (\dot{m}c_p)_w \Delta T_w \quad 3.23$$

The heat transfer rate calculated in equation 3.23 will be used to calculate the shell-side heat transfer coefficient and the overall heat conductance of the heat exchanger by equations 3.24 and 3.25 respectively ($T_{m,s}$ is the mean coil surface temperature).

$$h_o = \frac{q}{A(T_{m,s} - T_{m,w})} \quad 3.24$$

$$UA = \frac{q}{LMTD} \quad 3.25$$

The overall heat conductance, or the UA product of the heat exchanger, is an indication of the amount of heat rate that the heat exchanger can handle. Its definition rises

from any situation that involves a solid wall separating two streams of fluid at different temperatures. It is defined as in equation 3.26.

$$\frac{1}{UA} = \frac{1}{h_i A_i} + \frac{\ln(D_{t,o}/d)}{2\pi k_t L} + \frac{1}{h_o A_o} \quad 3.26$$

The second term on the right hand side of equation 3.26 is the thermal resistance of the tube wall, which can be neglected in case of high thermally conductive material and/or thin-walled tubes. Also in the case of thin-walled tubes, often the difference between the inner and outer surface area of the tube will be small and the equation 3.26 becomes simplified.

Equation 3.26 provides an alternative way in calculating h_o once h_i and the UA product are calculated from equations 3.9 and 3.25 respectively. Values of the shell-side heat transfer coefficient calculated from this method, can be compared to those calculated directly from equation 3.24.

The logarithmic mean temperature difference (LMTD) must be used in parallel flow heat exchangers since the temperature difference between the two fluids changes from inlet to outlet of the heat exchanger. It has also proved useful for counter-flow and cross-flow situations. For a pure counter-flow heat exchanger, $LMTD$ is defined in equation 3.27. Subscripts h and c refer to hot and cold flows respectively.

$$LMTD = \frac{(T_{h,i} - T_{c,o}) - (T_{h,o} - T_{c,i})}{\ln\left(\frac{T_{h,i} - T_{c,o}}{T_{h,o} - T_{c,i}}\right)} \quad 3.27$$

However it is recommended (Kays and London (1984)) to use correction factors for cases other than pure parallel and counter flow. Typical $LMTD$ correction factors can be found in Fraas (1989). A shell-and-coil heat exchanger utilizes a combination of counter and cross flow and none of the typical correction factors are applicable to it.

The effectiveness of any heat exchanger, ε is defined as the ratio of the actual heat rate to the maximum possible heat transfer rate in the heat exchanger. In terms of temperatures and flow rates it takes the form of equation 3.28.

$$\varepsilon = \frac{(\dot{m}c_p)_h(T_{h,i} - T_{h,o})}{(\dot{m}c_p)_{\min}(T_{h,i} - T_{c,i})} \quad 3.28$$

In equation 3.28 subscript 'min' indicates that the value can be taken from either cold or hot fluid whichever has the minimum value. A modified definition of effectiveness more suitable for natural convection heat exchangers was defined by Fraser *et al.* (1995) as in equation 3.29.

$$\varepsilon' = \frac{T_{h,i} - T_{h,o}}{T_{h,i} - T_{c,i}} \quad 3.29$$

The modified effectiveness is a sign of the success of the heat exchanger to lower the temperature of the hot fluid to the minimum temperature possible ($T_{c,i}$).

3.2.2.3. Scale analysis

Compared to a dimensional analysis, a scale analysis can reveal more information. If it is backed with good hypotheses, scale analysis can suggest the trend of change of parameters. However it is often difficult to develop a basic theory for a problem and the degree of difficulty increases with increased geometrical complexity and flow complexities such as turbulence. This makes the lack of a basic theory for turbulent natural convection flow over multiple helical coils excusable. In these situations reference to less complex but related problems is elucidating.

Turbulent natural convection next to a heated vertical wall has received attention in a scale analysis point of view (George and Capp 1979). The flow is divided into inner and outer regions. The inner region was divided into two subregions. A thin conductive and thermo-viscous sublayer adjacent to the wall and a relatively thicker buoyant sublayer on

the outside of the first layer. A heat transfer correlation in the form of equation 3.30 was yielded.

$$Nu_z = C(Pr) \cdot H_z^{*0.25} \quad 3.30$$

In equation 3.30 z is the vertical distance from the bottom of the wall, C is a function of the Prandtl number and H_z^* is a new dimensionless parameter defined in equation 3.31.

$$H_z^* = Ra_{q,z} Pr \quad 3.31$$

3.3. Physical property evaluation

In order to carry on the necessary calculation of the thermal parameters, evaluation of certain physical properties of the glycol and water flow was required. The properties of interest included the dynamic viscosity, specific heat, mass density, Prandtl number and the thermal conductivity for both water and glycol and also the coefficient of thermal expansion for water. The other physical properties can be calculated once the main properties are at hand. Tabular values of the desired property in each case were extracted from the sources and plotted as a function of the temperature. In order to computerize the process of property evaluation, the best fits to the plots were fed to the computer in forms of polynomials of at least third degree. Special attention was paid so that the error of the property evaluation was minimal. The plots and the associated polynomial equation of each property is presented in detail in appendix A.

3.4. Experimental uncertainty analysis

As with the report of every experimental research, the analysis of the experimental uncertainties in calculating the results must be given proper attention. The method proposed by Kline and McClintock (1953) seems to be widely accepted among the authors of technical papers. The uncertainty in calculating the major heat transfer and hydraulic

parameters were evaluated based on the mentioned method. The results are reported in table 3.3.

Table 3.3. Experimental uncertainties of important parameters

Parameter	Uncertainty	Parameter	Uncertainty
De	1%	Ra_{Dhx}	2%
ε	1%	Ra'_{Dhx}	2%
ε'	1%	Ra_{Dx}	2%
h_i	5%	Ra_H	2%
h_o	3%	Ra_L	2%
$LMTD$	2%	$Ra_{q,Dhx}$	3%
\dot{m}_g	1%	$Ra_{q,L}$	3%
\dot{m}_w	2%	Re_{Dhx}	2%
NTU	5%	Re_{Dx}	2%
Nu_{Dhx}	3%	Re_i	1%
Nu_{Dx}	3%	Ri	2%
Nu_H	3%	St	2%
Nu_L	3%	UA	5%
q	2%		

3.5. Summary

The geometry of a helical coil and important parameters involved in natural convection heat transfer from multiple helical coils in cylindrical shells were reviewed. For the tube-side heat transfer coefficient, available Nusselt number and friction factor correlations will be used. Results of the dimensional analysis was reproduced and additional parameters were defined. In a heat exchanger it is desirable to keep the logarithmic mean temperature difference as low as possible to make the heat exchanger thermodynamically more efficient. Also larger UA values are desirable since it leads to lower $LMTD$ values for a fixed heat rate. The total volume of the heat exchanger should be kept minimal for a fixed heat rate to lessen the initial costs.

CHAPTER 4

EXPERIMENTAL SETUP AND PROCEDURE

4.1 Experimental apparatus

The experimental apparatus consisted of the following: the glycol reservoir, glycol pump, heater, piping, heat exchanger, flow meters, thermocouples, pressure gauges, water storage tank and the data acquisition device. Each of the parts will be described in the sections that follow.

4.1.1. Glycol reservoir

A 22.7 liter plastic cylindrical container was used as the glycol reservoir filled with at least 15 liters of an aqueous solution of 40% propylene glycol. The glycol was pumped from the reservoir, circulated through the heater, the heat exchanger and other parts of the loop and back to the reservoir.

4.1.2. Glycol pump

A small pump was used to circulate the glycol solution. The pump is a positive displacement sliding-vane type manufactured by PROCON, Murfreesboro, Tennessee. It was driven by a MET, DC electric motor model 3B-A004082C with a nominal voltage requirement of 115 VDC. The input voltage to the motor was controlled via a POWERSTAT variable autotransformer of the type 216B.

4.1.3. Heater

The glycol solution was heated electrically by a 5000 W electric heater, manufactured by CHROMALOX CANADA rated at 240 VAC. The voltage input to the

heater was controlled via a POWERSTAT variable autotransformer of the type 136BT-2. The heater was selected based on its ability to raise the glycol temperature to that where the glycol is heated inside a standard 3 m² flat-plate solar collector on a sunny day.

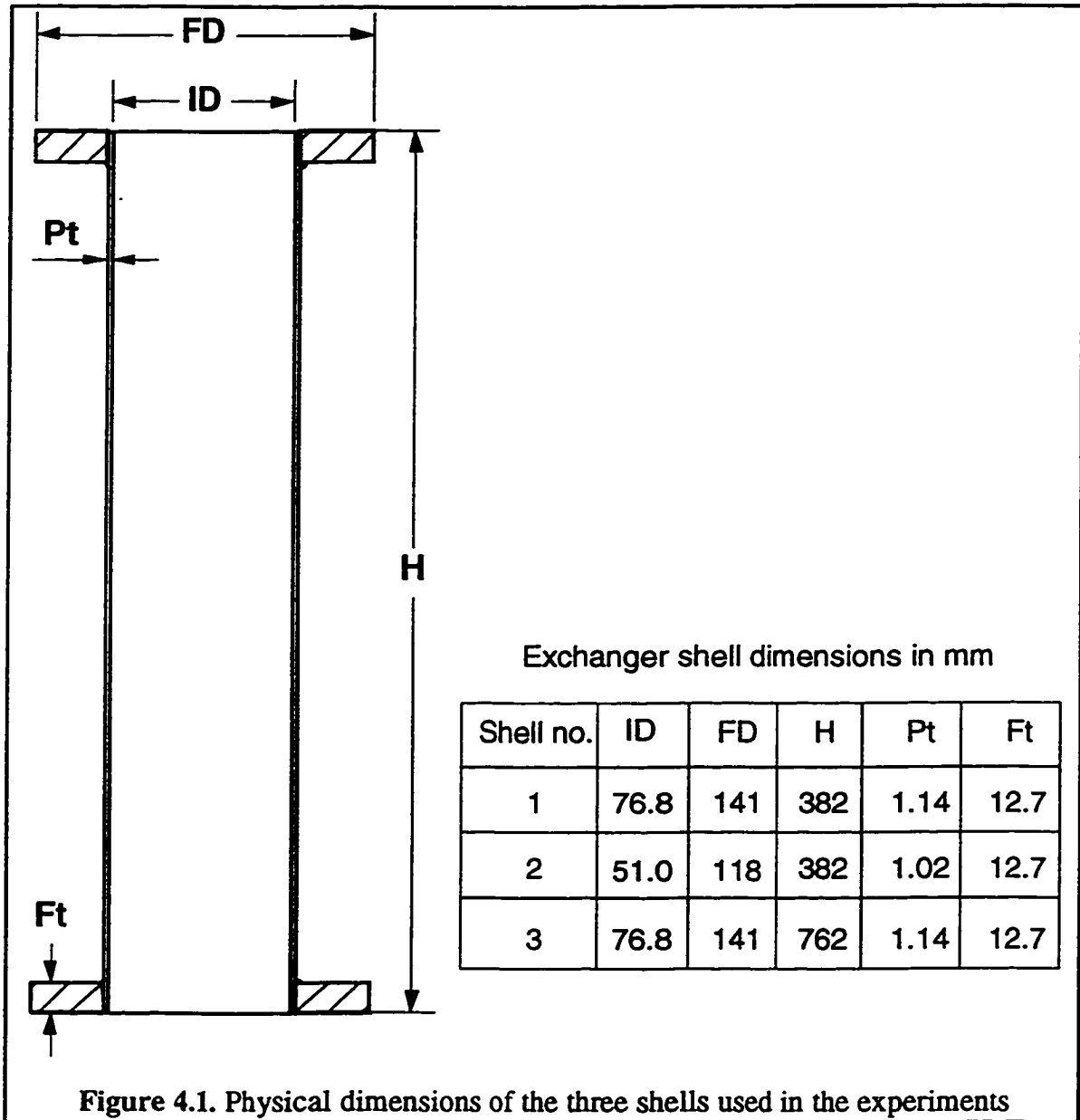
4.1.4. The shell-and-coil heat exchanger

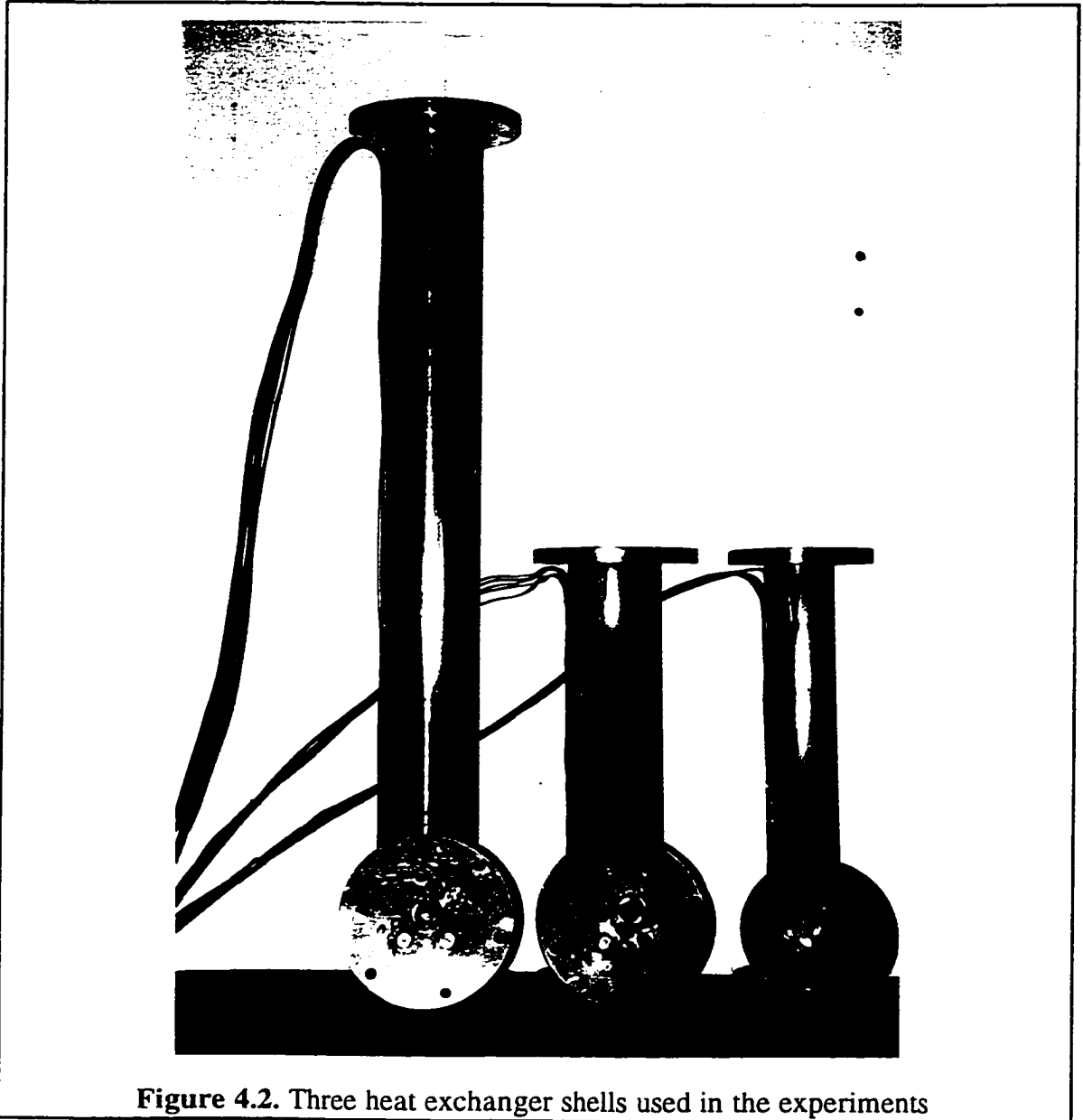
The heart of the apparatus is the heat exchanger. The shell-and-coil heat exchanger consists of a cylindrical shell, top and bottom caps and the helical coils inside.

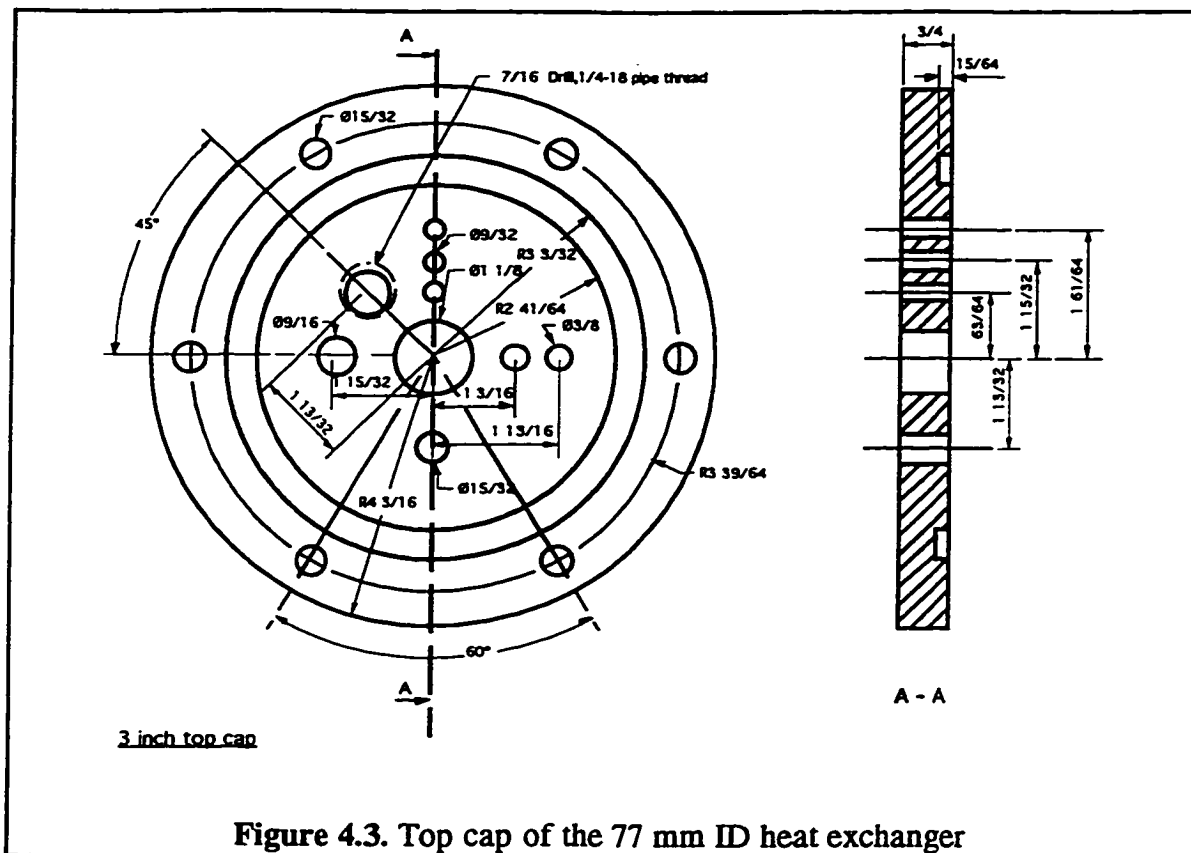
Standard copper water tube, type M, of 2" and 3" nominal diameter was used for the shell, with 12.7 mm thick brass flanges brazed to its both ends. Figure 4.1 is the sketch of the 77 mm ID × 382 mm long shell with the dimensions of all the three shells tabulated. Also figure 4.2 is a picture of the three shells with thermocouples attached to them.

The top and bottom caps were made of 12.7 mm thick brass. Figure 4.3 shows the sketch of the top cap of the 77 mm ID heat exchanger. At the center of the cap is the water outlet port. Also the central thermocouple probe is inserted through the same opening. The cap was equipped with various holes with different diameters in order to facilitate the change of the coils from one configuration to another. After a coil was installed, the other holes were covered with small caps and sealed by soldering. In addition to those, an extra pipe-threaded hole was provided so that the thermocouple wires measuring the coil surface temperature could be transferred outside. The thermocouple wires were passed through a short-length 6.35 mm copper tube and the gap was sealed by filling with epoxy. Six 5/16" steel bolts were used to fasten each cap to the flange. Since the storage tank was connected to the main water supply line at pressures of nearly 3.4 atm, rubber O-rings at both ends of the heat exchanger were necessary to prevent water leakage from the assembled heat exchanger.

The bottom cap was identical to the top one except that it did not require a threaded hole to accommodate a thermocouple feed-through. As for the 51 mm ID heat exchanger, the caps had generally the same layout but different dimensions.







All the coils were made by winding copper tubes around cylinders of different diameters. A spacer was placed between each two consecutive coil turns to ensure a uniform pitch along the coil. Different coil pitches were possible by increasing or decreasing the spacer size. Table 4.1 contains the specifications of all the coils tested, together with the specifications for double- and triple-coil configurations. Coil #22 was only used in a triple-coil configuration. Coils #1, #2 and #22 are shown in figure 4.4.

Table 4.1. Coil specifications

Coil #	D_{Lo} (mm)	D_{hyd} (mm)	Coil OD (mm)	D_{ex} (mm)	A (m ²)	S'	P	Number of turns
1	6.35	4.74	55.8	29.8	0.100	1.221	1.58	31.5
2	6.35	4.46	38.2	41.5	0.058	1.885	1.74	28.0
3	6.35	4.71	64.2	26.0	0.116	1.055	1.68	31.7
4	6.35	4.69	54.4	39.3	0.053	1.262	2.94	17.0
5	6.35	4.50	38.8	48.3	0.036	1.861	2.97	16.8
6	6.35	4.85	65.7	32.8	0.069	0.999	3.06	18.3
7	6.35	4.44	37.2	54.2	0.023	1.938	3.93	11.1
8	7.94	4.55	39.0	46.9	0.041	1.908	1.97	14.6
9	7.94	5.82	56.2	36.1	0.060	1.122	1.95	14.8
10	7.94	5.00	38.6	49.9	0.032	1.825	3.01	11.6
11	7.94	5.74	56.7	39.0	0.049	1.126	2.95	12.0
12	4.76	3.16	35.7	42.3	0.059	2.225	1.80	40.6
13	4.76	3.18	44.8	37.4	0.073	1.824	1.89	39.0
14	4.76	3.22	64.8	28.9	0.106	1.296	1.97	37.6
15	9.52	5.68	54.6	36.9	0.062	1.249	2.24	13.5
16	6.35	4.73	67.6	19.4	0.181	0.997	1.00	47.1
17	6.35	4.85	69.4	40.3	0.037	0.993	5.96	9.0
18	6.35	4.75	67.5	23.2	0.135	0.984	1.25	34.9
19	6.35	4.43	36.8	24.1	0.035	0.981	2.76	17.0
20	6.35	4.58	41.2	14.2	0.091	0.799	1.20	41.3
21	9.52	5.77	55.0	26.3	0.123	1.240	1.05	27.0
22	6.35	4.78	75.8	-	0.183	-	1.24	41.6
23	6.35	4.05	37.6	35.6	0.169	2.052	1.20	82.7
24	6.35	4.59	55.2	25.6	0.260	1.289	1.31	84.5
25	6.35	4.76	74.5	18.4	0.366	0.889	1.33	85.2
1+2	6.35	-	-	19.2	0.158	0.760	-	-
23+24	6.35	-	-	16.1	0.430	0.831	-	-
23+25	6.35	-	-	12.0	0.536	0.606	-	-
24+25	6.35	-	-	9.17	0.627	0.457	-	-
1+2+22	6.35	-	-	6.36	0.340	0.279	-	-
23+24+25	6.35	-	-	6.05	0.796	0.315	-	-

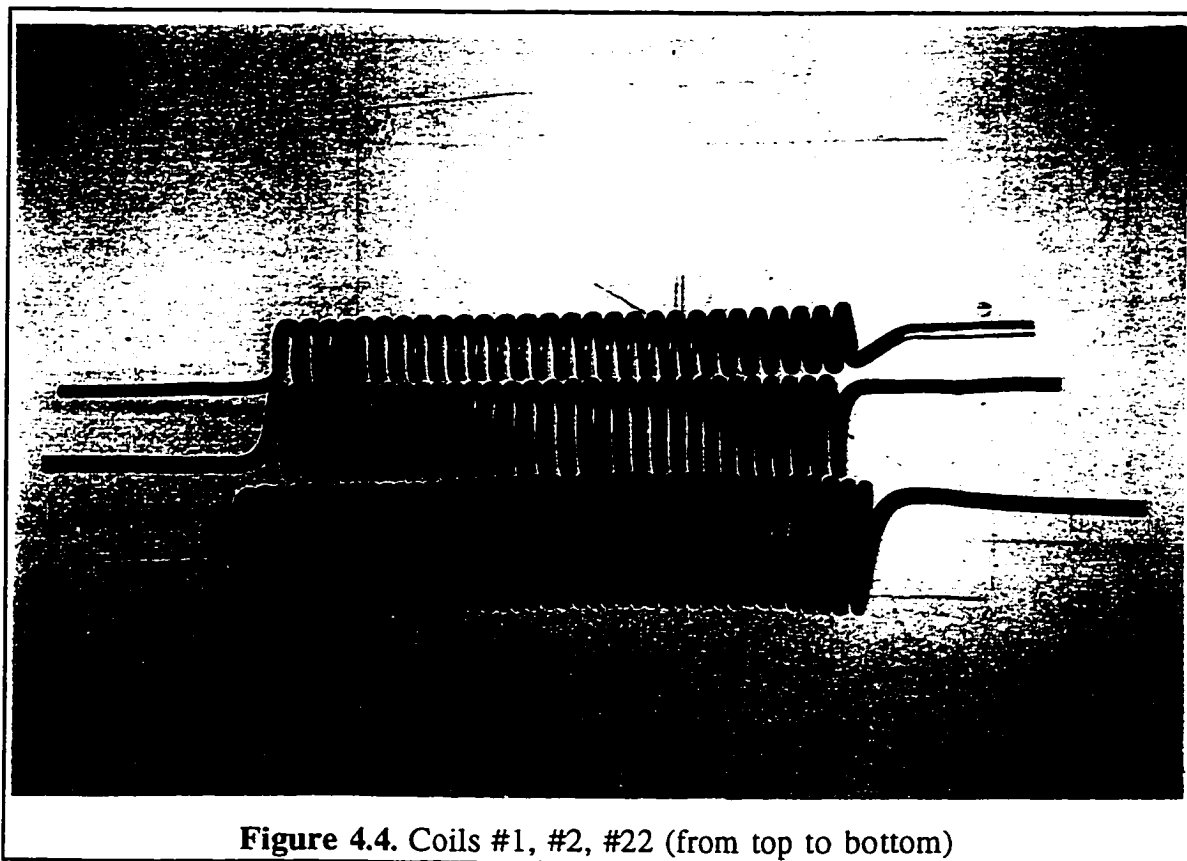
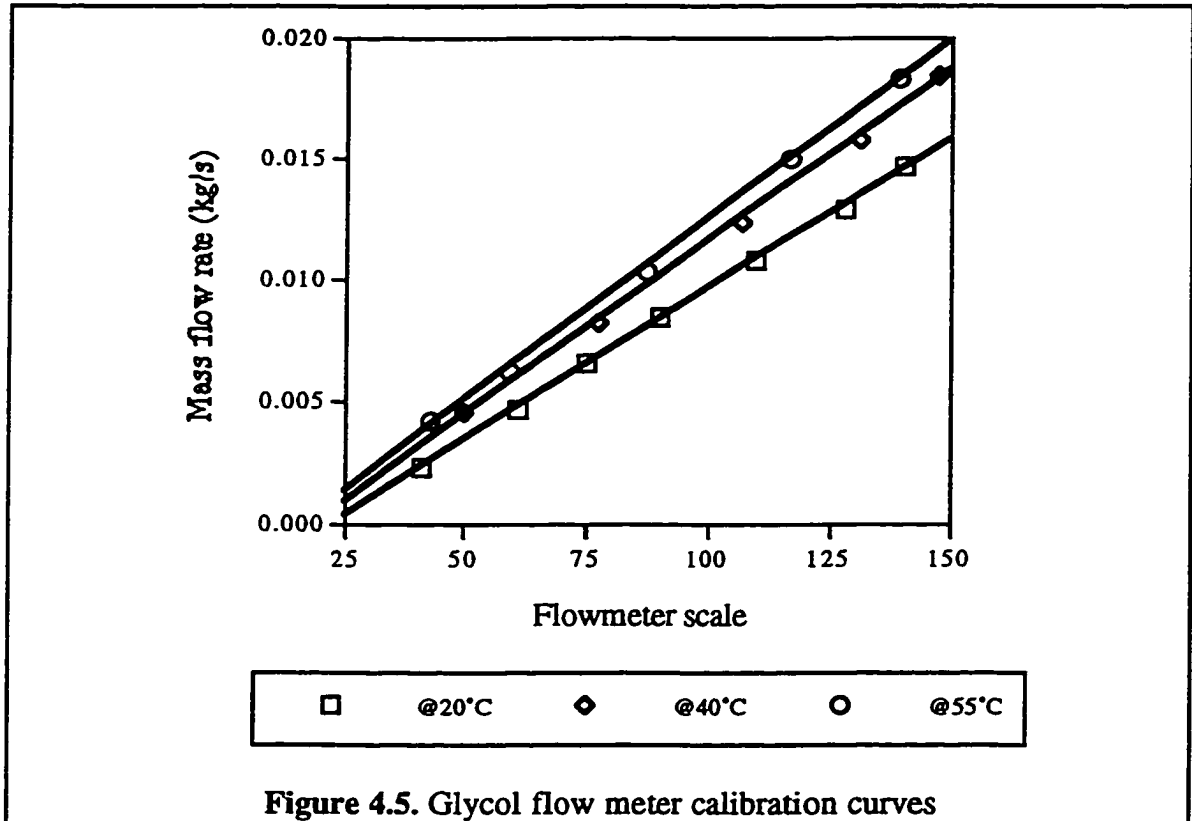


Figure 4.4. Coils #1, #2, #22 (from top to bottom)

4.1.5. Flow meters

For glycol flow rate measurements, three Cole-Parmer 150 mm variable-area flow meters were used. The measurement accuracy of the flow meters was $\pm 2\%$ of full scale. The flow meters were calibrated to measure the flow of a solution of 40% by volume of propylene glycol in water. The calibration was performed by running the glycol solution through each of the flow meters at different rates and measuring the flow rate by recording the time needed to collect a certain amount of glycol by weight. This made it possible to directly convert the reading on the flow meter to the mass flow rate of glycol. The process of calibration was repeated for three different temperatures of 20, 40 and 55°C. The average of the inlet and outlet temperatures of the flow meter was taken as the mean

temperature of glycol flowing through the flow meter. The calibration plots are illustrated in figure 4.5.



The linear behavior of the flow meters was confirmed by figure 4.5. Also significant temperature effects on the flow meter readings were observed. The equations of the three calibration lines were included in the computer code. Depending on the mean temperature of glycol flowing through the flow meters, the computer would calculate the mass flow rate based on each equation and the result would be interpolated to account for the temperature effects.

Flow measurement requirements on the shell-side were different from those on the tube-side. Weak natural-convective flows must be treated with special care. The flow disturbances must be kept at a minimal level. As a result conventional flow meters such as paddle-wheel, orifice or rotameters are not fit for this purpose. In the current experiments a

magnetic-resonance type flow meter was used to ensure that the flow would not be disturbed. In this type of flow meters, the voltage induced due to the passage of an electric conductor (water) through a magnetic field, is detected. The electronic circuitry will calculate the flow velocity from the measured voltage. The fact that there is no need for either a moving part or a protruding probe, makes this type of flow meter the preferred choice for flow measurements in buoyancy-induced flow situation.

A Clorius Combimeter (Ballerup, Denmark) model 1.5 VPD flow meter was used to measure the water flow rates. The error associated with the flow measurement was $\pm 2\%$. The range of flow measurement for the model 1.5 VPD was between 0.015 - 1.5 m³/h. The device consisted of a measuring unit and a processing unit. The processing unit is also capable of calculating the accumulated value of water flow over a period of time. In order to automate the process of flow measurement, a pulsed output was also provided.

4.1.6. Thermocouples

For all the temperature measurements, copper-constantan (T-type) thermocouples were used. Most of the thermocouples were of 26 AWG size. Thermocouple wires were soldered to various locations (at least five) along the coil surface, and also to six locations along the outside wall of the heat exchanger shell. The shell wall thermal resistance was negligible, and the shell was insulated from the outside. Therefore, the temperature measured by the thermocouples on the shell outer wall was very close to the water temperature in the vicinity of the shell wall on the inside. A special probe was built to measure the water temperatures on the centerline of the heat exchanger. The probe was made of 3.2 mm copper rod and the thermocouple wires were soldered to its surface at six positions equally apart. Proper tube fittings were soldered to the probe assembly to facilitate its insertion into the water outlet port of the heat exchanger.

Terminal temperatures were measured using factory-made (OMEGA) T-type thermocouple probes with inconel shielding. One-eighth inch probes were installed in the water inlet port and 1/16" probes were used in the inlet and outlet of the coils. The water outlet temperature was measured by the top most thermocouple junction of the specially-made central probe which was described above. The error associated with the temperature

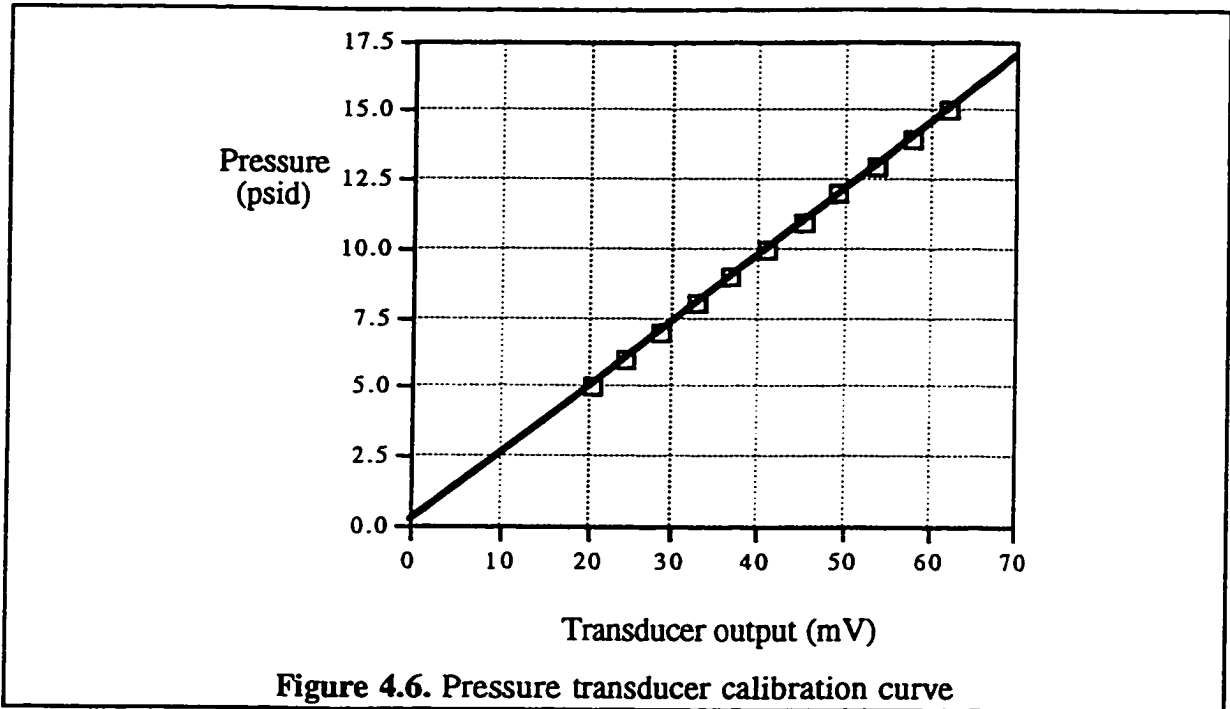
measurement by thermocouple wires and probes in the range of temperatures in the current thesis was less than 0.5°C according to the thermocouple technical information sheet (Omega Engineering Inc. 1992).

In addition to the above locations, the glycol temperature was measured at the heater exit and the heat exchanger inlet. It was used as a checkpoint for the glycol inlet temperature. Also the glycol temperature was measured at a location immediately after the variable-area flow meters in the outlet line. This was used to calculate the mean glycol temperature flowing through the flow meters. This mean temperature was needed for evaluating the glycol mass flow rate.

The temperature profile on the centerline of the storage tank was also measured. The probe used for this purpose was made of 9.52 mm hard copper tube and it was 173 cm long. Along the surface of the tube, constantan wires were soldered at 10 equally-spaced locations. The body of the copper tube was used as the common copper element of the copper-constantan thermocouple. A simple heat transfer model was developed and solved analytically to estimate the error level in measurement of temperature due to heat conduction along the probe wall. The error was found to be within acceptable range for the case of a thermally stratified tank. Temperature measurements on the tank centerline were necessary to confirm the establishment of thermal stratification inside the tank. Also the amount of water extracted from the tank was adjusted according to this temperature profile.

4.1.7. Pressure transducer

The pressure drop across the coils in the glycol loop was measured. An AMETEK (Feasterville, Pennsylvania) model 55AD002A diaphragm type differential pressure transducer was used for pressure measurements in the range 0-15 psid. Two 6 volt alkaline batteries connected in series were used as the 12 volt excitation source for the transducer. Since the output of the transducer is sensitive to the excitation voltage, the pressure transducer was calibrated again with the 12 V battery source. Figure 4.6 illustrates the calibration curve for the pressure transducer.



The linearity of the transducer output was confirmed. The equation of the line was used in the computer code to calculate the pressure difference from the measured output voltage of the transducer. In addition to the pressure transducer, dial pressure gauges were used to check the pressure at the inlet and outlet line of the glycol loop.

4.1.8. Water storage tank

In the water loop a 273 liter insulated tank model JWB805DF manufactured by JOHN WOOD, Toronto was used. The hot water from the heat exchanger was fed to the tank at the top and the bottom of the tank was connected to the main water supply. From a separate port at the top of the tank, water was extracted at a rate nearly equal to the water flow rate from the heat exchanger. The tank pressure was monitored to prevent pressure buildup. The tank was also equipped with a pressure relief valve. Since the tank was connected to the main supply line, its pressure was limited to 50 psia (3.4 atm).

4.1.9. Data acquisition system

All the voltage differences across the thermocouple leads were measured by the data acquisition device. A SCIOMETRIC electronic measurement system (Manotick, Ontario) model 8082A was used for this purpose. Some specifications of the data acquisition device are as follows. It is capable of measuring four primary quantities. DC voltage in the range ± 4.096 V with $2.0 \mu\text{V}$ resolution, DC current in the range ± 4.096 mA with $0.1 \mu\text{A}$ resolution, resistances of up to $1.3 \text{ M}\Omega$ with 0.5Ω resolution and frequencies from 0.03 to 3.8 Hz. A total of 80 independent input channels are provided, of which 64 are general purpose analog channels (Sciometric Instruments Inc. 1984).

The data acquisition device was connected to a SCIOMETRIC CPU module model 901. The CPU module was capable of converting the measured voltages to temperatures. In addition to that, the CPU module was programmed to continuously read the temperatures in certain periods of time and in some cases, averaging was also performed by the CPU module. The device is a microprocessor-based controlled, intelligent interface for the data acquisition system. The communication between the data acquisition CPU and the computer was made via the serial port of the computer. The maximum transmission speed was 9600 bits of data per second (Baud). It is also equipped with a battery-backed real time clock and is capable of transferring simple ASCII functions to and from a computer to the data acquisition device (Sciometric Instruments Inc. 1984).

As a part of the experimental apparatus, an APPLE Macintosh SE/30 computer was used to monitor the data continuously. A computer code was developed using the Microsoft QuickBasic 1.0 for Macintosh to monitor the measurements, produce continuous temperature graphs, and calculate the heat transfer and hydraulic parameters.

4.1.10. Piping

For the piping in the glycol loop mainly 6.35 mm nylon tubing was used, except for the inlet line to the pump, where 9.52 mm tubing was used instead. This was done to

avoid the cavitation phenomena at higher flow rates. In some parts of the loop, 12.7 mm copper tubes were employed.

Since the piping dimensions in the water loop are of significant importance in determining the water flow rate, more attention should be made to it. Figure 4.7 is a detailed sketch of the water piping in the experimental apparatus. The physical dimensions are given on the sketch.

Figure 4.8 is a schematic diagram of the experimental apparatus. Water piping is shown by the dashed line, and for the glycol piping, solid lines are used. To avoid complexity, the electrical connections and the thermocouple wires are not illustrated. All the thermocouple wires and the pressure transducer wires were connected to the data acquisition device, which in turn was connected to the CPU and from there to the computer for monitoring and processing.

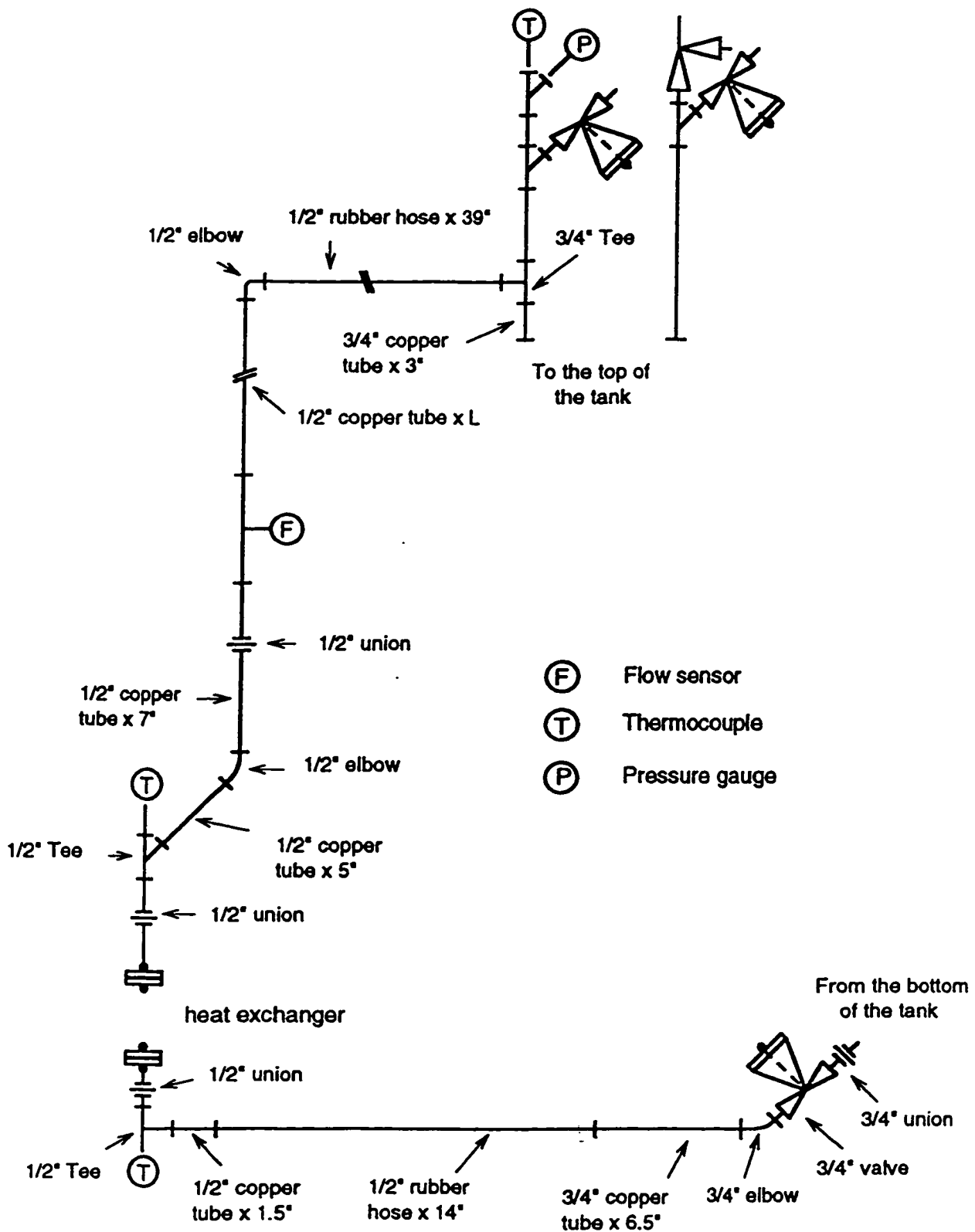


Figure 4.7. Water piping

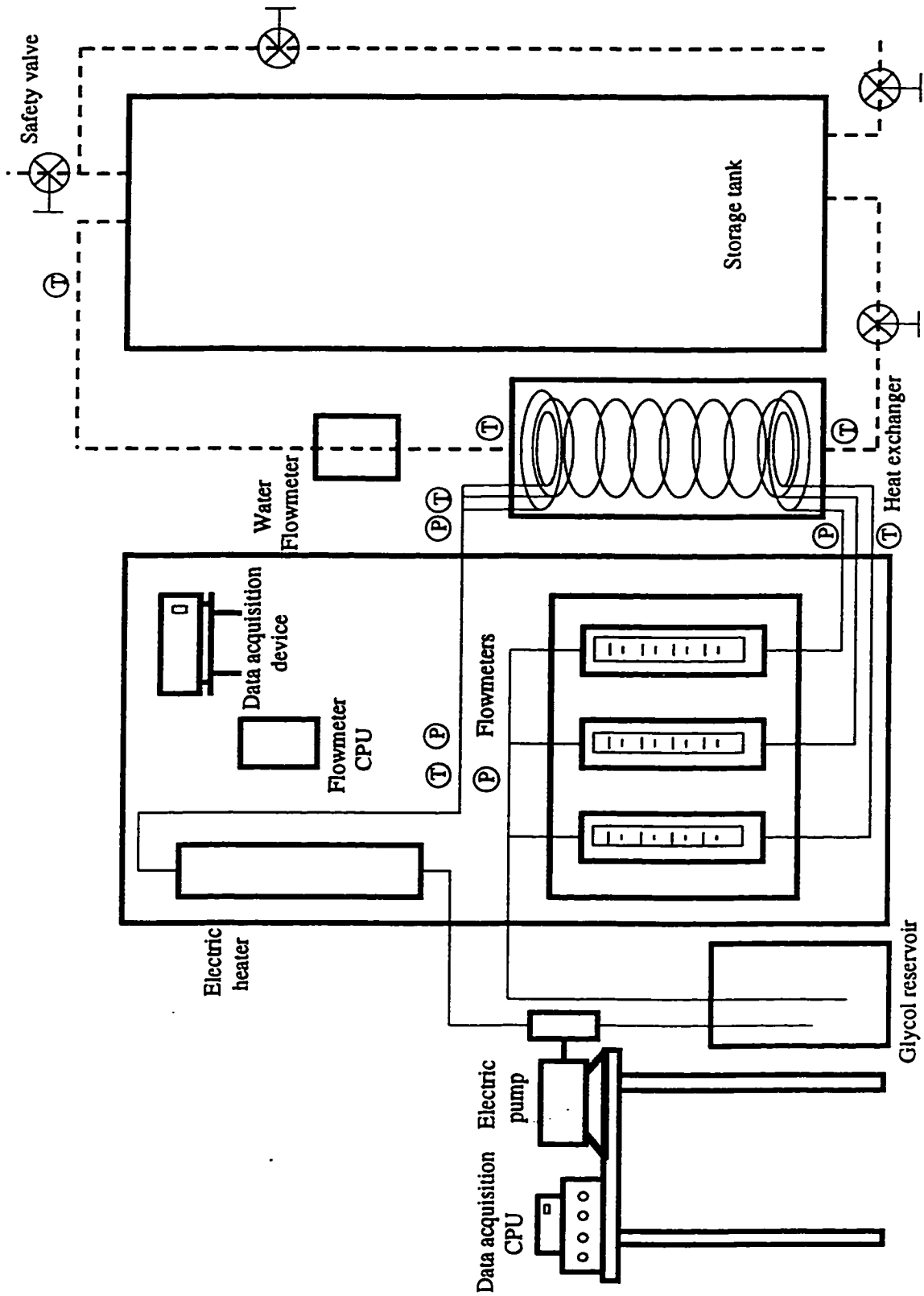


Figure 4.8. Experimental apparatus

4.2 Experimental procedure

The experimental procedure started by assembling the shell-and-coil heat exchanger having a specific configuration. Figure 4.9 is the sketch of a typical shell-and-coil NCHE and figure 4.10 is a picture of an actual heat exchanger. After measuring the physical dimensions of the coils, the constantan wires were soldered to the coil surface at six equally spaced locations vertically apart from each other. The coil wall was used as the common copper material to provide a copper-constantan junction. The constantan wires were then passed through a 5 cm long 6.35 mm copper tube and the tube was filled with epoxy glue to prevent from any water leakage. The straight length at the top end of the coils was passed through the holes of the top cap of the exchanger, the thermocouple feed-through was fixed in its port and the gap between the tubes and the cap holes were sealed with solder. The assembled part was then inserted in the shell. At last the bottom end of the tubes were passed through the holes in the bottom cap and soldered. The shell was tightened to the caps using six 5/16" steel bolts on each side and it was made water tight by using rubber O-rings. A copper wire was soldered to the coils at the top to be used as the copper lead for the thermocouple constantan wires.

The heat exchanger was installed in the test rig by making the water piping connections to the inlet and outlet. The water central temperature probe was installed. The main water supply line was connected to the bottom of the storage tank to prevent buildup of pressure in the water loop. Thermocouple wires were connected to the data acquisition system via multipin connectors. The multipin connectors consisted of pairs of 23 pairs of copper and constantan pins. This was done to avoid the measurement errors due to an intermediate junction. A total of 49 analog channels of the data acquisition system were used.

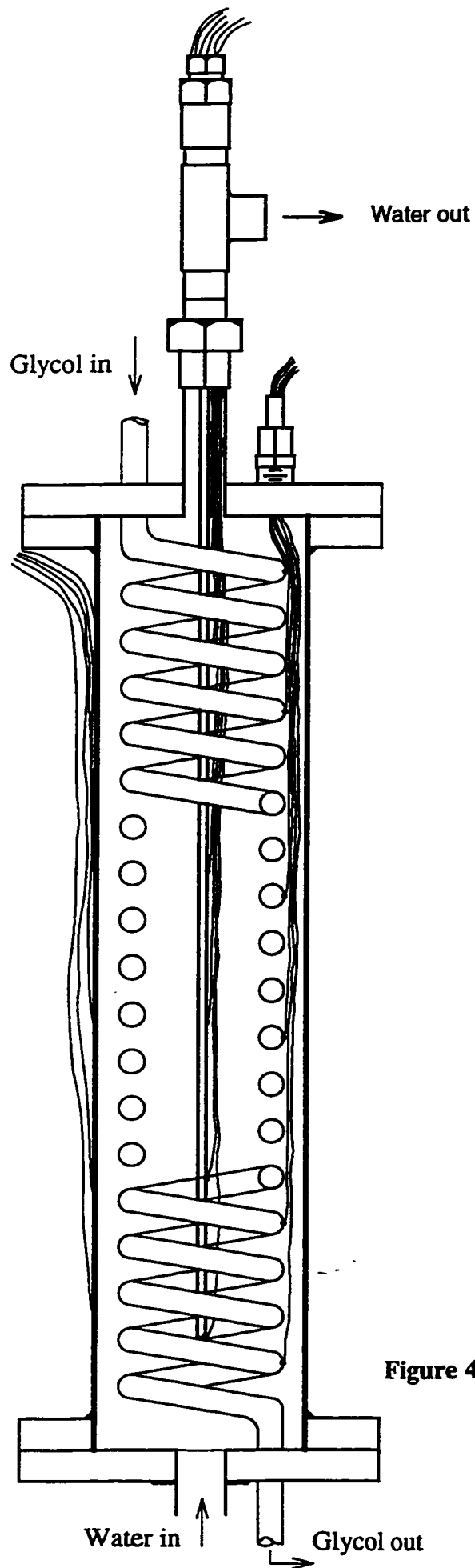
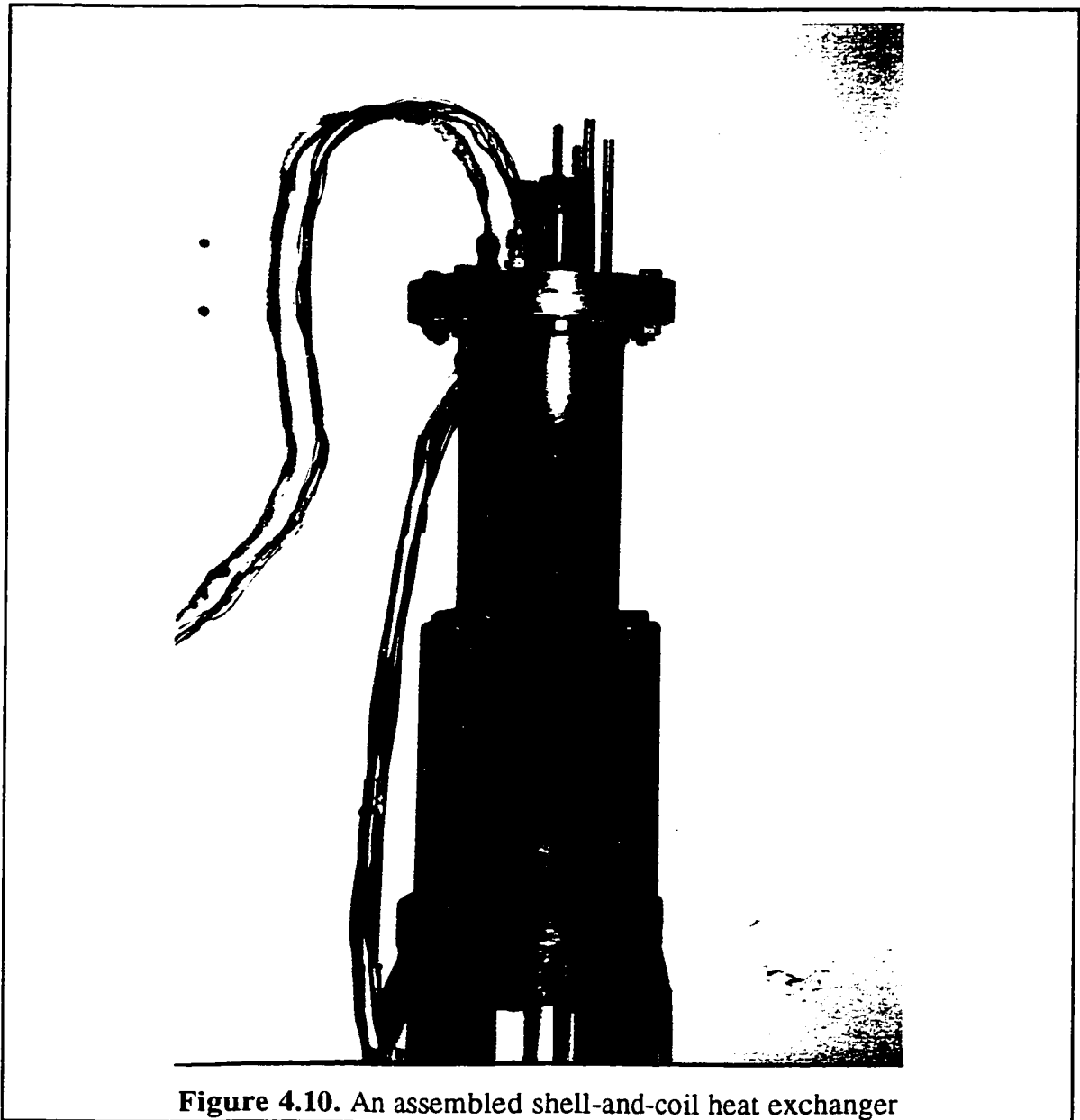


Figure 4.9. Shell-and-coil NCHE



The heat exchanger was insulated with 19 mm thick Armstrong ARMAFLEX pipe insulation material. At the glycol inlet and outlet, the tubing was connected to the coils using Parker PRESTOLOK connectors which provide the necessary sealing while they are easy to remove for disassembly.

The glycol concentration was checked at the start of the test to make sure that a solution of 40% by volume of glycol in tap water is maintained. The glycol solution refractive index was measured with an ATAGO hand refractometer. The value of the refractive index was then converted to the percentage of concentration using the tabulated data available (Dow Chemicals Inc. 1994).

Before starting the test, the mains supply water was passed through the heat exchanger to allow for the air trapped in the exchanger to escape. For each configuration, up to four values of glycol flow rate were set for a fixed heat rate. The heat rate was then changed and the tests were repeated with the four glycol flow rates. Up to four different heat rates were set. The glycol mass flow rate was varied from 0.00185 to 0.0343 kg/s and the range of the heat rate settings were from 160 to 2300 W. The combination of the heat rate and the glycol flow rate for each configuration was chosen so that the glycol inlet temperature did not exceed 85°C. All the temperatures were constantly monitored during the test until the condition of steady state was achieved. The time needed for the water loop to reach the point that the changes in temperatures were negligible with time, was approximately 65 minutes.

After the steady state condition was reached, the temperatures were sampled by the data acquisition system for a period of 3 minutes and the average value was sent to the computer. At the same time the water flow rate was read from the CPU of the flow meter and entered manually to the computer. Also the reading from the glycol flow meters was entered to the computer manually. The necessary heat transfer and hydraulic parameters were calculated from the raw data and the final results were saved in files for further reference.

At least ten data points were produced for each heat exchanger configuration. At the end, the heat exchanger was taken out of the test rig, dismantled and a new configuration was set up and made ready for a new set of test runs. 24 single-coil, 4 double-coil and 2 triple-coil configurations were tested.

4.3. Processing the data

A computer code was developed using Microsoft QuickBasic 1.0 for Macintosh to process the data. The code consisted of five major subroutines.

- 1) Calculating the geometrical parameters from the basic physical dimensions.
- 2) Communicating with the data acquisition CPU. The communication speed was set to 9600 Baud or bits per second.
- 3) Monitoring of the temperature data on the screen. The temperatures were constantly updating according to the values received from the data acquisition CPU. Each cycle of reading took about 15 seconds to complete. In each cycle a maximum of 49 channels were scanned.
- 4) Graphical presentation of individual temperature changes with time during the test runs. The user was able to access this feature through a menu of buttons on the computer screen.
- 5) Calculation of the heat transfer and hydraulic parameters.

The final graphical representation of data was done using CA-Cricket Graph III software. The curve-fitting task was also done by the same software.

CHAPTER 5

RESULTS AND DISCUSSION - I

In this chapter the effects of various parameters on the shell-side heat transfer coefficient is addressed. In addition, the temperature distribution inside the heat exchangers is discussed. Variations of tube-side heat transfer coefficient is also noted. The collective effect of all the parameters on the UA product of the heat exchanger and the results of the heat exchanger effectiveness is also discussed.

5.1. Temperature distribution

Temperature profiles inside a heat exchanger are revealing about the thermal behavior of the device. They can be helpful tools in determining if the space inside the heat exchanger is properly utilized or not.

5.1.1. Single coils

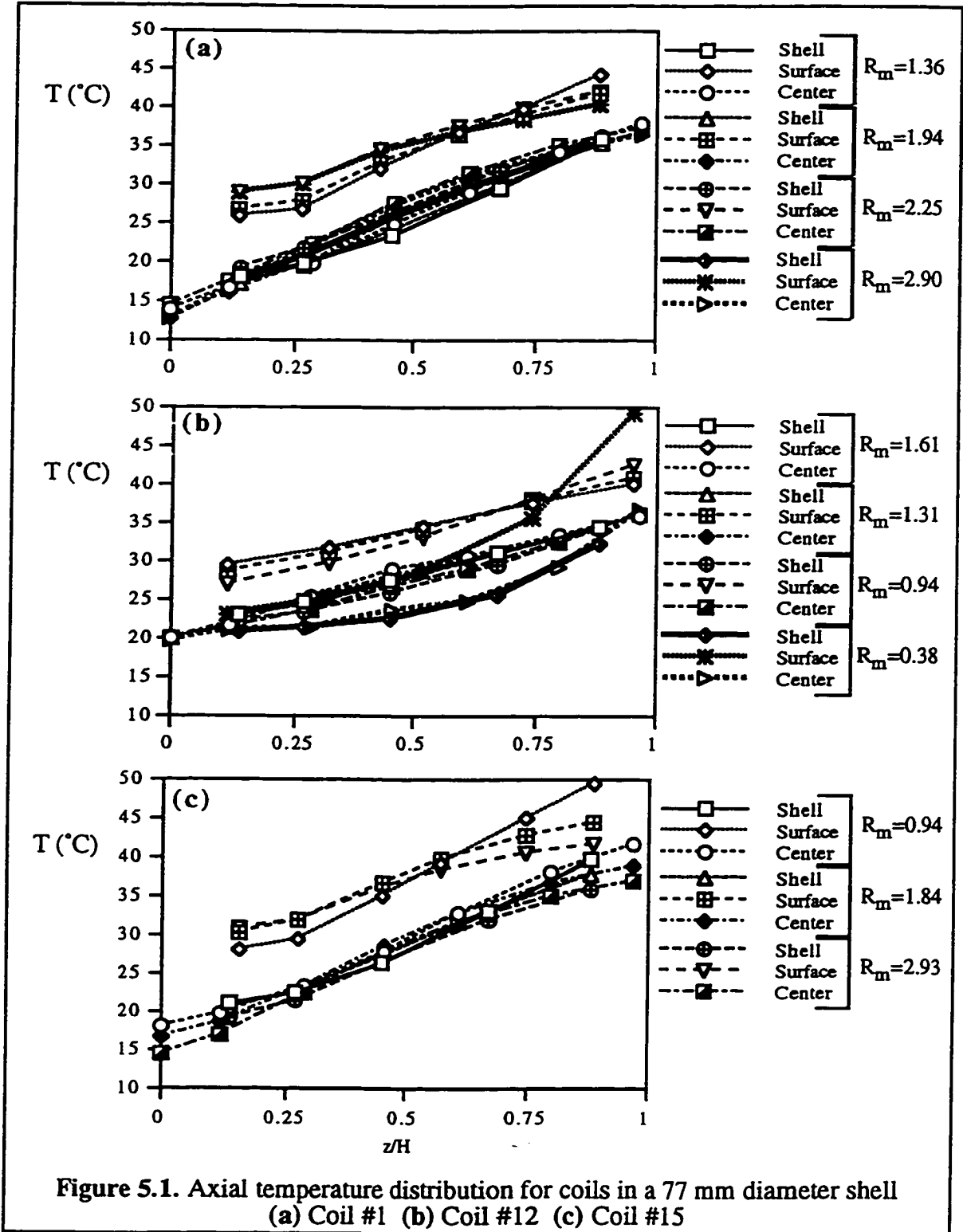
Figures 5.1 (a)-(c) and 5.4 (a)-(c) show typical temperature distributions inside the heat exchanger for various heat rates. In these figures R_m is the ratio of glycol to water mass flow rates, $\frac{\dot{m}_g}{\dot{m}_w}$. For all the graphs of the axial temperature profile, a value of zero on the abscissa corresponds to the bottom of the exchanger and a value of one indicates the top. The axial temperature profile is linear ($r^2 > 0.98$) for most values of R_m . However, for each coil there is a certain value of R_m for which the axial temperature profile of the coil surface is far from being linear. This deviation from a linear profile is influenced by the mass flow rate ratio. The smaller the glycol flow rate is relative to the water flow rate, the greater is the nonlinearity. This is illustrated for coil #12 in figure 5.2, where the r^2 values for linear curves fitted to data, are reported in the legend of the figure. As the mass flow rate ratio increases, the deviation from the linear profile increases, which is evident from

the decreased r^2 values. The nonlinearity is such that the profiles tend to be concave up, which means that the coil surface temperature is higher than usual at the top and then it drops faster than usual while moving towards the bottom of the heat exchanger. The value $R_m=1$ seems to be the critical point. For R_m significantly less than unity the curves deviate greatly from being linear whereas the curves are close to a straight line for R_m values approximately equal to or greater than one. A linear temperature profile means that the shell-side heat transfer coefficient is constant along the axis of the heat exchanger.

For coil #1 which is shown in figure 5.1(a) the profiles of water temperature are linear ($r^2>0.975$). The coil surface temperature profiles are also linear. This was expected since the mass flow rate ratios are all above unity. For the lowest value of R_m in this graph, the slope of the coil surface temperature profile is steeper.

The case of coil #12 [figure 5.1b] is significant because the deviation from linearity is highlighted where the mass flow rate ratio is well below unity. There is a notable drop in coil surface temperature as well as mean water temperature for $R_m=0.38$. The curves suggest that the shell-side heat transfer coefficient is no longer constant. Since it is reasonable to assume that the heat flux is uniform, the product ($h_o\Delta T$) is constant along the coil surface. Therefore a smaller temperature difference means a higher h_o value. The magnitude of h_o starts from a low value at the top and gradually decreases to its highest value at the bottom of the heat exchanger. Obviously this situation is not desirable since the hot stream loses its heat very quickly and therefore the heat exchanger does not operate at its full capacity. It can be concluded that for such a low glycol flow rate (and therefore a low heat rate) coil #12 is oversized in terms of the surface area. The coil has reduced the glycol temperature to the lowest value possible, i.e. the water inlet temperature. The case of $R_m=0.38$ for coil #12 is illustrated separately in figure 5.3.

In figure 5.1(c) again the profiles are mostly linear with the case $R_m=0.94$ having a steeper slope yet still linear. For coil #6 and #10 [figures 5.4(a) and (b)] where glycol mass flow rate is always higher than water flow rate, all profiles are close to linear. The same conditions for coil #12 prevailed for coil #13 in figure 5.4(c) for the case when the mass flow rate ratio is equal to 0.60.



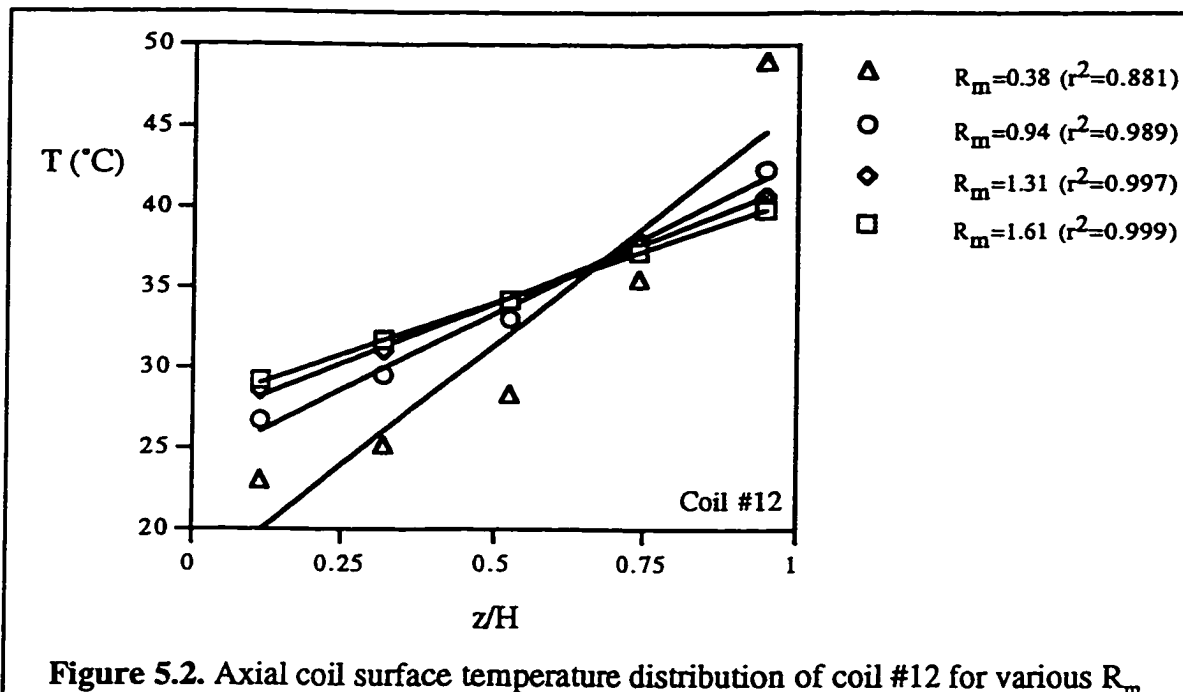


Figure 5.2. Axial coil surface temperature distribution of coil #12 for various R_m

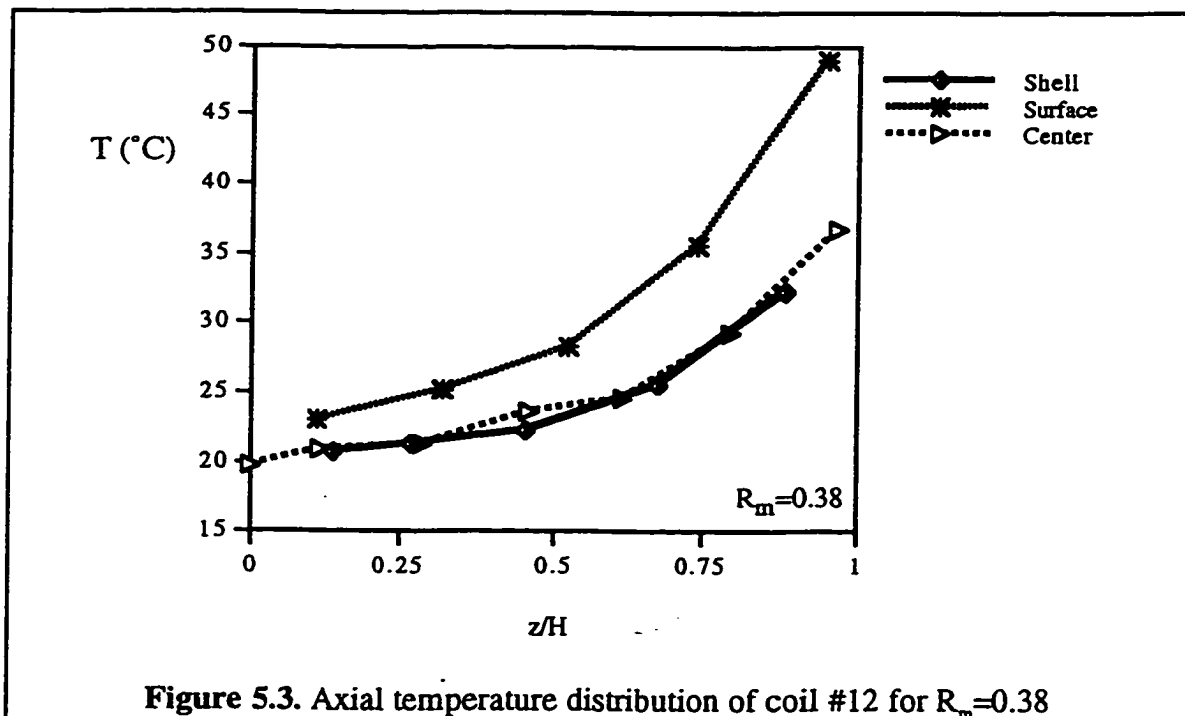
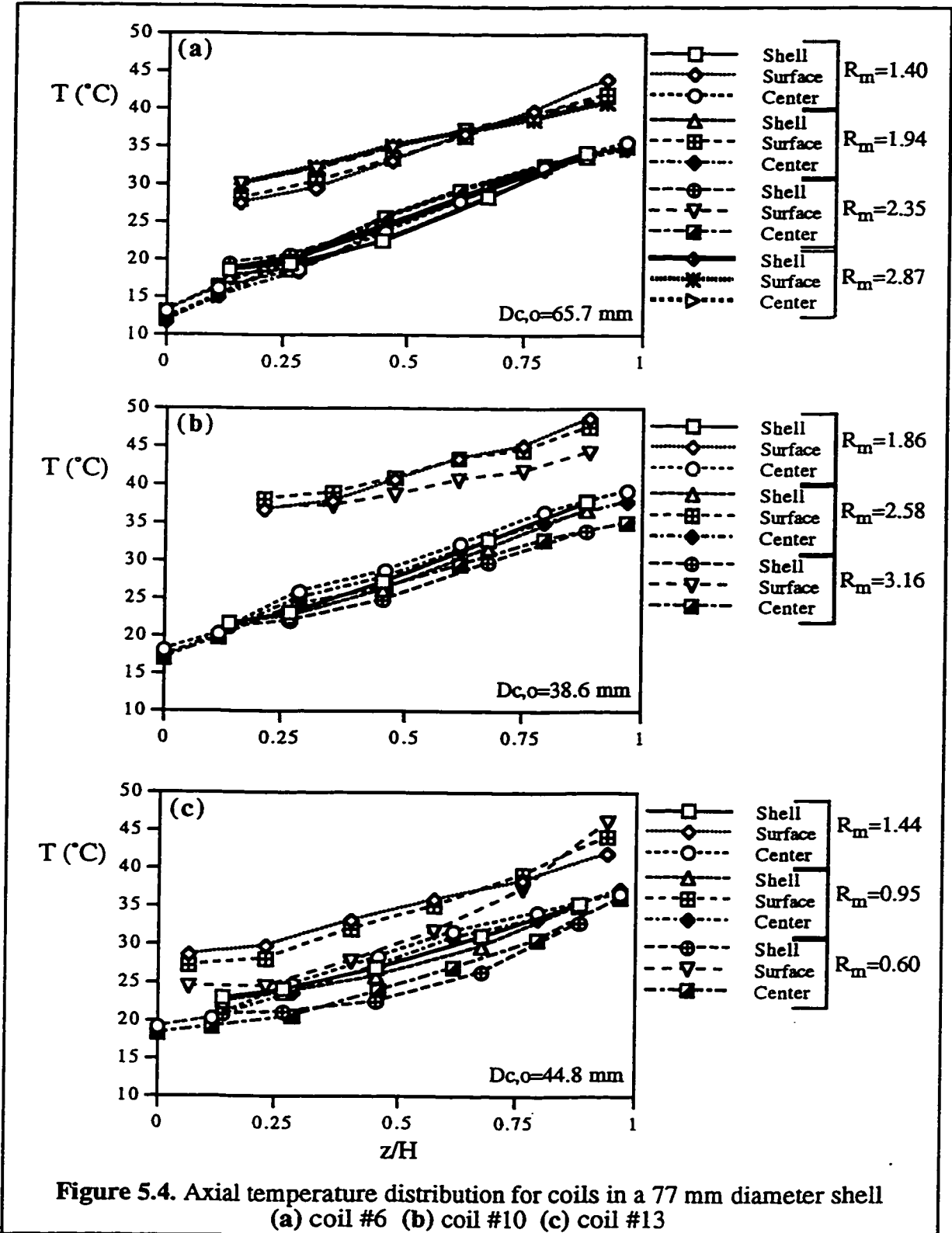


Figure 5.3. Axial temperature distribution of coil #12 for $R_m=0.38$



Figures 5.5(a) - (c) show that as the glycol mass flow rate increases beyond twice the value of the water flow rate, again the temperature profiles start diverting from their originally linear shape. This time the profiles tend to be concave down as opposed to concave up. Figure 5.6 illustrates this observation for coil #16. It can be seen that as the mass flow rate ratio changes from 0.95 to 2.62, the temperature profile changes from an initially concave-up profile to a concave-down one. In other words the coil surface is colder than usual at the top of the heat exchanger. This brings a higher shell-side heat transfer coefficient to the top part and it gradually decreases until it reaches its lowest value at the bottom of the heat exchanger. Also there is a faster drop in coil surface temperature at the bottom of the heat exchanger. This concave down profile results in higher mean water temperature compared to the linear profile. This, in turn, translates to higher water flow rates. It must be noted that the discussion so far has been based on a fixed heat rate for all the plots.

Based on these observations it can be concluded that regarding the buoyant driving force in the heat exchanger, the higher the glycol mass flow rate the higher the mean water temperature would be and therefore higher water flow rates can be achieved.

Based on the work of Hollands and Brunger (1992) there exists an optimum value for the glycol mass flow rate. Equation 2.1 defines this optimum value. The immediate result of equation 2.1 is that the glycol mass flow rate must be always kept higher than the water flow rate since the optimum value of the heat capacity ratio is always greater than one. This is confirmed by the observation made on the temperature profiles in the current work. Although the study of the temperature profiles does not lead to the value of the optimum mass flow rate ratio, it is obvious that there is a price to be paid in order to increase the glycol flow rate.

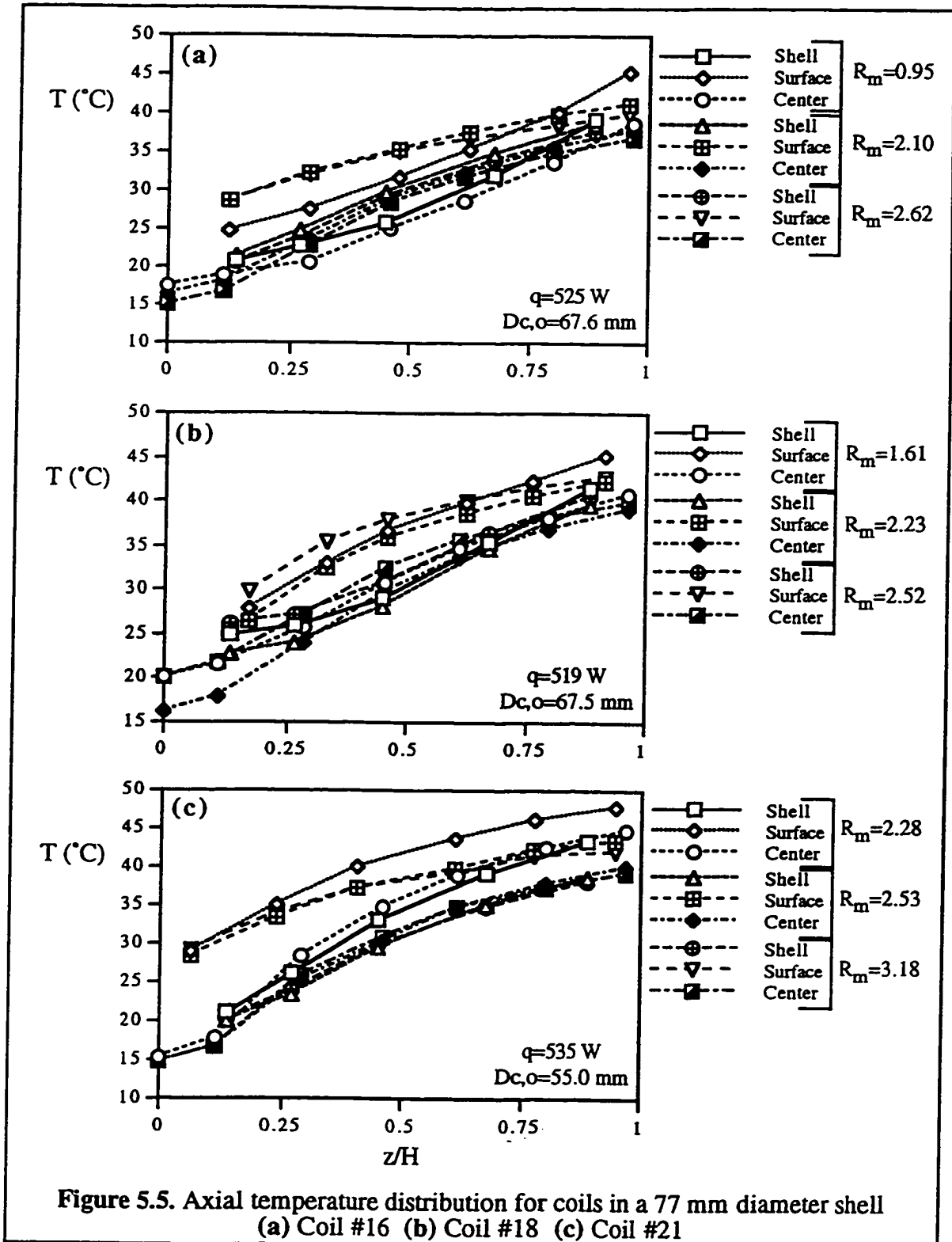
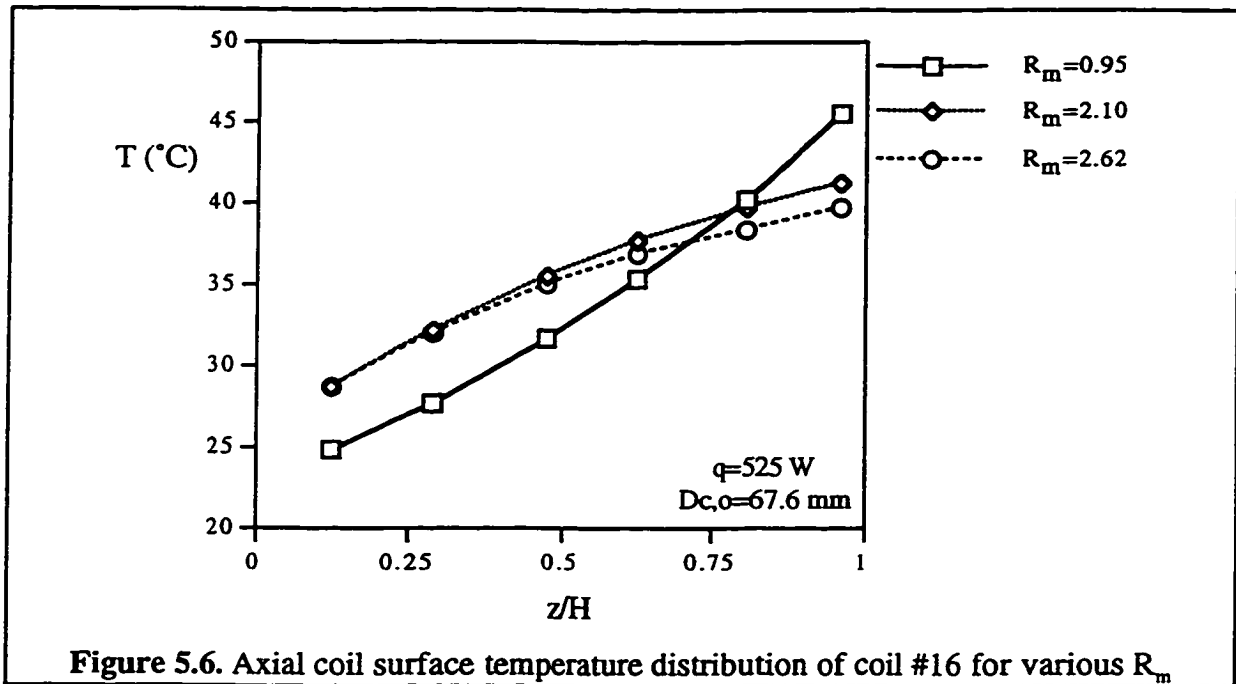


Figure 5.5. Axial temperature distribution for coils in a 77 mm diameter shell
 (a) Coil #16 (b) Coil #18 (c) Coil #21



It was found that the coil diameter does not have any influence on the shape of the temperature profiles. Figure 5.7 compares the temperature distribution along the exchanger axis for three coils with different outside diameters. It can be seen that the shape of the profiles are the same ($r^2 \geq 0.996$). The difference between the profile of the coil #3 with the others is because the water inlet temperature was higher for this coil during the test. In figure 5.5 the heat rate and the mass flow rate ratio are fixed. The same trend was observed for other coils.

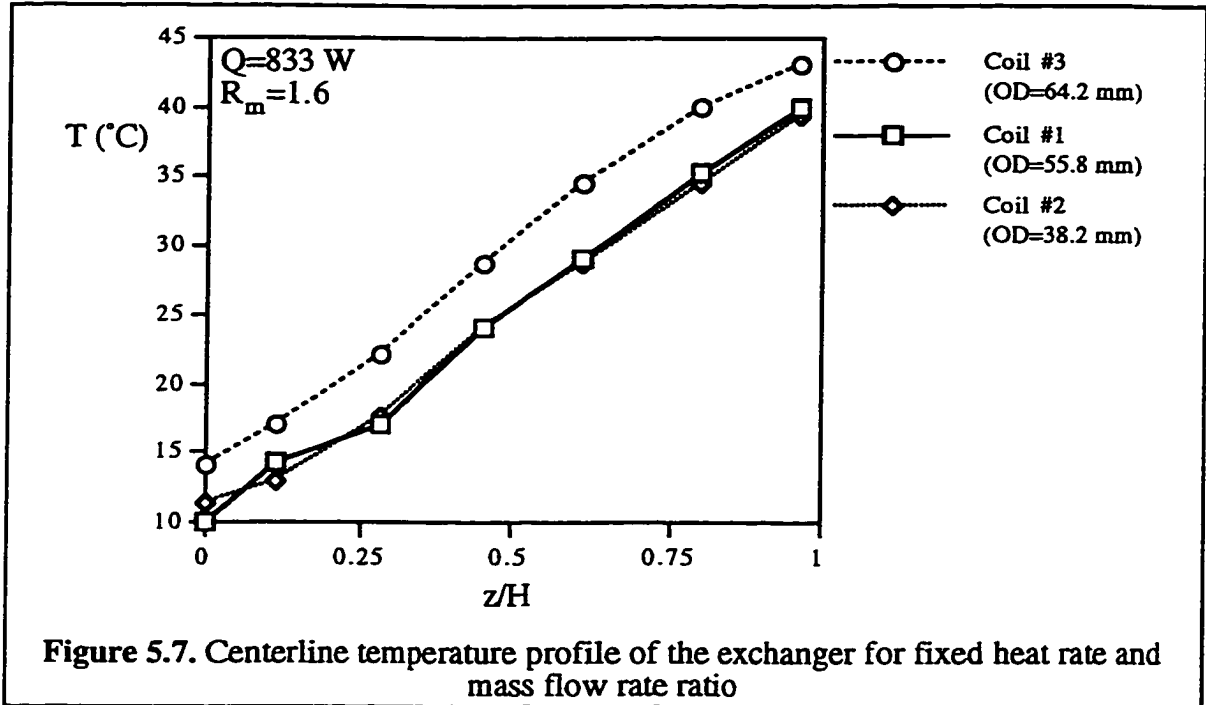
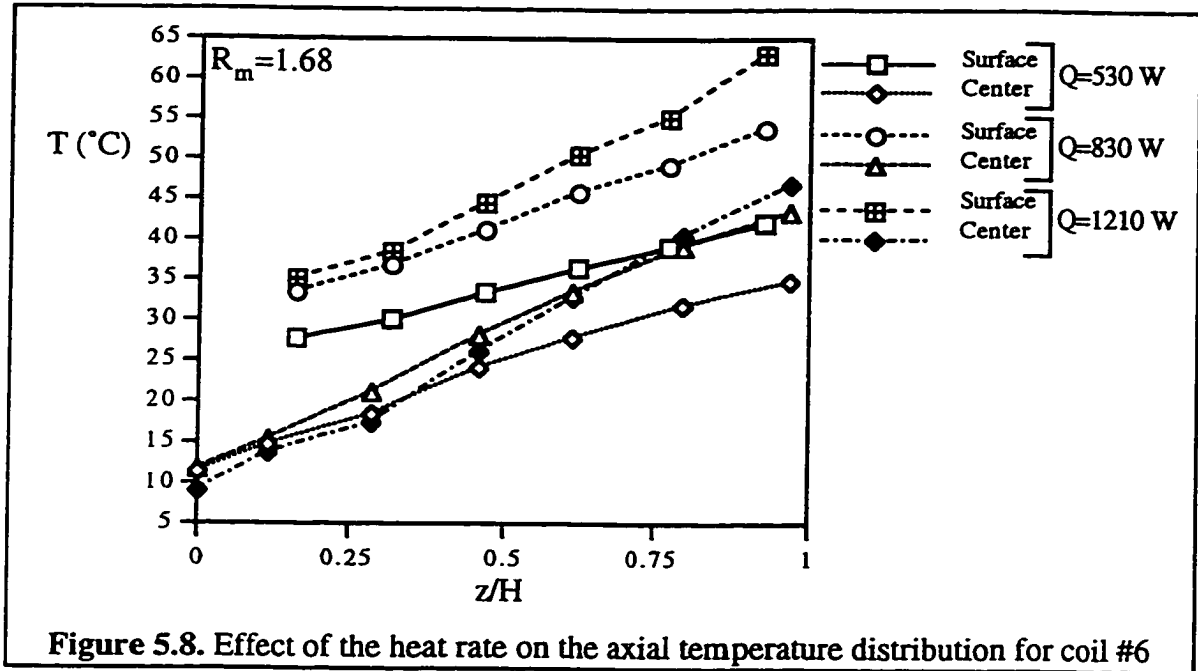


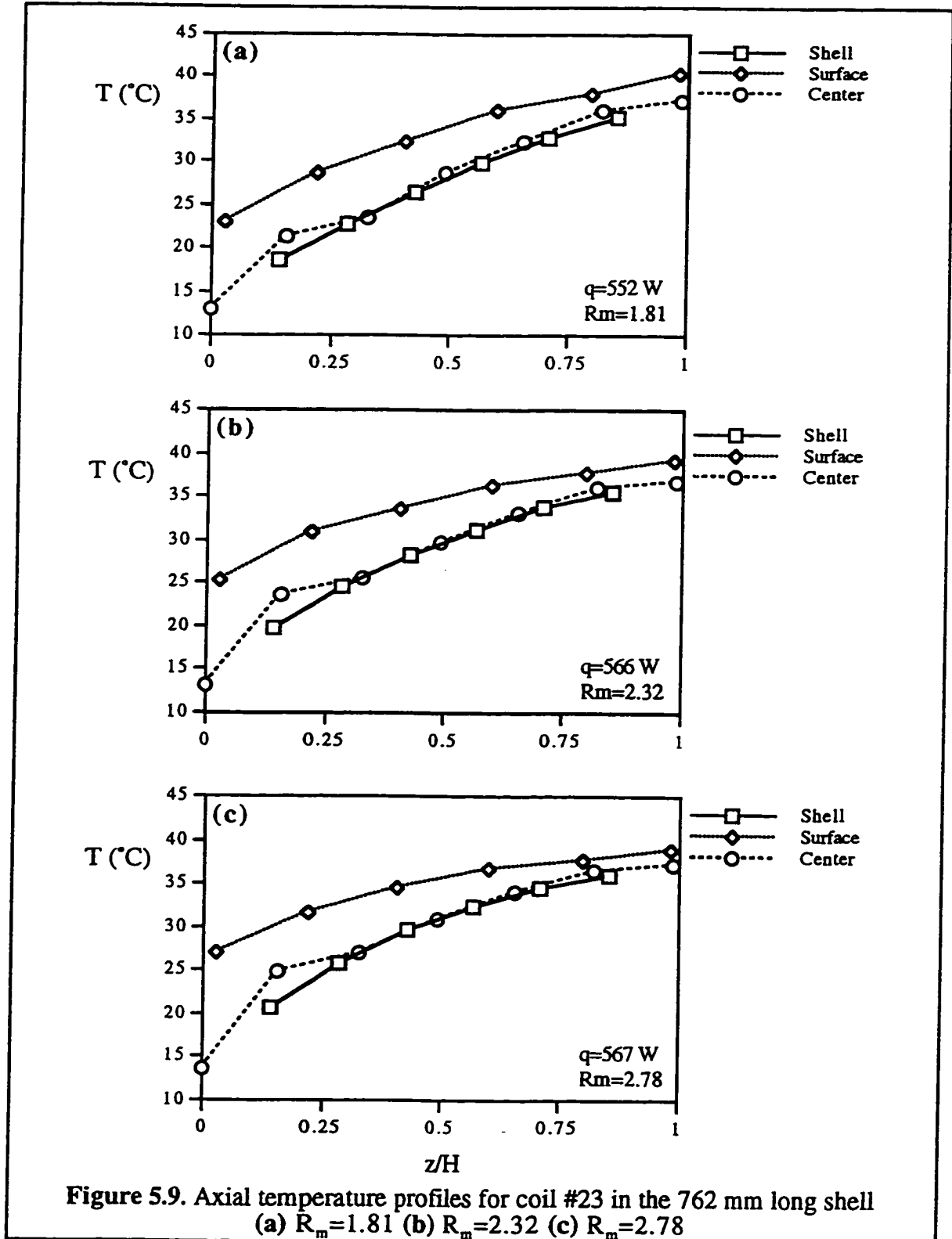
Figure 5.8 is a typical graph of the axial temperature distribution on the coil surface and the centerline of the exchanger for a fixed mass flow rate ratio but different rates of heat transfer. The effect of increasing the heat rate is to increase the slope of the profiles for both the coil surface and water on the centerline. A similar effect was always observed for all the coils. The value of $R_m=1.68$ was chosen so that a nearly linear profile ($r^2=0.994$) was attained.

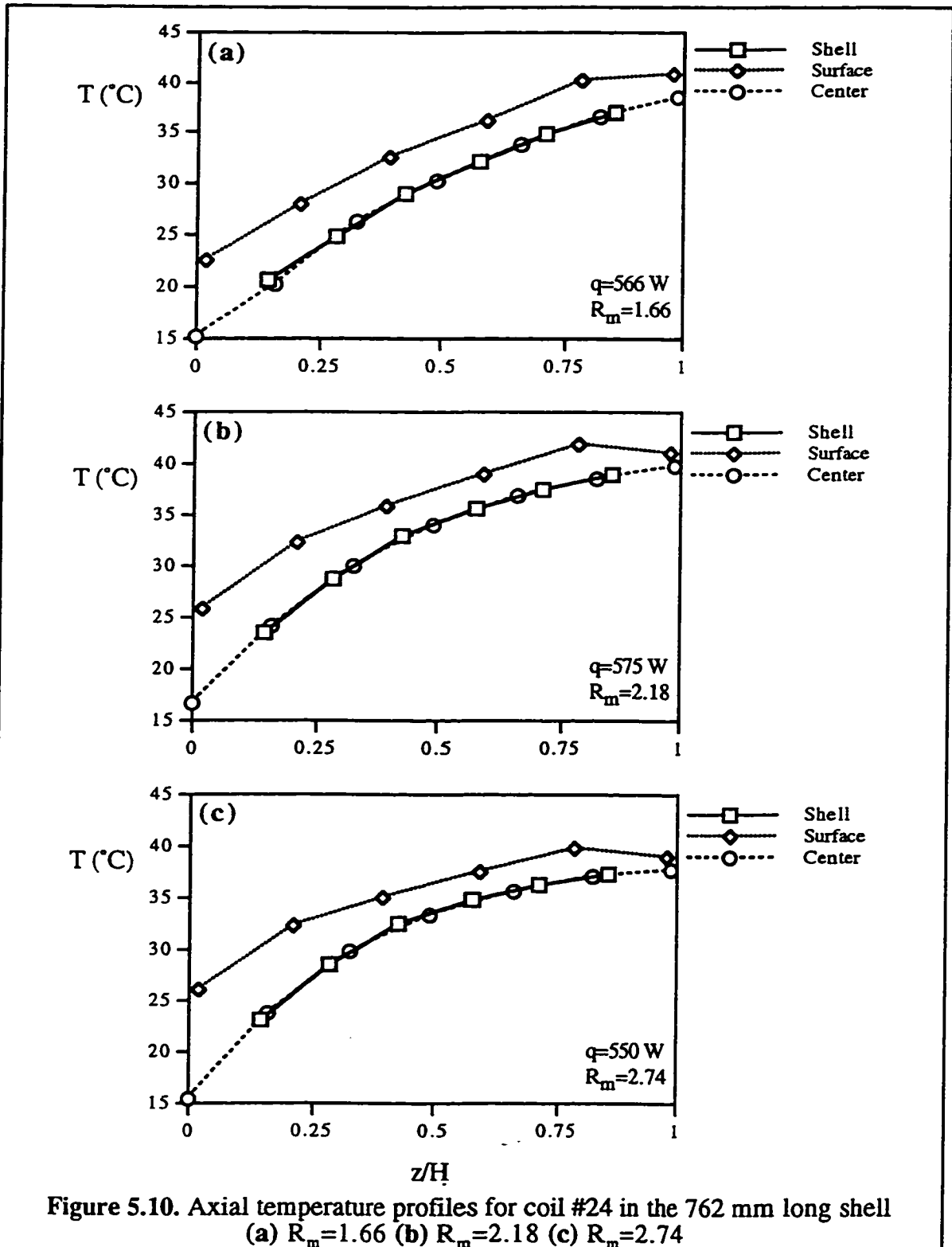


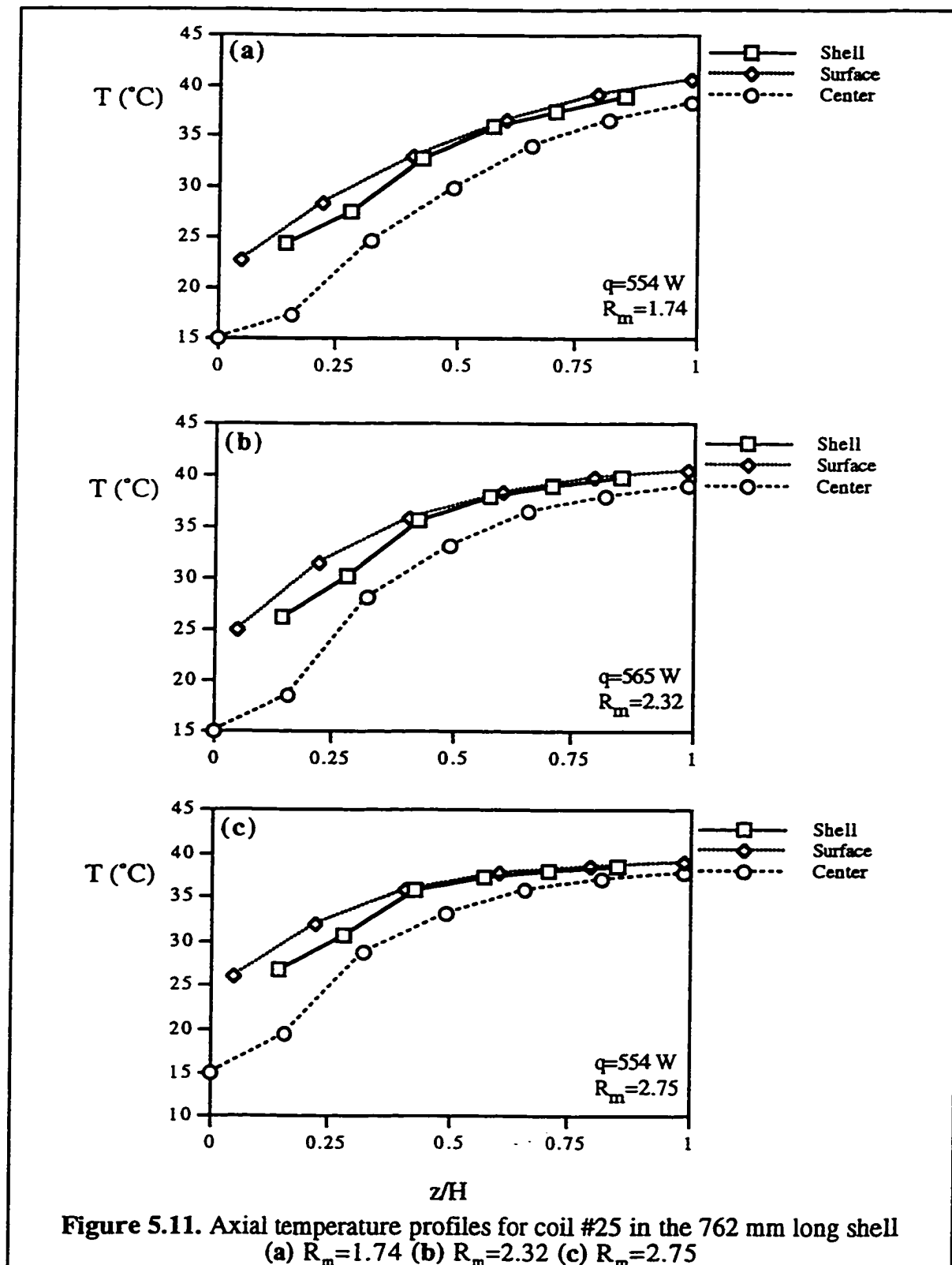
5.1.1.1. The effect of coil height

From figures 5.9 to 5.11 it is evident that the shape of the individual profiles does not change with the height of the heat exchanger and generally the same conditions of the 382 mm long shell prevail. Again the changing behavior of the local shell-side heat transfer coefficient along the axis of the exchanger can be observed. Since in all cases the value of R_m is greater than 1, the profiles take the quadratic form and therefore h_o decreases from its highest value at the top to its lowest point at the bottom of the exchanger.

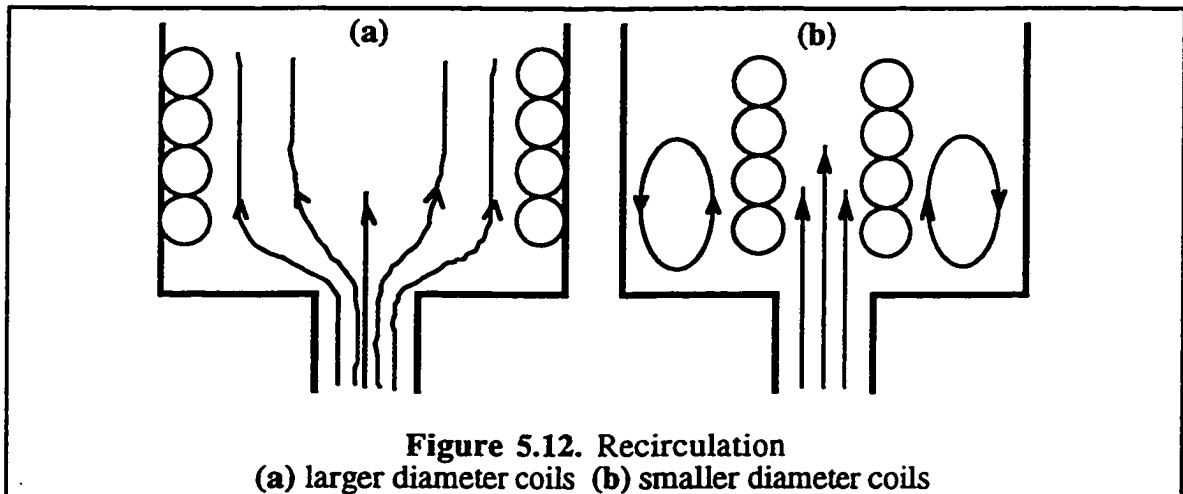
The water temperature outside the coil, which is noted as the shell temperature in the figures, is 16% closer to the coil surface temperature for coil #25 than those of coil #23. This was expected because coil #25 has the largest diameter among the three and also the outer side of its surface is nearly in contact with the heat exchanger shell. This is why in figure 5.11(a)-(c) a cold column of water exists in the core area of the bottom 25% of the exchanger height especially for the case $R_m=1.74$. It is then reasonable to assume that for the range tested, the height of the exchanger is not an influential factor in changing the temperature profiles in comparison with those for the 382 mm long shell.







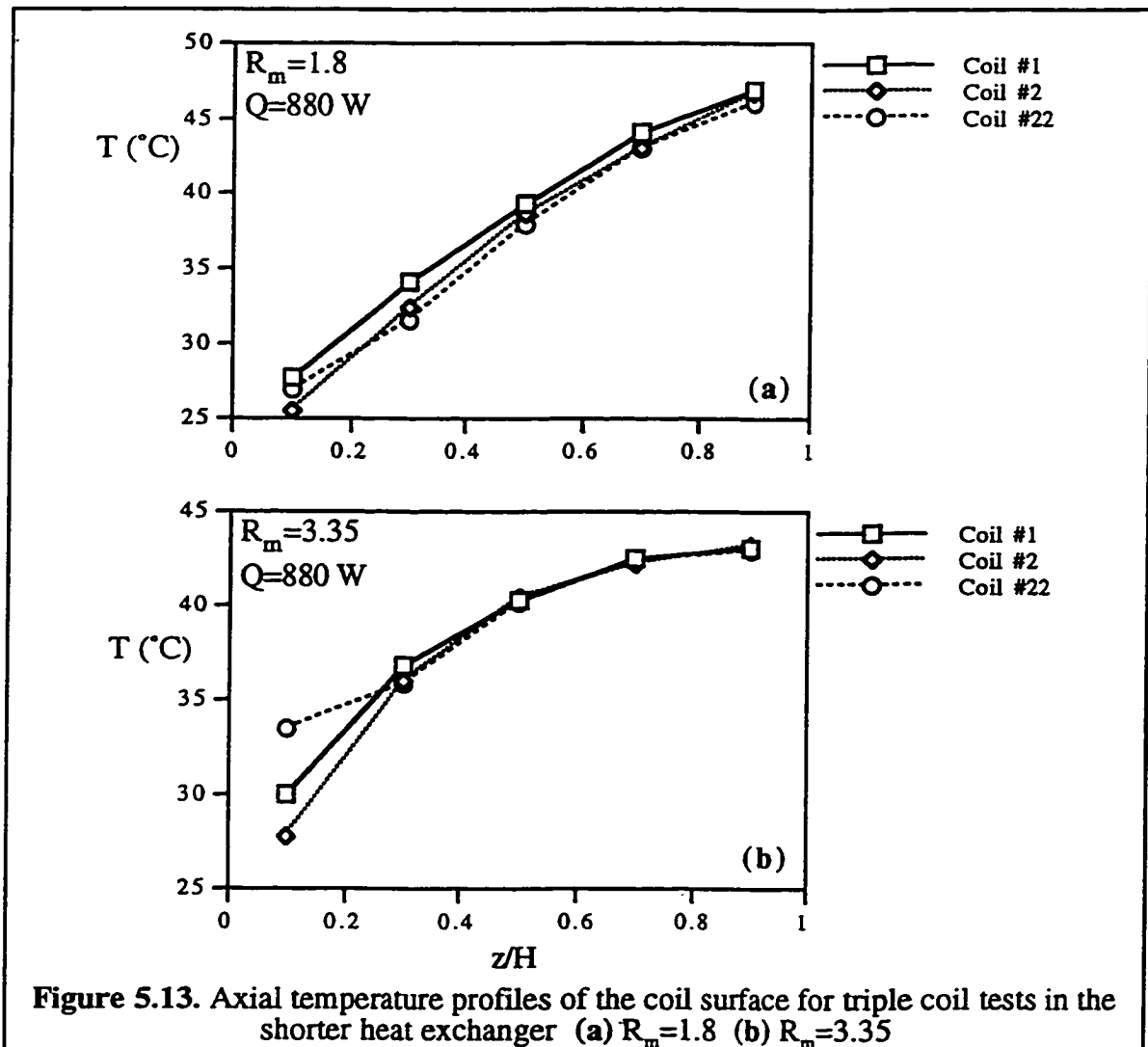
The above argument about the large diameter coils can be moved further to include its effect on possible flow recirculation. As it is shown schematically in figure 5.12 smaller diameter coils are more likely to cause recirculation between the coil and the shell. Flow recirculation was detected by temperature fluctuations especially in the lower part of the heat exchanger. This can be explained as follows. There is no doubt that the higher velocity streams are close to the coil surface regardless of the coil diameter. For larger diameter coils where the outer wall is nearly in touch with the inner side of the shell, the colder areas of water are limited only to the centerline of the exchanger. Since the water inlet port is located at the center, a jet flow in that area will be established which forces the cold stream of water at the center to mix with warmer streams near the coil surface. As a consequence, a relatively smooth flow of water can be achieved. For smaller diameter coils there exists a large space between the outer surface and the shell inner surface. In these areas there is no jet flow available to prevent the flow from recirculating. Therefore streams of water trapped between the hotter surface of the coil and the colder surface of the shell, not having enough driving force, start flowing in circulatory paths.



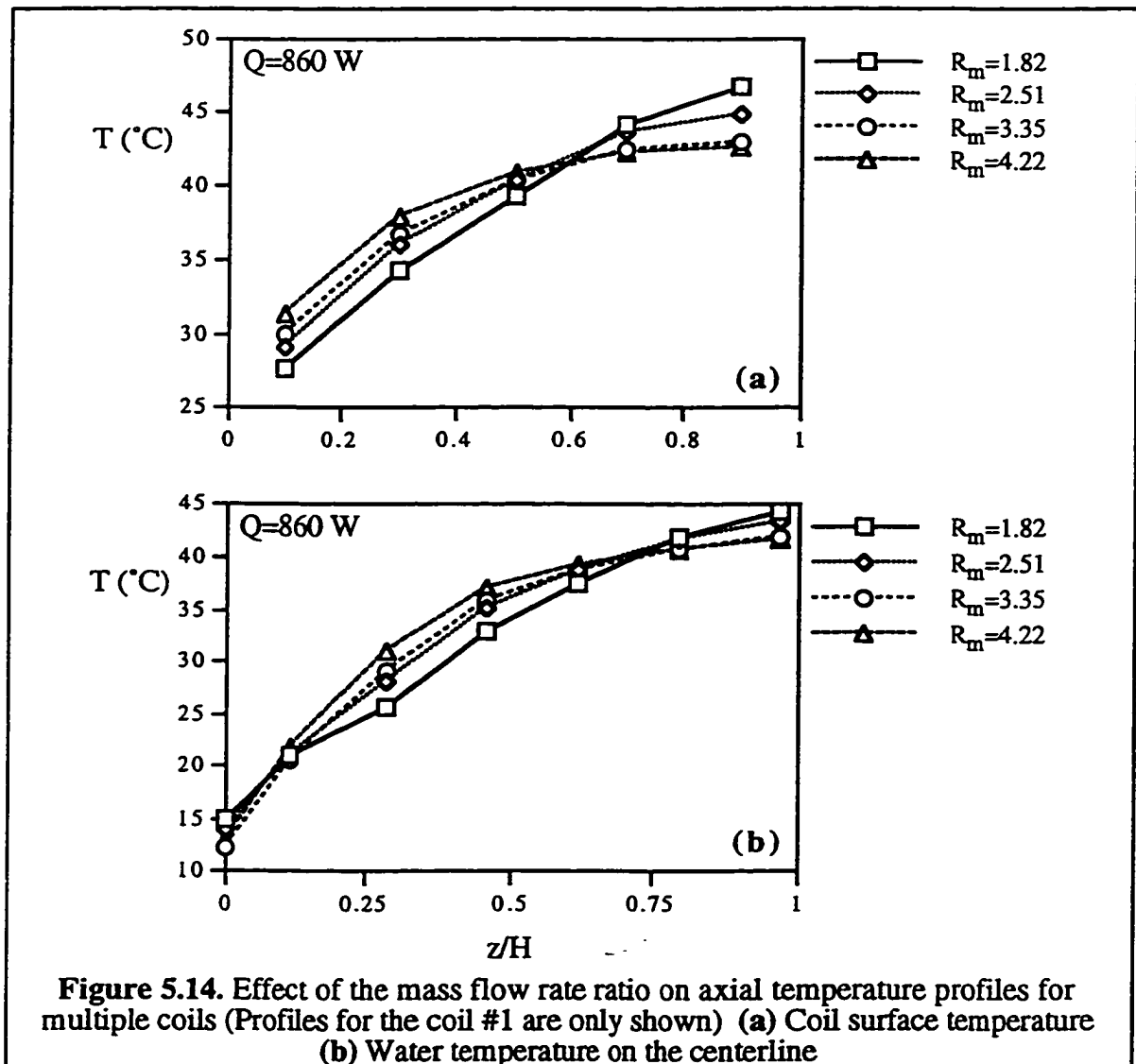
5.1.2. Multiple coils

The coil surface temperature profiles were found to be the same for all the three coils in triple coil tests provided that the heat rates and the mass flow rate ratios are kept the

same. Figure 5.13(a) compares these profiles for constant heat rate and mass flow rate ratio. A slight increase in temperatures with decreasing coil diameters can be detected. This slight increase vanishes when the mass flow rate ratio is high. It must be noted that here the total glycol mass flow rate passing through all three coils has been considered. Figure 5.13(b) repeats the same conditions as before except for a higher value of R_m . In both cases no significant difference ($r^2 > 0.996$) is detectable from the shape of the profiles for the individual coils.



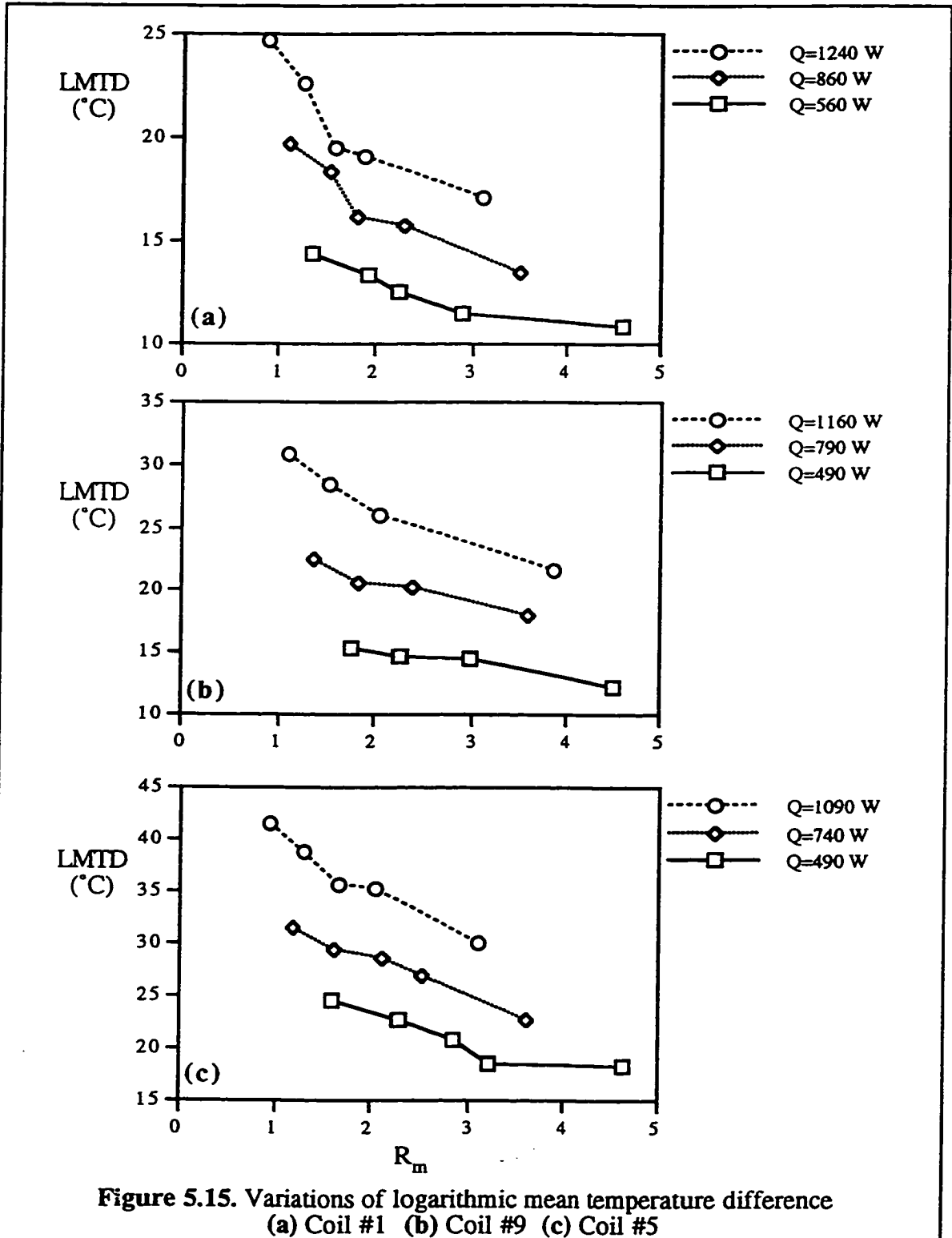
The effect of the mass flow rate ratio was found to be also the same as in single coils. Increasing R_m bends the profiles to a concave down shape. Again the total glycol flow rate was considered rather than the flow rate through each of the coils. Figure 5.14(a) indicates this trend for the coil #1 surface temperature in a triple coil configuration. The water temperature on the centerline is shown in figure 5.14(b) for the same exchanger with triple coils. It appears that the influence of R_m is not as strong on the water temperature compared to the coil surface temperature. However the concave down form of the profiles for relatively high R_m values are distinguishable.

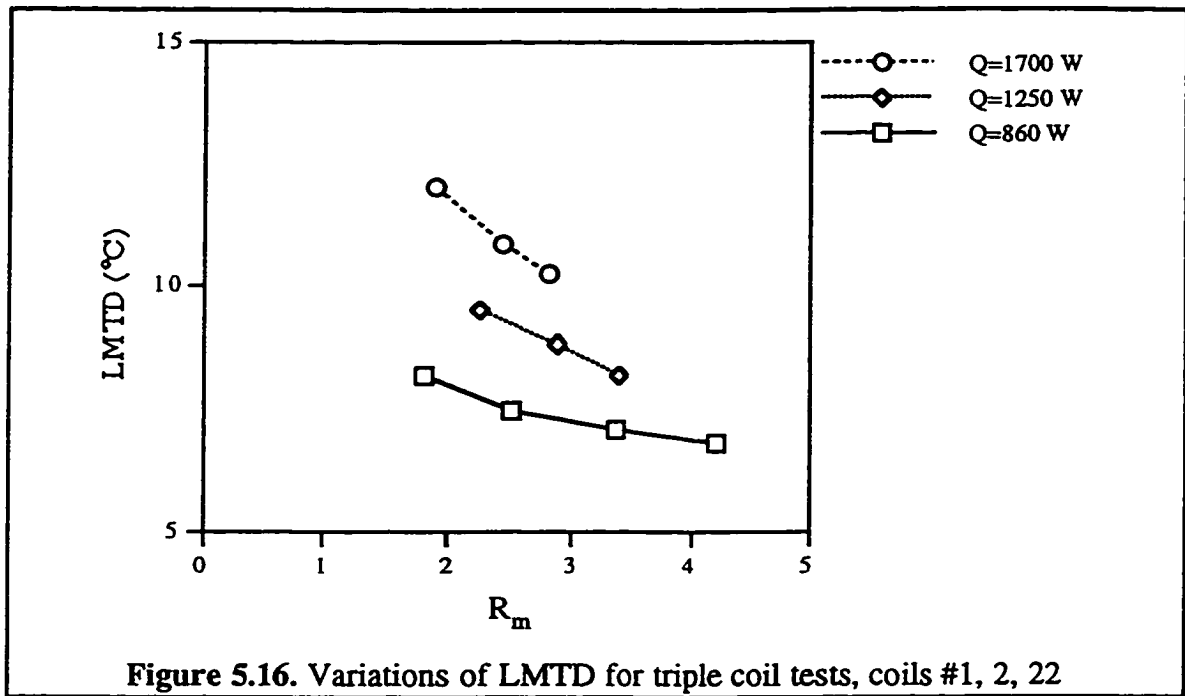


5.2. Logarithmic mean temperature difference

The logarithmic mean temperature difference (LMTD) decreases as the mass flow rate ratio increases for a fixed heat rate. This is evident from figures 5.15(a)-(c) which are typical of the behavior of LMTD. Also it is seen that for a fixed value of R_m , the effect of increased heat rate is to increase the value of LMTD. In these graphs the range of the heat rate and the mass flow rate ratio is nearly the same. The slope of the graphs becomes less as the heat rate decreases. This is in accord with the trend observed in graphs of coil surface temperature profiles.

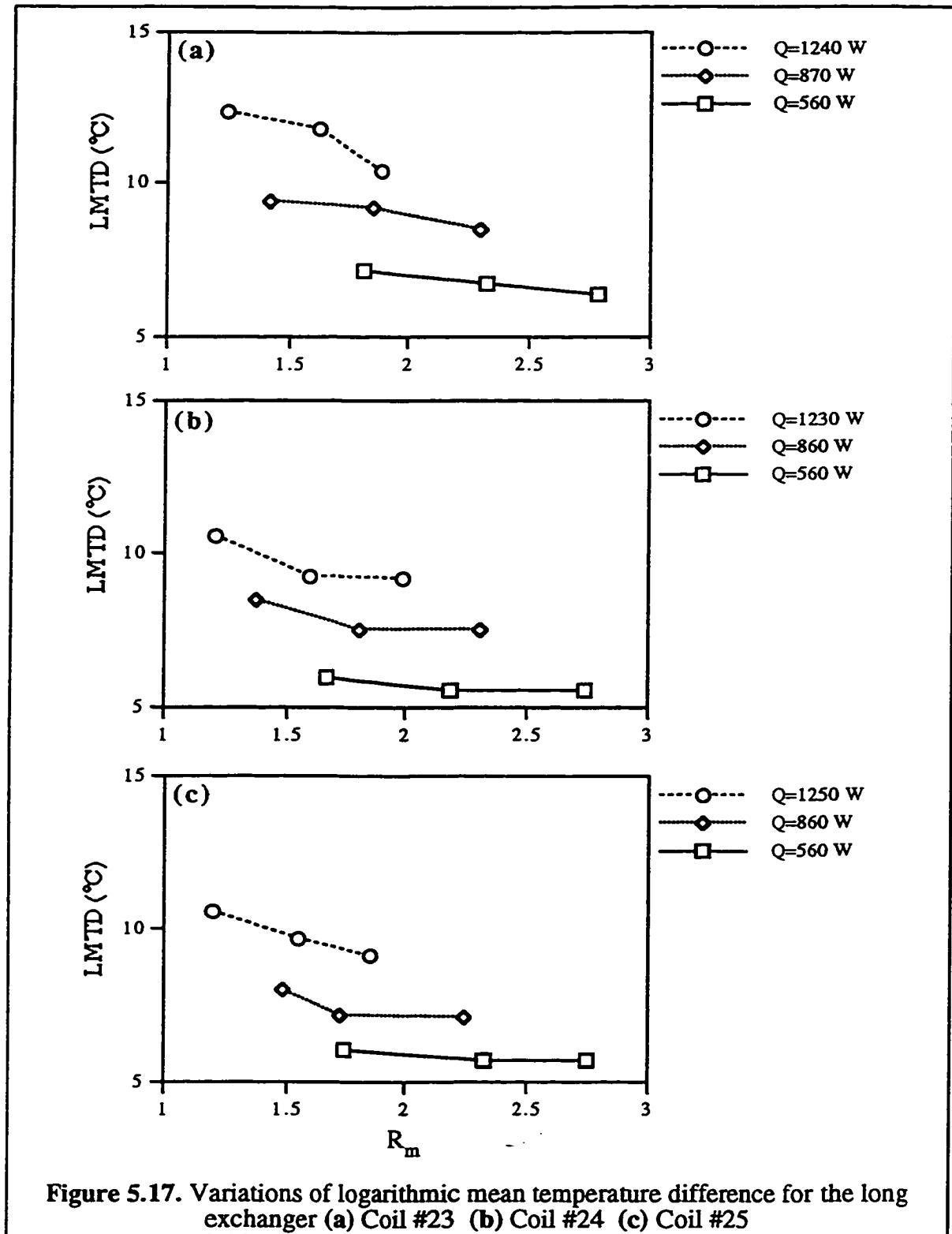
Also each individual curve experiences a flattening effect as the mass flow rate ratio increases, especially for lower rates of heat transfer. In other words, further increasing the glycol mass flow rate, when the heat rate is relatively low, will not decrease the value of LMTD further. This implies that the combination of low heat rate and high glycol flow rate is inefficient. This is because further increasing the glycol mass flow rate will not result in an increased UA value. Therefore the extra electrical power utilized by the glycol loop pump has not brought any extra performance to the heat transfer process. This once again points to the existence of an optimum value for the glycol mass flow rate as stated by Hollands and Brunger (1992).





Multiple coil tests also indicate that the same trends as explained for single coils are prevalent. This is seen in figure 5.16 which shows the variations of the logarithmic mean temperature difference with the heat rate and the mass flow rate ratio. Although the number of data points on each curve is not quite enough to firmly establish a trend, more or less the curves confirm the findings for the single coil tests. For the sake of ease of comparison the scale of the abscissa in figure 5.16 has been kept in the same range as in figures 5.15(a)-(c). Once again it must be mentioned that the total glycol flow rate was used in calculating R_m .

Figures 5.17(a)-(c) indicate that for the shell height of 762 mm also the same trends as in the 382 mm long shell are dominant. The LMTD drops with decreasing the heat rate for a fixed value of R_m . Moreover for low heat rates, the mass flow rate ratio has little effect on the variations of the logarithmic mean temperature difference. The diameter of the coils again is not influential.



5.3. Modified effectiveness

Fraser *et al.* (1995) assumed that the curves of the modified effectiveness versus the water mass flow rate are universal provided that the glycol mass flow rate is fixed. They made use of the assumption of universality in order to develop an empirical model for natural convection heat exchangers in SDHW systems. They also showed this universality by tests on one NCHE having four coils inside.

Current investigations showed that when the modified effectiveness is plotted versus the mass flow rate ratio the correlation between the data is not satisfactory. The length of the coil was found to be an influential parameter. Nevertheless, the assumption of universality made by Fraser *et al.* (1995) remains valid for a fixed heat exchanger. The mass flow rate ratio must be modified by a multiplier involving the length of the coil. Since the modified effectiveness was found to be higher for longer coils, a factor of $(H/L)^{0.3}$ was found suitable. In figure 5.18 the modified effectiveness as defined by equation 3.29 is plotted as a function of the mass flow rate ratio corrected for the effect of length for all the test configurations. This means that the data in figure 5.16 includes both shell diameters of 51 and 77 mm and shell heights of 382 and 762 mm.

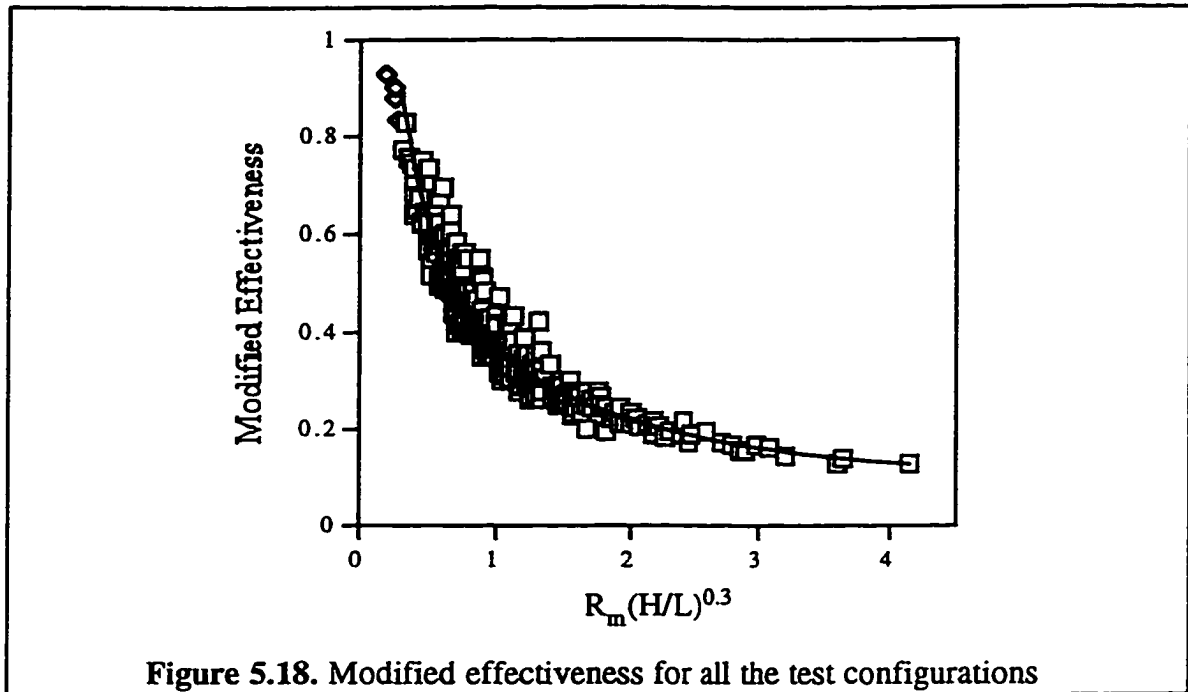


Figure 5.18. Modified effectiveness for all the test configurations

As can be seen in figure 5.18 the slope of the curve falls rapidly as the value of the corrected mass flow rate increases. For $R_m(H/L)^{0.3} < 1$ a slight decrease will result in a considerable improvement of the exchanger effectiveness, while for values larger than 2, the modified effectiveness remains nearly unchanged. This means that for a certain heat exchanger increasing the glycol mass flow rate will always downgrade the effectiveness. This effect is more intense for lower flow rates.

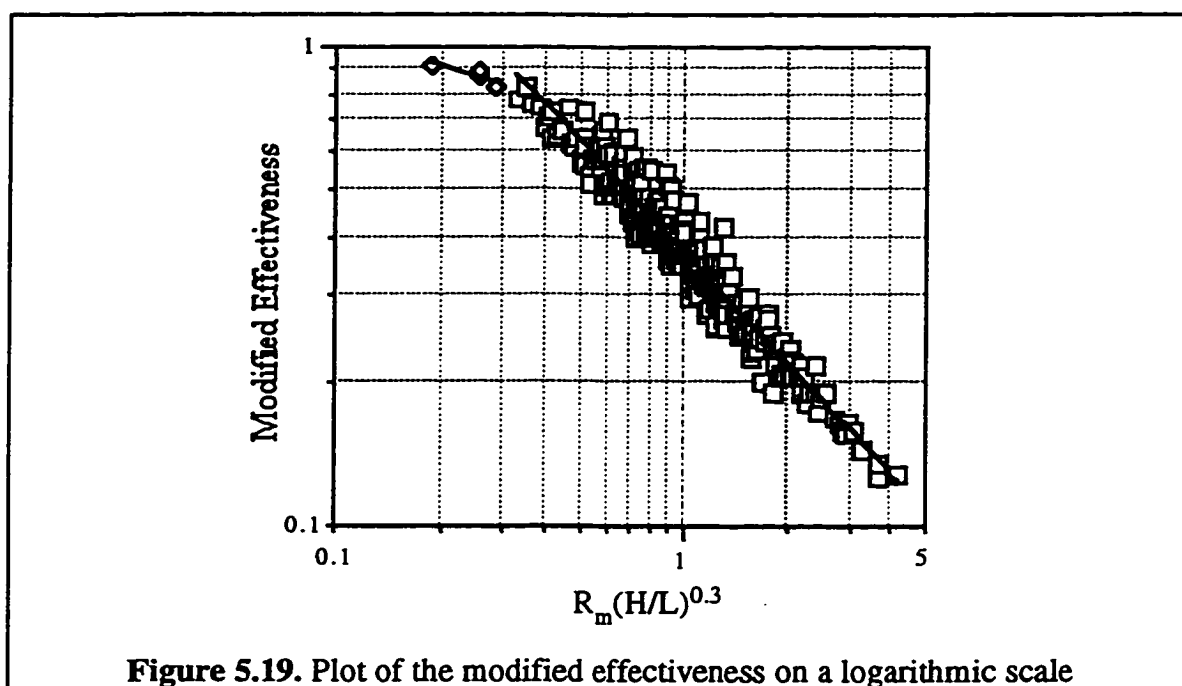
The data can be correlated by a simple power equation. Figure 5.19 is a replot of the data on figure 5.18 on log-log scales. The logarithmic-scale graph reveals that for the corrected mass flow rate ratios of less than 0.3, the data points tend to follow an asymptotic curve towards that maximum value of 1 for the modified effectiveness. This maximum value is achieved by very small glycol flow rates. Because of this asymptotic behavior the data must be divided into two ranges and different curves must be fit to the two regions. Equation 5.1 is recommended for predicting the effectiveness of the heat exchanger in the range $0.3 < R_m(H/L)^{0.3} < 5$ and $1.85 \times 10^{-3} \leq \dot{m}_g \leq 34.3 \times 10^{-3}$ kg/s.

$$\varepsilon' = 0.37 \left(\frac{\dot{m}_w}{\dot{m}_g} \right)^{0.77} \left(\frac{L}{H} \right)^{0.23} \quad 5.1$$

The coefficient of determination for equation 5.1 is 0.94. For the range $R_m(H/L)^{0.3} < 0.3$ a different correlation must be used (equation 5.2).

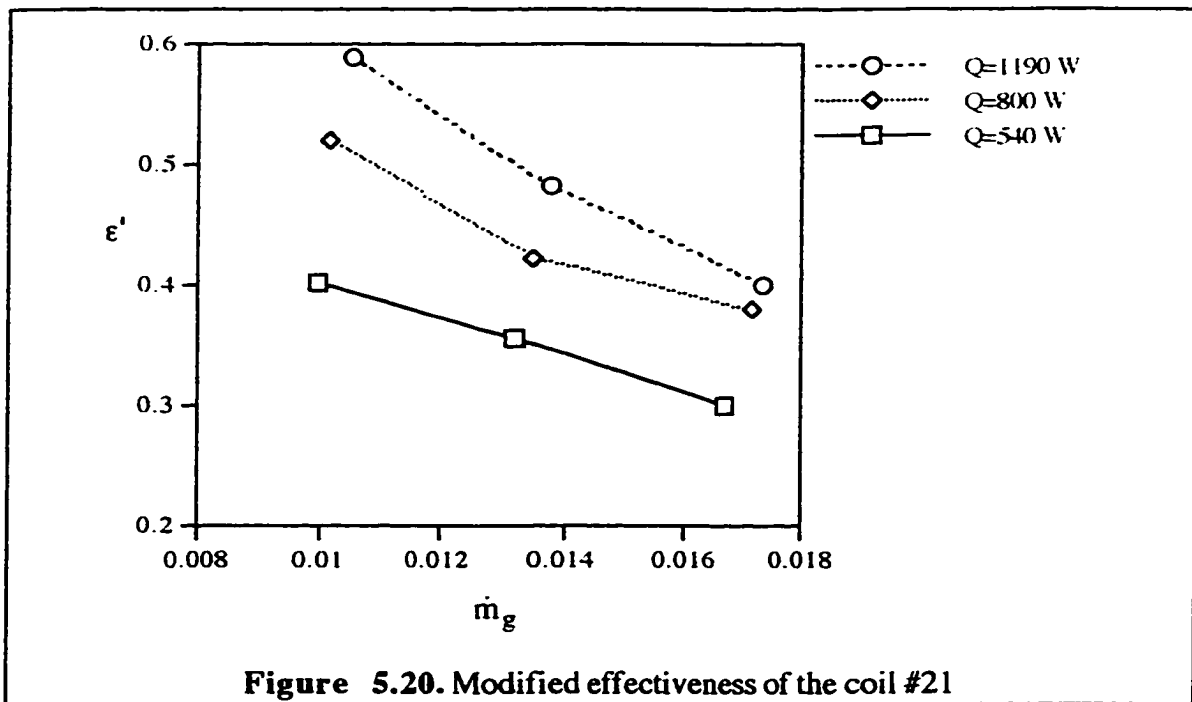
$$\varepsilon' = 0.64 \left(\frac{\dot{m}_w}{\dot{m}_g} \right)^{0.22} \left(\frac{L}{H} \right)^{0.066} \quad 5.2$$

The use of equation 5.2 is not recommended until additional data is at hand to confirm the trend. As can be seen from figure 5.19, very few data points are available in this range. As a result, the coefficient of determination for equation 5.2 is not better than 0.72.



The tube diameter has little effect on the modified effectiveness since it does not appear in equation 5.1. Also from equation 5.1 it can be found that the coil diameter and the shell diameter both are ineffectual in terms of influencing the modified effectiveness.

To look into more details of the behavior of the modified effectiveness, figure 5.20 must be considered. It was found that no matter what the shell diameter or height is, the modified effectiveness for a fixed heat rate always drops as the mass flow rate ratio increases. An increase in the heat rate always increases ϵ' provided that the value of \dot{m}_g is kept constant.



Equation 5.1 indicates that ϵ' is a strong function of the mass flow rates and a weaker function of heat exchanger height and coil length. The water flow rate has a favorable effect and glycol flow rate has an adverse effect on the modified effectiveness of the exchanger. Physically, more water flow means more heat extracted from the hot stream and therefore a greater temperature fall in that stream which translates to better effectiveness. On the contrary, more glycol flow leads to less temperature fall in the hot stream and consequently worsens the effectiveness of the exchanger. The two mass flow rates, therefore act against each other with the same strength. In natural convection

systems, the water flow rate is not directly under the control of the user but rather it is the collective effects of various parameters that determines its magnitude.

The term L/H in equation 5.1 can be called the exchanger compactness ratio since for a fixed exchanger height the more length of tube is fit into the exchanger the more compact the exchanger will be. Although the effectiveness is not influenced by the compactness ratio as strongly as by the mass flow rate ratio, still increasing the compactness ratio will improve it. In other words, adding more length to the coils inside the heat exchanger while its height is fixed, will moderately increase ε' and vice versa.

Ajele (1995) proposed a correlation for multiple coil tests of shell-and-coil natural convection heat exchangers, which differs from equation 5.1. Equation 5.3 is the equation proposed by Ajele for the range $0.01 < \dot{m}_g < 0.03$ kg/s.

$$\varepsilon' = 0.59(S')^{(-1/3N)} \left(\frac{\dot{m}_w}{\dot{m}_g} \right)^{0.80} \quad 5.3$$

In equation 5.3 the exponent of the term $\left(\frac{\dot{m}_w}{\dot{m}_g} \right)$ is in close agreement with the result of the current research. However, Ajele reached the conclusion that the other influential parameters are the modified dimensionless space of the heat exchanger and the number of coils. S' is related to the shell diameter as well as the coil diameters. Knowing that equation 5.3 is valid for exchangers with two to four coils, the exponent of S' varies between -0.08 to -0.17. In any case, this is a very weak dependence. In the current research, it was found that the data points from the 51 mm ID shell blend in nicely with other data, suggesting that the shell diameter does not have a strong influence on the modified effectiveness. As to the length of the coils and the exchanger height, Ajele's equation has no suggestion. This is not surprising since Ajele only tested coils in a fixed diameter and height shell and therefore did not have adequate data to draw any conclusions.

The effect of the coil pitch can not be separately addressed. It can be said that for a fixed height and a certain number of coils inside the heat exchanger, the lower the pitch value is, the longer the coil will be. In other words, lower pitch values contribute in

increasing the compactness ratio of the exchanger and hence the effect of the coil pitch can be integrated with the effect of the compactness ratio.

Using the definition of the modified effectiveness and equation 5.1, one can easily derive equations for predicting the glycol and water outlet temperatures.

$$T_{h,o} = T_{h,i} - 0.37 \left(\frac{\dot{m}_w}{\dot{m}_g} \right)^{0.77} \left(\frac{L}{H} \right)^{0.23} (T_{h,i} - T_{c,i}) \quad 5.4$$

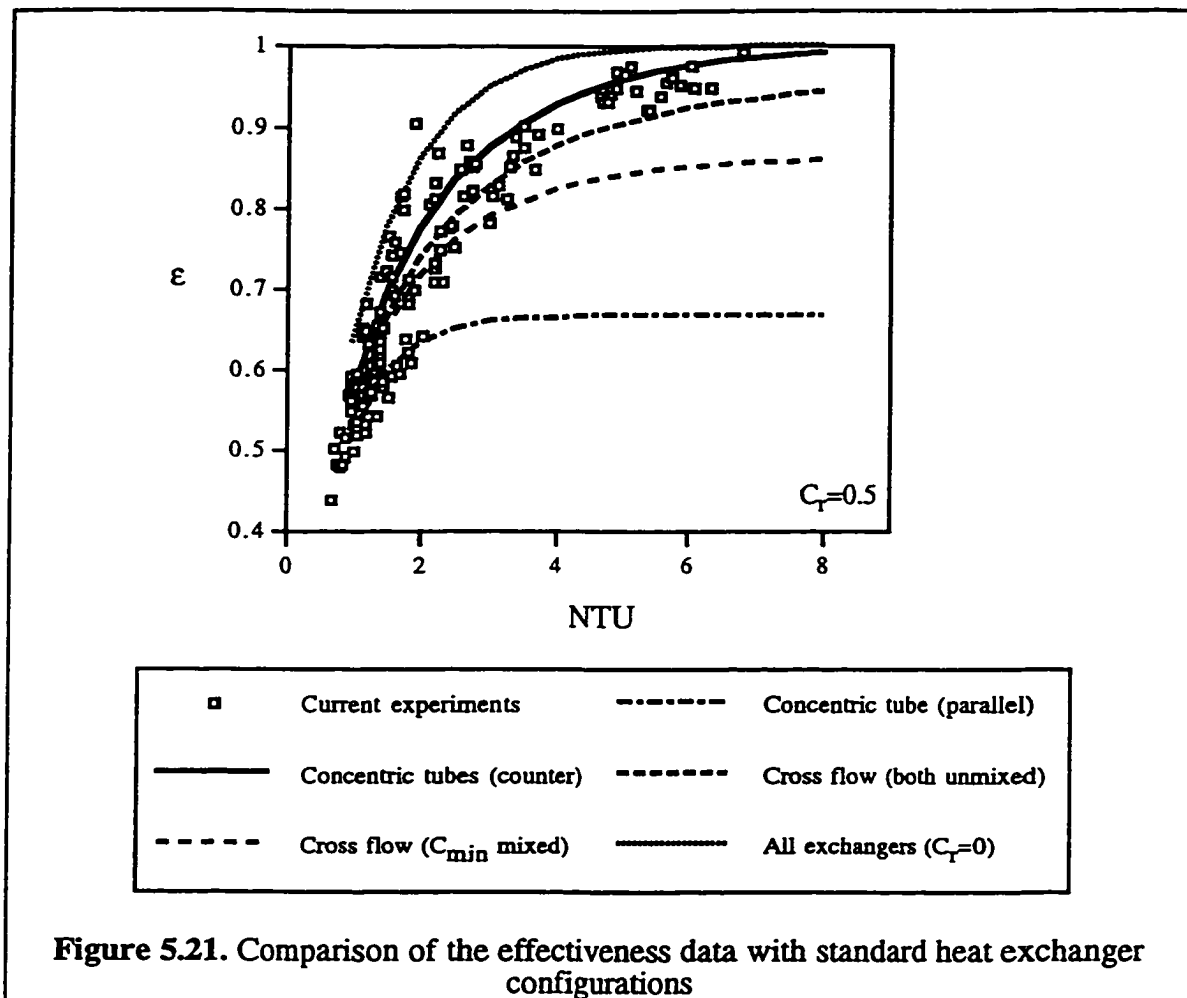
$$T_{c,o} = T_{c,i} + 0.37 \frac{c_{p,g}}{c_{p,w}} \left(R_m \frac{L}{H} \right)^{0.23} (T_{h,i} - T_{c,i}) \quad 5.5$$

In general, the inlet temperatures are known, thus making the prediction of the outlet temperatures possible by using equations 5.4 and 5.5. Equation 5.5 implies that increasing the compactness of the exchanger will increase the water outlet temperature but only to a slight degree. Glycol mass flow rate also has the exact same effect on $T_{c,o}$.

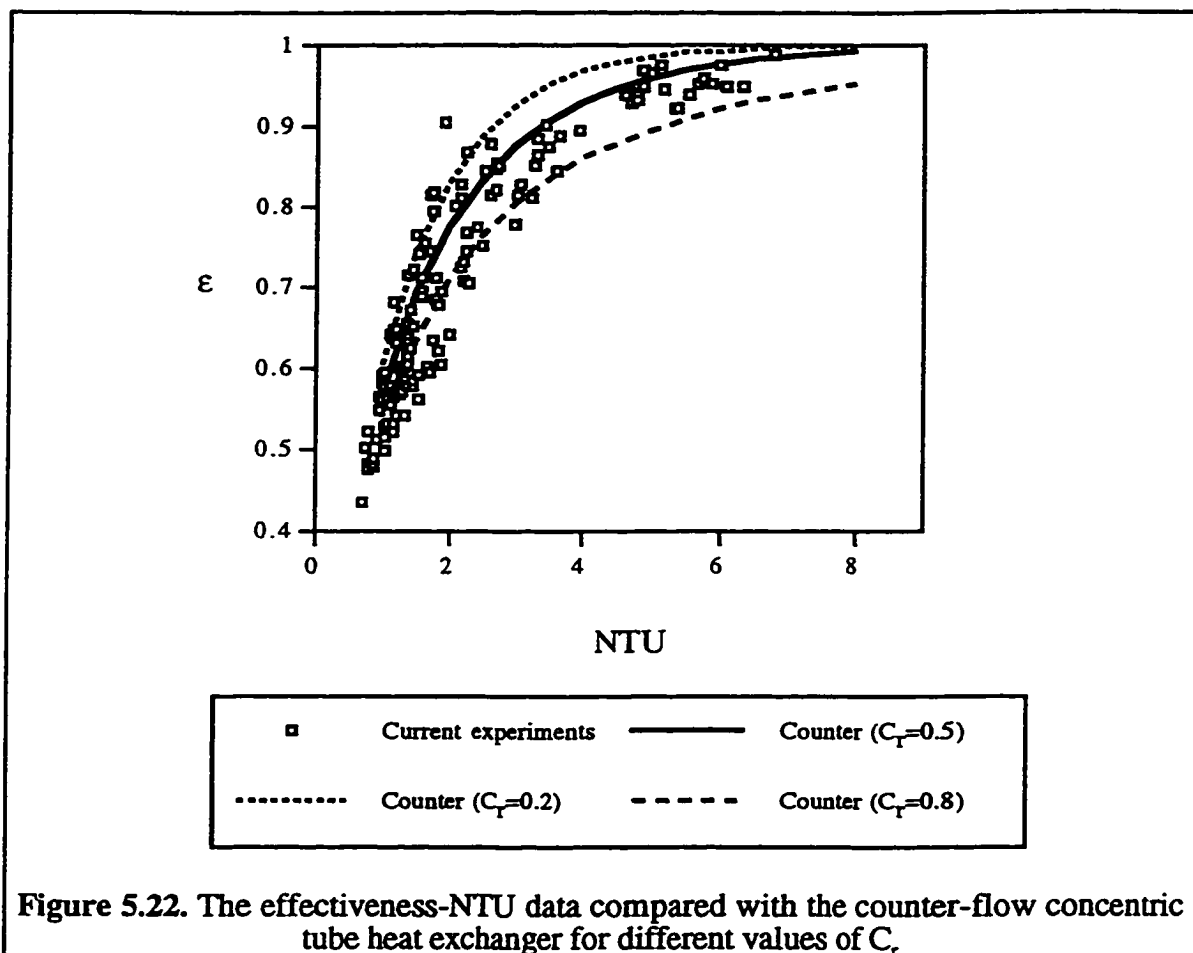
5.3.1. Effectiveness-NTU relation

In order to establish the effectiveness- NTU relations for the shell-and-coil heat exchangers, the data were plotted together with the plots for some standard configurations in figure 5.21.

In figure 5.21 the ε - NTU relationship for parallel and counter flow concentric tube heat exchangers, cross flow with both fluids unmixed and cross flow with the C_{min} fluid mixed are plotted for the case $C_r=0.5$ as an average value. In addition, for the sake of comparison the general ε - NTU for all heat exchangers with $C_r=0$ is also plotted in the same figure.



From figure 5.21 the effectiveness of the parallel-flow concentric tube heat exchanger is the lowest of all and is far below the values observed in the current experiments for $NTU > 2$. The case of $C_r=0$ would overpredict the effectiveness if used for the current case. This case can be attributed to the situation where the flow rate of one of the fluids is so small that it can be considered stagnant. The relation for the cross-flow case with one of the fluids mixed, if used for current situation would underpredict the data and therefore is not suitable. Two cases that can closely predict the data are the cross-flow with both fluids unmixed and the counter flow concentric tube heat exchanger. Among those two, the counter-flow configuration is the closest in reality and also on the graph. In order to double check this observation, figure 5.22 must be considered.



In figure 5.22, the results of the current experiments are compared with the standard counter-flow relations for C_r values of 0.2, 0.5 and 0.8. It is clear that the current data are reasonably correlated by the counter-flow relations. In conclusion, it is suggested to use the ϵ - NTU relations of the counter-flow heat exchanger to predict the effectiveness of the natural convection shell-and-coil heat exchangers and also for design purposes. The standard counter-flow relations, taken from Kays and London (1984) is reproduced here as equations 5.6 and 5.7.

$$\epsilon = \frac{1 - \exp[-NTU(1 - C_r)]}{1 - C_r \exp[-NTU(1 - C_r)]} \quad 5.6$$

$$NTU = \frac{1}{C_r - 1} \ln \left(\frac{\varepsilon - 1}{\varepsilon C_r - 1} \right) \quad 5.7$$

5.4. Water flow rate

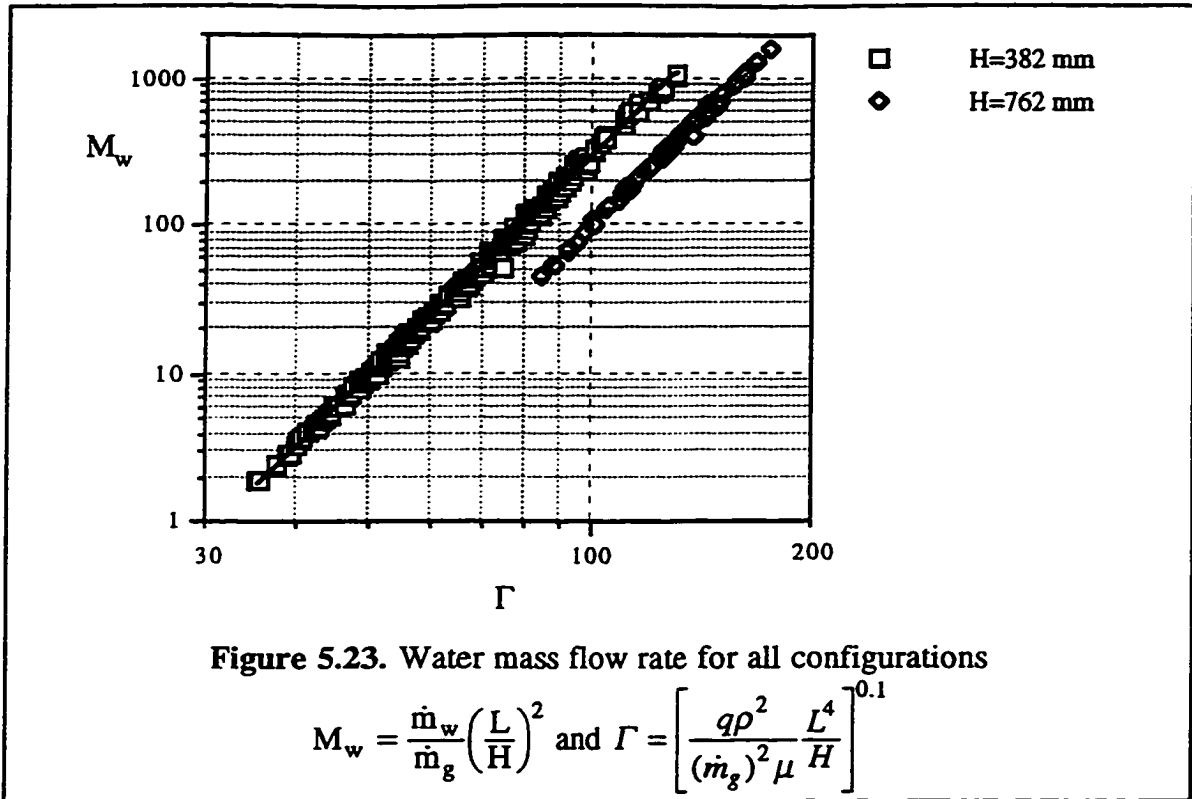
Understanding the effects of various relevant parameters on the magnitude of the water mass flow rate is of great significance. Achieving higher water flow rates is desirable since it speeds up the process of heat storage. However high flow rates will disturb stratification inside the storage tank which is damaging to the overall performance of the storage loop (Hollands and Lightstone 1989).

Figure 5.23 shows the plot of dimensionless water flow rate versus the dimensionless heat rate for all configurations. Dimensionless water flow rate and heat rate are defined in the figure caption. The best fit to the data in figure 5.23 results in equations 5.8 and 5.9 for shell heights of 382 and 762 mm respectively.

$$M_w = 4.07 \times 10^{-8} \Gamma^{4.9} \quad H=382 \text{ mm} \quad 5.8$$

$$M_w = 1.51 \times 10^{-8} \Gamma^{4.9} \quad H=762 \text{ mm} \quad 5.9$$

The coefficient of determination, r^2 , for these curve fits was 0.997. The equations are valid for $35 \leq \Gamma \leq 130$ and $80 \leq \Gamma \leq 180$ respectively. The exponent of the dimensionless heat rate is the same in both equations 5.8 and 5.9.



Equation 5.8 can be arranged in form of equation 5.10 for a better understanding of the role of each parameter on the water mass flow rate. In deriving equation 5.10 the exponents were rounded up without losing accuracy (C is a constant coefficient).

$$\dot{m}_w = Cq^{0.5} \rho \mu^{-0.5} H^{1.5} \quad 5.10$$

Heat transfer from the hot stream to the cold stream provides the driving force for the water flow and is the most influential factor. Equation 5.10 shows that increasing the heat rate will increase the magnitude of \dot{m}_w . The glycol mass flow rate does not appear in equation 5.10 meaning that it is not an influential factor in determining the water flow rate. This was expected since the glycol flow velocity at which the heat is transferred to water should not make any difference as long as the heat rate is constant.

Regarding the geometry of the exchanger, the effect of the shell height must be addressed separately because of some subtleties. The total length of the coils, L , was

canceled from both sides of equation 5.10. Therefore the length of the coils does not affect the water mass flow rate. This can be advanced further to conclude that for fixed heat rate, the surface area of the coils or the number of the coils inside the exchanger is immaterial to the value of \dot{m}_w .

Another geometrical parameter which at first appears important is the shell diameter. The fact that it was possible to obtain a best fit to the data with reasonable accuracy, without including the shell diameter suggests that D_s is also unimportant. This can be confirmed by a more detailed look at figure 5.23.

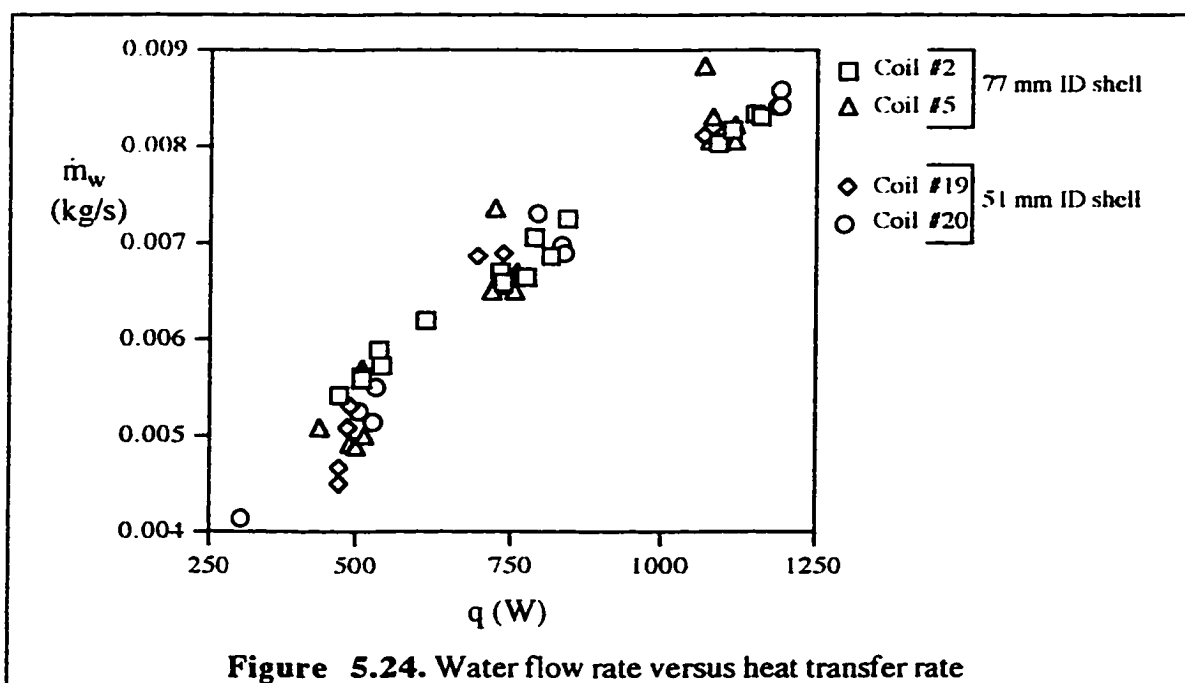


Figure 5.24 compares the water flow rate data for selected similar coils in 51 mm and 77 mm ID shell. This figure confirms that the shell diameter has little effect on \dot{m}_w since the correlation coefficient is greater than 0.975 for the data from each pair of coils. However, shell diameter has an effect on the mean velocity of water flow inside the exchanger. The smaller the shell diameter the higher the mean water velocity would be, which is likely to improve the heat transfer coefficient on the shell side.

Equation 5.10 gives an exponent of 1.5 for H suggesting a strong effect on the water mass flow rate. But this is not the case. In order to clarify the role of the shell height, equations 5.8 and 5.9 must be considered. When the shell height increases two-fold, from 382 to 762 mm, the constant multiplier of the equations decreases by a factor of 2.7. However the shell height has an exponent of 1.5 in both equations. This translates to an increase in water flow rate by a factor of 2.8. The inverse effect of the multiplier and the favorable effect of the exponent are nearly of the same magnitude. The consequent is that these two effects almost cancel each other out resulting in very little shell height influence on the water mass flow rate.

Physically, two separate effects act against each other to leave the heat exchanger height out of the correlation. On one hand, increasing H should decrease the mass flow rate by making the hot water column heavier compared to the shorter heat exchanger. This is because for a constant water temperature rise across both heat exchangers, the column of water with the longer heat exchanger is colder. On the other hand, increasing the heat exchanger height results in less hydraulic resistance in the loop thus higher water flow rates could be expected. In other words, lower water densities in the column with shorter heat exchanger also encounters more hydraulic resistance. Equation 5.10 can be modified, based on the above arguments and presented as equation 5.11.

$$\dot{m}_w = C_1 q^{0.5} \rho \mu^{-0.5} \quad 5.11$$

In equation 5.11, C_1 is a constant coefficient.

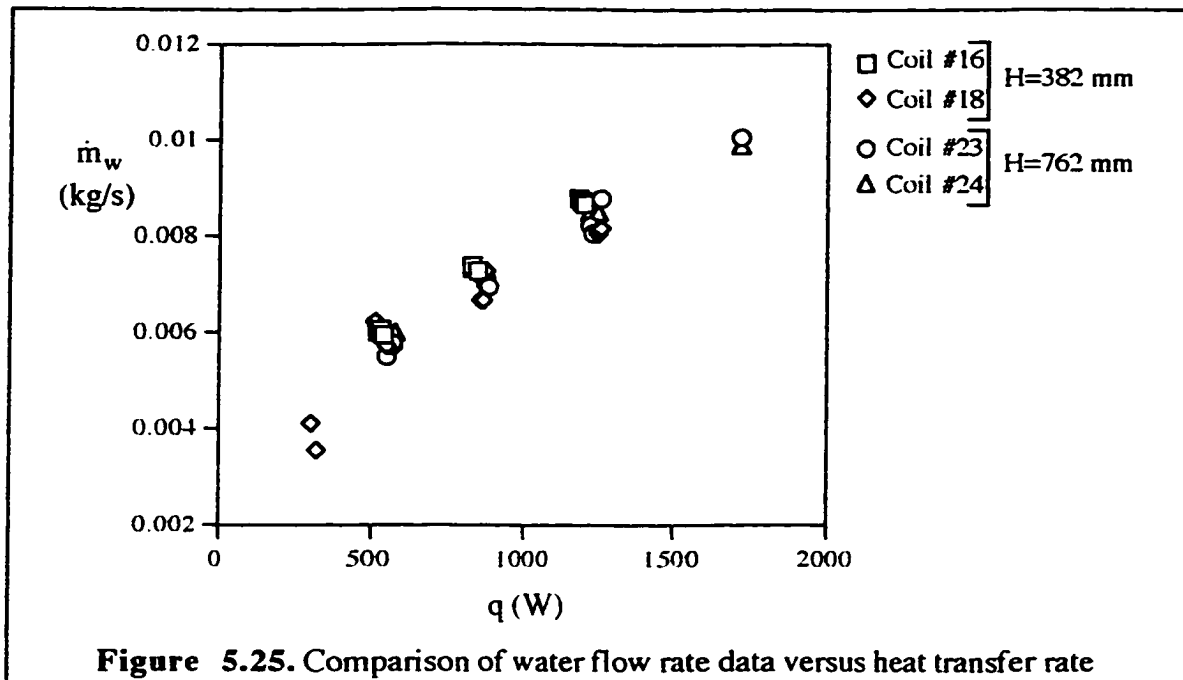


Figure 5.25 compares the water mass flow rate data from two coils in the 382 mm long shell and two coils in the 762 mm long one. Although the length of the coils was proved to be insignificant, the data presented in figure 5.25 are from coils with very close lengths. Figure 5.25 confirms that the shell height does not have any effect on the water mass flow rate (correlation coefficient is greater than 0.980).

It was found that contrary to what Ajele (1995) stated, the water flow rate data could not be correlated with the modified Rayleigh number. Ajele also proposed a correlation for the ratio of water to glycol flow rates as a function of the inlet temperatures of glycol and water. In the current thesis, attempts to obtain such a correlation produced no result with reasonable uncertainty neither for single nor multiple coils.

Finally regarding the water flow rate it must be noted that the storage tank temperature plays a crucial role. The density imbalance between the cold column of water in the storage tank and the warm column of water in the exchanger creates the flow. In all the experiments, by extracting water from the storage tank, at nearly the same rate as the exchanger water flow rate, an approximately constant temperature inside the storage tank

was ensured. This constant tank water temperature makes the comparisons made in the above paragraphs possible and reliable.

Also it must be noted that the auxiliary parts of the storage loop impose a significant effect on the water flow rate. These are the parts that define the total hydraulic resistance of the loop. They consisted of the connecting tubes and hoses, valves, tube fittings and the shape of the inlet and outlet ports. The dimensions of each of the auxiliary elements were given in chapter 4. The importance of the effects of those parts are discussed in Bergelt *et al.* (1993). Therefore, the equations 5.8 to 5.11 apply only to the loop geometry associated with the current experiments.

The arguments presented in this section can be summarized as follows. None of the geometrical parameters were found to have influence on the value of \dot{m}_w . This includes the shell diameter and height and the total length of the coils. This is true for both single and multiple coil heat exchangers. The heat rate is the main and most influential parameter. Correlations with reasonable uncertainty can not be obtained between \dot{m}_w and either Ra_{Dhx}^* or the inlet temperatures to the heat exchanger.

5.5. Heat transfer coefficients

Although calculation of the tube-side heat transfer coefficients has not been a major part of this thesis, addressing their variations provides a better understanding of the main subject. Therefore this section which is mainly dedicated to the shell-side heat transfer coefficients, will also address the tube-side coefficients with less importance given to them.

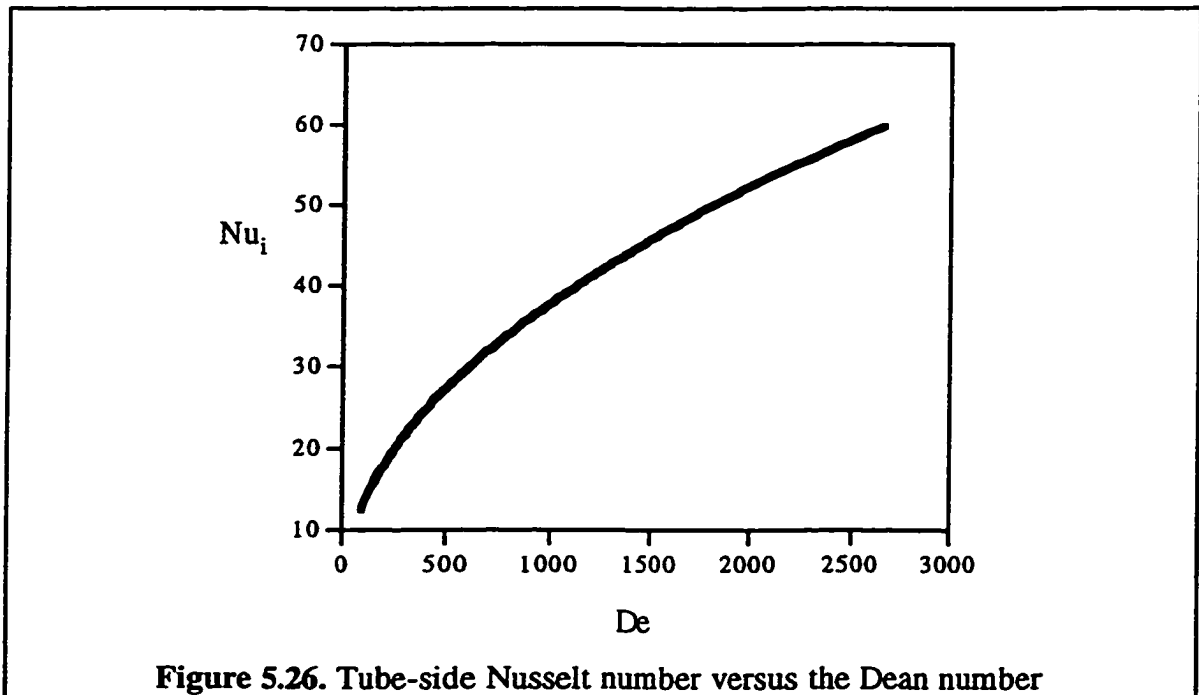
5.5.1. Tube-side heat transfer coefficient

The heat transfer coefficient on the tube side is a factor in determining the UA product of the heat exchanger. Moreover, as it was mentioned in chapter 3, h_i will be used to calculate h_o by an alternative way, using equation 3.26, for the sake of comparison. The effects of different coil geometrical parameters will be reviewed in the following sections.

Better understanding of these effects will help finding the optimum configuration of the heat exchanger.

5.5.1.1. Effect of tube diameter

Equation 3.7 can be simplified to give a clearer view of the tube diameter effect. Figure 5.26 is a plot of the data calculated from equation 3.7. The benefit of re-plotting the data lies in the ability to re-correlate the data by a simple power equation. This power equation facilitates the study of the effects of different parameters. Based on calculations in the current range of parameters, values of both x_3 and x_4 parameters in equation 3.8 are very close to unity.



The best fit to the graph of figure 5.26 leads to the simple correlation in equation 5.1.

$$Nu_i = 1.432De^{0.473}$$

5.12

For the range of coil sizes tested, equation 5.12 offers a simpler correlative form compared to equation 3.7 which is more complicated by itself and it is accompanied by another set of equations (equation 3.8) to calculate two of its variables. From equation 5.12, it is easy to derive the functional relationship between h_i and the tube hydraulic diameter on the inside. Keeping in mind that $De \propto d_{hyd}^{1.5}$, the functional relationship of equation 5.13 can be deduced.

$$h_i \propto d_{hyd}^{-0.29} \quad 5.13$$

Therefore the tube-side heat transfer coefficient increases with a decrease in tube diameter for a fixed coil diameter and pitch. The degree of the increase is such that a change of tube diameter from 9.52 mm to 4.76 mm (50% decrease) will bring a 22% improvement to the tube-side heat transfer coefficient. Since the above argument is based on the tube hydraulic diameter, a review of the factors affecting the hydraulic diameter is noteworthy.

During the process of winding the coils, the cross section of the tubes becomes distorted. The degree of the distortion depends on factors such as the tube diameter, the coil diameter and the pitch. Table 5.1 shows the coils specifications sorted with respect to the relative distortion. The percentage of distortion is the relative difference between the hydraulic tube diameter and the inner diameter of the undeformed tube.

Table 5.1. Percentage of distortion of the tubes cross section

Coil	d (mm)	d _{hyd} (mm)	D _{cm} (mm)	P	Distortion (%)
6	6.35	4.85	59.5	3.06	0.0
17	6.35	4.85	63.2	5.96	0.0
14	4.76	3.22	60.2	1.97	0.5
25	6.35	4.76	68.5	1.33	1.4
18	6.35	4.75	61.4	1.25	1.6
13	4.76	3.18	40.2	1.89	1.7
1	6.35	4.74	49.8	1.58	1.8
16	6.35	4.73	61.6	1.00	2.0
12	4.76	3.16	31.2	1.80	2.3
3	6.35	4.71	58.2	1.68	2.4
4	6.35	4.69	48.4	2.94	2.8
24	6.35	4.59	49.6	1.31	4.9
20	6.35	4.58	35.6	1.20	5.1
5	6.35	4.50	33.4	2.97	6.8
2	6.35	4.46	32.8	1.74	7.6
9	7.94	5.82	49.6	1.95	7.8
7	6.35	4.44	31.8	3.93	8.0
19	6.35	4.43	31.6	2.76	8.2
11	7.94	5.74	50.2	2.95	9.1
23	6.35	4.05	32.8	1.20	16.1
10	7.94	5.00	33.0	3.01	20.8
21	9.52	5.77	49.0	1.05	26.9
8	7.94	4.55	33.8	1.97	27.9
15	9.52	5.68	48.6	2.24	28.1

According to table 5.1 among 24 tested coils, five of them experienced distortions of more than 16% and the distortion of all the other coils was under 10%. Note that the distortion directly increases the pressure drop of the coil. It is evident from table 5.1 that the coil diameter is an important factor in determining the distortion. From the first two rows of the table it can be seen that when large coil diameters are combined with high pitch, there will be zero distortion. There seems to be a limit in the coil diameter to which a particular tube can be wound with reasonable distortion. As a rough figure it can be suggested that, to be within the limit of reasonable distortion, equation 5.14 must hold approximately.

$$D_c \cong 6 \times D_{t,o} \quad 5.14$$

In reaching to equation 5.2 the direct effect of cross section distortion on h_i was not addressed adequately. Addressing this issue, Truesdell and Adler (1970) stated that in elliptical tubes with their major axis perpendicular to helix axis, the secondary flow intensity is less. Less intense secondary flow equals to less heat transfer coefficient. In brief, distortion has also a negative effect on h_i .

The second important factor is the coil pitch. Higher pitch coils experience less distortion. As a result when the pitch is relatively high, smaller diameter coils can also be made. Another factor that adds to distortion is the tube wall thickness. Standard refrigeration tubes having diameters of 4.76 and 6.35 mm have a wall thickness of 0.762 mm whereas the wall thickness is 0.813 mm for tubes having 7.94 and 9.52 mm diameter. It should be mentioned that the uncertainty in calculating the cross section distortion has been 0.6%.

From the above facts it can be stated that the 9.52 mm tubes are not suitable for making coils that will fit in a 77 mm shell. Moreover, none can be fit inside a 51 mm shell.

5.5.1.2. Effect of coil diameter

From equation 5.12 the effect of coil mean diameter on the tube-side heat transfer coefficient can be derived as in equation 5.15.

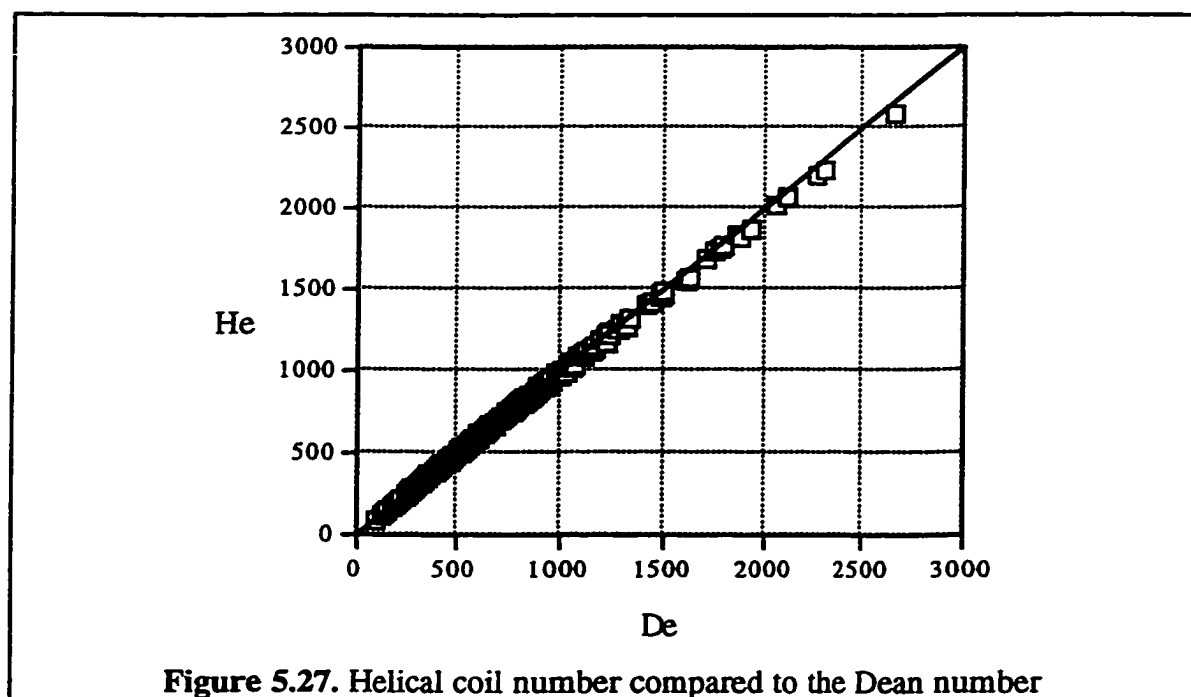
$$h_i \propto D_{c,m}^{-0.24} \quad 5.15$$

This means that tighter wound coils result in better h_i values than large diameter coils. However equation 5.15 suggests that reducing the coil diameter to half, will only improve h_i by 18%. It was argued in the previous section that there exists a limit to which the coil diameter can be reduced. This confirms that the 9.52 mm tube is inappropriate for the purpose. Another factor is the amount of work required by the process of coil winding. It is reasonable to believe that the work required is proportional to the tube diameter. The

7.94 and 9.52 mm tubes make the coil winding especially harder, because of the thicker tube wall they have.

5.5.1.3. Effect of coil pitch

In chapter 3, helical coil number (equation 3.4) was defined to take into account the effect of the coil pitch. Figure 5.27 shows the helical coil numbers for the current range of parameters, versus the Dean number.



Since the coil pitch values are much smaller than the coil radius of curvature for the range of parameters in the current experiments, there is little difference between the Dean number and the helical coil number. Figure 5.27 illustrates this fact and indicates that the use of helical coil number is not necessary since Only for $De > 2000$ do the points tend to fall below the dividing line number (a maximum deviation of 2.5%). From equation 3.4 it can be found that in order for the helical coil number to deviate from the Dean number by not more than 10%, equation 5.15 must be valid.

$$\frac{p_c}{D_{c,m}} \leq 1.5 \quad 5.16$$

In other words, equation 3.7 totally neglects the effect of coil pitch for moderate and small pitches. Mishra and Gupta (1978) found that if the coil pitch is less than the coil diameter, pressure drop receives negligible influence from the coil pitch. Also the numerical study by Futagami and Aoyama (1988) reached the same conclusion. From the definition of the coordinate system in Futagami and Aoyama's study the relationship between the inclination angle and the coil pitch can be expressed in equation 5.17.

$$\cos \alpha = \frac{1}{\sqrt{1 + \left(\frac{p_c}{\pi D_{c,m}}\right)^2}} \quad 5.17$$

Considering equations 2.68 and 5.17 it can be found that the coil pitch is influential on the tube-side heat transfer coefficient in a way that increasing pitch will decrease h_i . However, this influence is not significant for small and moderate pitches. The same result as in equation 5.16 can be reached here.

On the effect of pitch on the friction factor inside the coil, Yang *et al.* (1995) confirm that the coil pitch has almost no effect. Increasing pitch was found to decrease h_i , which is the same conclusion reached by Futagami and Aoyama (1988). For $Pr=10$, Yang *et al.* (1995) report a 30% decrease in h_i for the case when the coil pitch increases by a factor of 3. They did not report any Nusselt number values for $p/D_{c,m} > 1$.

Equation 5.16 holds for all the coils tested. Therefore it can be concluded that the Dean number is an adequate dimensionless parameter even for the case of very high pitch coils in the current experiments.

5.5.1.4. Effect of surface area

The collective effects of different geometrical parameters can be summarized in the effect of coil surface area on the tube-side heat transfer coefficient. An estimate on the effect

of coil surface area on h_i is required in order to determine its effect on the overall heat transfer coefficient or the UA product of the heat exchanger.

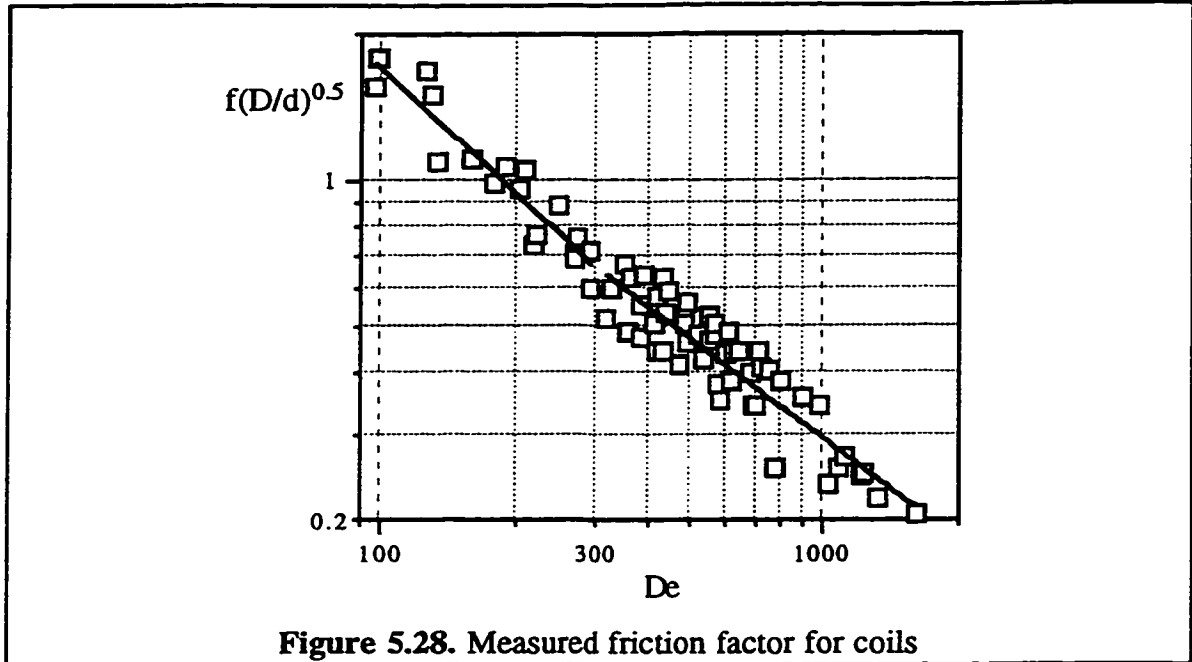
Tube diameter and coil length are the two parameters that define the surface area of a helical coil. In fully developed flow, the effect of length on the mean heat transfer coefficient is normally neglected as in the case of straight tubes. Therefore a conclusion can be drawn. Since the surface area increases with tube diameter in a one-to-one ratio, and knowing that the length does not have any effect, therefore h_i will decrease with increasing surface area. Furthermore if equation 5.13 be considered again, equation 5.18 can be derived.

$$h_i \propto A^{-0.29} \quad 5.18$$

The fact that h_i decreases with A can be verified by an alternative approach. In a constant height shell, the coil diameter and pitch work against each other to determine the surface area. It was concluded that the effect of the coil pitch can be ignored without any loss for moderate and small pitches. On the other hand, coil diameter is influential in a sense that increasing it, will decrease h_i . Considering the fact that the coil surface area is directly proportional to the coil diameter, the decrease of the tube-side heat transfer coefficient with increasing surface area can be verified.

5.5.2. Pressure drop in coils

Equations 2.50 to 2.52 by Srinivasan *et al.* (1970) can be verified by plotting the quantity $f(D_{c,m}/d)^{0.5}$ versus the Dean number for coils (figure 5.28).



Curve fits to the data on figure 5.28 reveal the following results.

$$f \propto De^{-0.86} \left(\frac{d}{D_{c,m}} \right)^{0.5} \quad 90 < De < 300 \quad 5.19$$

$$f \propto De^{-0.68} \left(\frac{d}{D_{c,m}} \right)^{0.5} \quad De > 300 \quad 5.20$$

The exponents of the Dean number in the above equations are different from those of equations 2.50 and 2.51. In equations 2.50 and 2.51 the exponents are -0.73 and -0.5 respectively. In figure 5.28 complete correlations can not be derived since additional tests were not performed to determine the pressure drop in the connecting tubes and fittings. However the trend can be confirmed.

Using equation 3.5 the friction factor for each coil can be calculated for various flow rate settings. Figure 5.29 shows the friction factor for all the single-coil tests. From this figure it is evident that the coils made of 4.76 mm tube have high friction factors

because of operating at low Dean numbers. Since high friction factor will lead to a high pressure drop along the coil, using coils of 4.76 mm tube in a heat exchanger will demand higher electrical power requirements to deliver a fixed amount of glycol flow rate. In a SDHW system where the objective is to minimize the amount of electricity required, this extra pressure drop is undoubtedly costly.

Also from figure 5.29 it is evident that there is little distinction between the friction factor for 6.35 mm tube coils and those of 7.94 mm tube coils. Therefore from the pressure drop point of view there is little difference between those two tube diameters. This is because the thicker wall of 7.94 mm tubes causes the cross section to deform more during the coil winding process. Therefore the pressure drop is expected to be in the same range as that for 6.35 mm tube coils.

In order to study the friction factors for 9.52 mm tube coils the area enclosed in the box in figure 5.29 is enlarged in figure 5.30. Figure 5.30 shows that the values of the friction factor for 9.52 mm tube coils are in the same range as those of 6.35 and 7.94 mm ones. This translates to much less pressure drop along 9.52 mm tube coils. As a consequence, these coils demand for less electrical power to circulate the glycol solution. However other disadvantages make the use of these coils impractical as mentioned earlier.

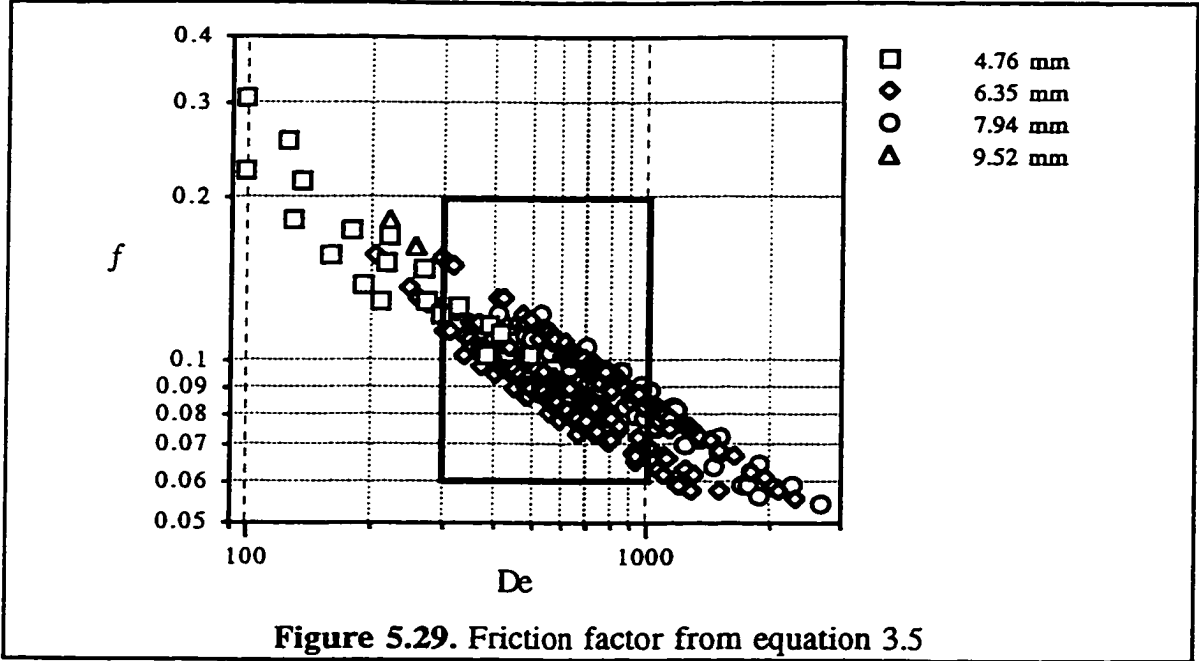


Figure 5.29. Friction factor from equation 3.5

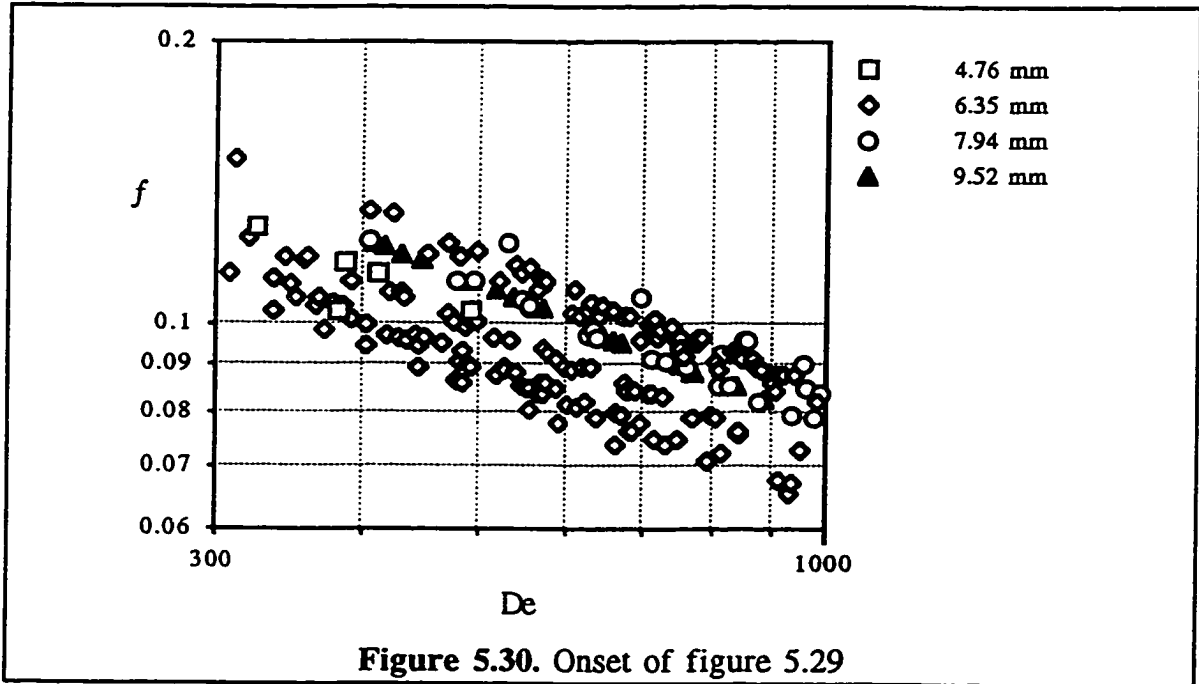


Figure 5.30. Onset of figure 5.29

5.5.3. Flow distribution in multiple coils

Multiple coil configurations in the current experiments are of the parallel type. This means that the pressure drop across all individual coils must be equal since the flow is mixed at the inlet and outlet.

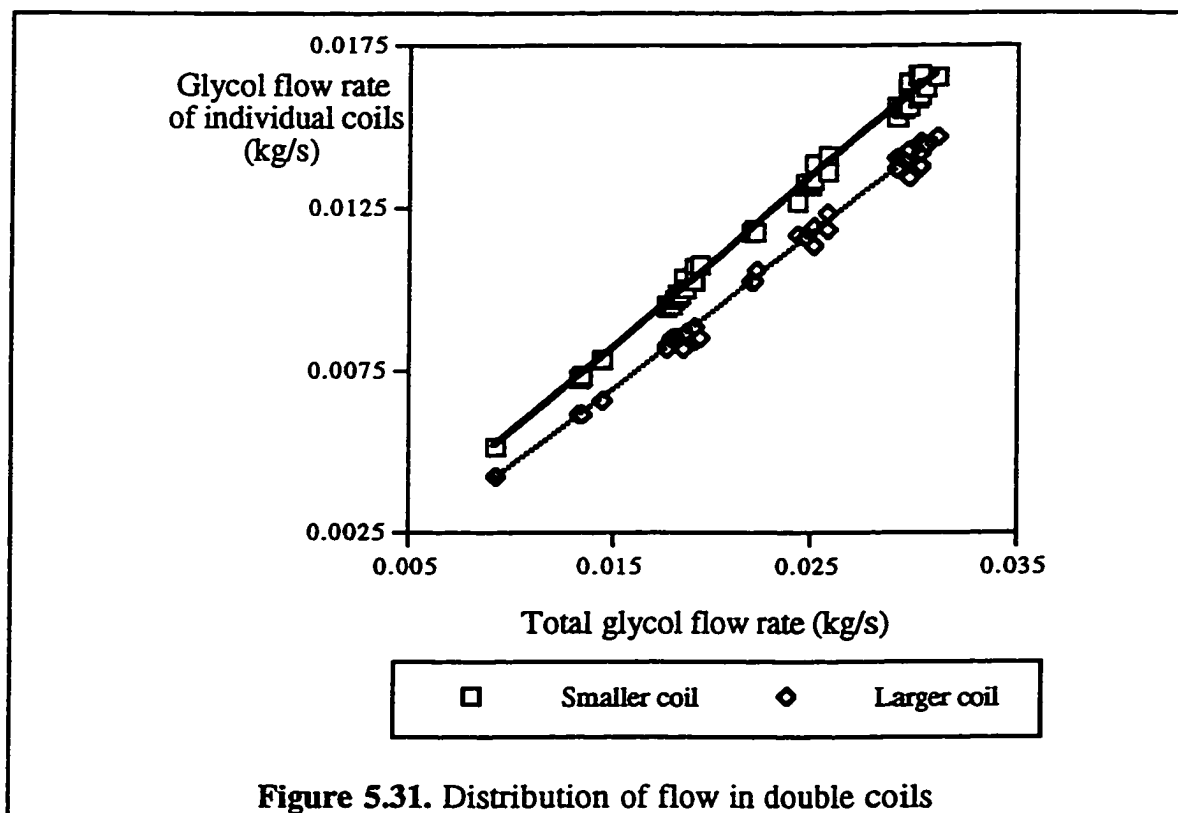
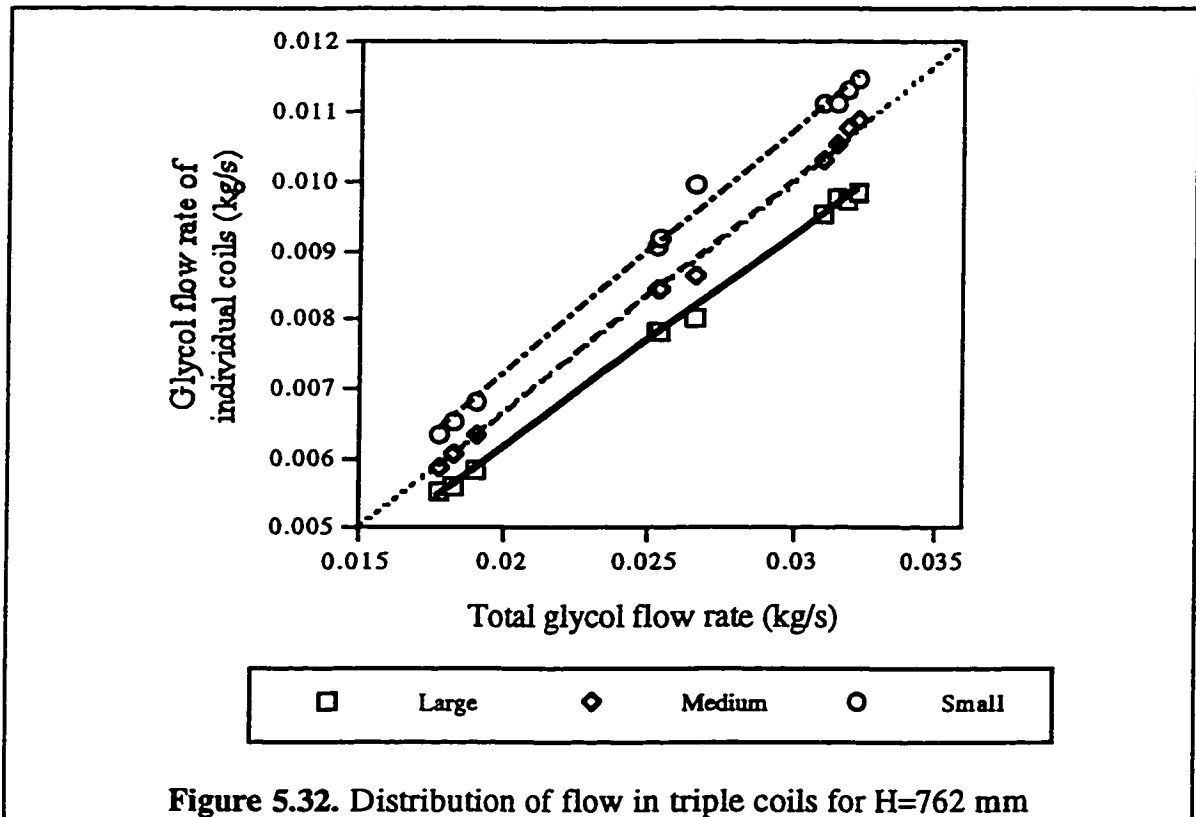


Figure 5.31 is a plot of the mass flow rate in each of the coils in a double coil configuration versus the total glycol flow rate to the heat exchanger. The general trend is that the difference between the mass flow rates of smaller and larger coils increases as the total glycol flow rate increases. Also they are both very close to the 50% line which indicates that the distribution is nearly even between the coils. Interestingly, it can be seen from figure 5.31 that all the data points of different coil diameters fall on a straight line. It indicates that the ratio of the diameters of the two coils in a double coil configuration does not influence the distribution of flow between the coils. From the definition of the friction coefficient inside the tubes and recalling the fact that the pressure drop must be equal for the

two coils, the following conclusion can be drawn. Since the larger coil is longer (increased L) and figure 5.31 implies that the mass flow rate remains constant (constant u), in order for ΔP to be equal for both coils, the friction coefficient must drop considerably for the larger coil. This change in the friction coefficient is inversely proportional to the change in the diameter of the coil.



The distribution of flow to each individual coil in a triple coil configuration is illustrated in figure 5.32. The diagonal dotted line is the one-third line. It can be seen that regardless of the value of the total mass flow rate, the middle coil always receives one-third of the share. This was also true for triple coils in the 382 mm long shell.

Ajele (1995) plotted the percentage of flow distribution versus the coil diameter for double, triple and quadruple coils. From the graphs of double and triple coils, it can be seen that the coil diameter has little effect on flow distribution. Also it is evident from the

triple coil graph that the middle coil receives 33% of the flow confirming the above observation in the current research.

5.5.4. Shell-side heat transfer coefficient

The performance of a heat exchanger is affected by the magnitude of its shell-side heat transfer coefficients. The effects of several parameters must be known in order to prescribe a method for improvement. Influential parameters can be divided into two categories: the geometrical and the heat transfer parameters. The heat transfer parameters include the heat rate, the glycol flow rate and the inlet temperatures. The geometrical parameters are the tube diameter, coil diameter, coil pitch, coil surface area, length, number of coils, shell diameter and shell height. The tests are divided into single and multiple coil cases and each case will be addressed separately.

5.5.4.1. Single coils

5.5.4.1.1. Effect of coil surface area

The coil surface area is determined by the values of its tube diameter and length. Studying the effect of coil surface area gives insight to better understanding of each parameter. First a macroscopic view will be presented and then a microscopic look into the details will follow.

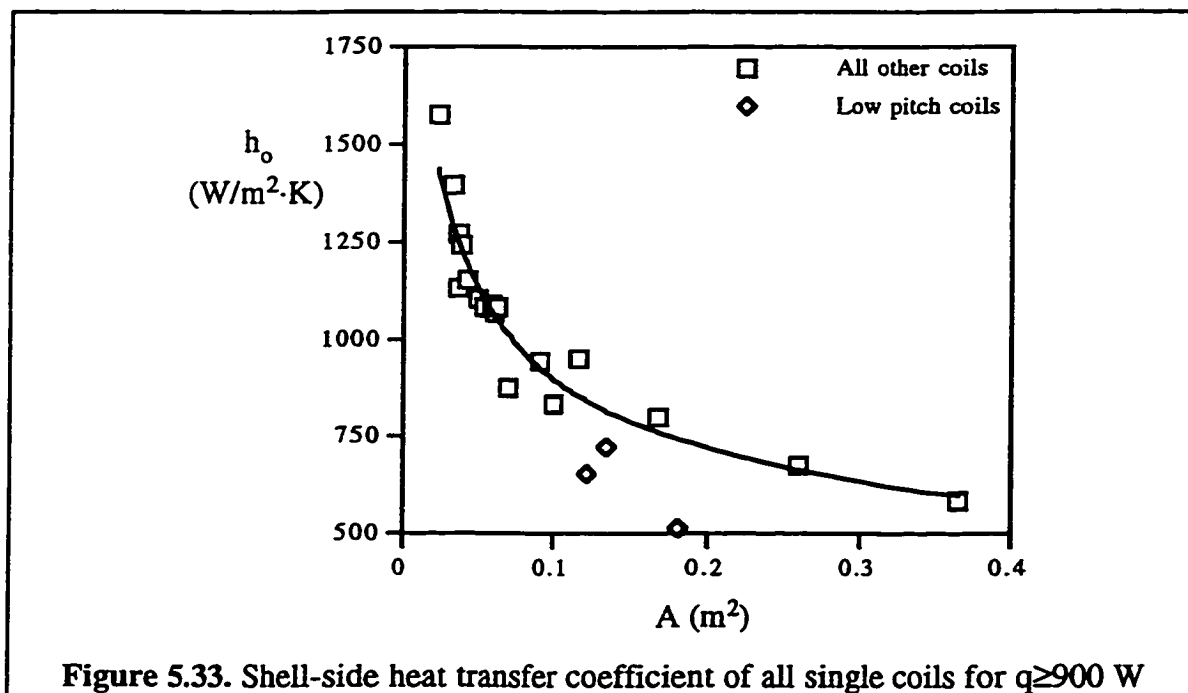
The shell-side heat transfer coefficient data of all single coils, averaged for a fixed heat rate, is presented in figure 5.33. As the coil surface area increases, h_s drops sharply for $A < 0.1 \text{ m}^2$ and continues to drop at a lower rate for $A > 0.1 \text{ m}^2$. The data from coils with $P \leq 1.25$ have been excluded from the rest of the data, because in those cases the heat transfer coefficients are considerably lower and the heat transfer performance of the exchanger is impaired.

The curve fit to the data in figure 5.33 suggests the functional relationship of equation 5.21 between h_s and A (the low-pitch coils data are not included in the curve fit).

$$h_o \propto A^{-0.32}$$

5.21

The conclusion is that the shell-side heat transfer coefficient is dependent on the coil surface area and equation 5.21 must be kept in mind before deciding to increase the surface area i.e. increase coil diameter, coil length, tube diameter etc.

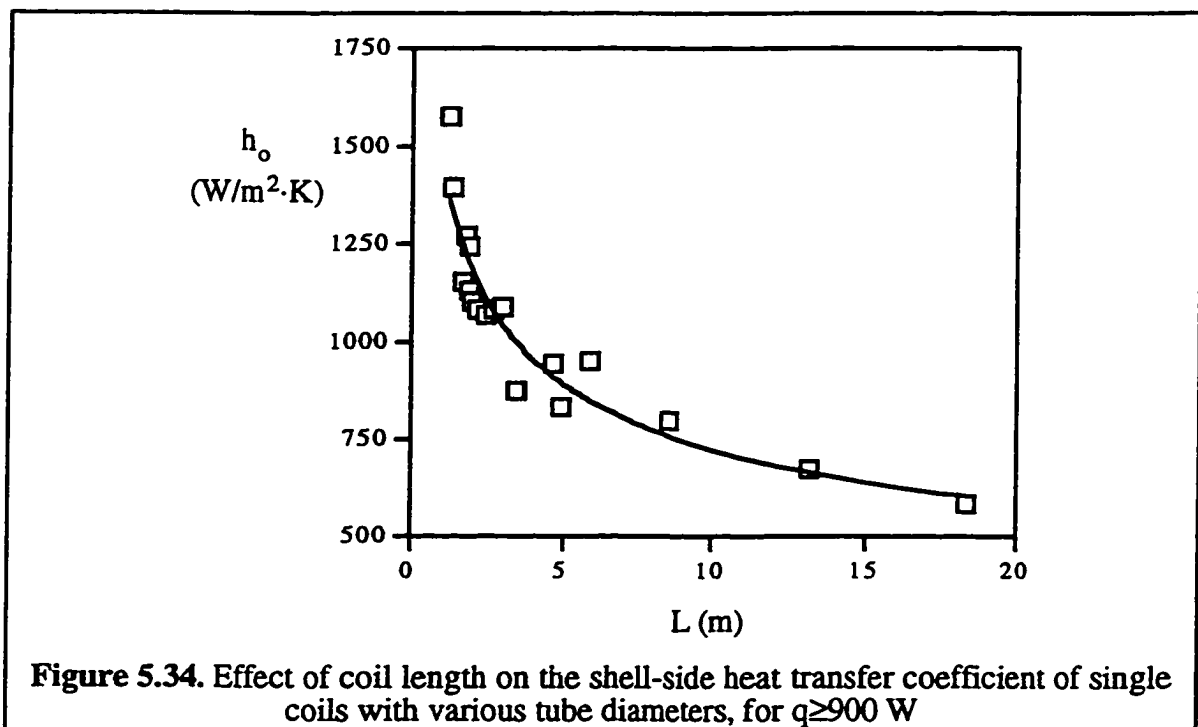


Ali (1994) found that for coils having a tube diameter of 8 mm the heat transfer coefficient increases with increasing coil surface area but when the tube diameter is 12 mm, increasing A will decrease h_o . The rate of decrease or increase was not indicated. In the current thesis Ali's finding for the 12 mm diameter tube was confirmed. It is shown in section 5.5.4.1.3 that the tube diameter has little effect on the shell-side heat transfer coefficient. Therefore, there is no evidence to confirm the result of Ali's experiment on the 8 mm tube coils.

It is now possible to investigate the effects of other geometrical parameters after having a general idea about their collective effect. Further comparison of the data must be done only on the cases where the coil surface areas are reasonably close to each other.

5.5.4.1.2. Effect of coil length

For a constant tube outside diameter, since the coil surface area is directly proportional to its length, the same relationship as in equation 5.21 must be reached with the coil length.



In fact the best fit to the data in figure 5.34 reveals a relationship of the form presented in equation 5.22.

$$h_o \propto L^{-0.30}$$

5.22

The exponent in equation 5.22 is 0.30 which indicates that the coil length plays the same role in influencing the shell-side heat transfer coefficient as the coil surface area. Noting that figure 5.34 is for various tube diameters, this observation leads to additional information regarding the role of the tube diameter. From the mathematical definition of the coil surface area this conclusion can be reached that the tube outside diameter has only a negligible effect on the shell-side heat transfer coefficient. This conclusion is addressed with more details in the following section.

Ali (1994) correlated the Nusselt number data with the Rayleigh number based on the coil length and obtained two different relationships for the two tube diameters he tested.

$$h_o \propto L^{-0.115} \quad \text{for } D_{t,o}=12 \text{ mm} \quad 5.23$$

$$h_o \propto L^{0.548} \quad \text{for } D_{t,o}=8 \text{ mm} \quad 5.24$$

No specific reason was given by Ali to explain this immense change of slope by changing the tube diameter from 12 mm to 8 mm.

5.5.4.1.3. Effect of tube outside diameter

In the preceding section it was shown that the effect of tube diameter on h_o can be neglected without any loss of accuracy. Figure 5.35 confirms this observation.

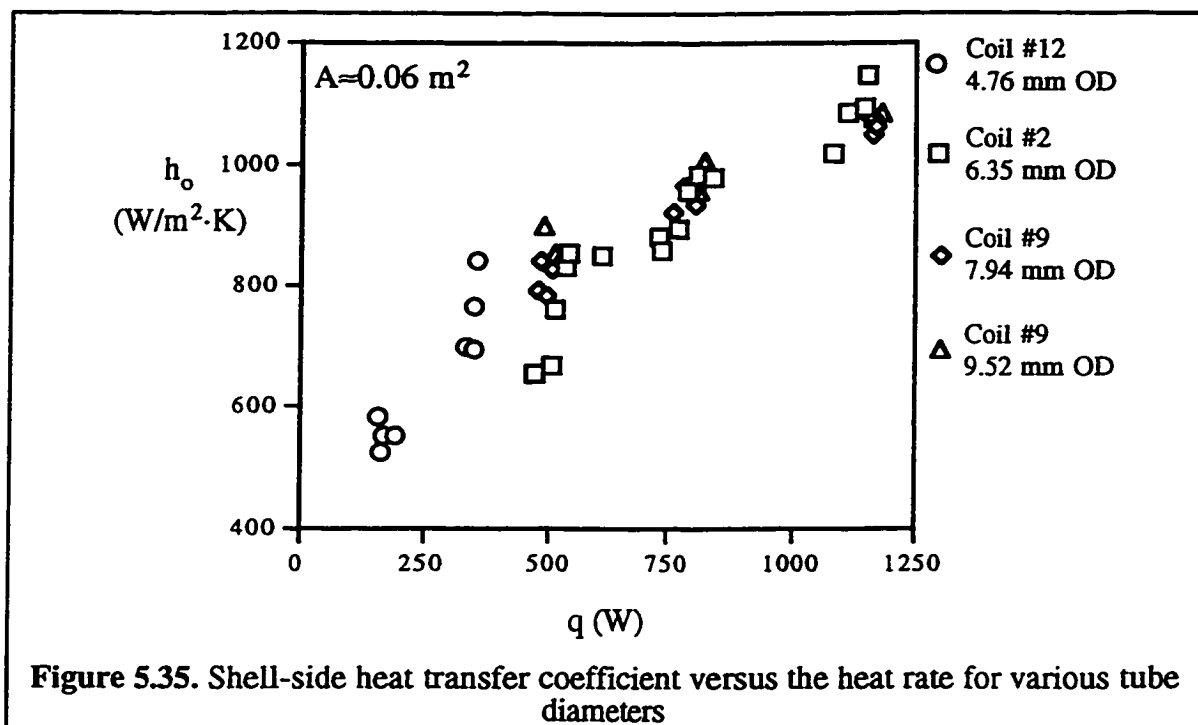


Figure 5.35. Shell-side heat transfer coefficient versus the heat rate for various tube diameters

Figure 5.35 covers the h_o data of four coils each of different tube diameter. On figure 5.35 no specific trend can be detected regarding the changes in tube diameter. Specially for higher values of heat rate all the points collapse on each other indicating the insignificance of the tube diameter. Concerning figure 5.35 it must be noted that in order to avoid very high glycol temperatures, no data points were made available for 4.76 mm OD coils at $q > 500$ W.

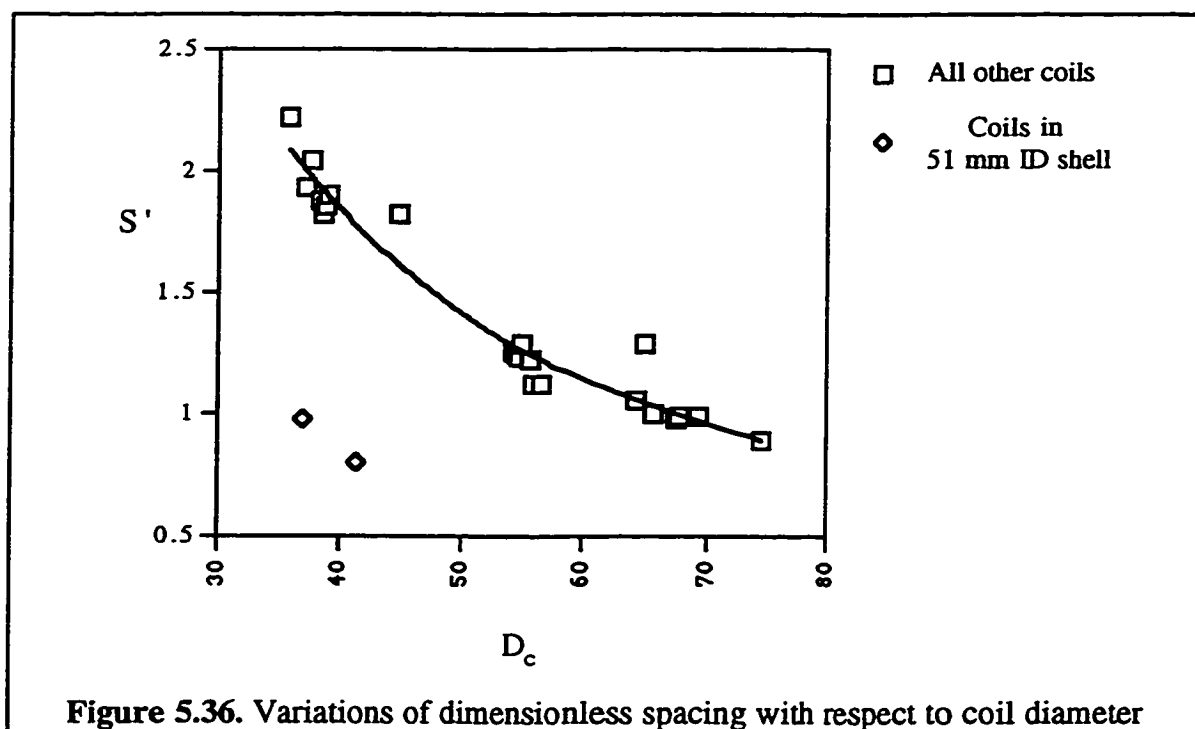
Equation 2.18 By Xin and Ebadian (1996) reveals a relationship between the tube diameter and the shell-side heat transfer coefficient as in equation 5.25.

$$h_o \propto D_{t,o}^{-0.12} \quad 5.25$$

This equation is the result of the tests on coils having tube diameters of 12.7 and 25.4 mm. Equation 5.25 suggests a weak dependence on the tube diameter. Therefore the insignificance of the tube diameter is confirmed. If only the magnitude of the shell-side heat transfer coefficient is considered, any tube diameter within the range 4.76 to 9.52 mm can be used to make coils, disregarding, at this time, the pressure drop through the coils.

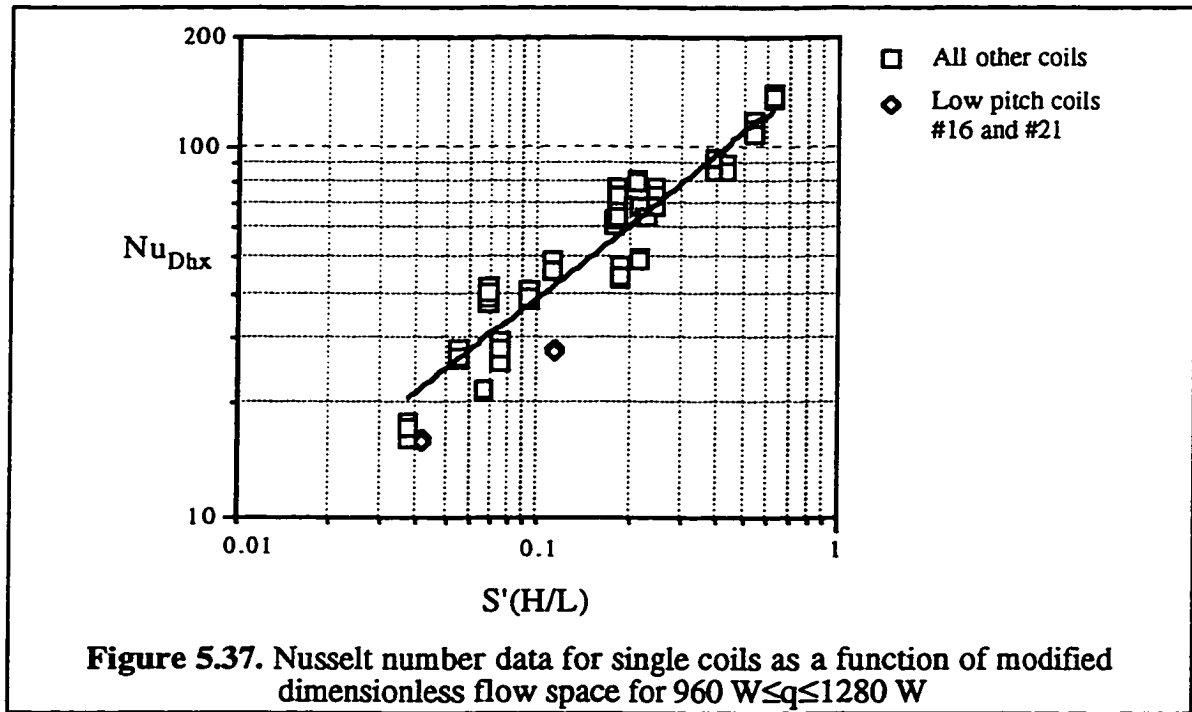
5.5.4.1.4. Effect of coil diameter

The changes in coil diameter are reflected in the modified dimensionless spacing of the exchanger. Figure 5.36 shows the relationship between these two quantities. As the coil diameter increases, the dimensionless spacing decreases at a nearly one-to-one ratio ($S' \propto D_c^{-1.16}$). It becomes possible then to study the effects of S' on various parameters, using S' as the representative for the coil diameter. The results can be easily related to the coil diameter with figure 5.36.



The Nusselt number data of all single coil tests are presented in figure 5.37 as a function of the modified dimensionless flow space. The data presented in the figure, are for a fixed power setting to the heater to eliminate the effect of the heat rate. It was found that the Nusselt number data can not be correlated with the dimensionless flow space without modification. Applying the modifying term H/L , which has also been used to modify the Rayleigh number, was found necessary in order for the data to be correlated well. The

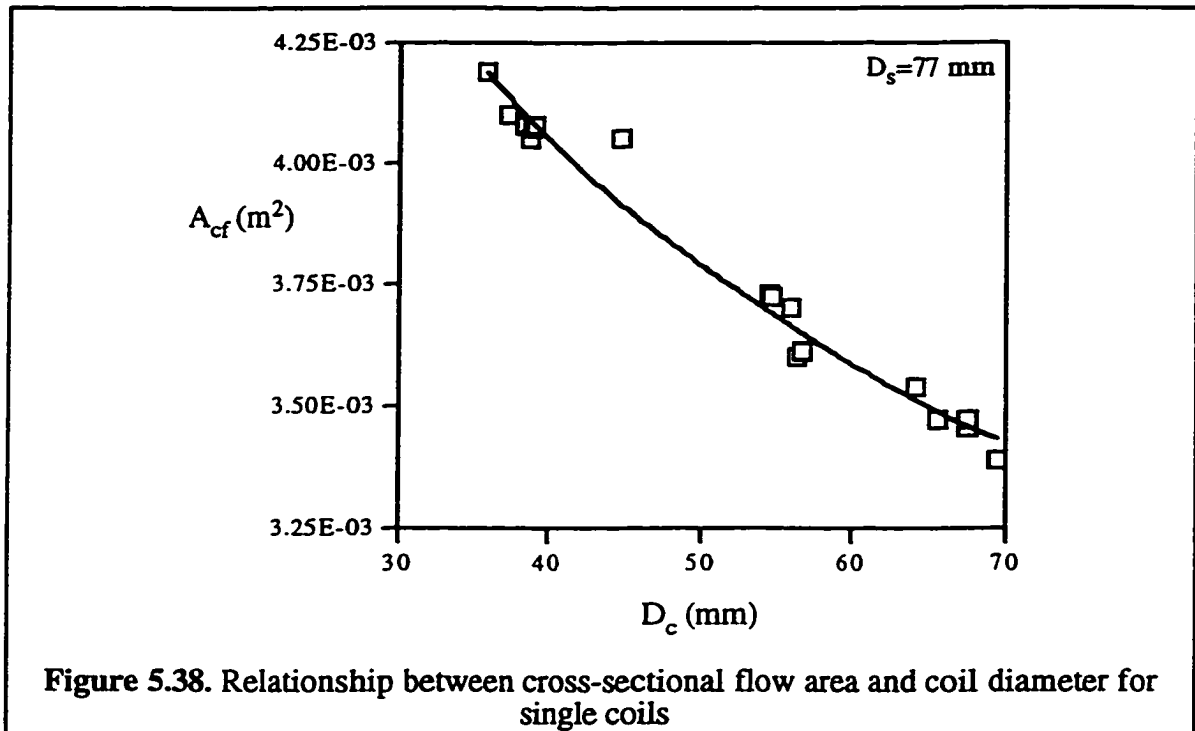
significance of this modifier lies in the fact that the coil surface area is crucial to be kept constant while studying the effects of other parameters on the shell-side heat transfer coefficient. Since the coil surface area is directly proportional to the coil length, the parameter L in the denominator of the term H/L eliminates the effect of the coil surface area. As a result the study of the exclusive effect of S' and the coil diameter becomes possible.



The best fit to the plot of figure 5.37 can be represented by equation 5.26 for the range $0.8 \leq S' \leq 2.0$ and $D_i = 77 \text{ mm}$.

$$Nu_{Dhx} = 174.4 \left(S' \frac{H}{L} \right)^{0.65} \quad 960 \text{ W} \leq q \leq 1280 \text{ W} \quad 5.26$$

From the definition of the heat exchanger hydraulic diameter (equation 3.18), one can observe its dependence on flow cross-sectional area. Therefore in order to further carry on the argument and reach a conclusion on the effect of the coil diameter on h_o , the relationship between the coil diameter and A_c must be understood first. Figure 5.38 offers an insight to this matter.



The flow cross-section area of all single coil tests in the 77 mm shell is plotted as a function of the coil diameter in figure 5.38. Flow cross-section area of single coil heat exchangers is defined as in equation 5.27.

$$A_{cf} = \frac{\pi}{4}(D_s^2 - D_{c,o}^2 + D_{c,i}^2) \cong \frac{\pi}{4}(D_s^2 - 4D_c D_{t,o}) \quad 5.27$$

Equation 5.27 reveals that, as the coil diameter increases, the flow cross-section area decreases. This decrease depends on the shell diameter and tube outer diameter as well. By fitting a curve to the data in figure 5.38 a simple functional relationship can be achieved between A_{cf} and the coil diameter. This relationship was found to be of the form presented in equation 5.28.

$$A_{cf} \propto D_c^{-0.3} \quad 5.28$$

Gathering all the above information, considering equations 5.26 and 5.28 and the definition of $Nu_{D_{hx}}$ and some mathematical manipulations, the rate of change of the shell-side heat transfer coefficient with the coil diameter can finally be determined. The result can be summarized in equation 5.29.

$$h_o \propto D_c^{-0.45} \quad 5.29$$

The shell-side heat transfer coefficient is therefore higher for smaller diameter coils. This conclusion is valid when the coil surface area does not change dramatically. The range of parameters for which equation 5.29 remains valid is, $0.8 \leq S' \leq 2.0$, $960 \text{ W} \leq q \leq 1280 \text{ W}$ and $D_s = 77 \text{ mm}$. Until extensive data concerning this effect is at hand, equation 5.29 should be relied upon only to the extent of the general statement that the smaller diameter coils offer better heat transfer coefficients.

Differentiating between the effects of the coil surface area and the coil diameter is not a straightforward task. Tests on coils with various diameters but equal surface areas in a fixed diameter and height shell might help in this regard. This can be done by varying the coil pitch within a reasonable range.

Although no particular reason was given, Ajele (1995) stated that, generally, tighter wound coils were expected to perform better. In his study of the effect of the modified flow space on Nu , Ajele encountered an initially constant Nusselt number with S' then increasing Nu with S' and finally, a constant or decreasing Nusselt number with S' . The coils tested were in the range $1.15 \leq S' \leq 2.91$. In the current study, the initially constant Nusselt number with S' was not experienced although the range of the modified flow space fell below the value of 1.15, which was the lower limit of Ajele's tests. At the other end of the spectrum, the current study stops at $S' = 2.0$ while Ajele's study range goes up to $S' = 2.91$. Therefore the state of constant or decreasing Nusselt number at higher S' values could neither be confirmed nor rejected because of lack of data.

For the sake of comparison the work of Hsu and Shih (1984) can be considered. It must be noted that their results are for helical coils inside cylindrical tanks which are stirred by a jet. It means that the situation is somewhat forced convective instead of natural

convective. For the effect of the coil diameter, Hsu and Shih (1984) reached to a relationship of the form of equation 5.30.

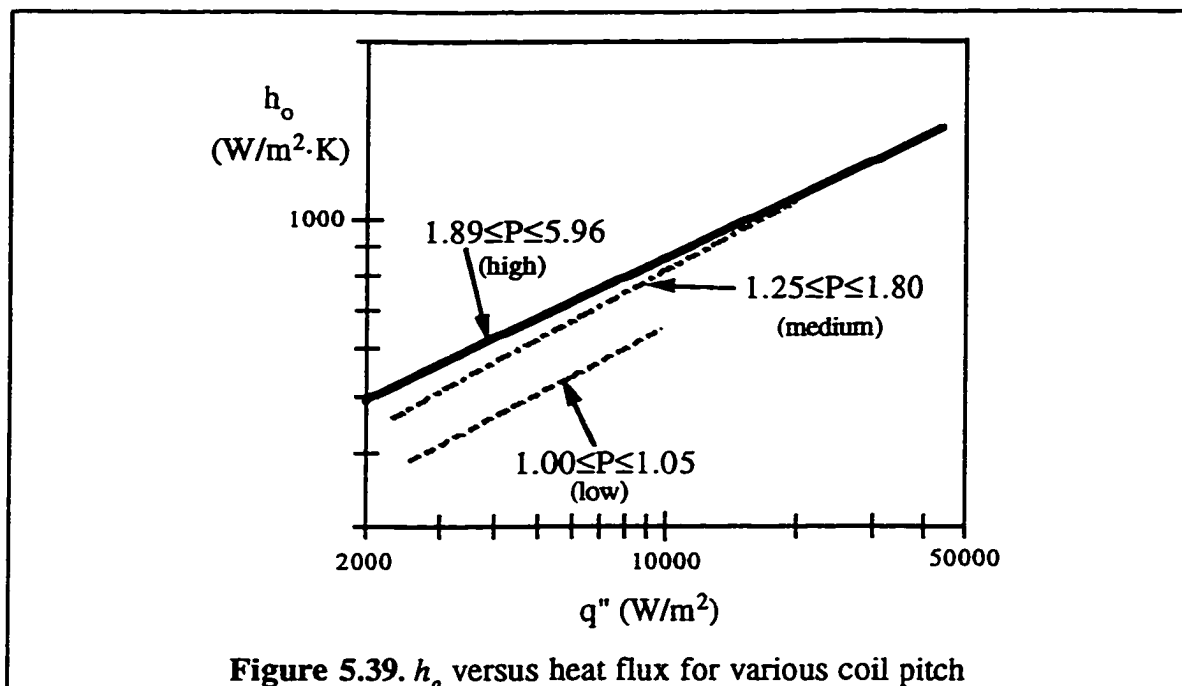
$$h_o \propto D_c^{-0.08} \quad 5.30$$

The results covers coils of diameters ranging from 115 to 216 mm also tube diameter varied between 6.35 and 19.05 mm. Equation 5.29 is an indication that the outside heat transfer coefficient is not influenced significantly by the variations of the coil diameter, when the flow is forced.

In summary, for a fixed coil surface area, h_o increases with decreasing D_c . This is because for smaller coil diameters the heat source is concentrated at the shell core more than the case of larger diameter coils, resulting in higher velocities of water in the core, producing higher values of h_o .

5.5.4.1.5. Effect of coil pitch

In order for the heat exchanger to be as compact as possible the minimum possible coil pitch which does not affect the coil performance greatly must be known. Also knowledge of the maximum acceptable coil pitch is important. In other words, search for an optimum coil pitch value is a necessity in determining the optimum heat exchanger configuration. There is no doubt that the value of the optimum coil pitch is affected by the behavior of thermal boundary layer around the coil surface. It was seen in section 5.1.1 that the glycol mass flow rate is influential in determining the thickness of the thermal boundary layer along the coil. For low mass flow rate ratios, the temperature profiles were concave down which translates to thicker boundary layer at the top of the exchanger. The effect of high mass flow rate ratio was to bend the profiles to form an upwardly concave shape. This means thinner boundary layer at the top compared to the bottom. However in the study of the coil pitch, it is only the thickness of the boundary layer at the top and bottom of the tube cross section that is important.



The shell-side heat transfer coefficient data was correlated with coil pitch and the result is illustrated in figure 5.39. The data in figure 5.39 covers all the single coil tests in the 77 mm shell to eliminate the effects of shell diameter and height.

Figure 5.39 reveals that by changing the coil pitch from the medium range to the low range, there will be a 20% drop in h_o . Changing from the medium range to high range will result in only a 7% increase in h_o . Considering the relative change in the coil pitch, it means that first, a 33% increase in coil pitch causes a 25% improvement in h_o , but further increasing the coil pitch by 157% will only improve the shell-side heat transfer coefficient by 7%. It is obvious that for a fixed shell height any increase in coil pitch will decrease the coil surface area and accordingly the UA value of the heat exchanger which is not desirable. Based on the above arguments, the medium coil pitch range, $1.25 \leq P \leq 1.80$, should be regarded as the optimum range.

No literature was cited regarding the optimum pitch value for helical coils. However there are a number of articles dealing with the optimum pitch for natural convection heat transfer from a horizontal bundle of circular tubes. Because of some similarities between

those geometries and that of a vertical helical coil, there is benefit in reviewing the mentioned articles.

Sparrow and Niethammer (1981), Farouk and Guceri (1983) and Sadeghipour and Asheghi (1994) confirmed that the heat transfer performance of a horizontal bundle of tubes is greatly affected by the tube spacing. Tillman (1976) found that for maximum heat transfer from arrays of horizontal cylinders there exists an optimum center-to-center distance between the cylinders. This optimum distance depended on the temperature difference between the cylinders and the air surrounding them. This was found to be in the range $1.25 \leq P \leq 1.5$.

Tokura *et al.* (1983) found that when the center-to-center distance is less than 4 tube diameters the Nusselt number of the intermediate tubes will decrease considerably in an array. They recommend a pitch value of 7 for which the heat transfer performance does not decrease and the compactness of the unit is also prevailed. However if the compactness is the primary concern, the results of Tokura *et al.* points to a pitch value of 2 to 3 tube diameters as the optimum value.

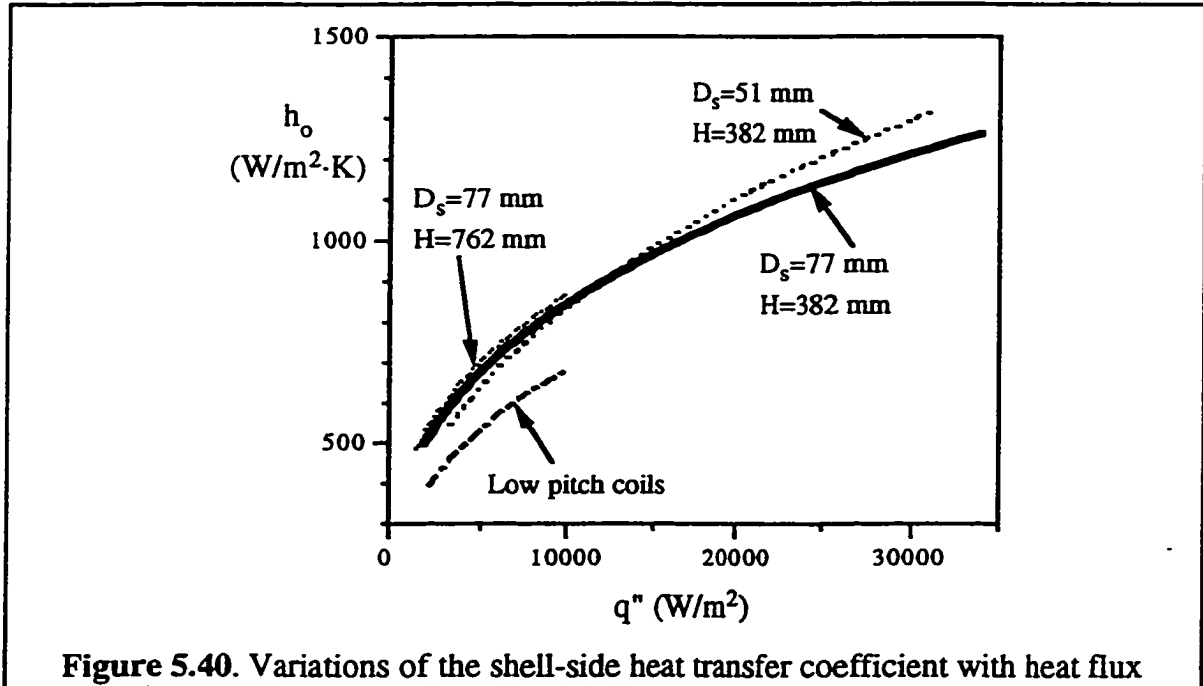
Sparrow and Vemuri (1985) suggested an optimum value for the number of pin fins in a highly populated array. Their conclusion was based on maximizing the rate of heat transfer from the array at a given temperature difference between air and the pins. This optimum number when translated to center-to-center distance will yield a pitch of 1.9 to 2.5 tube diameters.

Bejan *et al.* (1995) reported an optimum pitch value of 2.5 for which heat transfer from a bundle of horizontal cylinders in a fixed volume is maximum. They theoretically proved the existence of an optimum spacing between the cylinders.

Although physical dimensions of the test sections as well as the boundary conditions of the tests were diverse and in some cases totally different from each other, the optimum pitch value in the literature cited varied from 1.25 to 3. This is a strong confirmation of the current results. Therefore it is recommended to make coils of pitch values of 1.25 to 1.80 tube diameters. In case of a 6.35 mm tube, the recommended pitch value leads to a minimum wall to wall distance of 1.6 mm between two consecutive coil

turns. This means that very compact heat exchangers can be built without significant loss of thermal performance.

5.5.4.1.6. Effect of heat rate



There is no doubt that h_o increases as the heat rate increases. In figure 5.40 the effect of the coil surface area is isolated by plotting the h_o data versus the rate of heat transfer per unit area. The solid line represents the data from all single coil tests in the 77 mm ID and 382 mm long shell. This solid line can be taken as the typical plot of h_o versus q'' . From figure 5.38 the proportionality of h_o to the heat flux can be determined as $h_o \propto (q'')^{0.33}$.

5.5.4.1.7 Effect of glycol flow rate

Since the glycol mass flow rate is the main determining factor for the Dean number, it has a great influence on the tube-side heat transfer coefficient as it can be

deduced from figure 5.26. It is of great interest to know the degree of influence the glycol mass flow rate might have on the shell-side heat transfer coefficient as well.

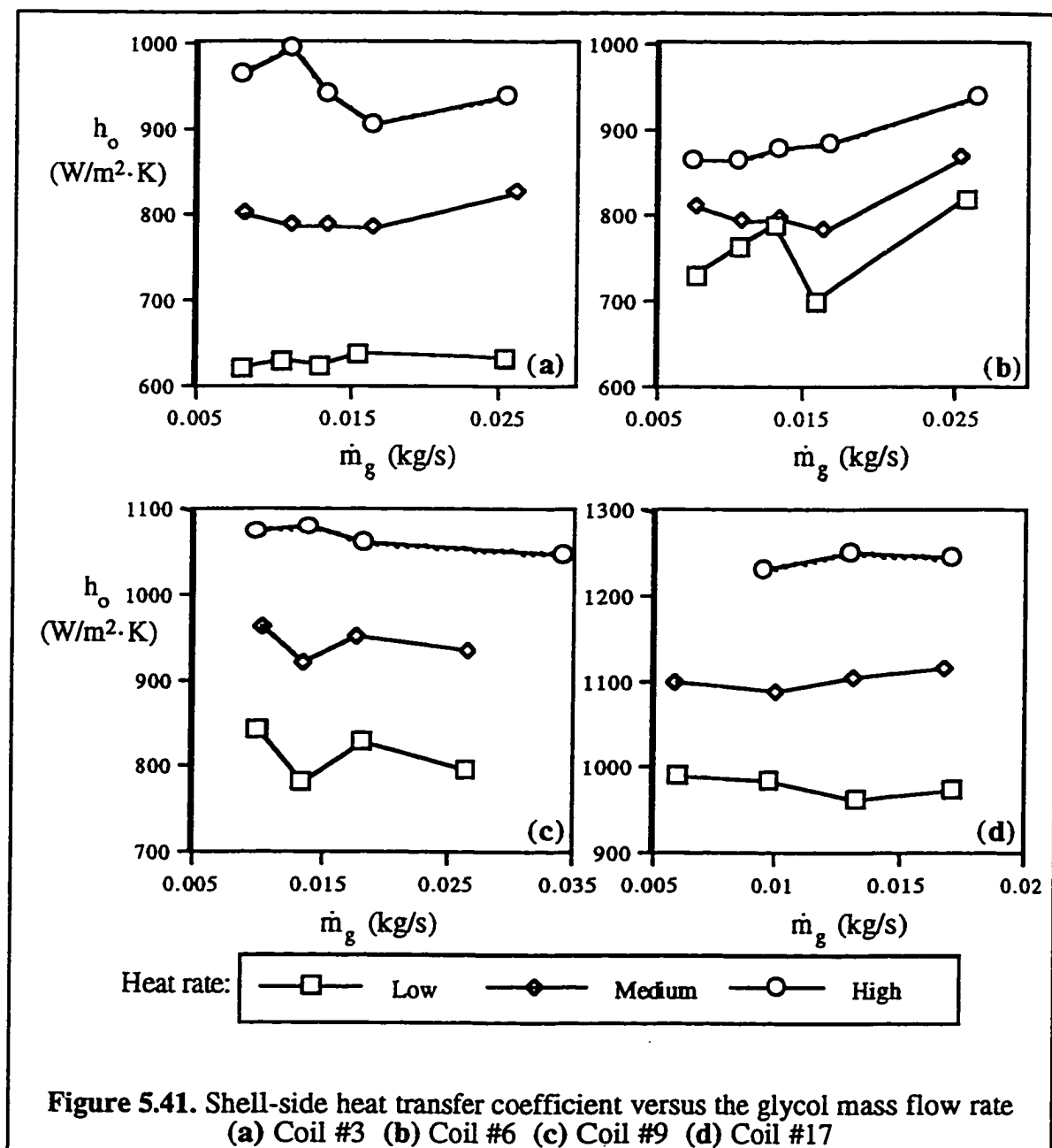


Figure 5.41 illustrates the insignificance of the glycol mass flow rate. The low, medium and high heat rates correspond to approximately 500, 800 and 1200 W

respectively. Coils #3, #6, #9 and #17 were chosen for plots but nearly the same behavior was demonstrated by other coils. No specific trend was distinguishable in studying the plots of h_o versus \dot{m}_g of various coils. Therefore it was concluded that the shell-side heat transfer coefficient is insensitive to the glycol mass flow rate as it was expected.

5.5.4.1.8. Effect of shell diameter

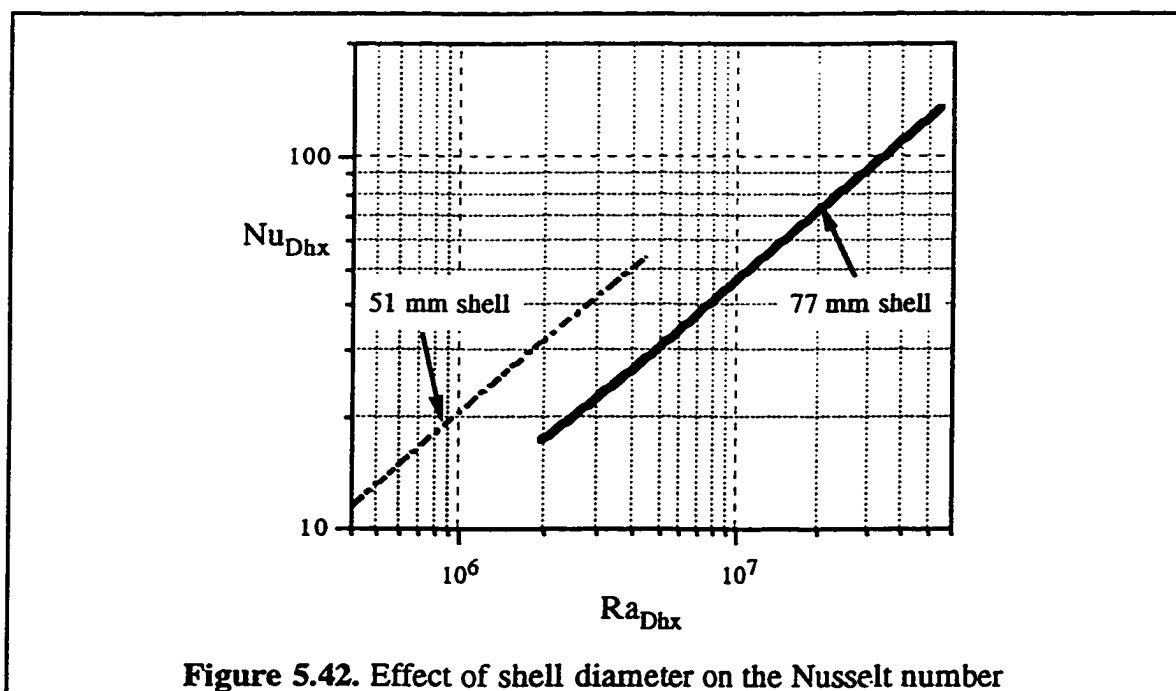


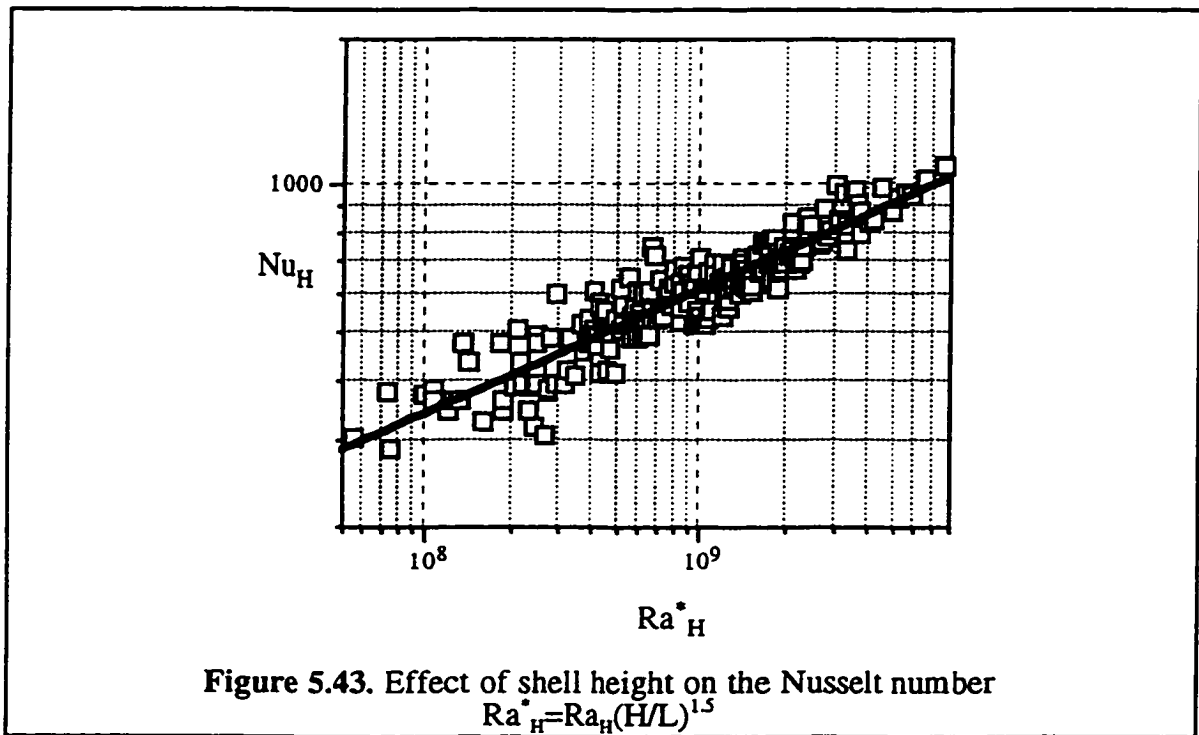
Figure 5.42. Effect of shell diameter on the Nusselt number

For a fixed water mass flow rate, the mean water velocity inside the heat exchanger is higher for smaller diameter shells. The heated water layers close to the coil surface will be washed away faster, lowering the coil surface temperature for constant wall heat flux. Therefore better shell-side heat transfer coefficients are expected to be achieved with smaller diameter shells. Figure 5.42 illustrates the Nusselt number data for two shell diameters tested. The two lines are the best fits to the data. An improvement in the Nusselt number due to a decrease in shell diameter is evident from the figure. The Rayleigh number ranges of the two sets of data only overlap for $2 \times 10^6 \leq Ra_{D_{hx}} \leq 4.5 \times 10^6$. At $Ra_{D_{hx}} = 3 \times 10^6$ there is an 86% increase in the Nusselt number for the 51 mm shell compared to that of the

77 mm shell. At a fixed Rayleigh number and heat exchanger hydraulic diameter, this means that the shell-side heat transfer coefficient is 86% higher in the smaller shell.

The heat exchanger hydraulic diameter is affected by the shell diameter according to equation 3.18. Therefore for Dhx to remain unchanged by changing the shell diameter, other parameters must change properly. It is very likely that the coil surface area must decrease, and some of the improvement in h_o is due to the decrease in the coil surface area which was discussed in section 5.5.4.1.1. There is the possibility to keep Dhx fixed without changing the coil surface area (e.g. by changing the coil and/or tube diameter), and it can be concluded that decreasing the shell diameter will increase the shell-side heat transfer coefficient significantly.

5.5.4.1.9. Effect of shell height



The height of the heat exchanger greatly affects exchanger compactness thus it is very important to know its effects on the shell-side heat transfer coefficient. It was

concluded in section 5.1.1.1 that the exchanger height does not influence the temperature profiles significantly. Therefore for a fixed heat rate it is expected to have no notable effect on the shell-side heat transfer coefficient.

Figure 5.43 is helpful in shedding light on this matter. The Nusselt number data based on the shell height is plotted against Ra_H^* . The Rayleigh number based on H was modified by multiplying it by $(H/L)^{1.5}$ which accounts for the length of the coil. A curve fit to the data results in equation 5.31 for the range $5 \times 10^7 < Ra_H^* < 8 \times 10^9$.

$$Nu_H = 3.23 Ra_H^{*0.25} \quad 5.31$$

It can be found from equation 5.31 that the dependence of the shell-side heat transfer coefficient on the shell height is weak ($h_o \propto H^{0.125}$). In other words there will be less than a 10% increase in h_o by using a shell two times longer, provided the same coil length is considered.

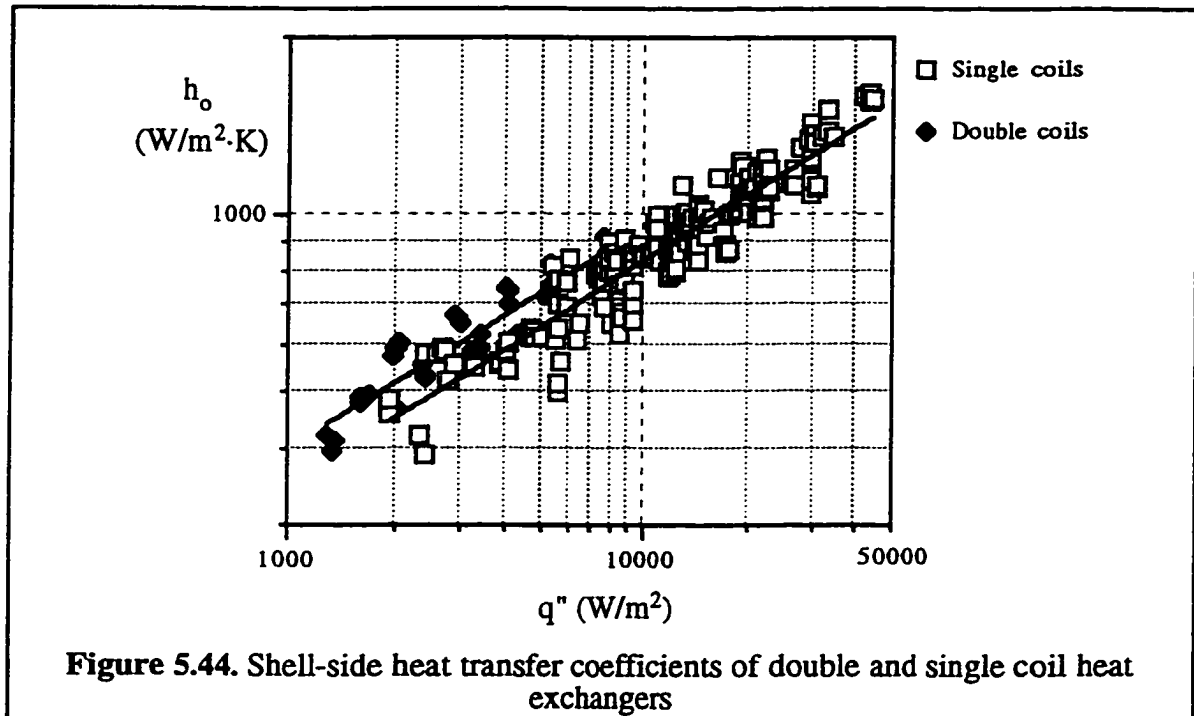
Khan and Kumar (1989) in their numerical study of natural convection in vertical annuli found that the effect of the aspect ratio is insignificant when the aspect ratio is greater than 5. The aspect ratio of a vertical annulus is defined as $H/(r_o - r_i)$, where H is the height of the annulus and r_o and r_i are the radii of the outer and inner cylinders, respectively.

In a way this behavior can be beneficial. The heat exchanger can be built longer with more coil surface area inside to increase the overall heat transfer coefficient.

5.5.4.2. Multiple coils

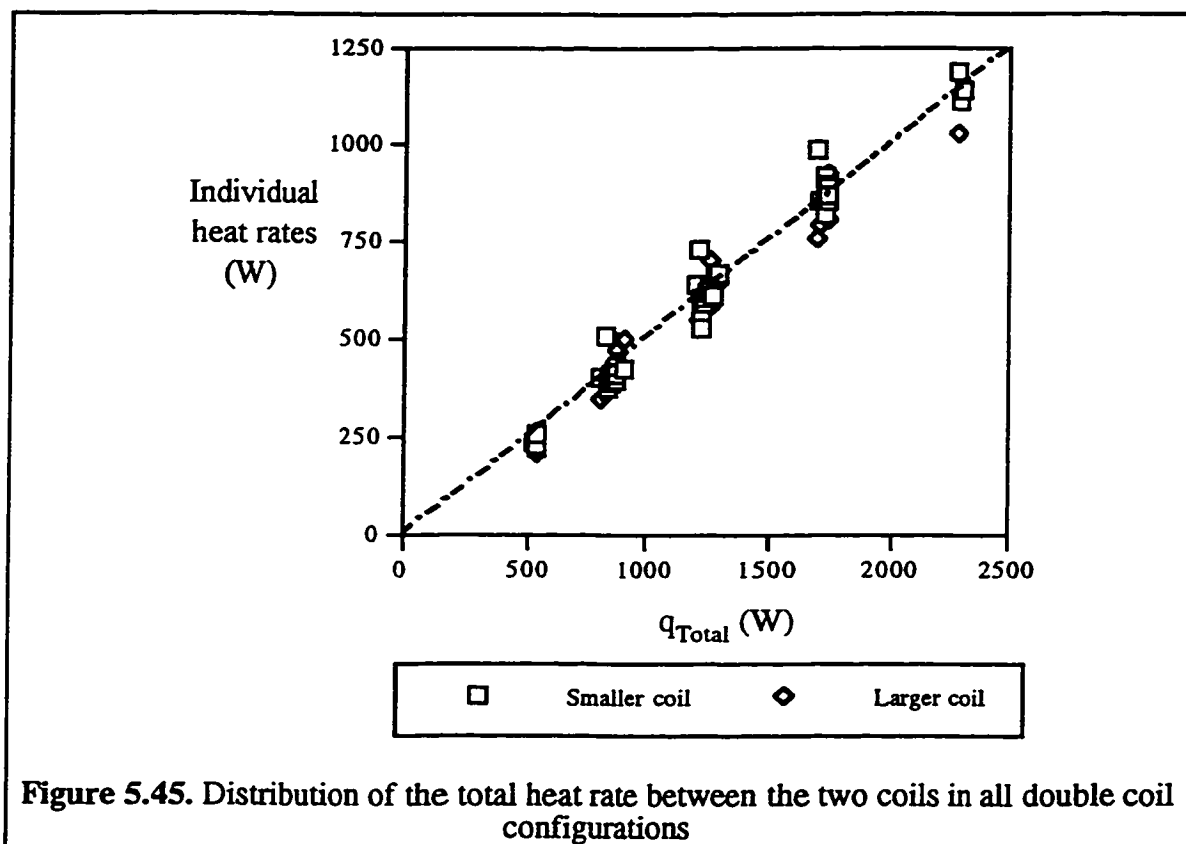
In this section the possible effects on the shell-side heat transfer coefficient due to the interaction between multiple coils in the heat exchanger will be examined.

5.5.4.2.1. Double coils

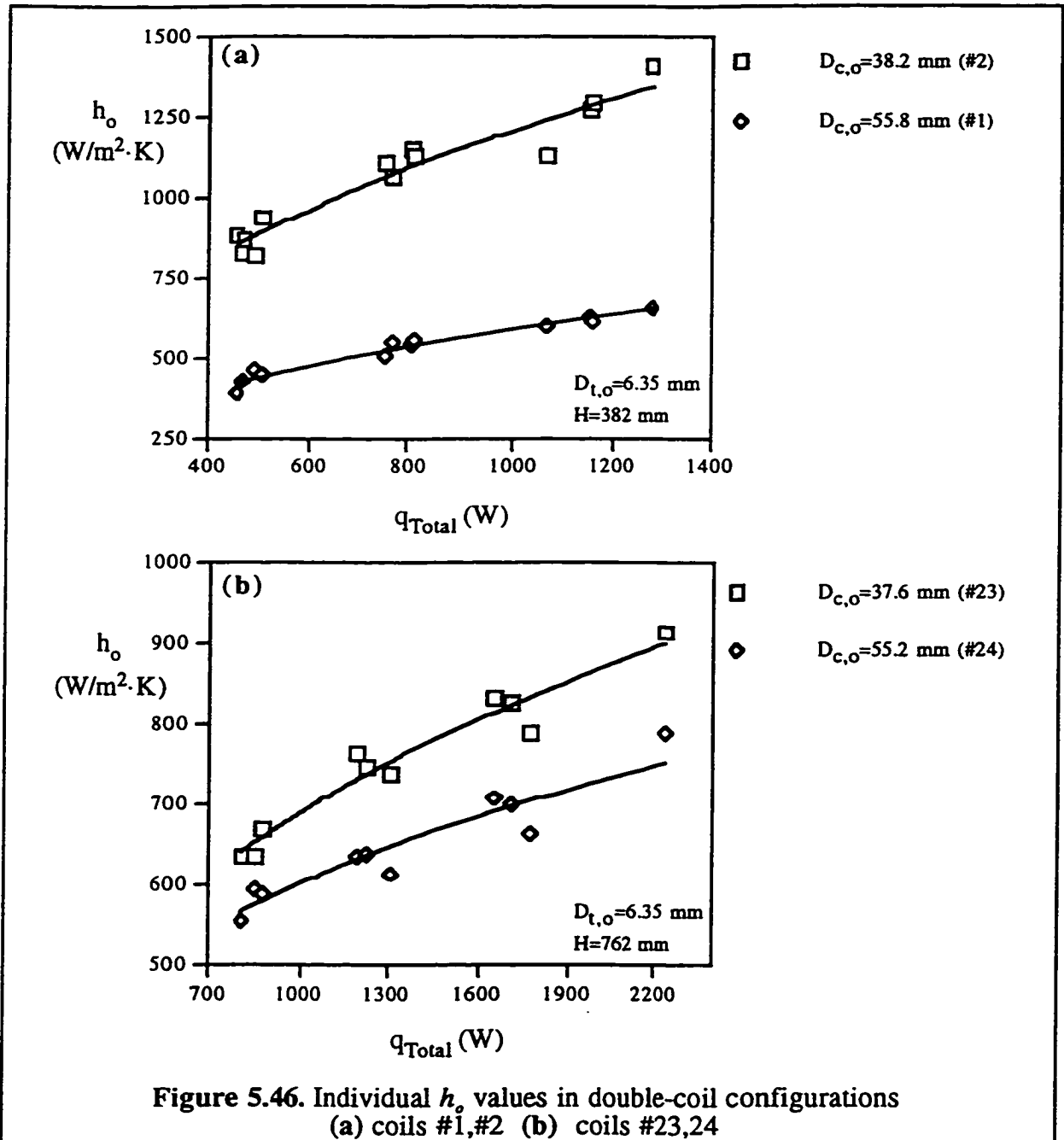


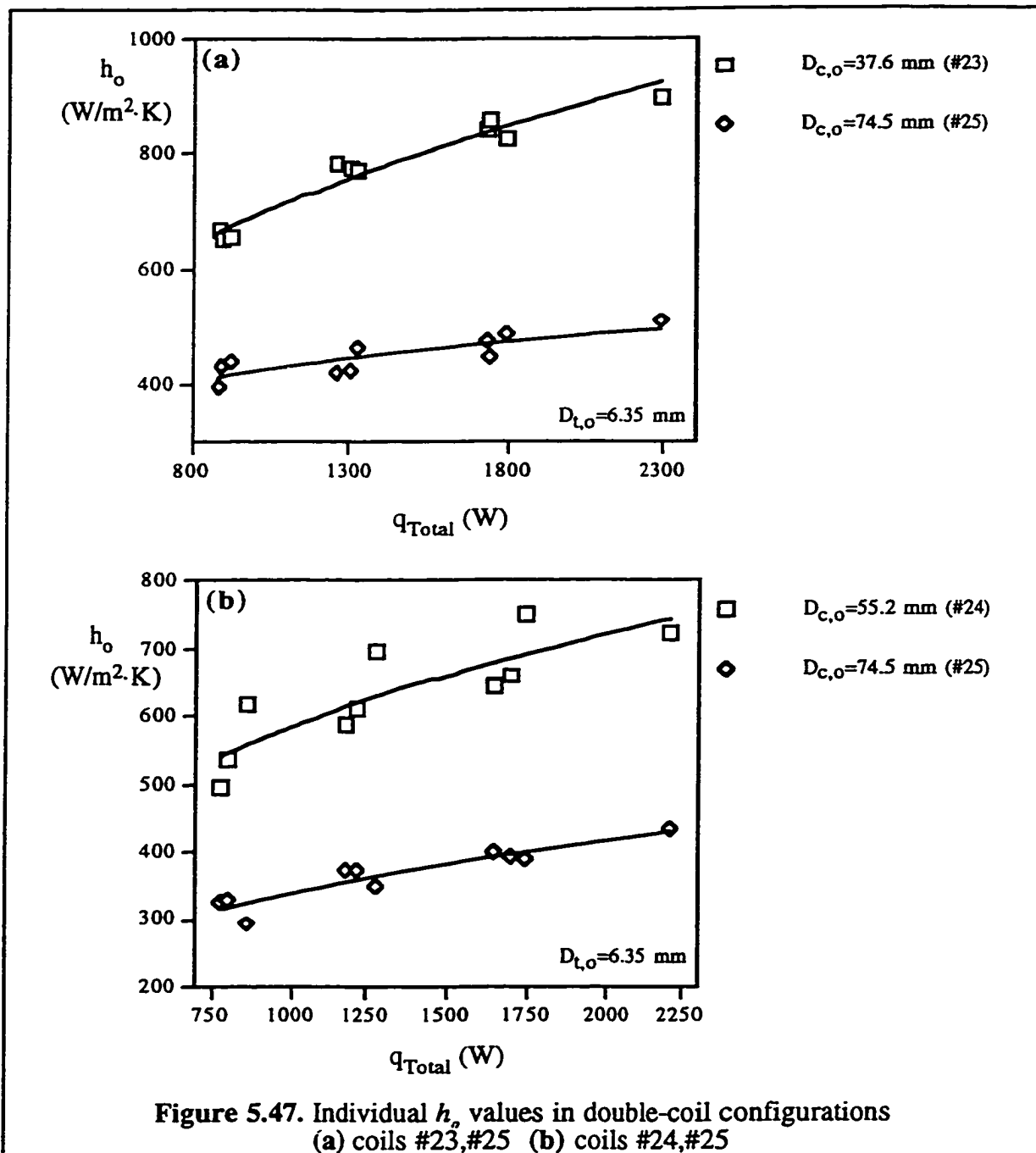
First it can be shown that the average shell-side heat transfer coefficient data for double coil tests correlate well with those for single coils when they are plotted against the heat flux (figure 5.44). The shell-side heat transfer coefficient of the double coil heat exchangers are in the range 410 to 920 $\text{W/m}^2\cdot\text{K}$ for 500 $\text{W} < q < 2300$ W , which is a slight increase in h_o compared to single ones. For the same heat transfer area and heat rate there is an average of about 13% improvement in h_o .

Secondly, it can be shown that regardless of the length and diameter of individual coils in a double coil configuration, both coils will always convey a nearly equal amount of heat to the cold stream. Figure 5.45 shows this nearly 50-50 division. The deviation of the data points for smaller and larger coils from the 50% diagonal line is very small. The maximum deviation is 20% for larger coil and 15% for the smaller coil. The plot of figure 5.45 covers the data from all double coil configurations having different diameter ratios (table 5.1). This makes for a fair comparison between the coils in a multiple coil configuration.



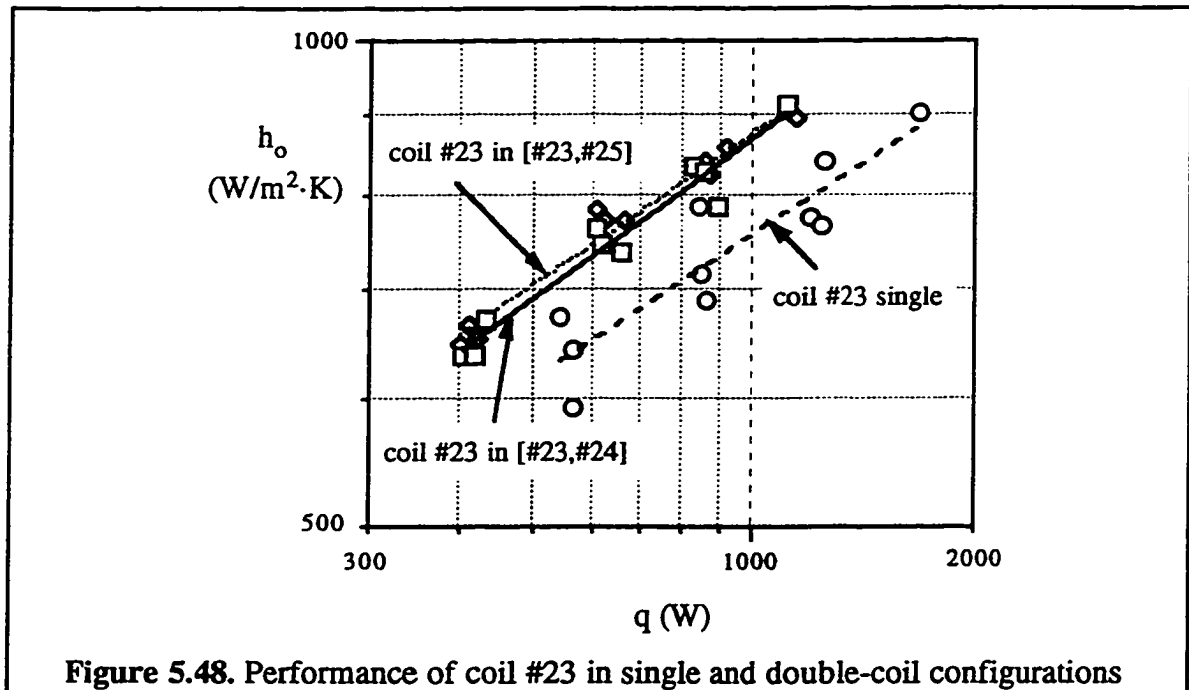
The effects of different parameters on the shell-side heat transfer coefficient in single coil configurations were discussed in previous sections. It is expected to see some changes in the value of h_o of individual coils in a multiple coil configuration. These changes are expected to happen due to the interaction between the boundary layers of each coil. Figures 5.46 and 5.47 compare the individual shell-side heat transfer coefficients for the coils in double-coil configurations.





The smaller coil always performs better than the larger one in the double-coil configuration. Some of this improved performance is because of the decreased area of the coil, as was found in section 5.5.4.1.1 that increasing coil surface area will decrease the shell-side heat transfer coefficient of single coils. The additional difference between the performance of the smaller and larger coil is mainly due to the inferior performance by the

larger coil. While the performance of the smaller coil in a double-coil configuration is slightly improved, the larger coil offers significantly lower h_o values compared to the case of single coils. This is evident first by comparing the h_o values of the coil #23 in the single and two double coil configurations.



It is clear from figure 5.48 that the performance of coil #23 is not affected by alteration of its accompanying coil in the double coil situation. Higher h_o values in double coil configurations can be achieved compared to those for single coil ones. The reason is that the second coil in a double coil configuration contributes to the heat transfer process by increasing the mean water temperature inside the heat exchanger. This results in a higher value for the shell-side heat transfer coefficient. Therefore the comparison between single and double coil configurations is not equitable.

The performance of coil #24 in single and double-coil configurations is plotted in figure 5.49. The same result was found for coil #24 except for the fact that the difference between the performance in single and double coil configurations was smaller. However, as it is evident from figure 5.50 the situation is different for coil #25.

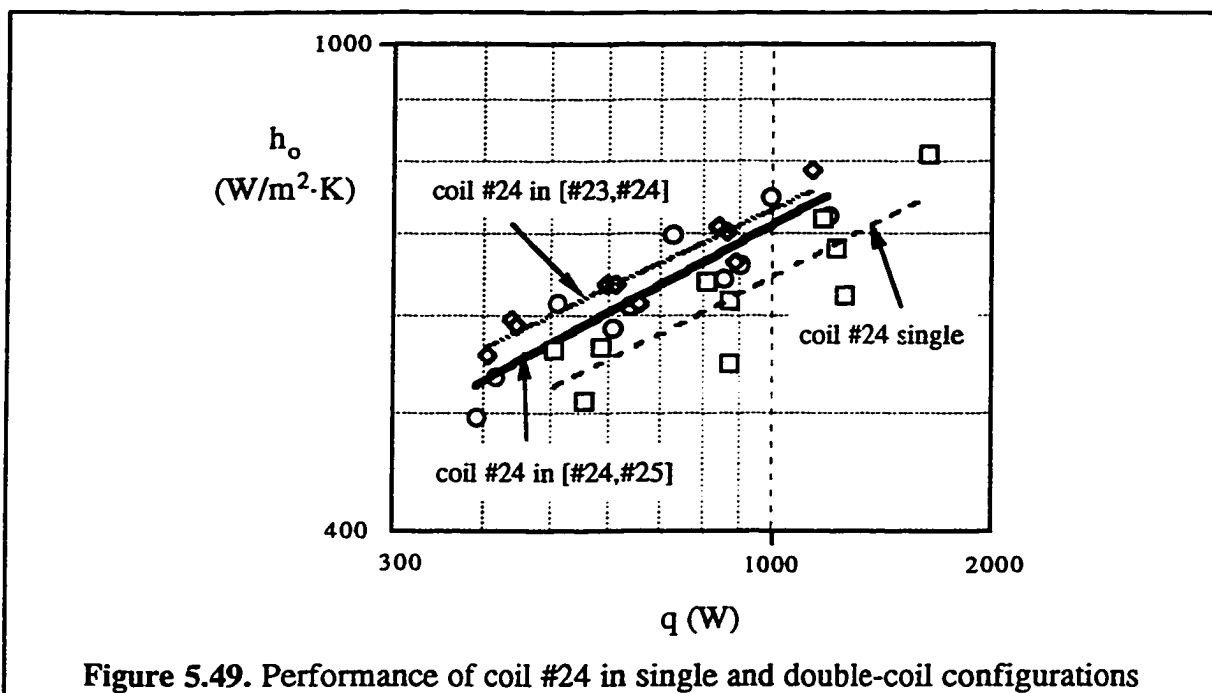


Figure 5.49. Performance of coil #24 in single and double-coil configurations

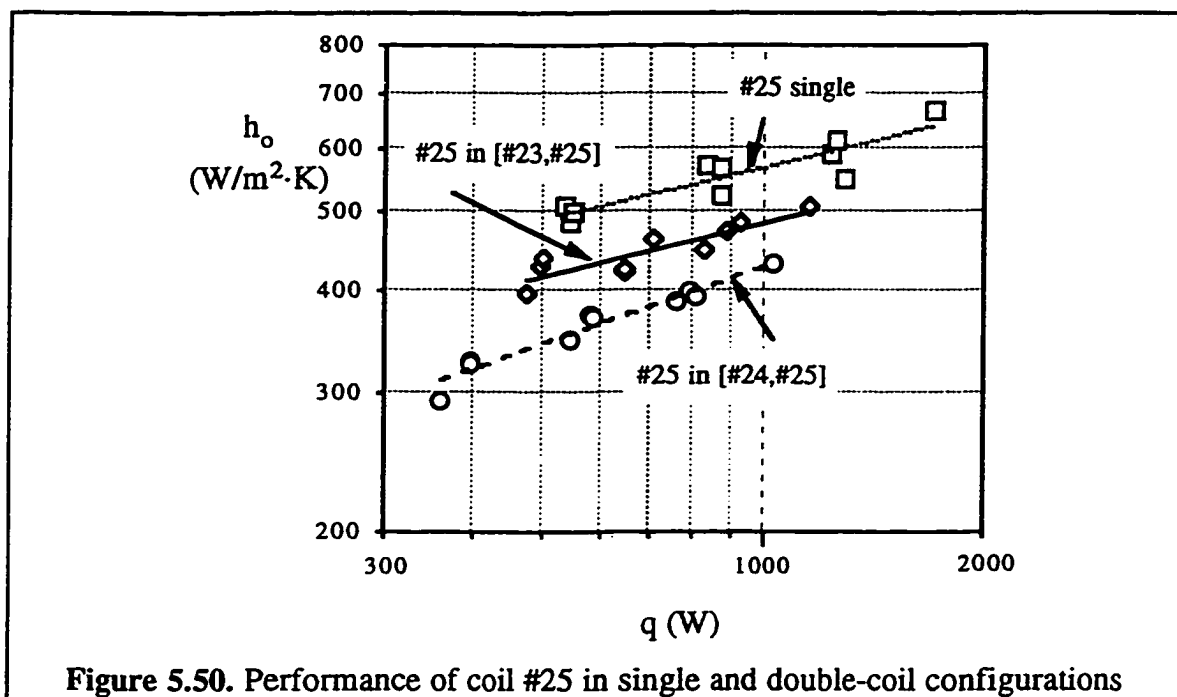


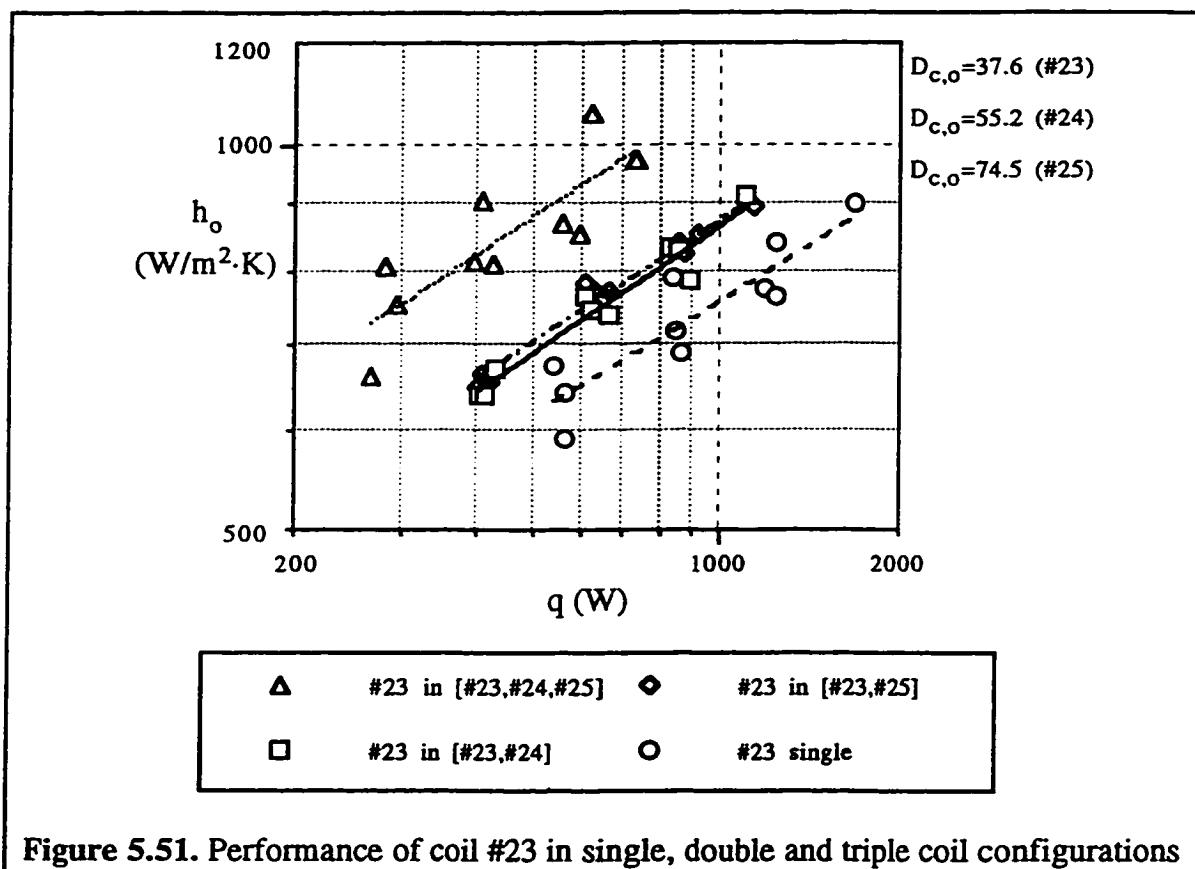
Figure 5.50. Performance of coil #25 in single and double-coil configurations

For coil #25 the performance is better in the case of single coil configuration. Also its performance in double coil configuration changes as its accompanying coil is altered. This different behavior can be explained as follows. In the case of coil #23 and coil #24, the water can flow along the both inner and outer areas of the coil, washing away the hot layer of water close to the coil surface. When they are accompanied by a second coil, acting as a barrier to heat transfer from that side, there always exists an alternate side to counter this barrier effect. Thus the heat transfer coefficient of the coils #23 and #24 will not be affected greatly in double coil situations.

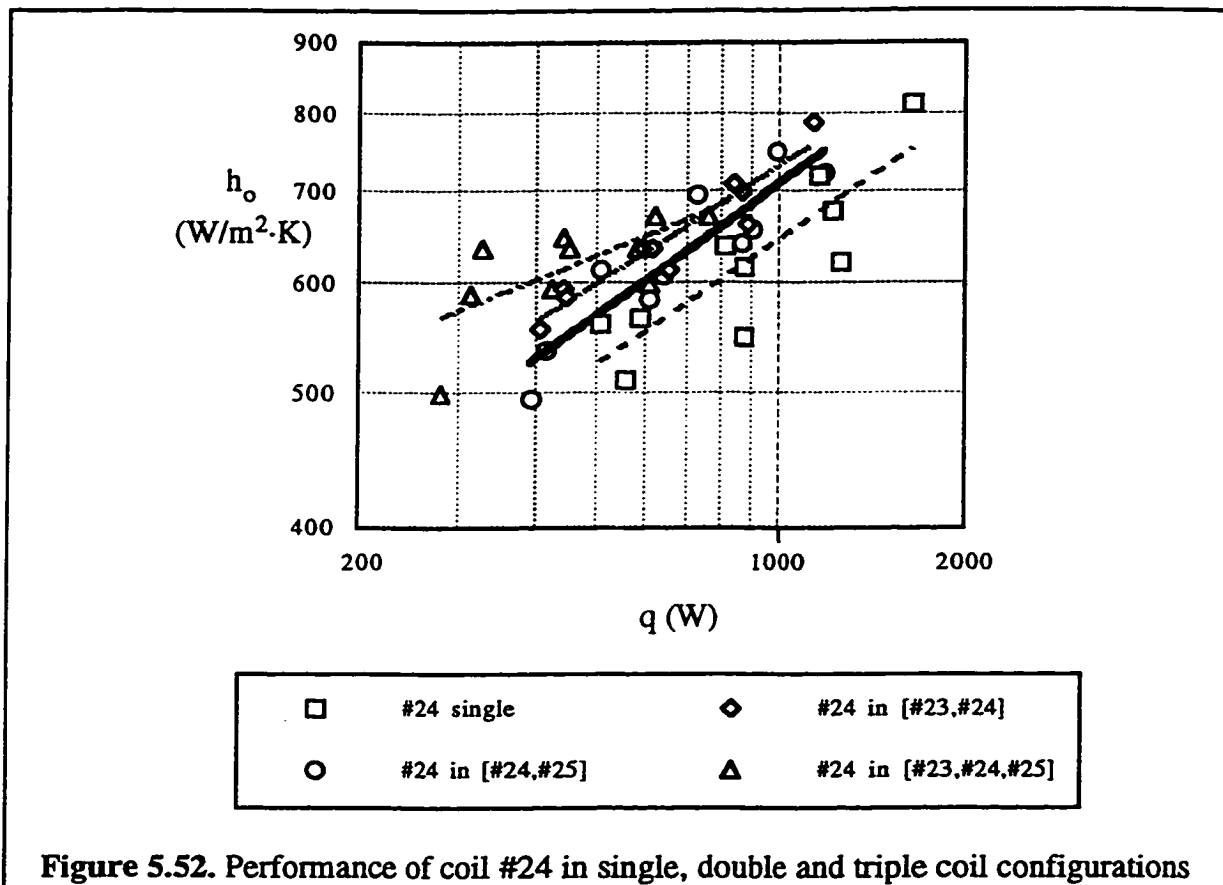
However, coil #25, being the largest of the three, is always located in such a way that its outer wall is against the heat exchanger shell. In fact the outer diameter of coil #25 is large enough to touch the shell wall. This, of course, completely blocks the flow of water along its outer surface and forces it to only rely on the inner surface for transfer of heat to the stream of water. When there is a second coil present on the inner side of coil #25, the role of this second coil is to insert a shield in front of the inner wall of coil #25 resulting in increased surface temperature for the coil #25 and consequently lower heat transfer coefficients. As the diameter of the inner coil increases, the shield comes closer to the coil, causing more drop in the h_o values.

Since the performance of coil #25 is better in a single-coil situation, it can be concluded that the effect of increased surface temperature is stronger than the increased mean water temperature due to heat transfer from the second coil.

5.5.4.2.2. Triple coils



Similar to the case of double coils, for coil #23 the performance is even better in triple coil configuration as illustrated in figure 5.51. Again this is due to higher mean water temperature caused by heat transfer from the other two coils. For coil #24 the distinction is not clear as with double-coil configurations as shown in figure 5.52.



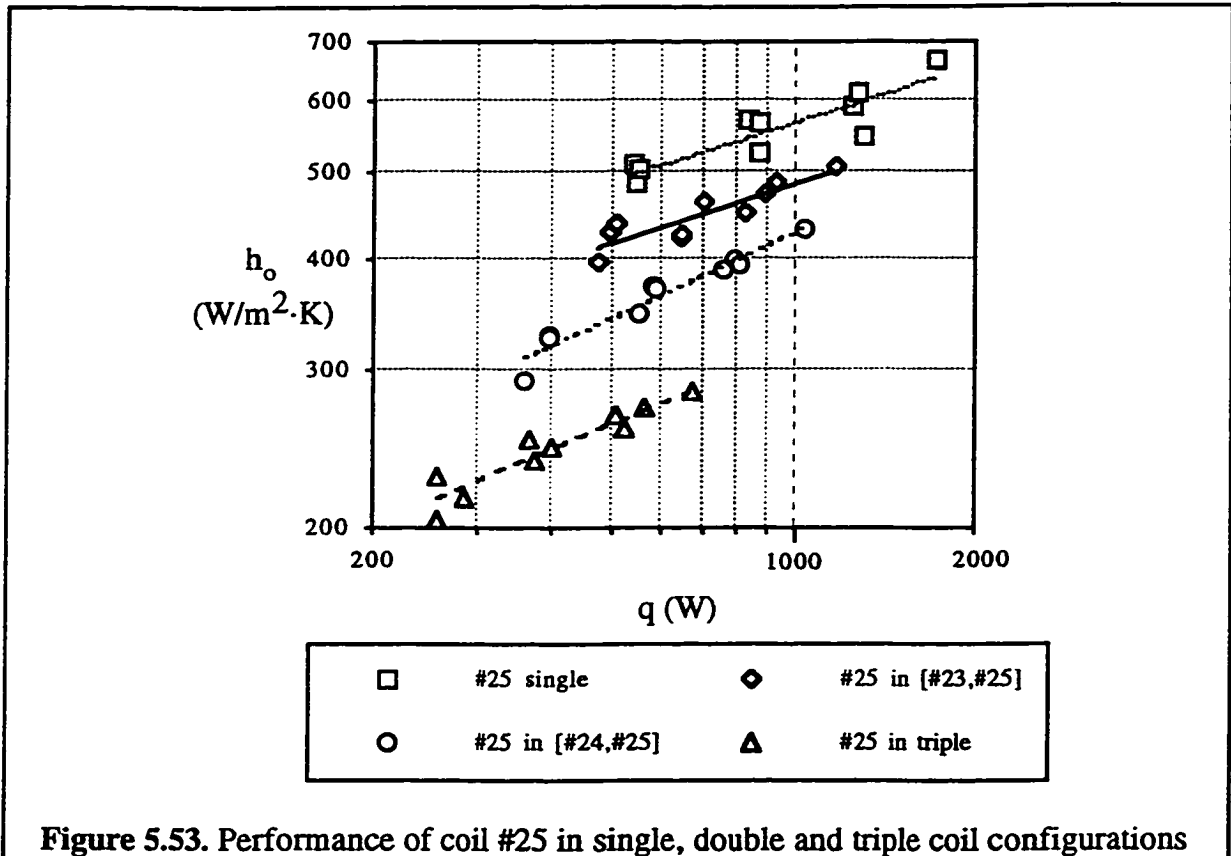


Figure 5.53 indicates that the behavior of coil #25 is the opposite of that of coil #23. Coil #25 performs best when there are no other coils present, second best when a small diameter coil is present (#23, #25), followed by the case that the inner coil has a diameter closer to that of coil #25. The worst case is when there are two coils accompanying coil #25. This can be explained as follows.

According to figure 5.32, the largest diameter coil conveys the lowest glycol flow rate among the three. This low flow rate will cause a rise in the mean surface temperature of the coil. The outer surface of the coil is nearly in contact with the shell inner wall, leaving no room for water to flow freely on that side. Moreover, in triple coil configuration, the role of the two smaller coils located in the core area of the larger coil is to provide a thermal wall in the inside area of the coil. The unavailability of free space on the outside, and the existence of the thermal wall on the inside of the coil will block the cold water stream from reaching the higher temperature surface of the largest coil. As a consequence the participation of the mentioned coil in the total process of heat transfer will become very

limited. This is exhibited by the heat transfer coefficients of considerably lower values than expected.

Based on the above observation the following recommendations can be made in order to improve the situation or optimize it. The diameter of the largest coil should be chosen so that there is a gap between its outside wall and the shell. A rough estimate for the size of the gap would be at least half the tube diameter. This condition might be difficult to fulfill because of limited space in the heat exchanger shell. In that case the largest coil should have less surface area than usual. In other words, the coil must be made with fewer turns i.e. higher pitch. This will reduce the amount of copper tube used to build the heat exchanger and yet the performance will remain unchanged. Again as a rough estimate, the surface area of the coil can be reduced to a value equal to that of the middle coil. For more precise figures additional experiments need be done.

This subject can also be looked at from a different angle by studying the glycol outlet temperatures of the three coils in the triple coil configuration. Figure 5.54 is the plot of the glycol outlet temperatures for individual coils in the triple coil configuration versus the total heat rate. For total glycol flow rates larger than 0.0258 kg/s it is evident from figure 5.54 that the outlet temperatures for the two inner coils (#23 and #24) are nearly identical for all heat rates. As for the outermost coil (#25), the outlet temperature stays at a higher value than that of the inner two coils. The excess temperature for the largest coil increases as the heat rate increases. The temperature differences at the outlet of the glycol side of the heat exchanger cause mixing. According to the second law of thermodynamics, mixing of streams of fluid at different temperatures generates entropy which translates to the loss of some available energy in the total flow. In other words, the exchanger will not perform as expected. The more the temperature difference is between the streams, the more severe will be the loss.

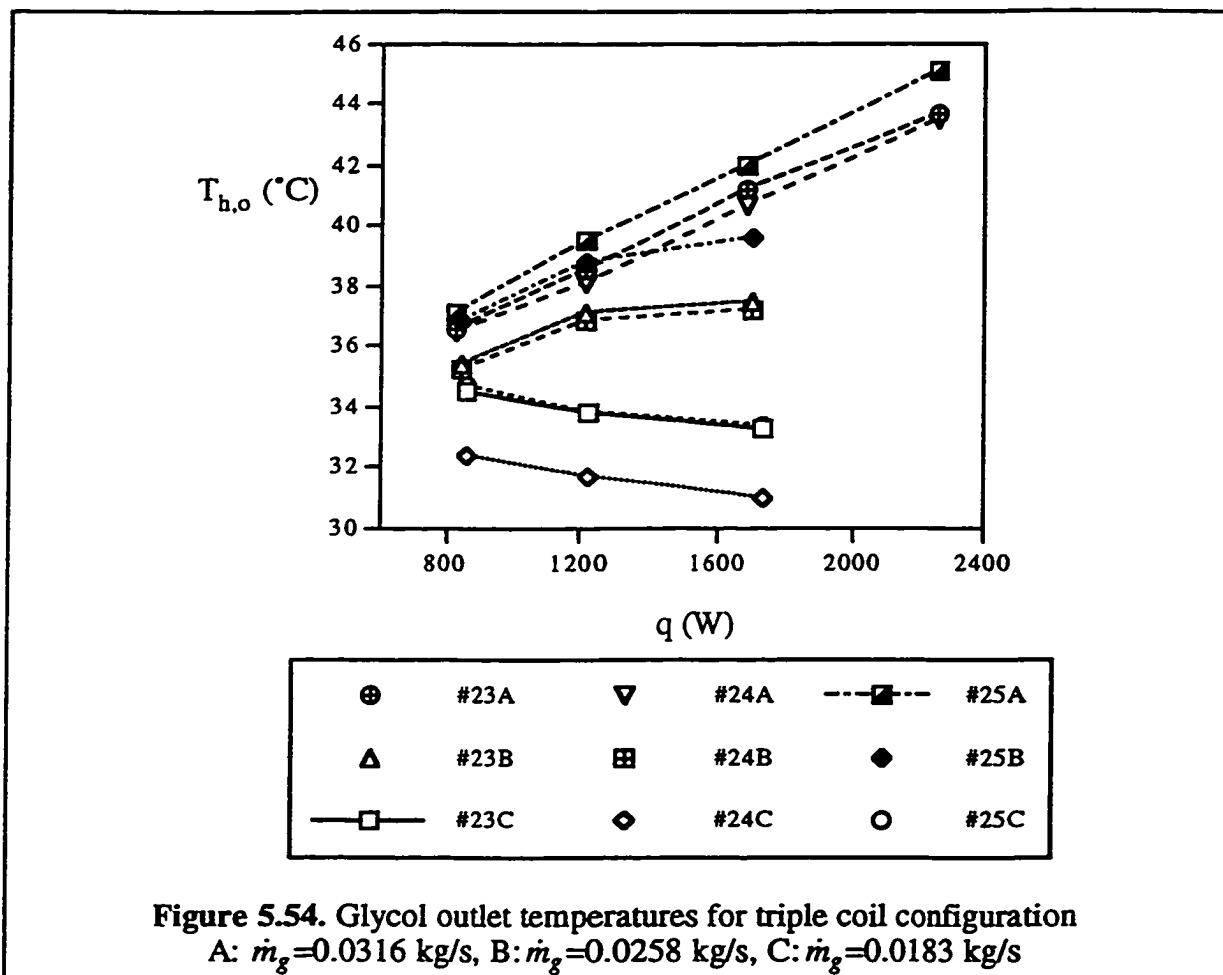


Figure 5.54 illustrates an additional interesting phenomenon. For higher flow rates ($\dot{m}_g=0.0316$ kg/s), as the total heat rate increases the outlet temperature of each coil increases as well. For lower flow rates ($\dot{m}_g=0.0183$ kg/s) the trend is reversed and increasing the heat rate results in decreased outlet temperatures. The intermediate value of the glycol flow rate produces plots that are flat for high heat rates. In other words, for intermediate glycol flow rate, the outlet temperature increases initially but tends to remain unchanged as the heat rate increases further. This behavior can be further explained as follows. For $\dot{m}_g=0.0316$ kg/s the hot stream of glycol carries enough heat capacity to transfer the heat at the required rate and as the heat rate increases this heat capacity remains strong. At $\dot{m}_g=0.0258$ kg/s the hot stream loses some of its heat capacity to carry the heat and therefore further increasing the heat rate does not lead to higher outlet temperatures. Whereas in the case of $\dot{m}_g=0.0183$ kg/s the glycol flow does not possess enough heat

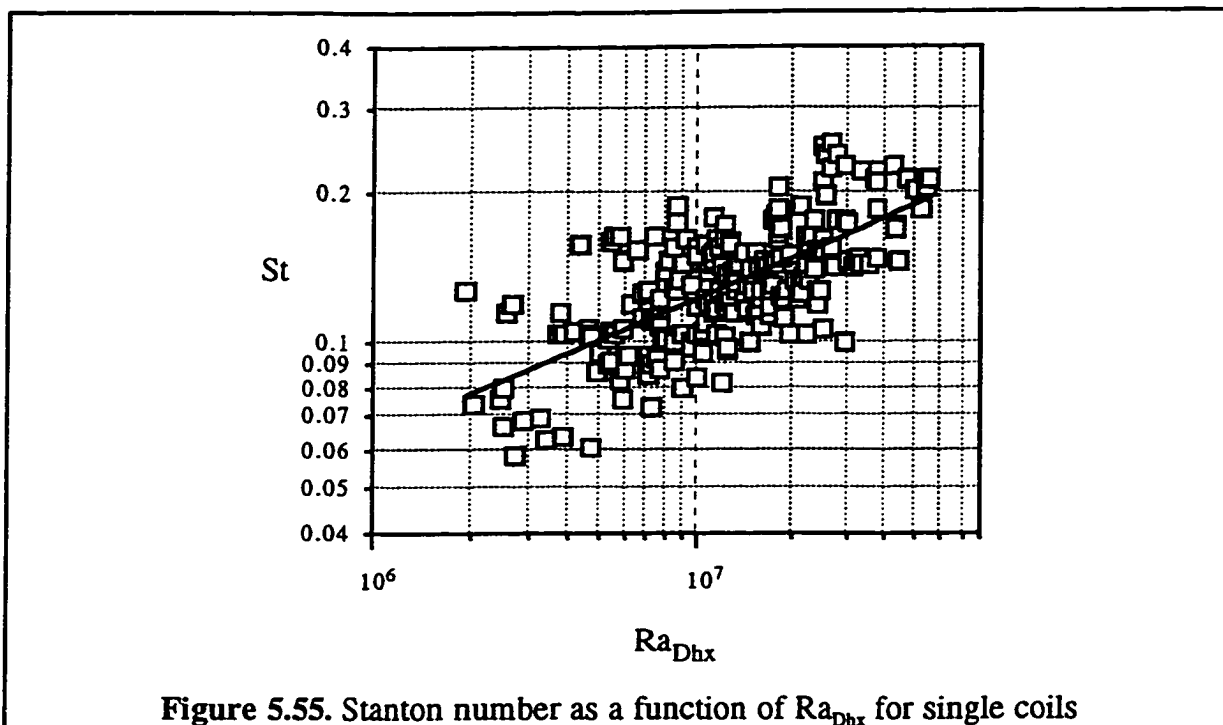
capacity to increase the temperature. As a result the situation gets worse when more heat transfer is demanded and the drop in outlet temperatures is unavoidable. This behavior suggests that somewhere around $\dot{m}_g=0.0258$ kg/s exists an optimum glycol mass flow rate for which the demand for heat transfer is fulfilled while unnecessary additional pump work is avoided.

5.6. The Stanton number

Considering that the flow is turbulent on the shell side, it is then justified to investigate the changes in the Stanton number of the heat exchanger. The Stanton number can be regarded as the Nusselt number, modified for the case of turbulent forced convection (Bejan 1984). It often appears in representing the thermal behavior of cases of mixed convection as well. The situation inside a natural convection shell-and-coil heat exchanger is believed to be of turbulent mixed convection nature with natural convection as the dominant mode of heat transfer. Figure 5.55 is a plot of Stanton number versus the Rayleigh number based on D_{hx}

The plot of figure 5.55 contains the data from single coil configurations in the 71 mm ID shells. As can be seen, the correlation is not satisfactory. The general trend in figure 5.55 is that the Stanton number increases as the Rayleigh number increases. It was however discovered that for a fixed heat exchanger the value of the Stanton number does not change significantly. In other words, the Stanton number for a heat exchanger is solely a function of the geometry of the exchanger and not a function of the thermal and hydraulic parameters. This indicates that once a heat exchanger is built, a unique Stanton number can be assigned to it which will not change with changes in the heat rate, glycol flow rate, or even the inlet temperatures of water and glycol.

Based on the above argument and considering that the only geometrical parameter in $Ra_{D_{hx}}$ is the heat exchanger hydraulic diameter, it can be concluded from figure 5.55 that the Stanton number increases with increasing heat exchanger hydraulic diameter.

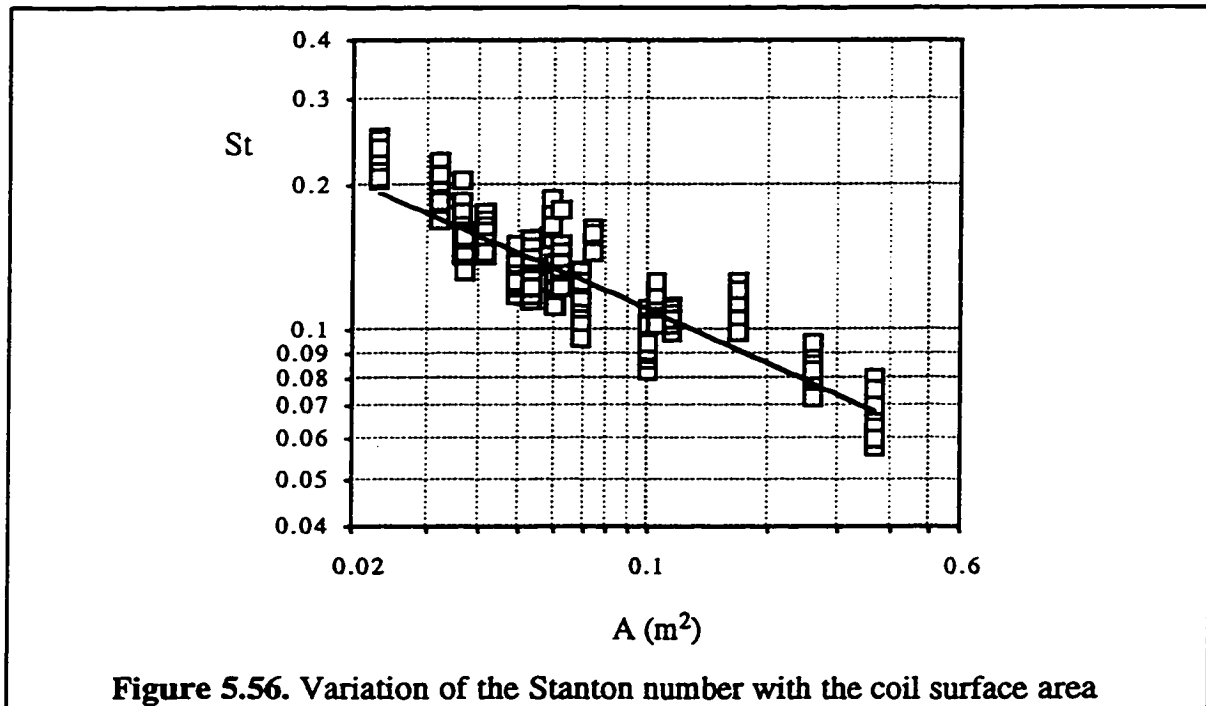


The uniqueness of the Stanton number for a particular heat exchanger leads to another fact regarding the friction coefficient for flow over the coils. In order to discuss this, reference should be made to the empirical equation known as the Colburn's formula which is reproduced here as equation 5.32.

$$St_x Pr^{2/3} = \frac{1}{2} C_{f,x} \quad 5.32$$

Equation 5.32 together with the observation of a fixed Stanton number for a heat exchanger suggests that the local friction coefficient on the shell side of a shell-and-coil heat exchanger is constant. This conclusion when extended to include the mean Stanton number, will point to the idea that once the heat exchanger is built, its friction factor on the shell side is fixed and does not change with thermal and hydraulic parameters. This in turn is a confirmation of the turbulent nature of the flow, since the weak dependence of the friction coefficient on the hydraulic parameters is a characteristic of turbulent flows.

The effect of the coil surface area on the Stanton number is plotted in figure 5.56. Increasing the coil surface area decreases the Stanton number as it is evident from figure 5.56.



The effect of the coil surface area can be discussed further as follows. The definition of the Stanton number, presented in the form of equation 5.33 reveals an important relationship between the heat transfer coefficient and the water mass flow rate of the heat exchanger.

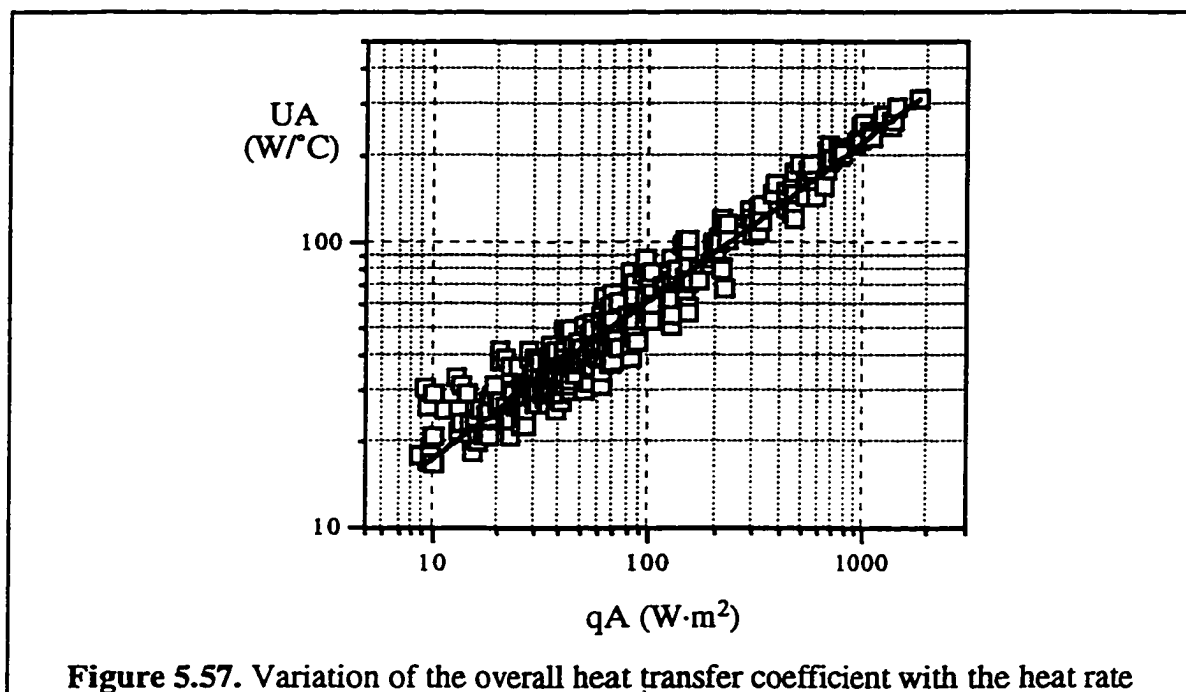
$$St = \frac{h_o A_{c,f}}{\dot{m}_w c_{p,w}} \quad 5.33$$

A fixed value of the Stanton number for a heat exchanger means a fixed value for the ratio of the shell-side heat transfer coefficient to the water flow rate for that particular heat exchanger. Figure 5.56 together with equation 5.33 suggest that as the coil surface area increases, the decrease in the Stanton number translates into a decreased ratio of h_o to \dot{m}_w for the heat exchanger. Since the shell-side heat transfer coefficient drops with

increasing the coil surface area at nearly the same rate as the drop of the Stanton number with the coil surface area, it can be concluded that the water mass flow rate remains unchanged. In other words, the magnitude of the water flow rate is not affected by the coil surface area and other geometrical parameters. This is an extension of the conclusions reached in section 5.4.

5.7. Overall heat transfer coefficient

So far the thermal performances of the glycol and water streams have been discussed separately. The knowledge of the combined behavior of the two streams is of greater importance for design purposes. Also the proposal of an optimum heat exchanger configuration could not be reliable unless the overall performance of the heat exchanger is known. The overall heat transfer coefficient or simply the UA product of the heat exchanger is a good measure of its thermal performance.



As the heat rate increases, the UA product of the heat exchanger increases for a fixed coil surface area. This is evident from figure 5.57 which includes the data from single

and multiple coil tests in both the short and the long heat exchanger shells. The UA product is plotted against the heat rate multiplied by the surface area to isolate the effect of the surface area on the UA product. The dominant influence of the heat rate was expected as it affects both the tube-side and the shell-side heat transfer coefficients in a constructive way. The other thermal-hydraulic parameter of influence is the glycol mass flow rate. Figure 5.57 implicitly points to the existence of a weak dependence on the glycol mass flow rate. This was concluded based on the fact that there is a good correlation between the data in figure 5.57 without including \dot{m}_g in the plot. Figure 5.58 can also confirm this weak dependence. It can be seen in figure 5.58 that the UA product of the heat exchanger changes only with $\dot{m}_g^{0.2}$ (the mass flow rate ratio is defined as, $R_m = \frac{\dot{m}_g}{\dot{m}_w}$).

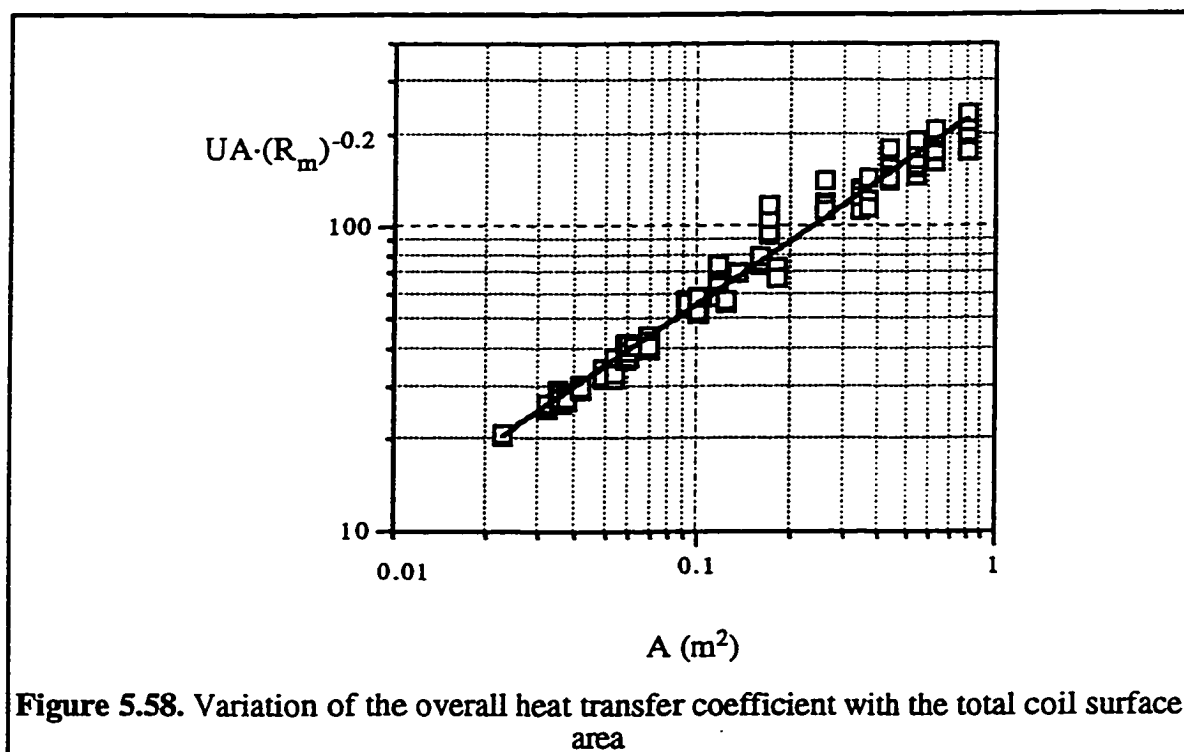


Figure 5.58. Variation of the overall heat transfer coefficient with the total coil surface area

The more important piece of information that can be deduced from figure 5.58 is the effect of the total coil surface area on the overall heat transfer coefficient of the exchanger. The effect of an increased coil surface area is to increase the value of the UA product. This seems quite obvious but the rate of the increase is less than expected. In

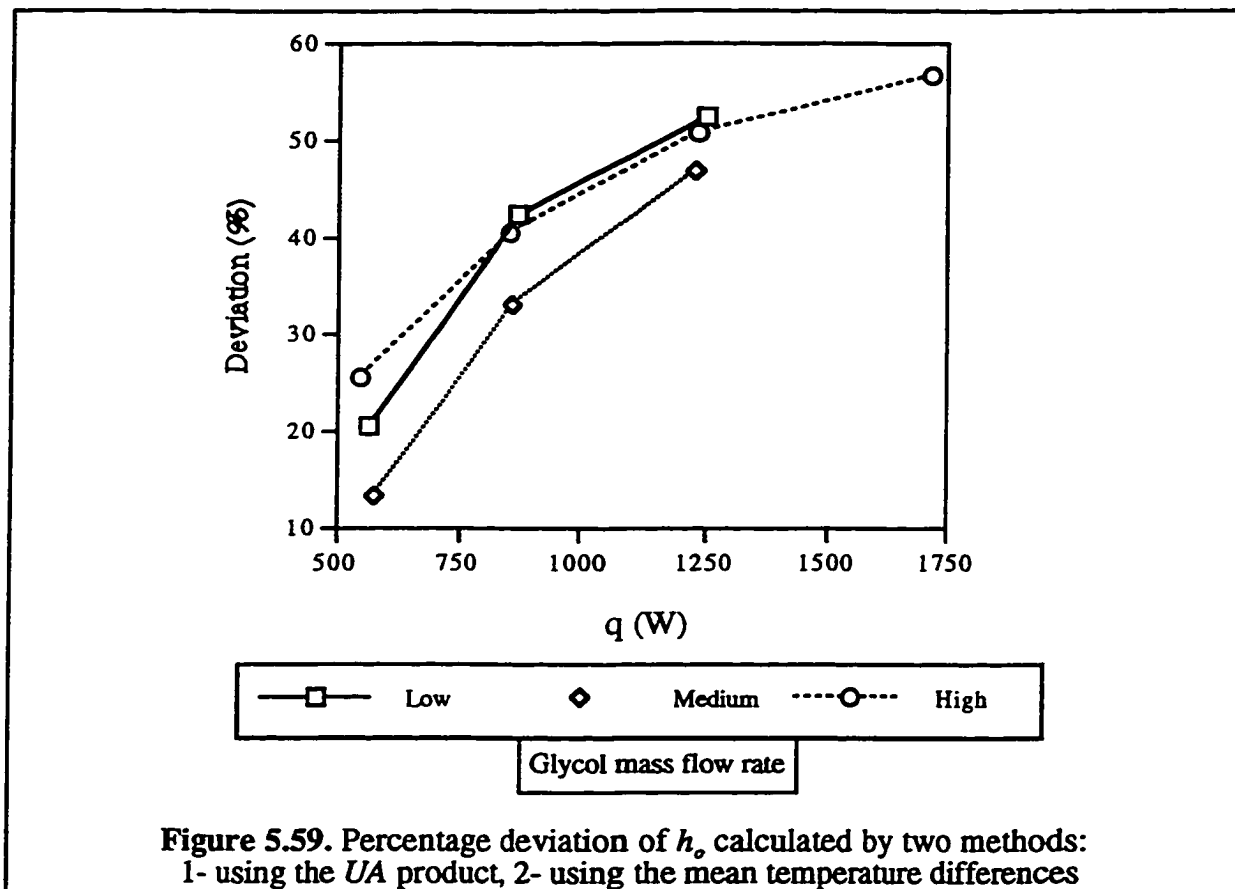
previous sections the adverse effect of the coil surface area on both the tube-side and the shell-side heat transfer coefficient was discussed. These combined effects lead to a relation of the form of equation 5.34 as extracted from figure 5.58.

$$UA \propto A^{0.67} \qquad 5.34$$

Therefore increasing the coil surface area will not result in an increase in the overall heat transfer coefficient in a one-to-one ratio. The UA values of some of the tested heat exchanger configurations are listed in appendix C.

The shell-side heat transfer coefficient was also calculated from the definition of the overall heat conductance of the heat exchanger. The h_o values calculated by this method had a deviation of between 10% to 60% from the h_o values calculated from the mean coil surface and water temperature difference. The glycol flow rate did not affect the amount of deviation, however, the deviation increased as the heat rate increased. Figure 5.59 is a typical plot of this deviation for various glycol flow rates versus the heat rate for coil #24.

The deviation exists mainly because of two reasons. First of all, evaluating the UA product from equation 3.25 involves the logarithmic mean temperature difference. The $LMTD$ is a mean value related to only the terminal temperatures and therefore might not be a very good representation of the actual mean temperature differences between the two streams of flow. Secondly, by calculating the h_o value from the UA product, the h_i must be first calculated from equation 3.7, which is an empirical correlation and contains a certain degree of uncertainty. This uncertainty will increase the magnitude of the deviation.

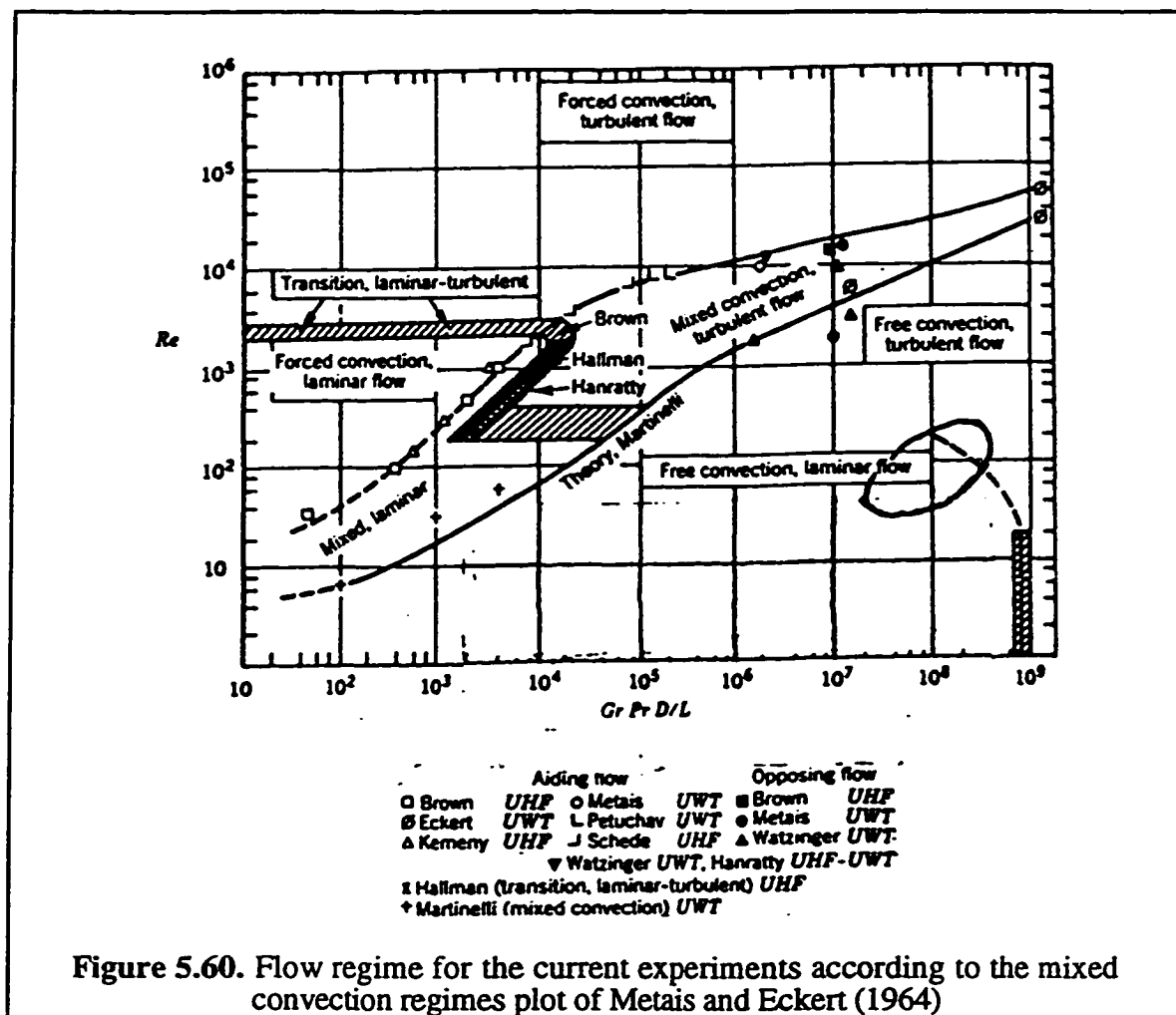


5.8. Regime of flow

Metais and Eckert (1964) proposed charts of mixed convection regimes in horizontal and vertical tubes indicating the boundaries between the various flow regimes. Figure 5.60 is a reproduction of the Metais and Eckert chart with the current thesis data included. The results of the current experiments always fell inside the area enclosed by an ellipse in the bottom right corner of the chart. As it is evident from the chart, the bottom right corner of the chart is the location of the boundary between laminar and turbulent natural convection regimes. It can therefore be concluded that, firstly the effects of forced convection are negligible in the current situation, and secondly, the regime of flow for the current experiments is in transition between laminar and turbulent.

However, the values of the Richardson number are always greater than 200, which are considerably higher than the transitional value of the order of unity. The high

Richardson number is an indication of fully turbulent natural convection regimes. As stated before, since the wavy surface of the coils act as a disturbance in the flow, the likelihood of the flow to be fully turbulent is higher.



CHAPTER 6

RESULTS AND DISCUSSION - II

6.1. Nusselt number correlations

In this chapter the Nusselt number based on different characteristic lengths is plotted against the Rayleigh number in order to obtain correlations of the form $Nu = CR\alpha^n$.

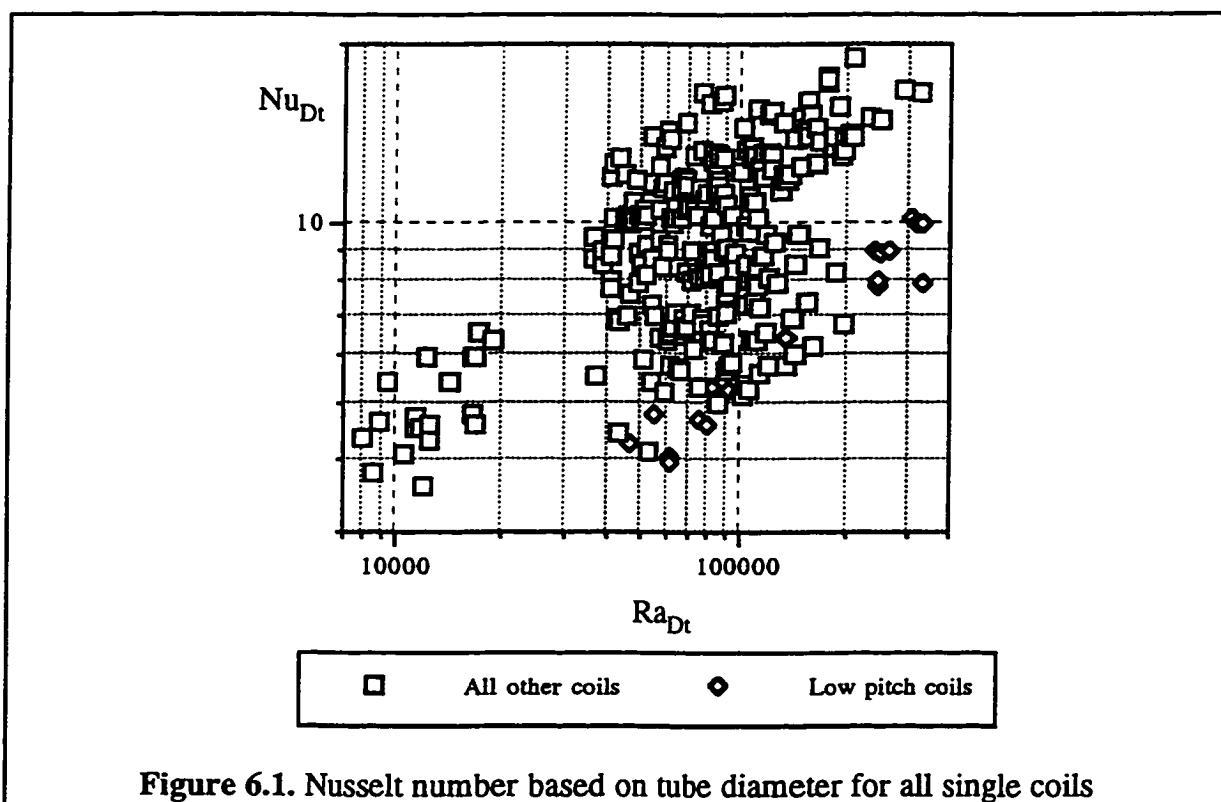
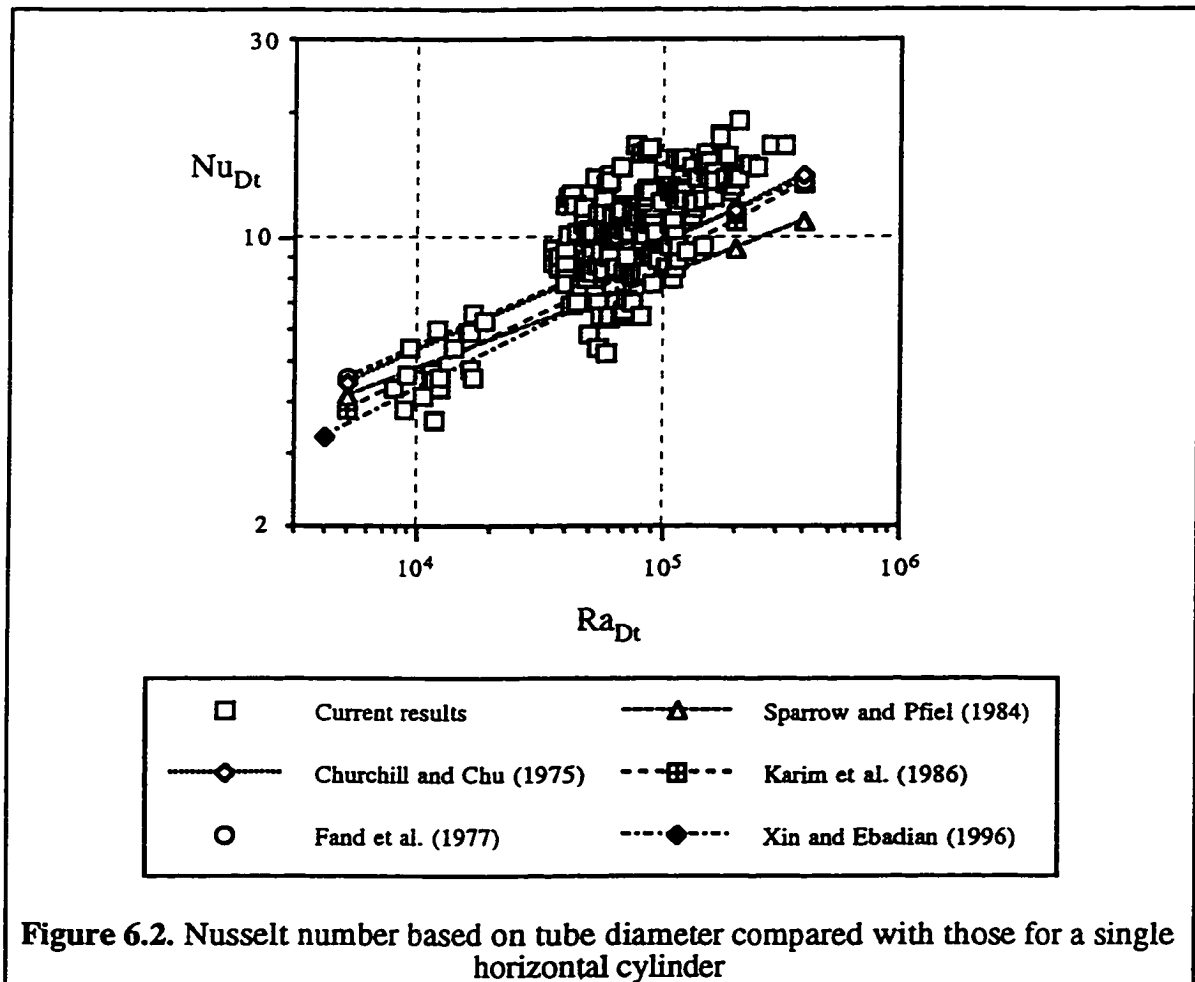


Figure 6.1. Nusselt number based on tube diameter for all single coils

Figure 6.1 indicates that the Nusselt number data can not be correlated with the Rayleigh number when tube diameter is the characteristic length. The characteristic length must represent the geometry of the system and clearly the tube diameter does not represent the geometry of a heat exchanger with multiple helical coils. Figure 6.1 contains the data from single coil experiments but multiple coils would make the outcome worse.

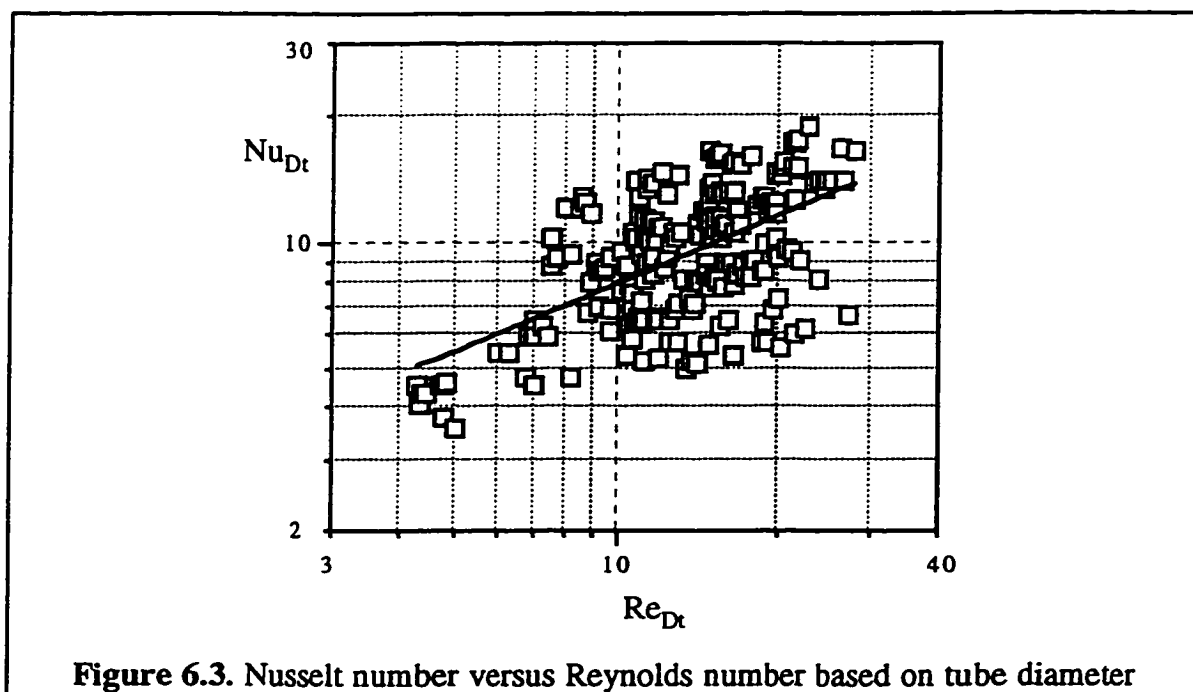
Nevertheless the results can be compared with those by previous authors. In figure 6.2 a comparison is made with Nusselt number for single horizontal cylinders. There has been conducted quite an amount of research on the subject of natural convection from single horizontal cylinders. For the sake of comparison, the most recent literature was taken into account.



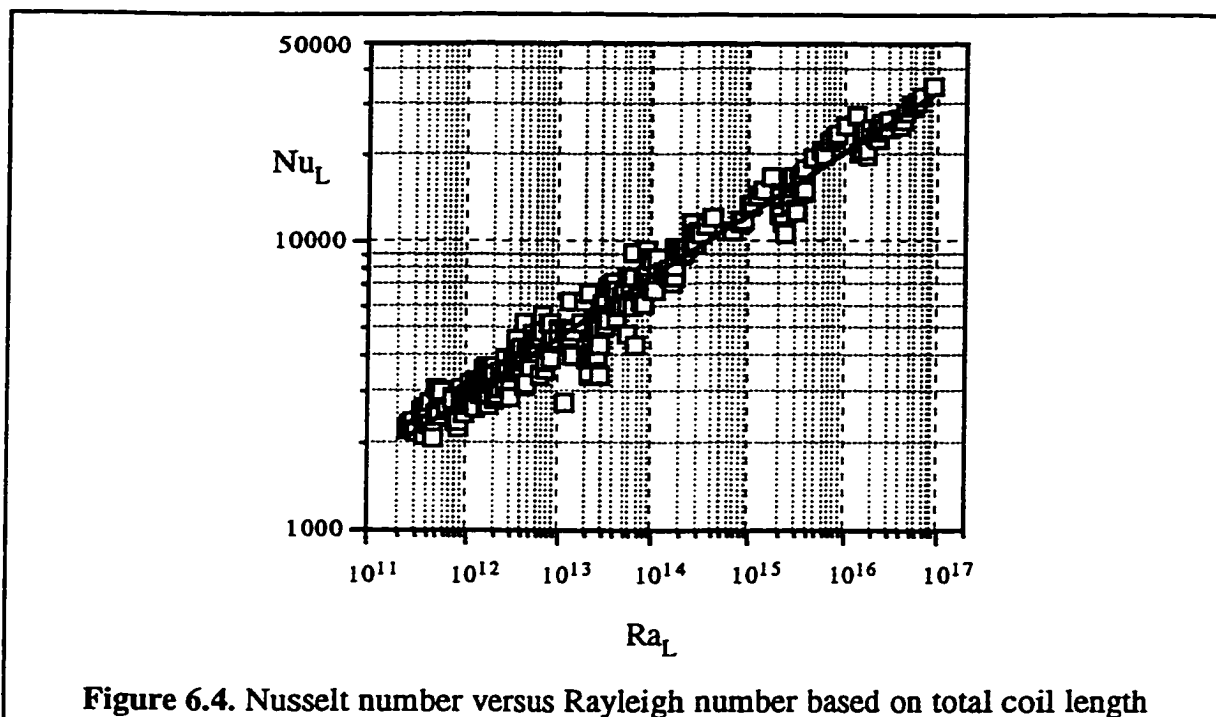
In general, the data is in good agreement with the literature. The current results have been plotted together with those by Churchill and Chu (1975), Fand, Morris and Lum (1977), Sparrow and Pfiel (1984) and Karim, Farouk and Namer (1986). The results of Xin and Ebadian (1996) for helical coils are also included in the figure. For $Ra_{Dt} < 3 \times 10^4$,

the heat transfer coefficient of a coiled tube is less than that of a horizontal cylinder. However, the coiled tube performs better than a single horizontal cylinder for $Ra_{Dt} > 3 \times 10^4$. Figure 6.2 can be considered as a validation of the current experiment results.

The Nusselt number based on the tube diameter can also be plotted against the Reynolds number. As can be seen from figure 6.3 the correlation is not acceptable. Figure 6.3 contains the data from single coil configurations in 77 mm shells.



The idea of seeking a $Nu-Re$ correlation was justified by considering that in this natural circulation loop, once the circulation starts, the flow mode is mixed convective. The flow of water is driven by the density difference between the water columns in the storage tank and the heat exchanger, and this can be viewed as a pump in the loop, creating the same velocity profile as produced by the buoyancy-induced flow.



In figure 6.4 the Nusselt number from all tests is plotted as a function of the Rayleigh number with the total coil length as the characteristic length. Figure 6.4 contains the data from all tested configurations (i.e. 51 mm and 77 mm ID shell, 382 mm and 762 mm long shell, single and multiple coils). Equation 6.1 correlates the data well for the range $2 \times 10^{11} < Ra_L < 1 \times 10^{17}$.

$$Nu_L = 7.34 Ra_L^{0.215} \quad 6.1$$

The coefficient of determination is 0.97 for the above correlation. As illustrated in figure 5.32 and equation 5.21, as the length of the coil increases the shell-side heat transfer coefficient decreases. Equation 6.1 suggests a relationship of the form $h_o \propto L^{-0.355}$ which is in agreement with equation 5.21.

Figure 6.5 was produced to compare the current results with those by previous authors.

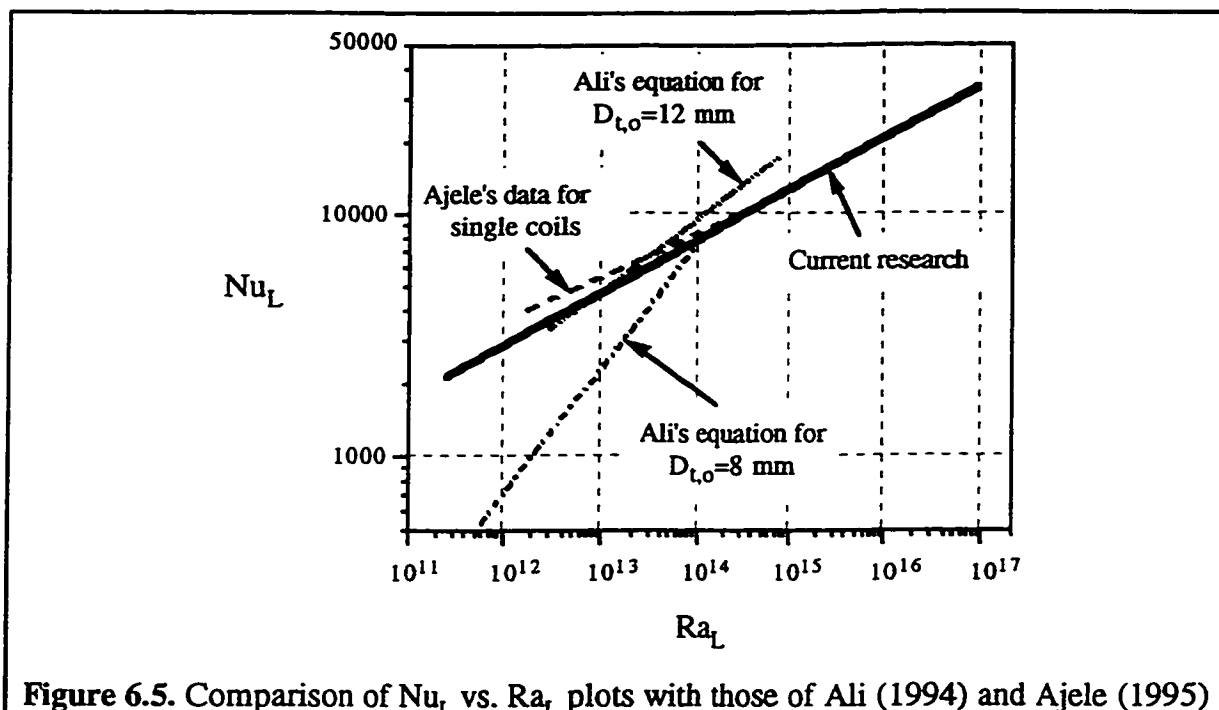


Figure 6.5. Comparison of Nu_L vs. Ra_L plots with those of Ali (1994) and Ajele (1995)

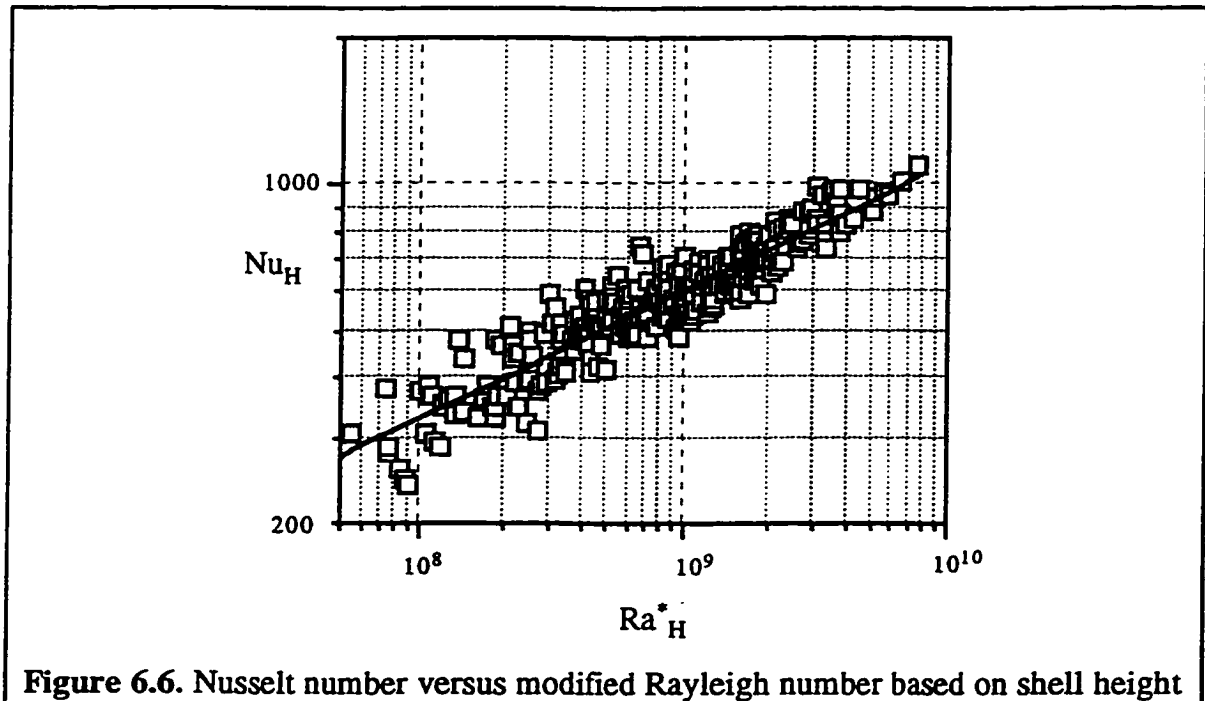
Ajele (1995) plotted the data for single coils based on the coil length but did not present a correlation for the plot. As can be seen in figure 6.5 there is a good agreement between Ajele's result and the result of the current thesis.

Ali (1994) presented two correlations for two different tube diameters tested. Ali's two correlations are not consistent with each other. The correlation for 12 mm tube is somewhat closer to the current research results at the lower end of its range and it departs from the current research results at the higher end of its range. The trend is reversed for the correlation for the 8 mm tube. Over its entire range, Ali's correlation for the 8 mm tube is far from the current data and only at the upper end of its range it is in agreement with the current research.

Because of the close agreement between the data of Ajele (1995) and those of the current work, it is reasonable to believe that some inaccuracies are involved in the work of Ali (1994).

A correlation based on the shell height was introduced in chapter 5 (equation 5.31). Figure 5.43 can be improved by including the data from multiple coil configurations. The

modified Rayleigh number based on the shell height ($Ra_H^* = Ra_H(H/L)^{1.5}$) was introduced in order to take into account the effect of various coil lengths inside each shell. Figure 6.6 is the improved version of figure 5.43. The data from 51 mm shell are not plotted on figure 6.6.



Equation 6.2 correlates the data well for the range $5 \times 10^7 < Ra_H^* < 8 \times 10^9$ or $4 \times 10^9 < Ra_H < 7 \times 10^{11}$, with a coefficient of determination of 0.86.

$$Nu_H = 2.52 Ra_H^{*0.265} \quad 6.2$$

The above correlation is valid for a shell diameter of 77 mm and for single as well as multiple coils. As was concluded before for single coils, the effect of the shell height on the heat transfer coefficient is minimal. Using equation 6.2, the same conclusion can be extended to multiple coil configurations. Equation 6.2 suggests that the relationship

between the shell-side heat transfer coefficient and the shell height is of the form,
 $h_o \propto H^{0.193}$.

In figure 6.7 the results of the current research are compared with those by Ajele (1995).

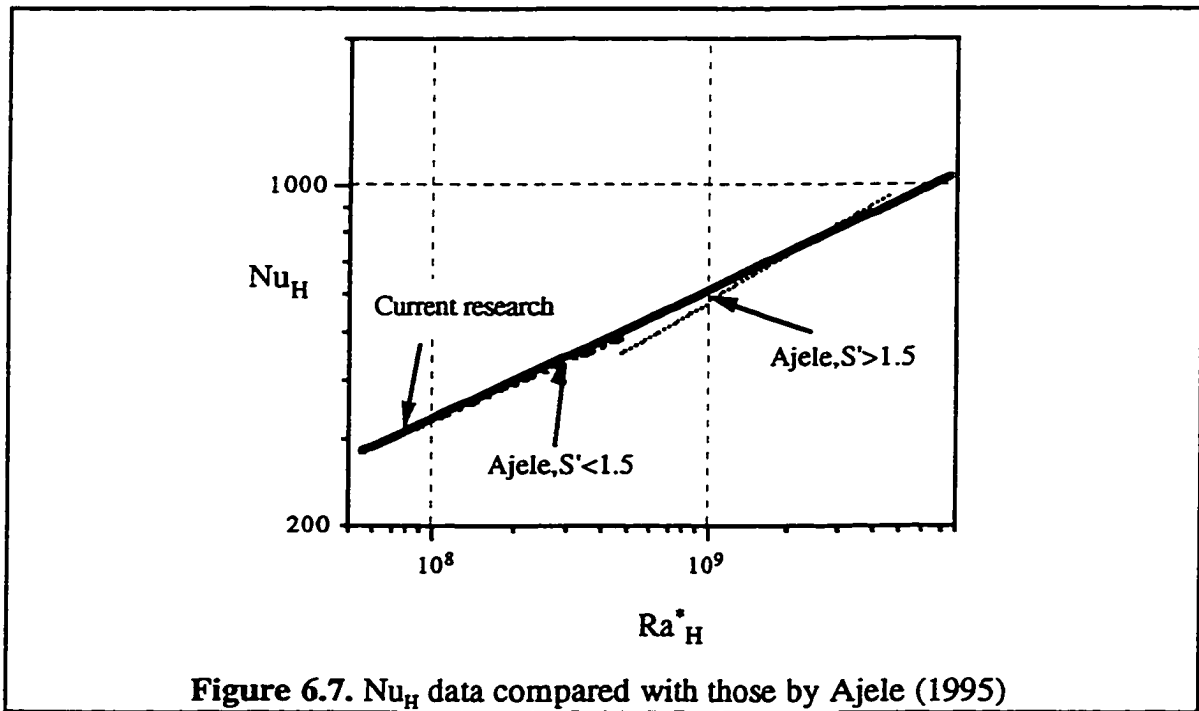


Figure 6.7. Nu_H data compared with those by Ajele (1995)

Ajele (1995) presented two correlations for the Nusselt number based on the shell height as a function of the modified Rayleigh number based on the shell height. Ajele's data covered only single coil configurations. In order to compare Ajele's data with the results of the current research some modifications were necessary. The fact that in Ajele's experiments the shell diameter was 102 mm, greater than that in the current thesis, makes equation 6.2 more reliable.

The heat exchanger hydraulic diameter, equation 3.18, offers a better representation of the geometry of the exchanger. In figure 6.8 the data for all the configurations are plotted against the Rayleigh number based on D_{hx} .

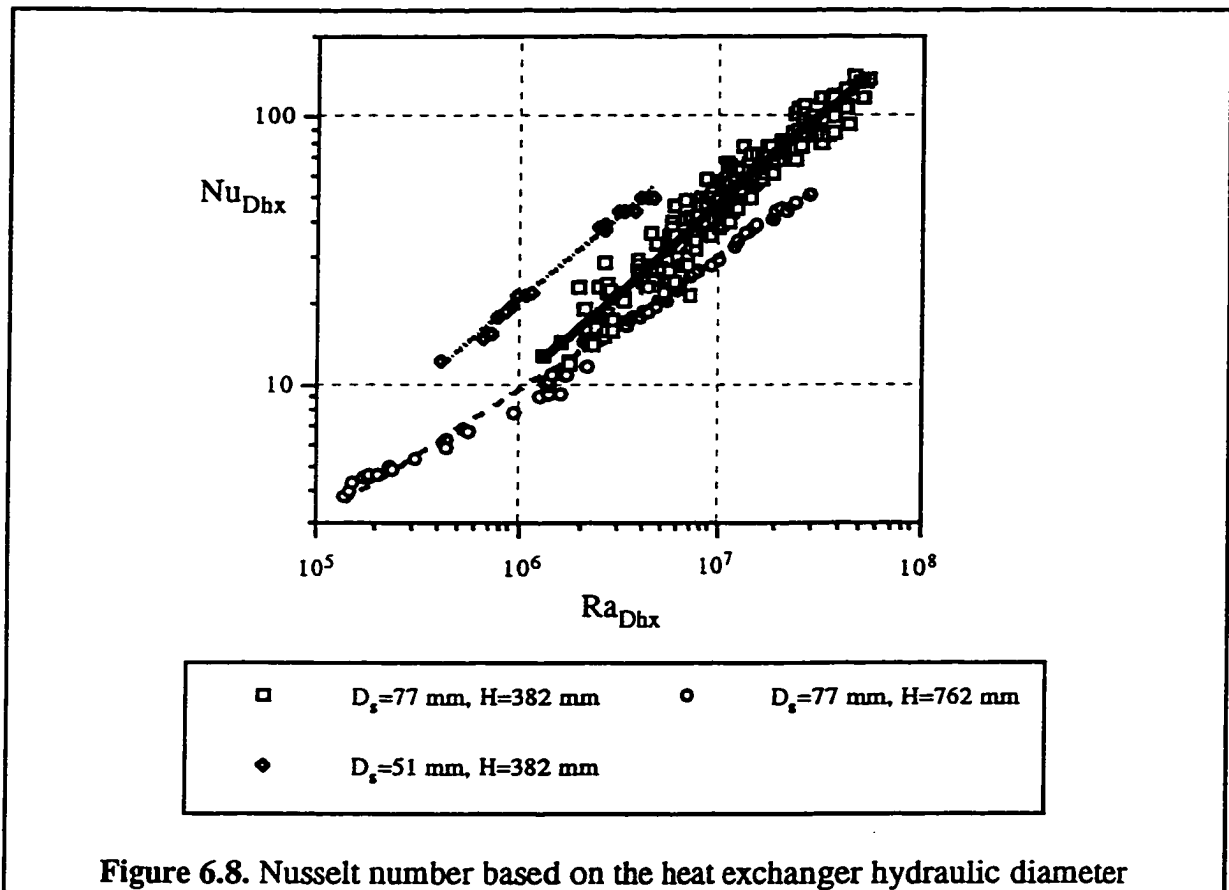


Figure 6.8. Nusselt number based on the heat exchanger hydraulic diameter

The data are divided based on the shell diameter and/or height into three categories. Equations were fitted to the data in order to obtain correlations for each category. Equations 6.3 to 6.5 are the results of the curve fitting.

For $D_s=51$ mm and $H=382$ mm,

$$Nu_{Dhx} = 0.0028 Ra_{Dhx}^{0.644} \quad 6.3$$

For $D_s=77$ mm and $H=382$ mm,

$$Nu_{Dhx} = 0.0014 Ra_{Dhx}^{0.647} \quad 6.4$$

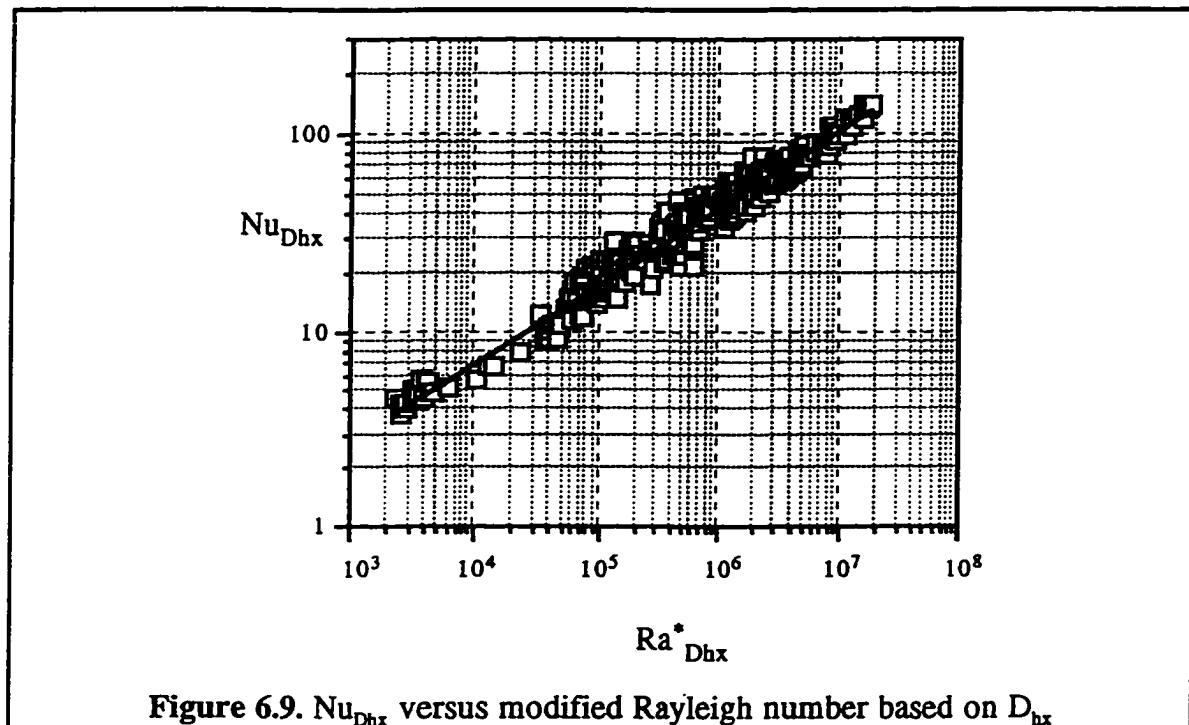
And for $D_s=77$ mm and $H=762$ mm equation 6.5 correlates the data well.

$$Nu_{D_{hx}} = 0.0105 Ra_{D_{hx}}^{0.493}$$

6.5

The second configuration is different from the first one in the shell diameter. In the third configuration, the shell diameter is the same as the second one but the shell height is nearly twice that of the second one.

The slope of the logarithmic graphs represented by equations 6.3 and 6.4 are nearly the same, suggesting that the changes in $Nu_{D_{hx}}$ will follow the same trend. However, at a fixed value of D_{hx} the smaller diameter shell has a Nusselt number twice that of the larger diameter shell. For the case of tall shell (equation 6.5) the slope is less. This means that at higher $Ra_{D_{hx}}$ values, the tall heat exchanger has Nusselt numbers which are much less than those of the shorter exchanger. The effects of the shell diameter and height were discussed in chapter 5 in detail.

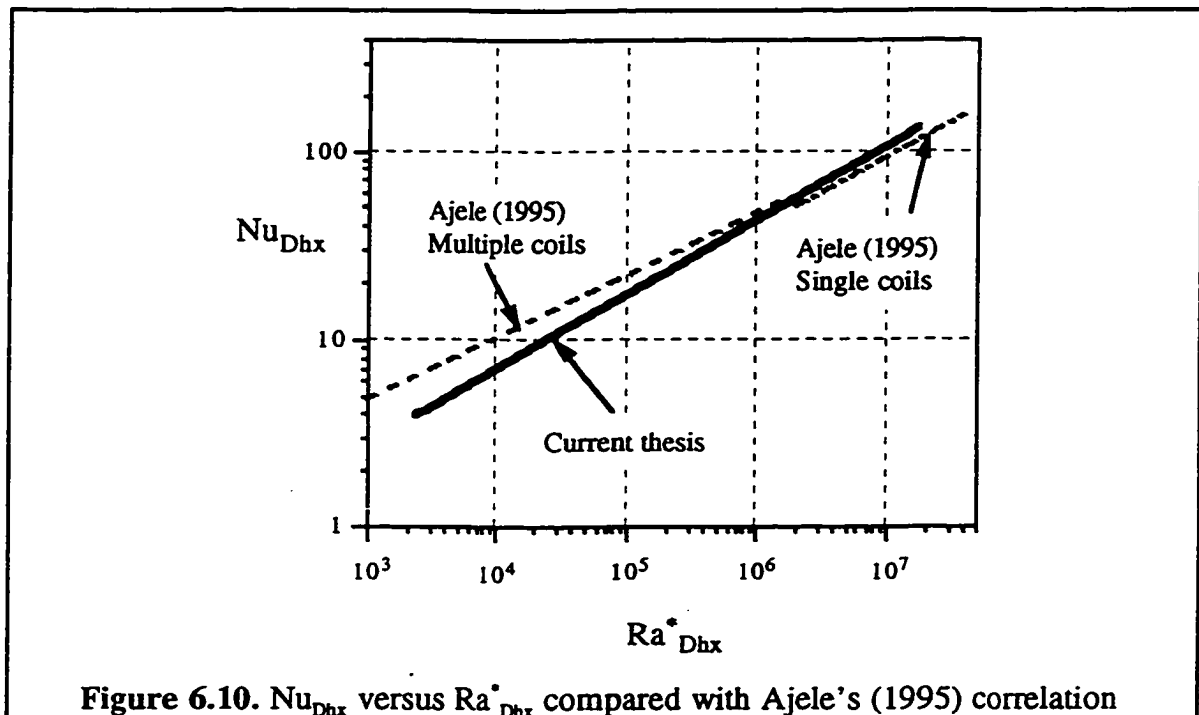


When the Rayleigh number is modified by multiplying it by H/L , the Nusselt number data are correlated well as is evident from figure 6.9. Equation 6.6 correlates the data with a coefficient of determination of 0.97.

$$Nu_{Dhx} = 0.182 Ra_{Dhx}^{* 0.394} \quad 6.6$$

Equation 6.6 includes the data for all configurations. Equation 6.6 provides a single correlation which represents all the data with reasonable accuracy. The Rayleigh number range covered by equation 6.6 is $2 \times 10^3 < Ra_{Dhx}^* < 2 \times 10^7$.

Ajele (1995) also presented correlations based on the modified Rayleigh number. Figure 6.10 compares the current results with those by Ajele. Ajele (1995) included the modified flow space and the flow number in his correlations and reported coefficients of determination of 2 to 3% better for his equations, compared to his correlations without inclusion of the modified flow space.



The dashed line in figure 6.10 represents Ajele's correlation for multiple coils before adjustments for F and S' . For the range of the flow number and the modified flow space in Ajele's experiments, equation 6.7 represents the data well with little loss of accuracy in the range $10^3 < Ra_{Dhx}^* < 2 \times 10^6$.

$$Nu_{Dhx} = 0.48 Ra_{Dhx}^{*0.33} \quad 6.7$$

The adjustments made to obtain equations 2.13 to 2.17 by Ajele, bring little improvement to the accuracy of the equations. On the other hand, those adjustments make the equations more complex and tedious, noting that the exponent m has to be extracted from table 2.1. Therefore for the sake of comparison, only Ajele's original equation (equation 6.7) will be considered.

For $S' > 1.5$, which includes only single coil configurations, equation 2.13 was proposed by Ajele for the range $2 \times 10^6 \leq Ra_{Dhx}^* < 4 \times 10^7$. Equation 2.13 for the average value of S' of the single coils can be modified with insignificant loss of accuracy to form equation 6.8. Equation 6.8 is indicated in figure 6.10 by the dash-dot line.

$$Nu_{Dhx} = 0.2 Ra_{Dhx}^{*0.38} \quad 6.8$$

As can be seen on figure 6.10 for most of the Rayleigh number range, equation 6.7 over-predicts the current results. This over-prediction is higher for lower values in the Rayleigh number range. However, for $Ra_{Dhx}^* \geq 10^5$ the current results are represented by equation 6.7 with less than 10% error.

As for equation 6.8 the agreement with the current results is very good over the range $10^5 \leq Ra_{Dhx}^* < 4 \times 10^7$. In order to be safe, for the range $10^3 < Ra_{Dhx}^* < 10^5$ the Nusselt number can be evaluated using both equations 6.6 and 6.7 and the average of the two can be used for design purposes. This recommendation is based on the fact that the

current experiments and those by Ajele (1995) each cover some heat exchanger configurations that are not covered by the other one. Therefore both should be considered valid in their own places.

The definition of the Rayleigh number based on the heat rate proves appropriate in cases with a uniform heat flux boundary condition. Also it could be more suitable for design purposes since it is easier to estimate the rate of heat transfer than the mean temperature difference in the heat exchanger as the traditional Rayleigh number definition requires.

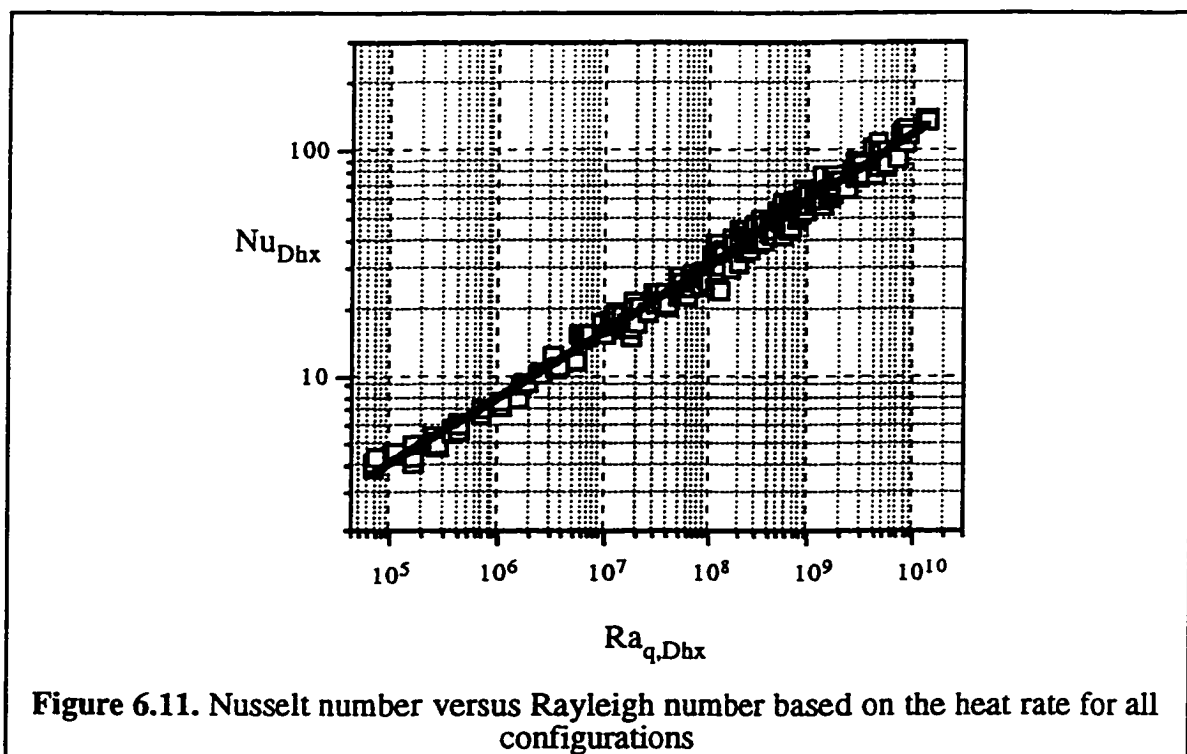
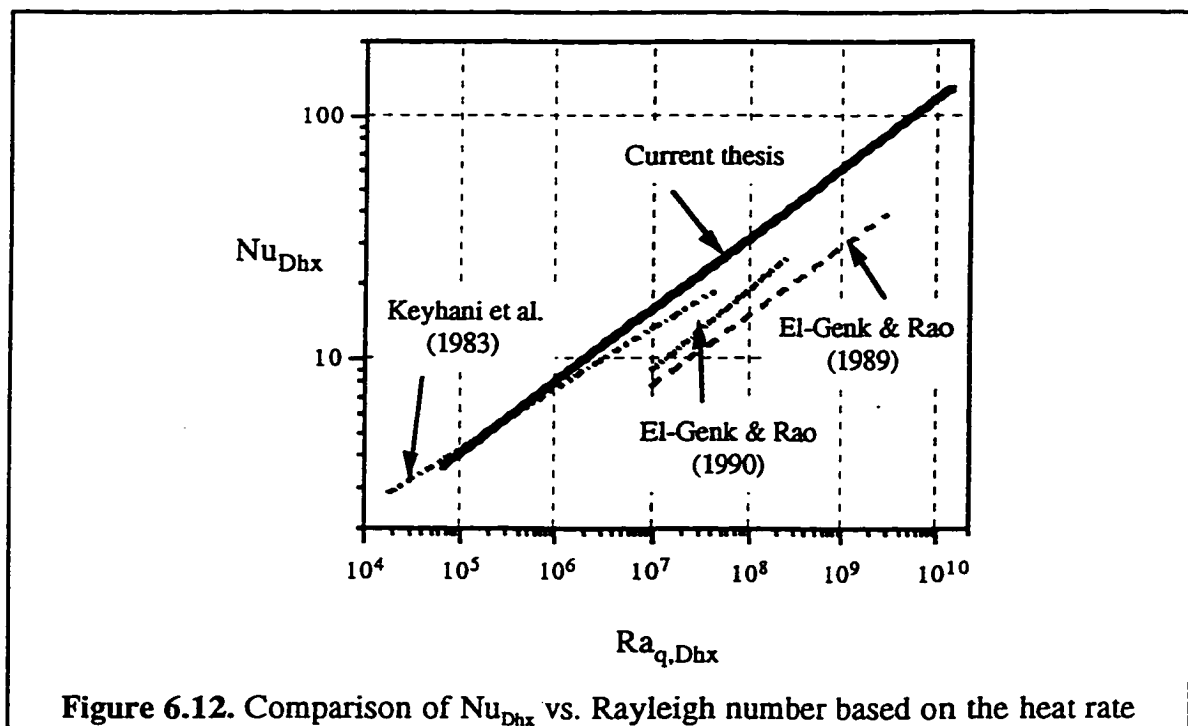


Figure 6.11 illustrates an excellent correlation between the data when the Rayleigh number is based on the heat rate ($r^2=0.99$). The best fit to the plot of figure 6.11, valid in the range $6 \times 10^4 \leq Ra_{q,Dhx} < 2 \times 10^{10}$, is represented by equation 6.9. The definition of $Ra_{q,Dhx}$ (equation 3.21) is reproduced here as equation 6.10.

$$Nu_{Dhx} = 0.139 Ra_{q,Dhx}^{0.293} \quad 6.9$$

$$Ra_{q,Dhx} = \frac{g\beta q''(Dhx)^4}{k\nu\alpha} \quad 6.10$$

All configurations are represented by the above correlation. This is very convenient since all the data is correlated by a single power equation without any different regions involved. Equation 6.9 suggests that increasing the heat exchanger hydraulic diameter will slightly increase the shell-side heat transfer coefficient.



There are no correlations available in the literature covering the same issue. However for the sake of comparison the results of natural convection in vertical annuli can be considered. In figure 6.12 the results of the current experiments are plotted together with those by Keyhani *et al.* (1983), El-Genk and Rao (1989) and El-Genk and Rao (1990). The current results exhibit good agreement with the data of Keyhani *et al.* (1983). The results of El-Genk and Rao (1989), (1990) fall below the current results for the entire range

of their validity. However the slope of the graphs are nearly the same. The data of El-Genk and Rao (1989), (1990) are for low Reynolds number forced convective flows of water.

Since the correlation based on the heat rate proved to be promising, other characteristic lengths can also be used to establish $Nu-Ra_q$ correlations. In figure 6.13 the total length of the coils is taken as the characteristic length.

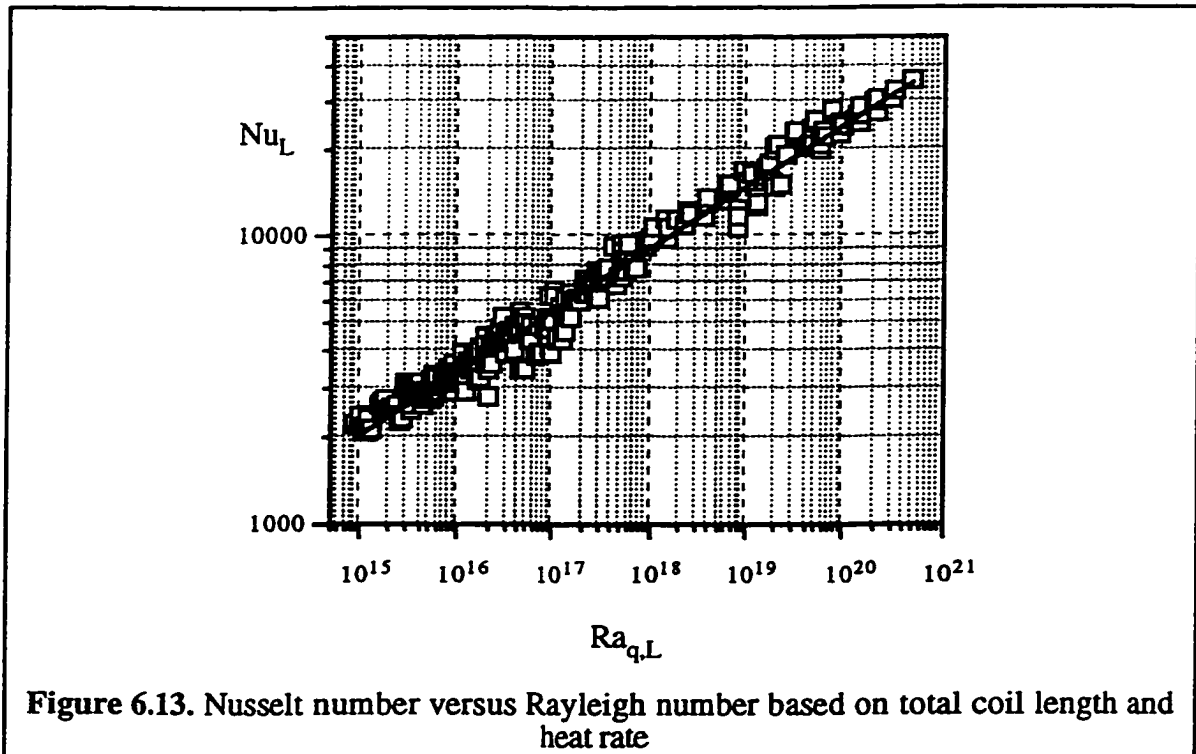


Figure 6.13 illustrates a good correlation between the data using $Ra_{q,L}$. Again the plot of figure 6.13 contains all the configurations tested in the current experiments. The correlating equation for this plot is presented as equation 6.11.

$$Nu_L = 1.183Ra_{q,L}^{0.216} \quad 6.11$$

The Rayleigh number range for equation 6.11 is $7 \times 10^{14} < Ra_{q,L} < 6 \times 10^{20}$ and the coefficient of determination is 0.98. It can be determined from equation 6.11 that for a

fixed heat rate any increase in the total length of the coils will slightly decrease the shell-side heat transfer coefficient. This was discussed in detail in chapter 5.

CHAPTER 7

APPLICATIONS

7.1. Optimum configuration

The effects of several parameters on the thermal performance of the shell-and-coil natural convection heat exchangers were presented in chapter 5. An optimum configuration for the heat exchanger will be proposed. This will be done by reviewing the effects of each parameter separately.

7.1.1. Tube diameter

Four tube diameters were used to make the coils. Those were 4.76, 6.35, 7.94 and 9.52 mm. From the heat transfer point of view, it was found that the diameter of the tube is not influential. The coils made from 4.76 mm copper tube have the advantage that more of them can be fit inside a fixed shell diameter, therefore increasing the heat transfer area without increasing the overall size of the exchanger. However, a major disadvantage of using 4.76 mm tube coils is in the pressure drop that occurs across such coils. To overcome the large pressure drop, a larger pump must be used which is costly. Consequently, the use of 4.76 mm tubes is not practical.

There are two reasons to disqualify the 9.52 mm tubes as the choice for making coils. One is due to the toughness of the tubes which demands more work in the process of coil winding. That could slow down the mass production of the coils and make it more energy consuming. The second reason is that due to the limitation on the minimum achievable coil diameter with 9.52 mm tubes, less number of coils can be placed in a certain shell diameter. This is not desirable considering that some available space inside the exchanger will not be utilized properly.

As regards to the 7.94 mm tube, there are no significant disadvantages other than the fact that their wall thickness is larger than that of 6.35 mm tubes, therefore making them slightly harder to bend compared to the 6.35 mm tubes. The minimum achievable coil diameter may also be a disadvantage. Also, 7.94 mm tubes and fittings for the same are not nearly so readily available as the mass produced 6.35 mm tubes and fittings.

However, for the optimum tube diameter, the recommendation is the 6.35 mm tubes. The advantages are, moderate pressure drops, less toughness and therefore easier to bend, reasonable minimum achievable coil diameter and less wall thickness compared with the 7.94 mm tubes. In addition to those, the fact that the 6.35 mm tubes are a more widely used size in industry makes them easier to purchase and more economical to use.

7.1.2. Shell diameter

The effect of the shell diameter on the shell-side heat transfer coefficient was found to be insignificant for the range of shell diameters tested. In order to comment on the optimum shell diameter, more data must become available especially for shell diameters larger than 100 mm. Based on the information currently available, no restriction can be imposed on the heat exchanger shell diameter. Once the required heat transfer area is known, the shell diameter should be selected based on its ability to accommodate the required number of coils. The minimum shell diameter which can offer the required number of coils must be selected in order to maintain the desired level of compactness. Since a 100 mm shell provides enough space to accommodate four 6.35 mm coils, it should be the choice for the heat exchanger.

7.1.3. Coil diameter

In practice, heat exchangers with single or double coils are not considered because of insufficient surface area. Therefore the recommendations here will be toward the improvement of triple-coil configurations. In a triple-coil configuration the performance of the largest coil was not satisfactory. In order to improve the situation the following guidelines should be followed. The diameters of the three coils should be selected so that a gap of at least half a tube diameter exists between two consecutive coils. This gap must

especially be maintained between the middle and the outermost coil. Also the same gap should exist between the largest coil and the inner surface of the heat exchanger shell.

The implementation of the above suggestion may cause difficulties due to the limitation in the minimum achievable coil diameter for the innermost coil. In case the suggested gaps can not be obtained, the optimization can be achieved by reducing the surface area of the largest coil. It was found that the shell-side heat transfer coefficient decreases as the coil surface area increases. Therefore, the largest coil can be made with less coil turns, i.e. higher coil pitch. The surface area of the largest coil should be decreased to a size nearly equal to the surface area of the middle coil.

7.1.4. Shell height

The shell-side heat transfer coefficient was influenced very little by the shell height. Therefore the only limitation in selecting a shell height would be the space limitations. Since the shell height has little effect on the water flow rate, the heat exchanger can be built nearly as tall as the storage tank if space permits. This issue was discussed in detail in sections 5.5.4.1.9 and 6.1.

7.1.5. Coil pitch

The optimum dimensionless pitch was from 1.25 to 1.80. A pitch of 1.25 tube diameters, for a 6.35 mm tube will result in a 1.5 to 2 mm gap between consecutive coil turns. However for the largest coil the pitch should be higher as mentioned above.

7.1.6. Recommended configuration

Based on the above, an optimum configuration for the shell-and-coil natural convection heat exchanger is proposed. The coils should be made using 6.35 mm outer diameter copper tubes. The shell diameter should be 100 mm, i.e. 4" standard copper water tube. The heat exchanger should contain 4 coils with diameters so that at least a 3 mm gap exists between adjacent coils. The coil pitch for the three inner coils should be 1.25 tube

diameters, i.e. a 2 mm gap between adjacent turns. The largest coil should have less coil turns than the others so that its surface area is approximately equal to that of the one immediately inside it. There is no limitation on the heat exchanger height. With a 400 mm tall heat exchanger, having 4 coils and a 100 mm diameter shell, a UA product as high as 395 W/K can be achieved. Such a heat exchanger will be able to transfer 3000 watts of heat with a log-mean temperature difference of approximately 8° C. The specifications of the proposed heat exchanger are given in table 7.1. Further improvement is possible by adjusting the heat transfer area so that the glycol exit temperatures are uniform.

Table 7.1. Specifications for the proposed heat exchanger

Coil #	$D_{c,i}$ (mm)	$D_{c,o}$ (mm)	L (m)	A (m ²)
1	25.0	37.7	4.3	0.086
2	43.7	56.4	6.8	0.136
3	62.4	75.1	9.3	0.185
4	81.1	93.8	11.8	0.235
Total coil surface area = 0.64 m ²				
Number of coil turns = 43				
Additional straight length on each end (included in L) = 20 mm				
Gap between adjacent coils = 3 mm				
$UA = 325 \text{ W/K @ } 1500 \text{ W and } \dot{m}_g = 0.02 \text{ kg/s}$				

7.2. Design procedure

In general, heat exchanger problems, when the inlet temperatures and the hot and cold fluid flow rates are known, and a particular outlet temperature is desired, are referred to as heat exchanger design problems. The problem is solved when the type and the size of the heat exchanger is determined. The general approach to the heat exchanger design problems is called the *LMTD* (log-mean temperature difference) method. When $T_{c,o}$ is known the corresponding q and $T_{h,o}$ can be calculated using the energy balance equations. The value of the *LMTD* can be determined. Finally, the required heat transfer area can be calculated but only after U has been determined.

On the other hand there are cases in which the size and type of the heat exchanger are given and the rate of heat transfer and the hot and cold outlet temperatures are unknown. The inlet temperatures and the flow rates must be known for this type of problems as well. In these cases, the problem is called a heat exchanger rating problem. The method usually used in the rating problems is called the effectiveness- NTU method. Since ε - NTU relationships are available for various types of heat exchangers, the effectiveness can be evaluated after determining the NTU value given the heat exchanger type and size and also the fluid flow rates. The actual q then can be calculated from the effectiveness and knowing $q_{\max} = (\dot{m}c_p)_{\min}(T_{h,i} - T_{h,o})$. The calculation of the fluid outlet temperatures would then be only a matter of applying the energy balance equations (Incropera and Dewitt 1990).

7.2.1. Design

In traditional heat exchanger design problems where the inlet temperatures and the mass flow rates are known, the $LMTD$ method will facilitate the calculation of the heat transfer area required to achieve the desired outlet temperatures. This process does not involve any iterations. However, application of the $LMTD$ method to the NCHE design problems is not possible without iterations. The reason is firstly because of the indeterminate value of the water mass flow rate. In addition, the evaluation of the shell-side heat transfer coefficient from the available Nu - Ra correlations, requires knowledge of the heat exchanger hydraulic diameter. As a result, the design procedure involves a first guess of the heat transfer area, which must be verified subsequently.

Also for NCHEs it is better to start with a desired value of the heat transfer rate rather than the outlet temperature. Eventually the heat transfer rate can be adjusted to match the desired outlet temperatures.

A design procedure for shell-and-coil NCHEs is proposed as follows. From the desired heat transfer rate, q , the glycol outlet temperature, $T_{h,o}$ can be calculated by applying an energy balance. The modified effectiveness of the exchanger, ε' can be evaluated using equation 3.29. The water mass flow rate will then be calculated from

equation 5.1. Applying the energy balance equation to the water flow, the water outlet temperature, $T_{c,o}$ will be evaluated. Since all the terminal temperatures are known at this point, the logarithmic mean temperature difference can be calculated. Evaluating the UA product of the heat exchanger is then only a matter of applying equation 3.25. If the value of the overall heat transfer coefficient, U is known, the problem is solved by calculating the required heat transfer area. However, the nature of the empirical equations are such that the calculation of U , requires a prior estimate of the heat exchanger configuration, i.e. D_{hx} , and area.

The rest of the process can be explained as follows. A configuration for the heat exchanger must be considered by deciding on the shell diameter and height, number of coils, coil pitches and diameters. Therefore the heat transfer area can be estimated and the heat exchanger hydraulic diameter calculated. Since the rate of heat transfer is known, the heat-rate Rayleigh number based on D_{hx} can be calculated. From equation 6.9 the Nusselt number based on D_{hx} can be evaluated and the shell-side heat transfer coefficient can be calculated from the Nusselt number definition. Parallel to the mentioned process, the tube-side heat transfer coefficient must be calculated via the following procedure.

From knowledge of the glycol mass flow rate, the Dean number is calculated. Equation 5.11 is used to evaluate the Nusselt number value inside the coil tube. After calculating the tube-side heat transfer coefficient from the Nusselt number, the overall heat transfer coefficient is calculated using equation 3.26. With U and UA known, the heat transfer area can be evaluated. This value must then be compared with the estimated value and the proper adjustments made. The process will yield the value of the surface area required for the desired heat transfer rate following a few trial-and-error iterations. The flowcharts of the above procedures are illustrated in figure 7.1.

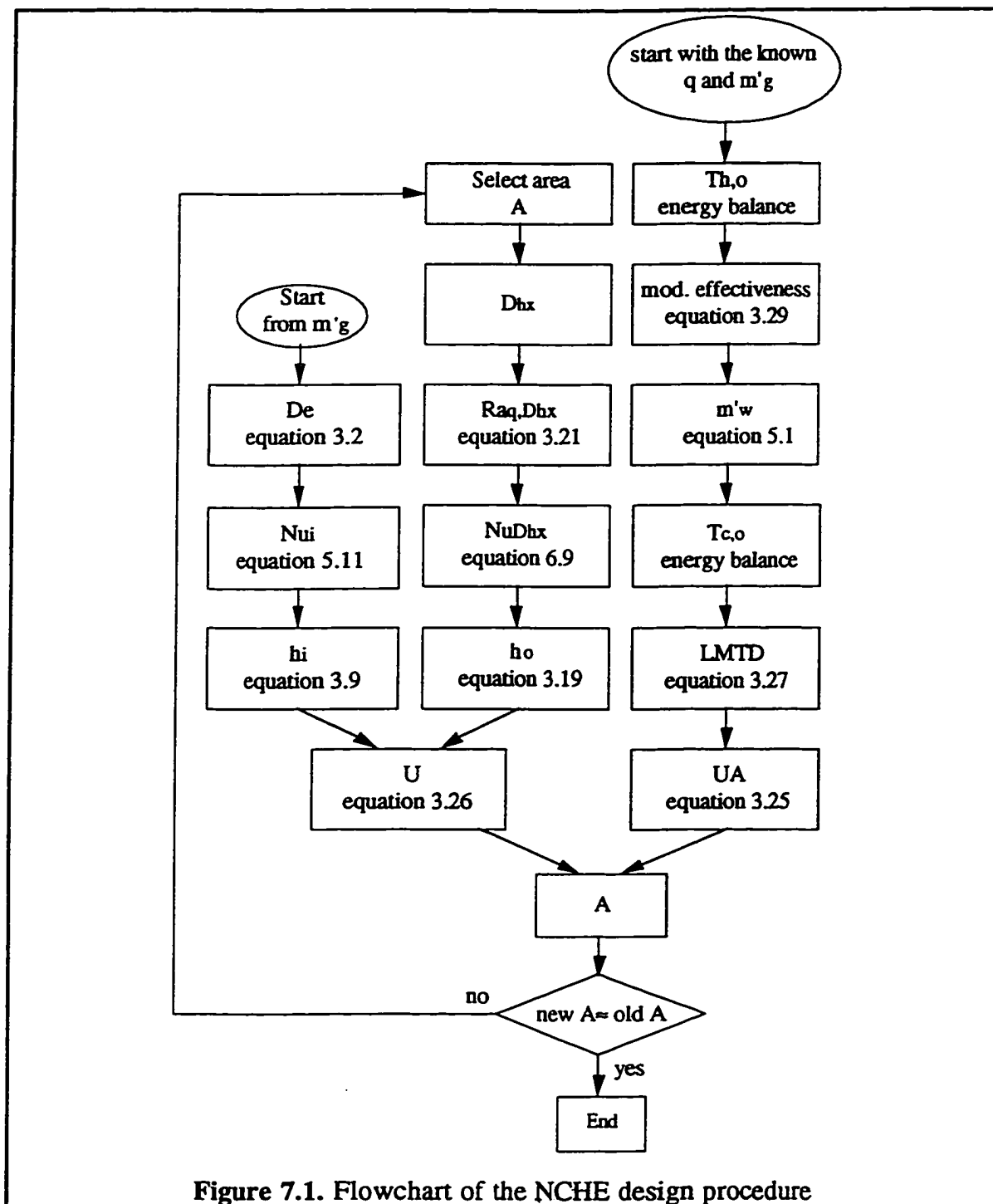


Figure 7.1. Flowchart of the NCHE design procedure

The results of some test runs are presented in table 7.2. The known parameters are selected so that the results can be compared with certain tested NCHE configurations.

Table 7.2. Results of the design procedure for the NCHE

S e l e c t e d	Parameter	Example 1		Example 2		Example 3	
		medium flow		low flow		short shell	
	q	838.2 W		1732 W		1704.9 W	
	$T_{c,i}$	17.7 °C		16.8 °C		11.5 °C	
	$T_{h,i}$	45 °C		58.2 °C		55.9 °C	
	m'_g	0.02531 kg/s		0.01774 kg/s		0.02419 kg/s	
	$D_{t,o}$	6.35 mm		6.35 mm		6.35 mm	
	D_s	76.8 mm		76.8 mm		76.8 mm	
	H	0.762 m		0.762 m		0.382 m	
	N	3 coils		3 coils		3 coils	
C a l c u l a t e d		measured	calculated	measured	calculated	measured	calculated
	$T_{c,o}$	44.8	48.5	56.3	57.1	52.7	49.7
	$T_{h,o}$	35.8	36.2	32.6	32.4	37.1	37.3
	m'_w	0.00741	0.00651	0.01048	0.01028	0.00993	0.01069
	e'	0.339	0.322	0.619	0.623	0.423	0.419
	$Ra_{q,Dhx}$	6.91E+04	3.72E+04	1.59E+05	4.25E+04	3.70E+05	1.87E+06
	Nu_{Dhx}	4.05	3.03	4.63	3.16	5.56	9.56
	h_o	422	361	486	428	548	706
	De	422	330	327	258	442	356
	h_i	2459	1925	2200	1725	2411	2007
	LMTD	4.1	3.5	6.5	5.6	10.8	13.8
	UA	214	238	264	310	157	123
	n	84.1	83.8	84.1	97.3	33.7	21
	A	0.796	0.781	0.796	0.905	0.340	0.236
	Error in A	1.90%		13.7%		30.6%	

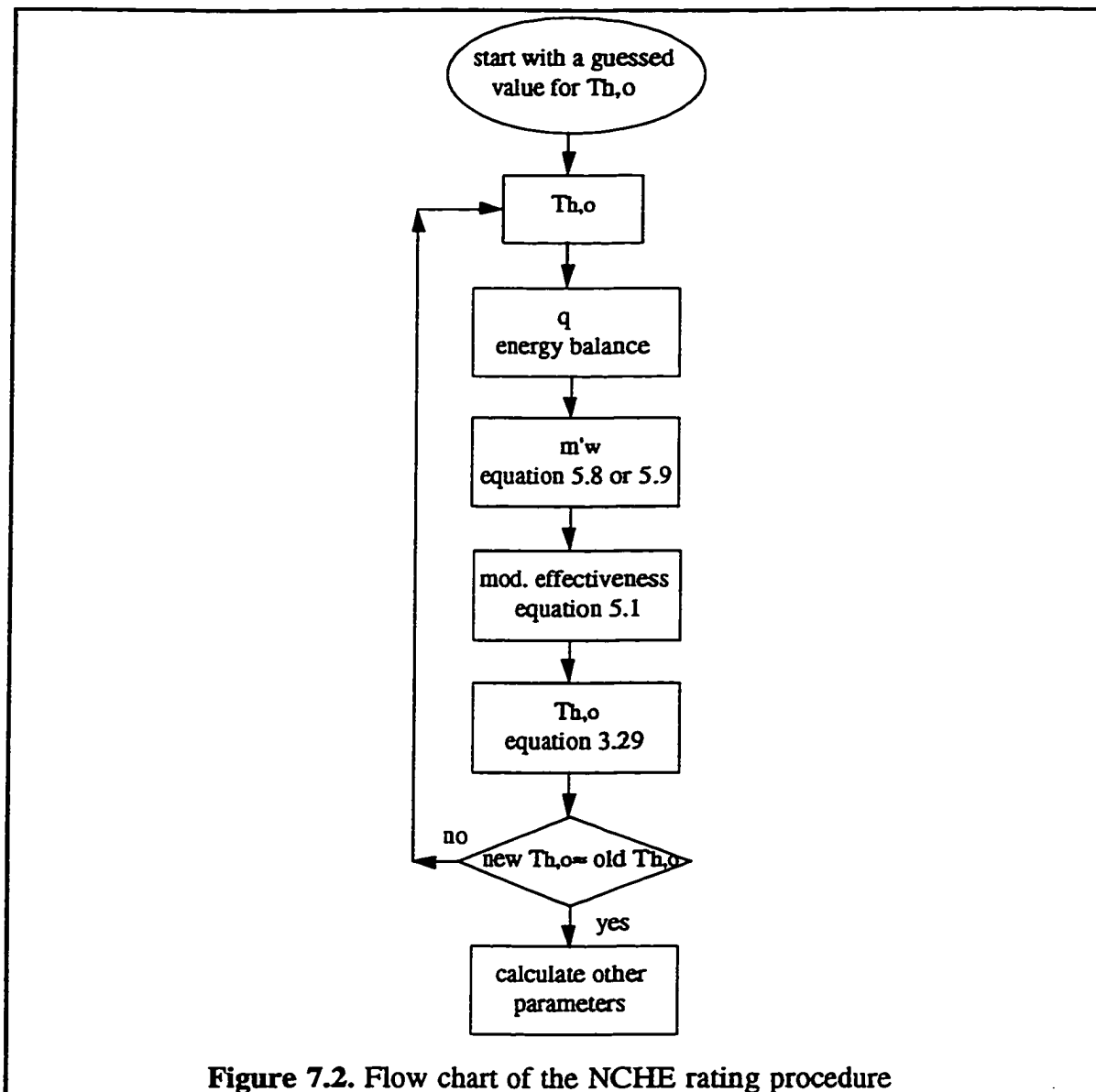
The error associated with the calculated area is reasonable for the long shell. For the short heat exchanger shell, the error is higher. The main source of error is in the calculation of the logarithmic mean temperature difference. By definition, *LMTD* is very sensitive to the temperature values and a slight uncertainty in any terminal temperature will result in a large error in the value of *LMTD*.

7.2.2. Rating

For the NCHE rating problems, the water mass flow rate is not known beforehand. This added unknown to the problem and the fact that the ϵ -*NTU* relations are not readily available, leaves no alternative than an iterative approach. The method that is proposed here starts with a guessed value for $T_{h,o}$. Knowing the glycol flow rate, q can be calculated from the energy balance. The water mass flow rate is evaluated using equation 5.8 or 5.9

depending on the height of the heat exchanger. For intermediate heights, linear interpolation can be performed. Equation 5.1 can then be used to evaluate the modified effectiveness of the heat exchanger. The definition of ε' will lead to the calculation of a new $T_{h,o}$. The procedure has to be repeated with the new value of $T_{h,o}$ until satisfactory convergence is reached. The calculation of other parameters of interest such as $Ra_{q,Dhx}$, Nu_{Dhx} , UA and $LMTD$ is straightforward. For better accuracy the temperature dependence of the water and glycol physical properties must be taken into account.

The rating procedure can be summarized in form of the flowchart in figure 7.2.



The above approach for the rating of a NCHE was applied to the conditions of a number of tested configurations and the results are tabulated in table 7.3.

Table 7.3. Typical results of the proposed rating procedure

K n o w n		Example 1		Example 2		Example 3	
	Parameter	single coil		double coil		triple coil	
	$T_{c,i}$	14.4 °C		15.4 °C		16.6 °C	
	$T_{h,i}$	44.8 °C		57.8 °C		56 °C	
	A	0.26 m ²		0.627 m ²		0.796 m ²	
	Dhx	0.02561 m		0.00917 m		0.00605 m	
	m'_w	0.01671 kg/s		0.01835 kg/s		0.0266 kg/s	
	H	0.762 m		0.762 m		0.762 m	
	L	13.166 m		31.532 m		40.065 m	
U n k n o w n		measured	calculated	measured	calculated	measured	calculated
	q	809.6	648.8	1733.7	1744.5	1816.2	2048.1
	m'_w	0.00728	0.00637	0.0103	0.01111	0.01054	0.01252
	ϵ'	0.423	0.339	0.576	0.592	0.457	0.515
	$Ra_{n,Dhx}$	5.62E+07	4.35E+07	1.01E+06	8.87E+05	1.65E+05	1.63E+05
	Nu_{Dhx}	26.39	24.05	7.29	7.69	4.92	4.68
	h_o	640	583	503	530	518	494
	LMTD	7.5	11.7	7.4	9.7	6.4	4.25
	UA	109	56	233	179	266	481
	$T_{h,o}$	31.9	34.5	33.4	32.7	38	35.7
$T_{c,o}$	42.5	38.8	55.7	53	55.2	55.8	
Error in $T_{c,o}$		8.70%		4.80%		1.10%	

As can be seen in table 7.3 the error associated with the water outlet temperature prediction by the proposed method is quite low. The prediction is significantly better for the triple-coil configurations which are of more interest in application. Among the heat transfer parameters predicted by this approach, the value of the UA product involves high errors. This is the case, because in the above table the UA product was calculated using the logarithmic mean temperature difference which is very sensitive to the terminal temperatures. However, the UA product of the heat exchanger can be calculated knowing h_o and h_i . Since the proposed method predicts the h_o values with reasonable accuracy, the error involved in calculating the UA product can be minimized. The above method is simple and straightforward and is recommended for the NCHE rating problems.

Applying the above approach to some cases might result in a $T_{c,o}$ value slightly higher than $T_{h,i}$. In such a case the water outlet temperature should be regarded as almost equal to the glycol inlet temperature. The review of the experimental results confirmed the above conclusion. The other heat transfer parameters can be calculated with no difficulty once the above modification is practiced.

7.3. The effect of the auxiliary parts

The above proposed procedures are valid for the common heat exchanger installation configurations. The heat exchanger is normally located beside the storage tank and connection is established through minimal tube lengths. However if this is not the case, or other flow-restricting devices are to be placed in the storage loop, the change in the hydraulic resistance of the loop must be taken into account in the design procedure.

The water mass flow rate must be estimated by an iterative process. This process can be summarized as below. The water temperature profile inside the heat exchanger must be guessed. Having an estimate of the storage tank temperature profile, the pressure drop of each of the components of the storage loop can be calculated using simple hydraulic equations. A water mass flow rate can then be selected so that the pressure drop due to friction, balances the pressure drop due to buoyancy. $T_{c,o}$ is determined and the temperature profile inside the heat exchanger corrected. With the new temperature profile, the process must be repeated. The design procedure presented in section 7.2.1 can be followed with the calculated value of the water mass flow rate. The result will be a new estimate for the water temperature profile inside the heat exchanger. The process must be repeated until detection of a reasonable convergence.

The above methods are by no means the only possible ways to perform a natural convection heat exchanger design and/or rating task. Numerous empirical equations are provided to facilitate the NCHE design and rating tasks in whichever way they may be carried on.

CHAPTER 8

CONCLUSIONS

8.1. Summary

Heat transfer in shell-and-coil natural convection heat exchangers was investigated experimentally. The shell-and-coil NCHE consisted of a cylindrical shell with one to three helical coils placed inside it. Coils of several different sizes were tested in various diameter and height shells. Coils were made of copper tubes of 4.76, 6.35, 7.94 and 9.52 mm outer diameter. Coil outside diameter varied from 35.7 to 74.5 mm. Coil pitch values of 1 to 6 were tested. Two shells of 51 and 77 mm ID were used. The shell height was 382 mm for the 51 mm ID shell and two shell heights of 382 and 762 mm were set for the 77 mm ID shell. Heated glycol was pumped through the coils with water circulating naturally on the shell side. Various combinations of heat rate and glycol flow rate were set to obtain at least 10 data points for each heat exchanger configuration. A total of 30 heat exchanger configurations were tested.

The effects of the tube diameter, coil diameter, coil surface area, coil pitch, shell diameter and height on the shell-side heat transfer coefficient were studied. Temperature profiles in the heat exchanger were measured. The thermal performance of individual coils in double and triple-coil configurations was analyzed. Nusselt number correlations based on the heat exchanger hydraulic diameter, heat exchanger height, coil length and heat rate were obtained. Design and rating procedures were proposed for shell-and-coil NCHE.

8.2. Conclusions

- 1) The ratio of the glycol to water mass flow rate (R_m) was found to be influential on the axial temperature profiles of the heat exchanger. For R_m greater than unity, the temperature profiles were of quadratic form from bottom to top of the heat exchanger. The profiles were linear for R_m close to unity and when the mass

flow rate ratio was considerably less than unity, the temperature profiles were of the logarithmic form.

- 2) The heat exchanger shell height and shell diameter did not influence the shape of the temperature profiles. The same observations were made with the multiple-coil configurations.
- 3) The effect of increasing the heat rate was to increase the slope of the axial temperature profiles.
- 4) In single-coil configurations, the smaller diameter coils were more likely to encounter recirculating flows at the bottom of the heat exchanger.
- 5) The logarithmic mean temperature difference was found to decrease with increasing the mass flow rate ratio.
- 6) The modified effectiveness decreased with increasing mass flow rate ratio. Equation 5.1 was found to correlate the modified effectiveness data to the mass flow rate ratio and the shell-and-coil NCHE compactness ratio, for $0.3 < R_m (H/L)^{0.3} < 5$ and $1.85 \times 10^{-3} \leq \dot{m}_g \leq 34.3 \times 10^{-3}$ kg/s,

$$\varepsilon' = 0.37 \left(\frac{\dot{m}_w}{\dot{m}_g} \right)^{0.77} \left(\frac{L}{H} \right)^{0.23} \quad 5.1$$

- 7) The ε - NTU relation of the NCHEs was similar to those of a pure counter flow heat exchanger.
- 8) Two correlations were presented for predicting the water flow rate. The two correlations are equation 5.8 for the shorter heat exchanger shell and equation 5.9 for the taller shell. The major factor in determining the water mass flow rate was the heat rate. The heat exchanger shell height and shell diameter did not produce any significant effect.

$$M_w = 4.07 \times 10^{-8} \Gamma^{-4.9} \quad H=382 \text{ mm} \quad 5.8$$

$$M_w = 1.51 \times 10^{-8} \Gamma^{-4.9} \quad H=762 \text{ mm} \quad 5.9$$

- 9) Increasing the coil surface area and consequently its length decreased the value of the shell-side heat transfer coefficient.
- 10) The shell-side heat transfer coefficient was not affected by the coil tube diameter.
- 11) The value of h_o is believed to be slightly higher for the smaller diameter coils.
- 12) The optimum value for the coil pitch is from 1.25 to 1.80 tube diameters. For smaller pitch the performance of the heat exchanger is inferior. Also there is no significant improvement in performance for the coils having pitches greater than 1.8 tube diameters.
- 13) The glycol flow rate did not have any considerable effect on h_o .
- 14) Decreasing the shell diameter was found to increase h_o .
- 15) The value of h_o was unaffected by changes in the heat exchanger shell height.
- 16) In triple-coil configurations, the largest coil had a considerably lower heat transfer coefficient compared to the other two coils. It was suggested to increase the coil-to-coil gap and the gap between the heat exchanger inner wall and the outer surface of the largest coil to facilitate the flow of water. In case the above modification is not possible, the largest coil must be made with a higher pitch to decrease its surface area.

- 17) The increase in the UA product of the heat exchanger was not directly proportional to increases in A . The UA product was proportional to the coil surface area to the power 0.67, ($UA \propto A^{0.67}$).
- 18) The flow regime for most tests was in the transition region.
- 19) The heat exchanger hydraulic diameter, D_{hx} was a relatively better parameter to serve as the characteristic length in the $Nu-Ra$ correlations.
- 20) Several $Nu-Ra$ correlations based on various choices of the characteristic length are presented. Equation 6.6 correlates the data the best. Also the Nusselt number based on D_{hx} was correlated with the heat rate Rayleigh number, $Ra_{q,Dhx}$ in equation 6.9. The Rayleigh number based on q was correlated with Nu_L as well.

$$Nu_{Dhx} = 0.182 Ra_{Dhx}^{*0.394} \quad 2 \times 10^3 < Ra_{Dhx}^* < 2 \times 10^7 \quad 6.6$$

$$Nu_{Dhx} = 0.139 Ra_{q,Dhx}^{0.293} \quad 6 \times 10^4 \leq Ra_{q,Dhx} < 2 \times 10^{10} \quad 6.9$$

- 21) Wherever possible, comparison was made with the results of other authors and in most cases the level of agreement was found to be satisfactory.

8.3. Recommendations for future work

In order to advance the current knowledge on the subject of the shell-and-coil NCHES, the following recommendations are presented.

- 1) A numerical model must be developed to predict the temperature distribution in the heat exchanger and the values of the shell-side heat transfer coefficient. The model must be a three-dimensional one with consideration of the turbulent behavior of the flow. Initially, the temperature boundary condition on the coil surface can be considered linear. Also the storage tank can be modeled as a

semi-infinite pool of constant temperature water. For the connecting tubes and fittings, simple hydraulic equations can be employed.

- 2) Further improvements can be made to the model as follows. Since the glycol temperature profile can not be considered linear, the shell-side heat transfer model must be coupled with a suitable model for the flow inside the helical coils. Preferably, the entrance effects on both sides should be taken into account. A third model for the storage tank must be used and solved simultaneously to account for the effects of the thermal stratification in the tank on the overall performance of the heat exchanger.
- 3) Flow visualization techniques such as dye injection, aluminum powder, hydrogen bubble generation or even more sophisticated optical techniques can be used to provide a qualitative image of the fluid and/or heat flow in the heat exchanger. Quantitative methods such as Laser Doppler Velocimetry can surely provide a great deal of information. For these purposes, heat exchangers with transparent shells must be built.
- 4) A study of forced convection heat transfer from vertical helical coils at low water flow rates will be quite beneficial since it will provide a source of data for comparison. This is because the heat transfer mode in the shell-and-coil heat exchangers, being used in SDHW systems storage loop is likely to be of mixed-convection type rather than pure natural convection.

REFERENCES

- Ajele, O. J. , 1995, Natural Convection Heat Transfer from Enclosed Helical Coils, Ph.D. thesis, Technical University of Nova Scotia, Halifax
- Akiyama, M., Cheng, K. C. , 1971, Boundary vorticity method for laminar forced convection heat transfer in curved pipes, *International Journal of Heat and Mass Transfer*, vol. 14, pp. 1659-1675
- Allen, P. L., Ajele, O. J. , 1993, Heat transfer in a natural convection shell-and-coil heat exchanger, 19th Annual Conference of the Solar Energy Society of Canada, Quebec city, Canada
- Allen, P. L., Ajele, O. J. , 1994, Natural convection from enclosed multiple coils, Solar Energy Society of Canada, Renewables '94 conference, Ottawa, Canada
- Allen, P. L., Ajele, O. J. , 1994, Optimum configuration of natural convection shell-and-coil heat exchanger with respect to thermal performance, Proceedings of the 1994 Annual Conference of the American Solar Energy Society, San Jose, U.S.A
- Allen, P. L., MacLeod, B. K. , 1994, Performance of solar water heaters with PV powered pumps, Proceedings of the Solar Energy Society of Canada, Renewables '94 Conference, Ottawa, Canada
- Ali, M. E. , 1994, Experimental investigation of natural convection from vertical helical coiled tubes, *International Journal of Heat and Mass Transfer*, vol. 37, no. 4, pp. 665-671
- Ali, S. , 1989, Pressure drop performance of coiled tubes, *Chemical Engineering Research and Design*, vol. 67, pp. 428-432

- Avina, J. , 1995, The Modeling of a Natural Convection Heat Exchanger in a Solar Domestic Hot Water System, M.Sc. thesis, University of Wisconsin-Madison, Madison, U.S.A
- Bejan, A., Fowler, A. J., Stanescu, G. , 1995, The optimal spacing between horizontal cylinders in a fixed volume cooled by natural convection, *International Journal of Heat and Mass Transfer*, vol. 38, no. 11, pp. 2047-2055
- Bergelt, T. K., Brunger, A. P., Hollands, K. G. T. , 1993, Optimum hydraulic resistance for natural convection SDHW heat exchanger loops, 19th Annual Conference of the Solar Energy Society of Canada, Quebec city, Canada
- Brown, C. K., Gauvin, W. H. , 1965, Combined free-and-forced convection I. Heat transfer in aiding flow, *The Canadian Journal of Chemical Engineering*, pp. 306-312
- Chapman, A. J. , 1967, *Heat Transfer Second Edition*, Macmillan Co., New York
- Churchill, S. W. , 1977, A comprehensive correlating equation for laminar, assisting, forced and free convection, *AIChE Journal*, vol. 23, no. 1, pp. 10-16
- Churchill, S. W., Chu, H. H. S. , 1975, Correlation equations for laminar and turbulent free convection from a horizontal cylinder, *International Journal of Heat and Mass Transfer*, vol. 18, pp. 1049-1053
- Clemes, S. B., Hollands, K. G. T., Brunger, A. P. , 1994, Natural convection heat transfer from long horizontal isothermal cylinders, *Journal of Heat Transfer*, vol. 116, pp. 96-104
- Dow Chemical Inc., 1994, *Engineering and Operating guide for DOWFROST and DOWFROST HD inhibited propylene glycol-based heat transfer fluids*, Michigan, U.S.A

- Dravid, A. N., Smith, K. A., Merrill, E. W., Brian, P. L. T. , 1971, Effect of secondary fluid motion on laminar flow heat transfer in helically coiled tubes, *AIChE Journal*, vol. 17, no. 5, pp. 1114-1122
- Dyer, J. R. , 1975, The development of laminar natural-convective flow in a vertical uniform heat flux duct, *International Journal of Heat and Mass Transfer*, vol. 18, pp. 1455-1465
- El-Genk, M. S., Bedrose, S. D., Rao, D. V. , 1990, Forced and combined convection of water in rod bundles, *Heat Transfer Engineering*, vol. 11, no. 4, pp. 32-43
- El-Genk, M. S., Rao, D. V. , 1989, Heat transfer experiments and correlations for low-Reynolds-Number flows of water in vertical annuli, *Heat Transfer Engineering*, vol.10, pp. 44-57
- El-Genk, M. S., Rao, D. V. , 1990, Buoyancy induced instability of laminar flows in vertical annuli - I. Flow visualization and heat transfer experiments, *International Journal of Heat and Mass Transfer*, vol. 33, pp. 2145-2159
- El-Genk, M. S., Su, B., Guo, Z. , 1993, Experimental studies of forced, combined and natural convection of water in vertical nine-rod bundles with a square lattice, *International Journal of Heat and Mass Transfer*, vol. 36, no. 9, pp. 2359-2374
- El-Shaarawi, M. A. I., Al-Nimr, M. A. , 1990, Fully developed laminar natural convection in open-ended vertical concentric annuli, *International Journal of Heat and Mass Transfer*, vol. 33, no. 9, pp. 1873-1884
- Eshghy, S. , 1964, Forced-flow effects on free-convection flow and heat transfer, *Journal of Heat Transfer*, pp. 290-291
- Fand, R. M., Morris, E. W., Lum, M. , 1977, Natural convection heat transfer from horizontal cylinders to air, water and silicone oils for Rayleigh numbers between

- 3×10^2 and 2×10^7 , *International Journal of Heat and Mass Transfer*, vol. 20, pp. 1173-1184
- Farouk, B., Guceri, S. I. , 1983, Natural convection from horizontal cylinders in interacting flow fields, *International Journal of Heat and Mass Transfer*, vol. 26, no. 2, pp. 231-243
- Fraas, A. P. , 1989, *Heat Exchanger Design Second Edition*, John Wiley & Sons Inc., New York
- Fraser, K. F., Hollands, K. G. T., Brunger, A. P. , 1995, An empirical model for natural convection heat exchangers in SDHW systems, *Solar Energy*, vol. 55, no. 2, pp. 75-84
- Fujii, T., Takeuchi, M, Fujii, M., Suzaki, K., Uehara, H. , 1970, Experiments on natural-convection heat transfer from the outer surface of a vertical cylinder to liquids, *International Journal of Heat and Mass Transfer*, vol. 13, pp. 753-787
- Futagami, K., Aoyama, Y. , 1988, Laminar heat transfer in a helically coiled tube, *International Journal of Heat and Mass Transfer*, vol. 31, no. 2, pp. 387-396
- George, W. K., Capp, S. P. , 1979, A theory for natural convection turbulent boundary layers next to heated vertical surfaces, *International Journal of Heat and Mass Transfer*, vol. 22, pp. 813-826
- Gnielinski, V. , 1986, Correlations for the pressure drop in helically coiled tubes, *International Chemical Engineering*, vol. 26, no. 1, pp. 36-44
- Hollands, K. G. T., Brunger, A. P. , 1992, Optimum flow rates in solar water heating systems with a counterflow exchanger, *Solar Energy*, vol. 48, pp. 15-19
- Hollands, K. G. T., Lightstone, M. F. , 1989, A review of low-flow, stratified-tank solar water heating systems, *Solar Energy*, vol. 43, pp. 97-105

- Hsu, Y. C., Shih, R. F. , 1984, Heat transfer from a heating helical coil immersed in a jet-stirred vessel, *The Canadian Journal of Chemical Engineering*, vol. 62, pp.474-481
- Incropera, F. P., DeWitt, D. P. , 1990, *Introduction to Heat Transfer*, Second Edition, John Wiley & Sons, Inc., New York, U.S.A
- Janssen, L. A. M., Hoogendoorn, C. J. , 1978, Laminar convective heat transfer in helical coiled tubes, *International Journal of Heat and Mass Transfer*, vol. 21, pp. 1197-1206
- Karim, F., Farouk, B., Namer, I. , 1986, Natural convection heat transfer from a horizontal cylinder between vertical confining adiabatic walls, *Journal of Heat Transfer*, vol. 108, pp. 291-298
- Kays, W. M., London, A. L. , 1984, *Compact Heat Exchangers Third Edition*, p. 8, McGraw-Hill Inc., New York
- Kemeny, G. A., Somers, E. V. , 1975, Combined free and forced-convective flow in vertical circular tubes -- Experiments with water and oil, *Journal of Heat Transfer*, pp. 339-346
- Keyhani, M., Dalton, T. , 1996, Natural convection heat transfer in horizontal rod-bundle enclosures, *Journal of Heat Transfer*, vol. 118, pp. 598-605
- Keyhani, M., Kulacki, F. A., Christensen, R. N. , 1983, Free convection in a vertical annulus with constant heat flux on the inner wall, *Journal of Heat Transfer*, vol. 105, pp. 454-459
- Keyhani, M., Kulacki, F. A., Christensen, R. N. , 1985, Experimental investigation of free convection in a vertical rod bundle -- A general correlation for Nusselt numbers, *Journal of Heat Transfer*, vol. 107, pp. 611-623

- Khan, J. A., Kumar, R. , 1989, Natural convection in vertical annuli: A numerical study for constant heat flux on the inner wall, *Journal of Heat Transfer*, vol. 111, pp. 909-915
- Kim, S., El-Genk, M. S. , 1989, Heat transfer experiments for low flow of water in rod bundles, *International Journal of Heat and Mass Transfer*, vol. 32, no. 7, pp. 1321-1336
- Kline, S. J., McClintock, F. A. , 1953, Describing uncertainties in single-sample experiments, *Mechanical Engineering*, vol. 75, pp. 3-9
- Kumar, R. , 1997, Three-dimensional natural convective flow in a vertical annulus with longitudinal fins, *International Journal of Heat and Mass Transfer*, vol. 40, no. 14, pp. 3323-3334
- Lieberman, J., Gebhart, B. , 1969, Interactions in natural convection from an array of heated elements, experimental, *International Journal of Heat and Mass Transfer*, vol. 12, pp. 1385-1396
- Manlapaz, R. L., Churchill, S. W. , 1980, Fully developed laminar flow in a helically coiled tube of finite pitch, *Chemical Engineering Communications*, vol. 7, pp. 57-78
- Manlapaz, R. L., Churchill, S. W. , 1981, Fully developed laminar convection from a helical coil, *Chemical Engineering Communications*, vol. 9, pp. 185-200
- Marsters, G. F. , 1972, Arrays of heated horizontal cylinders in natural convection, *International Journal of Heat and Mass Transfer*, vol. 15, pp. 921-933
- Marsters, G. F., Paulus, G. , 1972, Effects of confining walls on heat transfer from a vertical array of heated horizontal cylinders, *Transactions of the CSME*, vol. 1, no. 4, pp. 219-223
- Metais, B., Eckert, E. R. G. , 1964, Forced, mixed, and free convection regimes, *Journal of Heat Transfer*, vol. 86, pp. 295-296

- Mishra, P., Gupta, S. N. , 1979, Momentum transfer in curved pipes. 1. Newtonian fluids, *Industrial and Engineering Chemistry Process Design and Development*, vol. 18, no. 1, pp. 130-137
- Morgan, V. T. , 1997, Heat transfer by natural convection from a horizontal isothermal circular cylinder in air, *Heat Transfer Engineering*, vol. 18, no. 1, pp. 25-33
- Mori, Y., Nakayama, W. , 1965, Study on forced convective heat transfer in curved pipes, *International Journal of Heat and Mass Transfer*, vol. 8, pp. 67-82
- Omega Engineering Inc., 1992, *OMEGA Temperature Measurement Handbook & Encyclopedia*, Stamford, U.S.A., pp. Z41-Z42
- Parent, M. G. , 1988, *Natural Convection Heat Exchangers: Theory and Experiment*, M.A.Sc. thesis, University of Waterloo, Waterloo, Canada
- Parent, M. G., Van Der Meer, T. H., Hollands, K. G. T. , 1990, Natural convection heat exchangers in solar water heating systems: theory and experiment, *Solar Energy*, vol. 45, pp. 43-52
- Patankar, S. V., Prata, V. S., Spalding, D. B. , 1974, Prediction of laminar flow and heat transfer in helically coiled pipes, *Journal of Fluid Mechanics*, vol. 62, part 3, pp. 539-551
- Raithby, G. D., Hollands, K. G. T. , 1976, Laminar and turbulent free convection from elliptic cylinders, with a vertical plate and horizontal circular cylinder as special cases, *Journal of Heat Transfer*, vol. 98, pp. 72-80
- Rao, D. V., El-Genk, M. S., 1989, Buoyancy induced instability of laminar flows in vertical annuli - II, *International Journal of Heat and Mass Transfer*, vol. 33, no. 10, pp. 2160-2171

- Richmond, D. A., Hollands, K. G. T. , 1989, Numerical solution of an open cavity natural convection heat exchanger, *Journal of Heat Transfer*, vol. 111, pp. 80-85
- Rogers, G. F. C., Mayhew, Y. R. , 1964, Heat transfer and pressure loss in helically coiled tubes with turbulent flow, *International Journal of Heat and Mass Transfer*, vol. 7, pp. 1207-1216
- Rogers, B. B., Yao, L. S. , 1990, The effect of mixed convection instability on heat transfer in a vertical annulus, *International Journal of Heat and Mass Transfer*, vol. 33, no. 1, pp. 79-90
- Sadeghipour, M. S., Asheghi, M. , 1994, Free convection heat transfer from arrays of vertically separated horizontal cylinders at low Rayleigh numbers, *International Journal of Heat and Mass Transfer*, vol. 37, no. 1, pp. 103-109
- Scheele, G. F., Hanratty, T. J. , 1962, Effect of natural convection on stability of flow in a vertical pipe, *Journal of Fluid Mechanics*, vol. 14, part 2, pp. 244-257
- Sciometric Instruments Inc., 1984, CPU module and intelligent serial interface model 901 user guide, Manotick, Ontario, Canada
- Sciometric Instruments Inc., 1984, Electronics measurement system model 8082A users' manual, Manotick, Ontario, Canada
- Seban, R. A., McLaughlin, E. F. , 1963, Heat transfer in tube coils with laminar and turbulent flow, *International Journal of Heat and Mass Transfer*, vol. 6, pp. 387-395
- Shah, R. K., Joshi, S. D. , 1987, Convective heat transfer in curved ducts, *Handbook of Single-Phase Convective Heat Transfer*, John Wiley & Sons Inc., New York
- Sparrow, E. M., Niethammer, J. E. , 1981, Effect of vertical separation distance and cylinder-to-cylinder temperature imbalance on natural convection for a pair of horizontal cylinders, *Journal of Heat Transfer*, vol. 103, pp. 638-644

- Sparrow, E. M., Pfeil, D. R. , 1984, Enhancement of natural convection heat transfer from a horizontal cylinder due to vertical shrouding surfaces, *Journal of Heat Transfer*, vol. 106, pp. 124-130
- Sparrow, E. M., Vemuri, S. B. , 1985, Natural convection/radiation heat transfer from highly populated pin fin arrays, *Journal of Heat Transfer*, vol. 107, pp. 190-197
- Srinivasan, P. S., Nandapurkar, S. S., Holland, F. A. , 1970, Friction factors for coils, *Institution of Chemical Engineers Transactions*, vol. 48, pp. T156-T161
- Srinivasan, V., Christensen, R. , 1994, Design, full-scale testing, and analysis of an innovative natural-convection-driven heat-recovery heat exchanger for space-conditioning applications, *Heat Transfer Engineering*, vol. 15, pp. 44-54
- Taherian, H., Allen, P. L. , 1997, Natural convection from enclosed vertical helical coils, *7th International Conference on Solar Energy at High Latitudes*, Espoo-Oteniem, Finland
- Taherian, H., Allen, P. L. , 1997, Natural convection from vertical helical coils in a cylindrical enclosure, *Proceedings of the ASME Heat Transfer Division*, vol. 3, pp. 135-142
- Tillman, E. S. , 1976, Natural convection heat transfer from horizontal tube bundles, *ASME paper 76-HT-35*
- Tokura, I., Saito, H., Kishinami, K., Muramoto, K. , 1983, An experimental study of free convection heat transfer from a horizontal cylinder in a vertical array set in free space between parallel walls, *Journal of Heat Transfer*, vol. 105, pp. 102-107
- Topakoglu, H. C., Ebdian, M. A. , 1987, Viscous laminar flow in a curved pipe of elliptical cross-section, *Journal of Fluid Mechanics*, vol. 184, pp. 571-580
- Truesdell, L. C. Jr., Adler, R. J. , 1970, Numerical treatment of fully developed laminar flow in helically coiled tubes, *AIChE Journal*, vol. 16, no. 6, pp. 1010-1015

- Van Rossum, N. J. , 1990, **Natural Convection in Vertical Circular Tubes with and without Twisted Tape Inserts**, M.A.Sc. thesis, Technical University of Nova Scotia, Halifax, Canada
- Wang, P., Kahawita, R., Nguyen, D. L. , 1991, **Transient laminar natural convection from horizontal cylinders**, *International Journal of Heat and Mass Transfer*, vol. 34, no. 6, pp. 1429-1442
- Webster, D. R., Humphrey, J. A. C. , 1993, **Experimental observations of flow instability in a helical coil**, *Journal of Fluids Engineering*, vol. 115, pp. 436-443
- White, L. M., Allen, P. L., Van Rossum, N. J. , 1990, **Development of a new SDHW heat exchanger**, 16th Annual Conference of the Solar Energy Society of Canada, Halifax, Canada
- Xin, R. C., Ebdian, M. A. , 1996, **Natural convection heat transfer from helicoidal pipes**, *Journal of Thermophysics and Heat Transfer*, vol. 10, no. 2, pp. 297-302
- Yang, G., Dong, Z. F., Ebdian, M. A. , 1995, **Laminar forced convection in a helicoidal pipe with finite pitch**, *International Journal of Heat and Mass Transfer*, vol. 38, no. 5, pp. 853-862
- Zukauskas, A. , 1987, **Convective heat transfer in cross flow**, *Handbook of Single-Phase Convective Heat Transfer*, John Wiley & Sons Inc., New York

APPENDIX A

PHYSICAL PROPERTIES OF GLYCOL

Physical properties of an aqueous solution of 40% propylene glycol by volume are reported here (Dow Frost (1986)). For each property, a third-degree polynomial curve is fitted to the data.

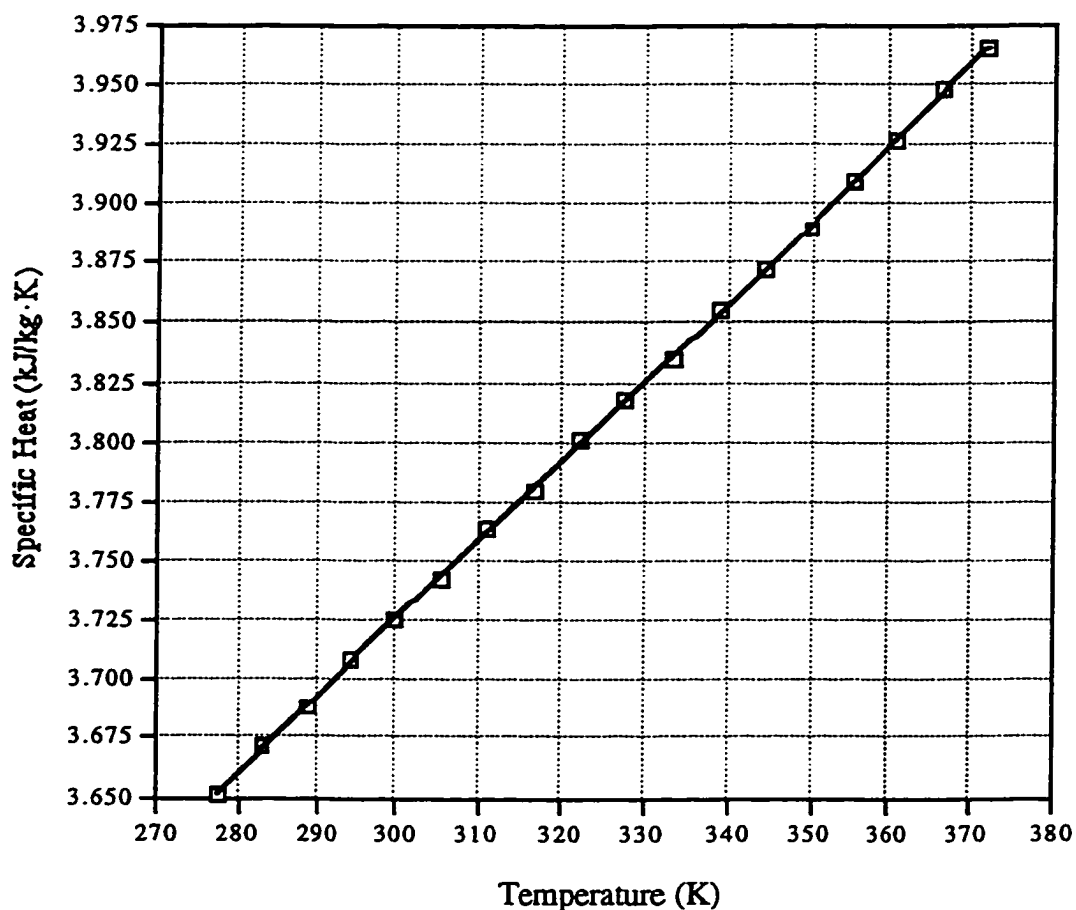


Figure A.1. Specific heat of 40/60 propylene glycol

$$c_{p,g} = 2.093 + 9.262 \times 10^{-3} T - 1.836 \times 10^{-5} T^2 + 1.878 \times 10^{-8} T^3 \quad \text{A.1}$$

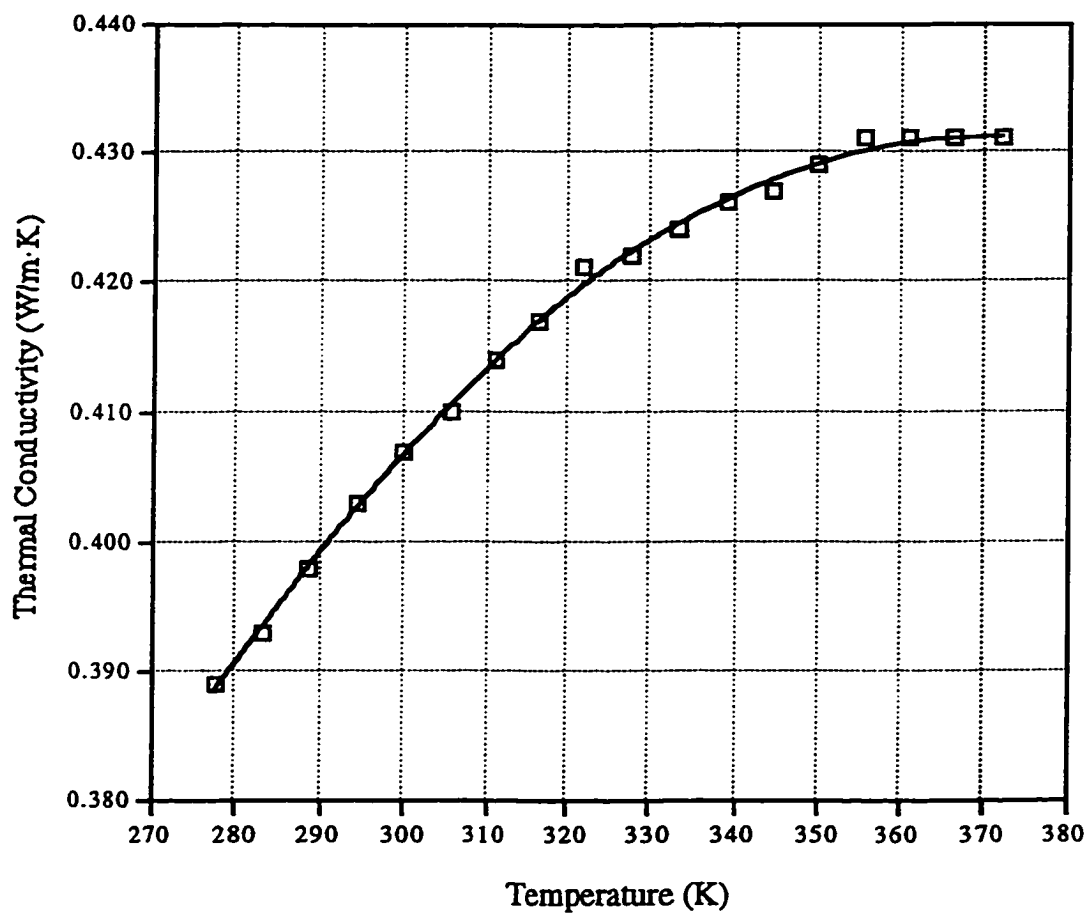


Figure A.2. Thermal conductivity of 40/60 propylene glycol

$$k_g = -0.2996 + 3.944 \times 10^{-3} T - 4.578 \times 10^{-6} T^2 - 4.052 \times 10^{-9} T^3 + 5.529 \times 10^{-12} T^4$$

A.2

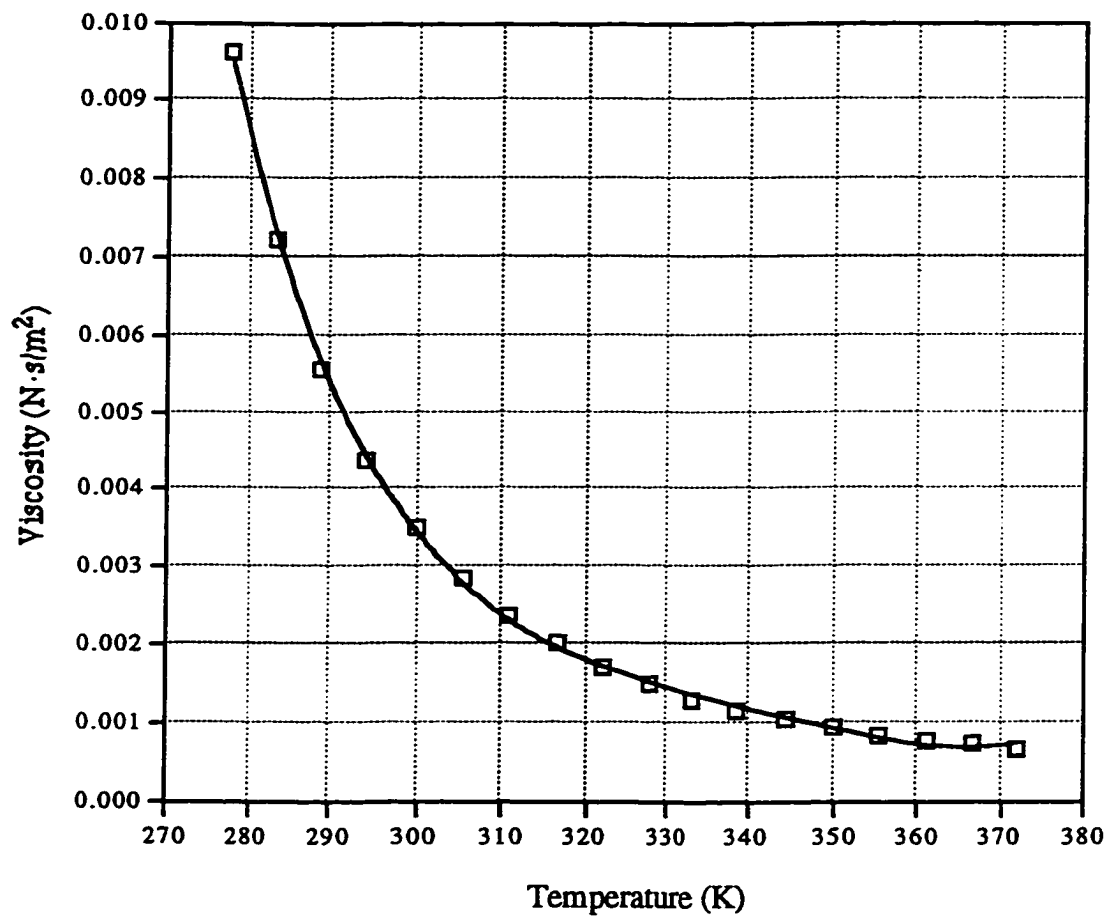


Figure A.3. Dynamic viscosity of 40/60 propylene glycol

$$\mu_g = 5.485 - 6.419 \times 10^{-2} T + 2.820 \times 10^{-4} T^2 - 5.510 \times 10^{-7} T^3 + 4.037 \times 10^{-10} T^4$$

A.3

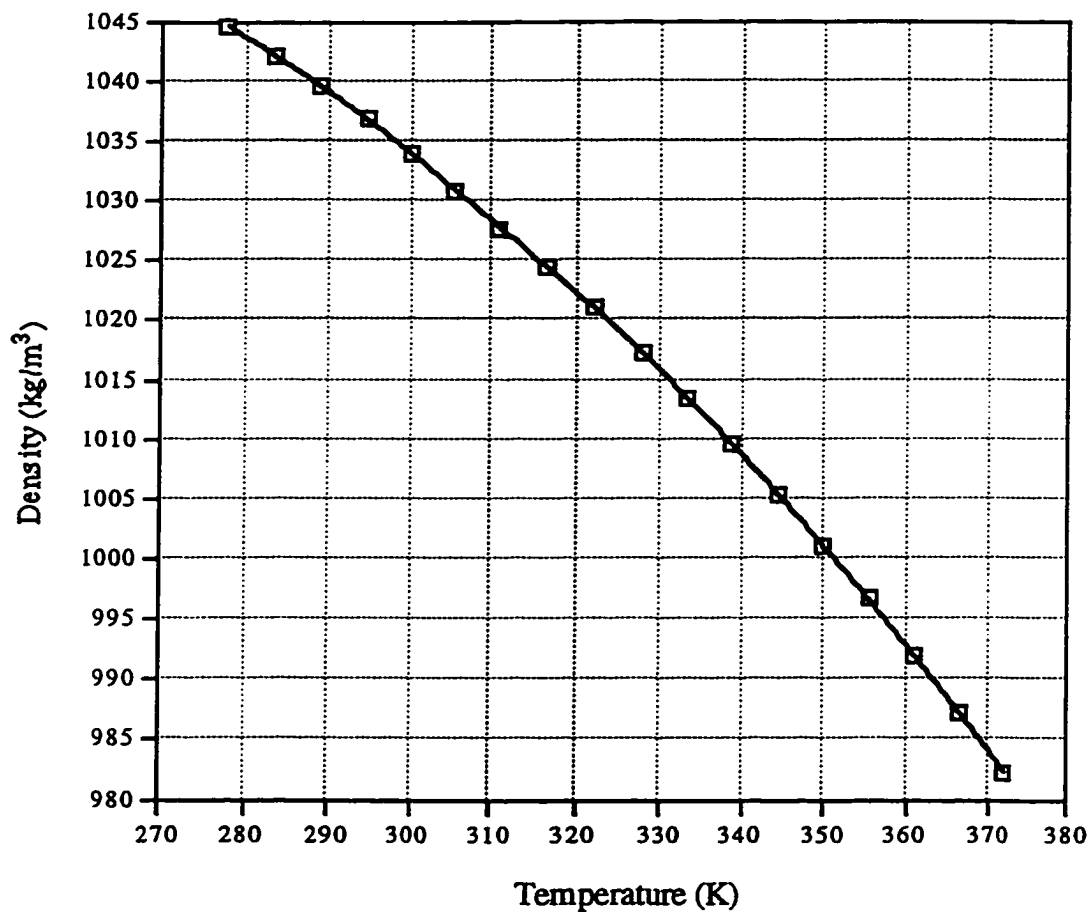


Figure A.4. Density of 40/60 propylene glycol

$$\rho_g = 1012 + 0.5557T - 1.189 \times 10^{-3}T^2 - 1.393 \times 10^{-6}T^3$$

A.4

APPENDIX B

COMPUTER CODE

```

'!!!!!!!! Triple coil monitoring program for coils #23, #24, #25
'!!!!!!!! June 1997
'*****
'***** NOTES *****
'Coil A is the outermost one and coil C is the innermost one.
'Rotameter1 reads flow rate of coil C (smallest)
'*****
DIM xiist$(66),t(66),frozenscr(5500)
pi=3.141593
kcu=387 ' Copper thermal conductivity (W/m.K)
grav=9.81 ' m/s^2
'*****
' >>> Physical dimensions
'-----
'Coil A -> Outermost
REM coil #25 nominal size :1/4" tube , 74.5 mm coil OD
DcoiloutA=.0745 ' Coil outer diameter (m)
DcoilinA=.0625 ' Coil inner diameter (m)
aout=.00635 ' Tube OD (undeformed)
a=.0048 ' Tube ID (undeformed)
tubethickness=(aout-a)/2
aloutA=.00602/2 : bloutA=.00667/2 ' radii deformed
alinA=aloutA-tubethickness : blinA=bloutA-tubethickness ' Semiaxes of the ellipse (distorted tube)
nturnsA=85.2 ' number of coil turns
coilpitchA=1.33
fstlengtA=.007 : fstlengbA=.013 ' extra straight tube length on either ends of the coil
Dshell=.0766 ' Shell inside diameter
Hshell=.762 ' Shell height
'Coil B -> middle
REM coil #24 nominal size :1/4" tube , 55.2 mm coil OD
DcoiloutB=.0552 ' Coil outer diameter (m)
DcoilinB=.0439 ' Coil inner diameter (m)
aloutB=.00563/2 : bloutB=.0069/2 ' radii deformed
alinB=aloutB-tubethickness : blinB=bloutB-tubethickness ' Semiaxes of the ellipse (distorted tube)
nturnsB=84.5 ' number of coil turns
coilpitchB=1.31
fstlengtB=.007 : fstlengbB=.005 ' extra straight tube length on either ends of the coil
'Coil C -> Innermost
REM coil #23 nominal size :1/4" tube , 37.6 mm coil OD
DcoiloutC=.0376 ' Coil outer diameter (m)
DcoilinC=.028 ' Coil inner diameter (m)
aloutC=.00482/2 : bloutC=.0075/2 ' radii deformed
alinC=aloutC-tubethickness : blinC=bloutC-tubethickness ' Semiaxes of the ellipse (distorted tube)
nturnsC=82.7 ' number of coil turns
coilpitchC=1.2
fstlengtC=.008 : fstlengbC=.015 ' extra straight tube length on either ends of the coil
'-----
' >>> Deriving other geometrical properties
coilpitchm=(coilpitchA+coilpitchB+coilpitchC)/3
rA=(DcoiloutA+DcoilinA)/4 ' Radius of curvature of the coil
rB=(DcoiloutB+DcoilinB)/4 ' Radius of curvature of the coil
rC=(DcoiloutC+DcoilinC)/4 ' Radius of curvature of the coil
DhydrA=2*alinA*blinA/SQR((alinA^2+blinA^2)/2) ' Hydraulic diameter of the tube
DhydrB=2*alinB*blinB/SQR((alinB^2+blinB^2)/2)
DhydrC=2*alinC*blinC/SQR((alinC^2+blinC^2)/2)
Dhydrm=(DhydrA+DhydrB+DhydrC)/3
TotalLCA=2*pi*rA*nturnsA+fstlengtA+fstlengbA
TotalLCB=2*pi*rB*nturnsB+fstlengtB+fstlengbB
TotalLCC=2*pi*rC*nturnsC+fstlengtC+fstlengbC
TotalLC=TotalLCA+TotalLCB+TotalLCC ' total coil length (m)
coiloutAA=2*pi*SQR((aloutA^2+bloutA^2)/2)*TotalLCA

```

```

coiloutAB=2*pi*SQR((a1outB^2+b1outB^2)/2)*TotalLCB
coiloutAC=2*pi*SQR((a1outC^2+b1outC^2)/2)*TotalLCC
coiloutA=coiloutAA+coiloutAB+coiloutAC      ' Outside area of the coil (m^2)
coilinAA=2*pi*SQR((a1inA^2+b1inA^2)/2)*TotalLCA
coilinAB=2*pi*SQR((a1inB^2+b1inB^2)/2)*TotalLCB
coilinAC=2*pi*SQR((a1inC^2+b1inC^2)/2)*TotalLCC
coilinA=coilinAA+coilinAB+coilinAC      ' Inside area of the coil surface (m^2)
Dequival=SQR((DcoiloutA^2-DcoilinA^2)+(DcoiloutB^2-DcoilinB^2)+(DcoiloutC^2-DcoilinC^2))
Acf=pi*(Dshell^2-Dequival^2)/4      ' Cross sectional flow area
Ainshell=pi*Dshell*Hshell      ' Shell inner surface area
Ap=coiloutA+Ainshell
Dhx=4*Acf*Hshell/Ap      ' Hydraulic diameter of the heat exchanger
Smodified=(Dshell-Dequival)/Dequival      ' S' is the dimensionless flow space
-----
REM   connecting to the Data Acquisition System
OPEN "COM1:9600,N,8,1" AS #1 LEN=10000
REM   Initialisation and calibration
send$="SETCAL 1,10,100,496,1001,999,10020,682400,1000000"
CALL putget
send$="ECHO 0":CALL putget
REM   Channels definition
xlist$(5)="TCP 5,3,0":xlist$(6)="TCP 6,3,0"
xlist$(7)="TCP 7,3,0":xlist$(8)="TCP 8,3,0"
xlist$(9)="TCP 9,3,0":xlist$(10)="TCP 10,3,0"
xlist$(11)="TCP 11,3,0":xlist$(12)="TCP 12,3,0"
xlist$(13)="TCP 13,3,0":xlist$(14)="TCP 14,3,0"
xlist$(15)="TCP 15,3,0":xlist$(16)="TCP 16,3,0"
xlist$(17)="TCP 17,3,0":xlist$(18)="TCP 18,3,0"
xlist$(19)="TCP 19,3,0":xlist$(20)="TCP 20,3,0"
xlist$(21)="TCP 21,3,0":xlist$(22)="TCP 22,3,0"
xlist$(23)="TCP 23,3,0":xlist$(24)="TCP 24,3,0"
xlist$(25)="TCP 25,3,0":xlist$(26)="TCP 26,3,0"
xlist$(27)="TCP 27,3,0"
xlist$(28)="DCV 28,1"      'pressure transducer-gain of 10
xlist$(31)="TCP 31,3,0":xlist$(32)="TCP 32,3,0"
xlist$(33)="TCP 33,3,0":xlist$(34)="TCP 34,3,0"
xlist$(35)="TCP 35,3,0":xlist$(36)="TCP 36,3,0"
xlist$(37)="TCP 37,3,0":xlist$(38)="TCP 38,3,0"
xlist$(39)="TCP 39,3,0"
xlist$(41)="TCP 41,3,0":xlist$(42)="TCP 42,3,0"
xlist$(43)="TCP 43,3,0":xlist$(44)="TCP 44,3,0"
xlist$(45)="TCP 45,3,0":xlist$(46)="TCP 46,3,0"
xlist$(47)="TCP 47,3,0":xlist$(48)="TCP 48,3,0"
xlist$(49)="TCP 49,3,0":xlist$(50)="TCP 50,3,0"
xlist$(51)="TCP 51,3,0":xlist$(52)="TCP 52,3,0"
xlist$(53)="TCP 53,3,0":xlist$(54)="TCP 54,3,0"
xlist$(55)="TCP 55,3,0":xlist$(56)="TCP 56,3,0"
CALL putget
OPEN "Fireball 520:desktop folder:programs:tempdata" FOR OUTPUT AS 3
PRINT #3,"Date :";DATE$," Time :";TIME$
PRINT #3,"*****"
CLOSE #3
REM   The main loop
*****
stime=TIMER
stime$=TIME$
picload:
WINDOW 1,,(1,21)-(511,341),3
OPEN "propic" FOR INPUT AS 2
image$=INPUT$(LOF(2),2)
PICTURE,image$
CLOSE 2
TEXTSIZE 9:TEXTFONT 3
LINE (5,297)-(50,313),b
LINE (413,1)-(439,122),b
LOCATE 5,64 : PRINT "Tank :"
BUTTON 1,1,"EXIT",(450,235)-(498,260),1
BUTTON 2,1,"Reload",(450,200)-(498,225),1
BUTTON 3,1,"Freeze",(450,165)-(498,190),1
BUTTON 4,1,"Calc.",(450,130)-(498,155),1
BUTTON 5,1,"Test",(450,95)-(498,120),1
BUTTON 6,1,"Graph",(450,60)-(498,85),1
LOCATE 26,10:PRINT "Minutes"
LOCATE 24,1 :PRINT "Started at ";CHR$(200);" ";stime$
WHILE DIALOG(0) <> 1      'waits for a button to be pushed
secondspassed=(TIMER-stime)

```

```

minutespassed=secondspassed/60
LOCATE 26,3:PRINT USING "###.#";minutespassed;
*****
BIN:
  Scanning all used channels
  FOR nt%= 5 TO 25
    IF nt%≠24 THEN nextchannel
    send$=xlist$(nt%):CALL putget
    t(nt%)=temp
  nextchannel:
  NEXT nt%
    LOCATE 20,20 :PRINT USING "###.#";t(5)      ' Shell surface
    LOCATE 18,20 :PRINT USING "###.#";t(6)
    LOCATE 16,20 :PRINT USING "###.#";t(7)
    LOCATE 14,20 :PRINT USING "###.#";t(8)
    LOCATE 12,20 :PRINT USING "###.#";t(9)
    LOCATE 11,20 :PRINT USING "###.#";t(25)     ' Shell surface
    LOCATE 20,26 :PRINT USING "###.#";t(10)     ' Coil surfaceA
    LOCATE 18,26 :PRINT USING "###.#";t(11)
    LOCATE 16,26 :PRINT USING "###.#";t(12)
    LOCATE 14,26 :PRINT USING "###.#";t(13)
    LOCATE 12,26 :PRINT USING "###.#";t(14)
    LOCATE 20,36 :PRINT USING "###.#";t(15)     ' Coil surfaceB
    LOCATE 18,36 :PRINT USING "###.#";t(16)
    LOCATE 16,36 :PRINT USING "###.#";t(17)
    LOCATE 14,36 :PRINT USING "###.#";t(18)
    LOCATE 12,36 :PRINT USING "###.#";t(19)
    LOCATE 20,51 :PRINT USING "###.#";t(20)     ' Coil surfaceC
    LOCATE 18,51 :PRINT USING "###.#";t(21)
    LOCATE 16,51 :PRINT USING "###.#";t(22)
    LOCATE 14,51 :PRINT USING "###.#";t(23)
    LOCATE 12,51 :PRINT USING "###.#";t(19)
  FOR nt%=31 TO 56
    IF nt%>=39 AND nt%<=40 THEN GOTO skipch
    send$=xlist$(nt%):CALL putget
    t(nt%)=temp
  skipch:
  NEXT nt%
    LOCATE 2,34 :PRINT USING "###.#";t(31)      'Glycol Low
    LINE (200,5)-(200,9)
    LOCATE 8,33 :PRINT USING "###.#";t(32)      'Glycol High
    LOCATE 25,80 :PRINT USING "###.#";t(36)     'Ambient
    LOCATE 25,72 :PRINT "Ambient : "
    LOCATE 10,48 :PRINT USING "###.#";t(46)     'WO
    LOCATE 12,45 :PRINT USING "###.#";t(45)     ' Water center
    LOCATE 14,45 :PRINT USING "###.#";t(44)
    LOCATE 16,45 :PRINT USING "###.#";t(43)
    LOCATE 18,45 :PRINT USING "###.#";t(42)
    LOCATE 20,45 :PRINT USING "###.#";t(41)     ' Water center
    LOCATE 10,31 :PRINT USING "###.#";t(33)     'GI
    LOCATE 23,31 :PRINT USING "###.#";t(34)     'GO A
    LOCATE 23,41 :PRINT USING "###.#";t(35)     ' B
    LOCATE 23,56 :PRINT USING "###.#";t(38)     ' C
    LOCATE 24,48 :PRINT USING "###.#";t(37)     'WI
    LOCATE 10,70 :PRINT USING "###.#";t(47)     ' Tank bottom
    LOCATE 9,70 :PRINT USING "###.#";t(48)
    LOCATE 8,70 :PRINT USING "###.#";t(49)
    LOCATE 7,70 :PRINT USING "###.#";t(50)
    LOCATE 6,70 :PRINT USING "###.#";t(51)
    LOCATE 5,70 :PRINT USING "###.#";t(52)
    LOCATE 4,70 :PRINT USING "###.#";t(53)
    LOCATE 3,70 :PRINT USING "###.#";t(54)
    LOCATE 2,70 :PRINT USING "###.#";t(55)
    LOCATE 1,70 :PRINT USING "###.#";t(56)     ' Tank top
    send$=xlist$(28):CALL putget
    DCmV2=temp*1000
    psid=241*DCmV2+.129
    LOCATE 26,73:PRINT "psid : "
    IF DCmV2<.1 THEN
      LOCATE 26,78:PRINT " Off "
    ELSE
      LOCATE 26,78 :PRINT USING "###.##";psid
    END IF
  WEND
*****
buttoncheck:

```



```

DelTtop=t(33)-t(46)
DelTbotA=t(34)-t(37)
DelTbotB=t(35)-t(37)
DelTbotC=t(38)-t(37)
LMTDA=(DelTtop-DelTbotA)/LOG(DelTtop/DelTbotA)
LMTDB=(DelTtop-DelTbotB)/LOG(DelTtop/DelTbotB)
LMTDC=(DelTtop-DelTbotC)/LOG(DelTtop/DelTbotC)
=====
>> Glycol properties
Tgoutav=(t(34)+t(35)+t(38))/3
Tmeanglycol=(Tgoutav+t(33))/2
Tg1=(Tgoutav+t(31))/2      Glycol temperature through the rotameter
Tg=Tmeanglycol+273        Absolute temperature
RhoG=(-1.3929E-06*Tg^3)-(0.011886*Tg^2)+(.55574*Tg)+1011.7
CpG=1000*((1.8782E-08*Tg^3)-(1.8356E-05*Tg^2)+(.0092619*Tg)+2.0932)
muG=(4.0369E-10*Tg^4)-(5.5097E-07*Tg^3)+(2.8203E-04*Tg^2)-(0.64193*Tg)+5.4852
PrG=(3.9303E-06*Tg^4)-(0.005362*Tg^3)+(2.7433*Tg^2)-(624.02*Tg)+53282&
kG=(5.5285E-12*Tg^4)-(4.0518E-09*Tg^3)-(4.5785E-06*Tg^2)+(.003944*Tg)-.29965
nuG=muG/RhoG
=====
>> Interpolation for Glycol flowrate (mL/S)
IF Tg1<=40 THEN
  yy1=.0001237*rotscaleA-.00272
  yy2=.0001422*rotscaleA-.002631
  yyA=yy1+((Tg1-20)/20)*(yy2-yy1)      ' interpolation
ELSE
  yy1=.0001422*rotscaleA-.002631
  yy2=.0001489*rotscaleA-.002384
  yyA=yy1+((Tg1-40)/15)*(yy2-yy1)      ' interpolation
END IF
IF Tg1<=40 THEN
  yy1=.0001237*rotscaleB-.00272
  yy2=.0001422*rotscaleB-.002631
  yyB=yy1+((Tg1-20)/20)*(yy2-yy1)      ' interpolation
ELSE
  yy1=.0001422*rotscaleB-.002631
  yy2=.0001489*rotscaleB-.002384
  yyB=yy1+((Tg1-40)/15)*(yy2-yy1)      ' interpolation
END IF
IF Tg1<=40 THEN
  yy1=.0001237*rotscaleC-.00272
  yy2=.0001422*rotscaleC-.002631
  yyC=yy1+((Tg1-20)/20)*(yy2-yy1)      ' interpolation
ELSE
  yy1=.0001422*rotscaleC-.002631
  yy2=.0001489*rotscaleC-.002384
  yyC=yy1+((Tg1-40)/15)*(yy2-yy1)      ' interpolation
END IF
=====
>> Hot liquid important parameters
massgflowA=yyA : massgflowB=yyB : massgflowC=yyC
massgflow=yyA+yyB+yyC      Kg/S
Flownum=massgflow*CpG*acout/(2*kW*coiloutA) ' Flow number F
RecritA=2100*(1+12*(rA/a)^(-.5))      ' Critical Reynolds
RecritB=2100*(1+12*(rB/a)^(-.5))
RecritC=2100*(1+12*(rC/a)^(-.5))
ReglycolA=4*massgflowA/(pi*DhydrA*muG)      ' Reynolds number
ReglycolB=4*massgflowB/(pi*DhydrB*muG)
ReglycolC=4*massgflowC/(pi*DhydrC*muG)
DeglycolA=ReglycolA*SQR(a/rA)      ' Dean number
DeglycolB=ReglycolB*SQR(a/rB)
DeglycolC=ReglycolC*SQR(a/rC)
>> x3 and x4 are parameters from eq. (5.33)
x3A=(1+1342/(DeglycolA^2*PrG))^2 : x4=1+1.15/PrG
x3B=(1+1342/(DeglycolB^2*PrG))^2
x3C=(1+1342/(DeglycolC^2*PrG))^2
NussglycolA=((4.364+4.636/x3A)^3+1.816*(DeglycolA/x4)^1.5)^(1/3) ' Nusselt number inside
NussglycolB=((4.364+4.636/x3B)^3+1.816*(DeglycolB/x4)^1.5)^(1/3)
NussglycolC=((4.364+4.636/x3C)^3+1.816*(DeglycolC/x4)^1.5)^(1/3)
hinsideA=NussglycolA*kG/DhydrA      h inside (W/m^2.K)
hinsideB=NussglycolB*kG/DhydrB
hinsideC=NussglycolC*kG/DhydrC
hinside=(hinsideA*massgflowA+hinsideB*massgflowB+hinsideC*massgflowC)/massgflow
wallthres=(LOG(acout/a))/(2*pi*kcw*TotalLC) ' tube wall thermal resistance
intheres=1/(coilinA*hinside)      ' internal thermal resistance
QoutglycolA=massgflowA*CpG*(t(33)-t(34))

```

```

QoutglycolB=massgflowB*CpG*(t(33)-t(35))
QoutglycolC=massgflowC*CpG*(t(33)-t(38))
tgoutwa=(t(34)*massgflowA+t(35)*massgflowB+t(38)*massgflowC)/massgflow
Qoutglycol=QoutglycolA+QoutglycolB+QoutglycolC      ' Watts
DelTbotwa=(DelTbotA*massgflowA+DelTbotB*massgflowB+DelTbotC*massgflowC)/massgflow
LMTD=(DelTtop-DelTbotwa)/LOG(DelTtop/DelTbotwa)
UAh=Qoutglycol/LMTD
UAc=Qinwater/LMTD
Uoh=UAh/coiloutA
ch=massgflow*CpG

```

```

REM      >>> natural convection coefficient <<<

```

```

' h and Nu from [Q=UoAo(LMTD)]
houtsideU=1/(coiloutA*(1/UAh-intheres-wallthres))  ' W/m^2.K
NusswdhxU=houtsideU*Dhx/kW
' h and Nu from the surface temps and mean water temp
t(10)=(t(14)+4*(t(11)-t(14))/3      ' extrapolation
Tmeansur=(t(10)+t(11)+t(12)+t(13)+t(14)+t(15)+t(16)+t(17)+t(18)+t(19)+t(20)+t(21)+t(22)+t(23)+t(19))/15
houtsideS=Qinwater/(coiloutA*(Tmeansur-Tmeancore))
TmeansurA=(t(10)+t(11)+t(12)+t(13)+t(14))/5
TmeansurB=(t(15)+t(16)+t(17)+t(18)+t(19))/5
TmeansurC=(t(20)+t(21)+t(22)+t(23)+t(19))/5
houtsideSA=QoutglycolA/(coiloutAA*(TmeansurA-Tmeancore))
houtsideSB=QoutglycolB/(coiloutAB*(TmeansurB-Tmeancore))
houtsideSC=QoutglycolC/(coiloutAC*(TmeansurC-Tmeancore))
NusswdhxSA=houtsideSA*Dhx/kW
NusswdhxSB=houtsideSB*Dhx/kW
NusswdhxSC=houtsideSC*Dhx/kW
NusswdtSA=houtsideSA*aout/kW
NusswdtSB=houtsideSB*aout/kW
NusswdtSC=houtsideSC*aout/kW
NusswLA=houtsideSA*TotalLCA/kW
NusswLB=houtsideSB*TotalLCB/kW
NusswLC=houtsideSC*TotalLCC/kW
NusswdhxS=houtsideS*Dhx/kW
NusswdtS=houtsideS*aout/kW      ' Nusselt based on the tube diameter
NusswL=houtsideS*TotalLC/kW      ' Nusselt based on the coil length
RayDt=grav*betaW*aout^3*(Tmeancore-Tinf)*PrW/(nuW^2)  ' Rayleigh number based on the tube diam.
RayDhx=grav*betaW*Dhx^3*(Tmeancore-Tinf)*PrW/(nuW^2)  ' Ra based on the heat exchanger diam.
RaySDhx=RayDhx*Hshell/TotalLC      ' Modified Rayleigh number
RayqDhx=grav*betaW*Qinwater*Dhx^4*PrW/(coiloutA*kW*nuW^2)
RayqL=grav*betaW*Qinwater*TotalLC^4*PrW/(coiloutA*kW*nuW^2)
RayL=grav*betaW*TotalLC^3*(Tmeancore-Tinf)*PrW/(nuW^2)
Velocity=masswflow/(RhoW*Acf)
ReDt=Velocity*aout/nuW
ReDhx=Velocity*Dhx/nuW

```

```

' >> Effectiveness and modified effectiveness
IF Cc>ch THEN Cmin=ch ELSE Cmin=Cc
Eff=ch*(t(33)-tgoutwa)/(Cmin*(t(33)-t(37)))
Effmod=(t(33)-tgoutwa)/(t(33)-t(37))

```

```

PRINT "ΔT,cold = ";t(46)-t(37)
PRINT "ΔT,hot = ";t(33)-tgoutwa
PRINT "LMTD = " USING "###.##":LMTD
PRINT "Flowrate,Hot side (L/S) = ";USING "#####.yy*1000/RhoG
PRINT "Electrical Power to the Heater = ";elecpower
PRINT "Q from Glycol (W) = ";USING "#####.##":Qoutglycol
PRINT "Q to Water (W) = ";USING "#####.##":Qinwater
DeltaQ=Qoutglycol-Qinwater
PRINT "Heat Loss (Qg-Qw) = ";USING "#####.##":DeltaQ
PRINT " ~~~~~~ "

```

```

' Calculate water flowrate from energy balance
Wcalcflow=1000*Qoutglycol/(CpW*(t(46)-t(37))*RhoW)    L/S
BUTTON 1,1,"Return",(5,228)-(70,240),3
BUTTON 2,1,"Write to file",(5,242)-(110,260),3
WHILE DIALOG(0)<=1: WEND
pushed=DIALOG(1)
IF pushed=2 THEN GOSUB wrdata
GOTO picload

```

```

REM The CPU scanning and averaging subroutine
scanave:
REM CPU module scan and save subprogram
send$="@crlst":CALL putget

```

```

FOR ch%=5 TO 46
  IF ch%>25 AND ch%<41 OR ch%=24 THEN forgetit
  cha$=STR$(ch%)
  send$="+A TCP "+cha$+",3,0" : CALL putget
forgetit:
NEXT ch%
'>> scans every 2 seconds and averages over a period of 120 seconds
send$="@scan 1,2,120" : CALL putget
'send$="@prlist" : CALL PUTGET
RETURN
REM steady state check subroutine
-----
steadcheck:
  IF Cc$="checkon" THEN
    Cc$="checkoff"
  ELSE
    Cc$="checkon"
  END IF
  GOTO picload
-----
wrdata: ' >> subroutine to write specific data into a file
-----
OPEN "Fireball 520:desktop folder:programs:tempdata" FOR APPEND AS 3
PRINT #3,">Temperatures : " :PRINT #3," "
PRINT #3,"Tc,i " : Tc,o " :Th,i " : Th,o(wa) "
PRINT #3,USING "###.# " :i(37);i(46);i(33);i(goutwa) :PRINT #3," "
PRINT #3,"Th,o1 " : Th,o2 " : Th,o3 "
PRINT #3,USING "###.# " :i(38);i(35);i(34) : PRINT #3," "
PRINT #3,"SH01 " : SH02 " : SH03 " : SH04 " : SH05 " : SH06 "
PRINT #3,USING "###.# " :i(5);i(6);i(7);i(8);i(9);i(25) :PRINT #3," "
PRINT #3,"CS01 CS02 CS03 CS04 CS05 -> Coil 3"
PRINT #3,USING "###.# " :i(10);i(11);i(12);i(13);i(14) :PRINT #3," "
PRINT #3,"CS01 CS02 CS03 CS04 CS05 -> Coil 2"
PRINT #3,USING "###.# " :i(15);i(16);i(17);i(18);i(19) :PRINT #3," "
PRINT #3,"CS01 CS02 CS03 CS04 CS05 -> Coil 1"
PRINT #3,USING "###.# " :i(20);i(21);i(22);i(23);i(19) :PRINT #3," "
PRINT #3,"Tm,s = " :USING "###.#" :Tmeansur :PRINT #3," "
PRINT #3,"WC01 WC02 WC03 WC04 WC05"
PRINT #3,USING "###.# " :i(41);i(42);i(43);i(44);i(45) :PRINT #3," "
PRINT #3,"Tm,w = " :USING "###.#" :Tmeancore :PRINT #3," "
PRINT #3,"TK01 TK02 TK03 TK04 TK05 TK06 TK07 TK08 TK09 TK10"
PRINT #3,USING "###.# " :i(47);i(48);i(49);i(50);i(51);i(52);i(53);i(54);i(55);i(56)
PRINT #3,"-----"
PRINT #3,">Properties : " :PRINT #3," "
PRINT #3,"CpW RhoW CpG RhoG"
PRINT #3,USING "###.# " :CpW,RhoW,CpG,RhoG :PRINT #3," "
PRINT #3,"muW nuW muG nuG"
PRINT #3,USING "###.#" :muW,nuW,muG,nuG :PRINT #3," "
PRINT #3,"kW PrW kG PrG"
PRINT #3,USING "###.# " :kW,PrW,kG,PrG
PRINT #3,"-----"
PRINT #3,">Readings : " :PRINT #3," "
PRINT #3,"Water flowrate Wflow calc. (L/s) Power (W)*"
PRINT #3,USING "###.# " :volwflow,Wcalcflow; :PRINT #3,SPC(12);
PRINT #3,USING "###.#" :elecpower :PRINT #3," "
PRINT #3,"psid rotameterA rotameterB rotameterC" :PRINT #3,USING "###.#" "psid;
PRINT #3,USING "###.# " :rotscaleA,rotscaleB,rotscaleC
PRINT #3,"-----"
PRINT #3,">Results (overall): " : PRINT #3," "
PRINT #3,"LMTD QCold QHot mdotW mdotG"
PRINT #3,USING "###.# " :LMTD;
PRINT #3,USING "###.# " :Qinwater,Qoutglycol;
PRINT #3,USING "###.#" :masswflow;massgflow :PRINT #3," "
PRINT #3,"Ambient UAh UAc Effectvsss Modified Eff."
PRINT #3,USING "###.# " :i(36);
PRINT #3,USING "###.# " :UAh;UAc;
PRINT #3,USING "###.# " :Eff;Effmod :PRINT #3," "
PRINT #3,"F = " :USING "###.#" :Flownum : PRINT #3," "
PRINT #3,"h inside (weighted ave.) = " :USING "###.#" :hinside : PRINT #3," "
PRINT #3,"> Coil 3:"
PRINT #3,"Re Critical Re De "
PRINT #3,USING "###.# " :ReglycolA,RecritA,DeglycolA
PRINT #3,"Nu inside = " :USING "###.#" :NussglycolA
PRINT #3,"h inside = " :USING "###.#" :hinsideA
PRINT #3,"h outside3 = " :USING "###.#" :houtsideSA
PRINT #3,"NuDhx3 = " :USING "###.#" :NusswdhxSA

```

```

PRINT #3,"NuDt3 = ";USING "###.##";NusswdtSC
PRINT #3,"> Coil 2:"
PRINT #3,"Re Critical Re De "
PRINT #3,USING "####";ReglycolB,RecritB,DeglycolB
PRINT #3,"Nu inside = ";USING "###.##";NussglycolB
PRINT #3,"h inside = ";USING "###.##";hinsideB
PRINT #3,"h outside2 = ";USING "###.##";houtsideSB
PRINT #3,"NuDhx2 = ";USING "###.##";NusswdhxSB
PRINT #3,"NuDt2 = ";USING "###.##";NusswdtSB
PRINT #3,"> Coil 1:"
PRINT #3,"Re Critical Re De "
PRINT #3,USING "####";ReglycolC,RecritC,DeglycolC
PRINT #3,"Nu inside = ";USING "###.##";NussglycolC
PRINT #3,"h inside = ";USING "###.##";hinsideC
PRINT #3,"h outside1 = ";USING "###.##";houtsideSC
PRINT #3,"NuDhx1 = ";USING "###.##";NusswdhxSC
PRINT #3,"NuDt1 = ";USING "###.##";NusswdtSC
PRINT #3,"*****"
PRINT #3,"From : Q=UoAo(LMTD)"
PRINT #3,"h outside = ";USING "###.##";houtsideU
PRINT #3,"NuDhx = ";USING "###.##";NusswdhxU
PRINT #3,"From the mean surface and water temperatures :"
PRINT #3,"h outside = ";USING "###.##";houtsideS
PRINT #3,"NuDhx = ";USING "###.##";NusswdhxS
PRINT #3,"NuDt = ";USING "###.##";NusswdtS
PRINT #3,"NuL = ";USING "###.##";NusswL
PRINT #3,"*****"
PRINT #3,"Rayleigh Dt = ";USING "###.###^###";RayDt
PRINT #3,"Rayleigh Dhx = ";USING "###.###^###";RayDhx
PRINT #3,"Rayleigh* Dhx = ";USING "###.###^###";RaySDhx
PRINT #3,"Rayleigh q" Dhx = ";USING "###.###^###";RayqDhx
PRINT #3,"Rayleigh q" L = ";USING "###.###^###";RayqL
PRINT #3,"Rayleigh L = ";USING "###.###^###";RayL
PRINT #3,"Flow velocity (m/s) = ";USING "###.###";Velocity
PRINT #3,"Reynolds Dt = ";USING "###.###";ReDt
PRINT #3,"Reynolds Dhx = ";USING "###.###";ReDhx
PRINT #3,"*****"
PRINT #3,"Dimensionless flow space S' = ";USING "###.###";Smodified
PRINT #3,"Coil pitch P (mean)= ";coilpitchm
PRINT #3,"Mean tubing hydraulic diameter (m) = ";USING "###.###";Dhydrrm
PRINT #3,"Heat exchanger hydraulic diameter (m) = ";USING "###.###";Dhx
PRINT #3,"Total surface area of the coils (m^2) = ";USING "###.###";coiloutA
PRINT #3,"Coils outside diameter (m) = ";USING "###.###";Dcoilout
PRINT #3,"Total length of the coils (m) = ";USING "###.###";TotalLC
CLOSE 3
GOTO picload

```

```

REM Subroutine to capture the screen for further printing
freeze: >> Freezes the screen and copies it to clipboard for further use
GET (1,1)-(497,320),frozenscr
PICTURE ON : PUT (1,1)-(497,320),frozenscr : PICTURE OFF
OPEN "clip:picture" FOR OUTPUT AS #4
PRINT #4,PICTURES$
CLOSE #4 : BEEP
GOTO picload

```

```

REM Subroutine "dograph" to monitor one particular channel
dograph:
xspan=370 : yspan=215
x2=400:x1=30
y1=245:y2=30
t1=0
WINDOW 5,"Value",(454,45)-(500,330),4
TEXTSIZE (9)
WINDOW 4,"Graph",(20,45)-(449,330),4
TEXTSIZE (9)
INPUT "Which channel : ",nt
INPUT "Temperature from : ",twat1
INPUT " to : ",twat2
INPUT "Time span in minutes : ",t2
IF twat2<=twat1 OR t2<=0 THEN GOTO dograph
PRINT :PRINT "channel # ";nt
PRINT "temperature from ";twat1;" to ";twat2
PRINT "Monitor for ";t2;" minutes"
INPUT "O.K (y/n) ",cor$
IF cor$="y" OR cor$="Y" THEN

```

```

ELSE
  CLS : GOTO dograph
END IF
CLS
LOCATE 2,30 : PRINT "Channel # ";nt
BUTTON 1,1,"Channel",(350,5)-(425,30)
BUTTON 2,1,"Return",(350,35)-(425,60)
LINE (30,245)-(400,245)
LINE (30,246)-(400,246)
LINE -(400,100)
LINE (30,247)-(30,30)
LINE (29,247)-(29,30)
LOCATE 22,66 : PRINT USING "##";t2
LOCATE 21,2 : PRINT USING "##";twat1
LOCATE 3,2 : PRINT USING "##";twat2
REM ***** The Main LOOP *****
stim=TIMER : tp=0 : i=0
WHILE tp<2 AND DIALOG(0)<>1
  secondspassed=(TIMER-stim)
  tp=secondspassed/60
  send$=xlist$(nt) :CALL putget
  twat=temp
  IF i>0 THEN
    IF twat<tmin THEN tmin=twat
    IF twat>tmax THEN tmax=twat
  ELSE
    tmin=twat
    tmax=twat
  END IF
  x=(tp-t1)*(x2-x1)/(t2-t1)+x1
  y=(twat-twat1)*(y2-y1)/(twat2-twat1)+y1
  WINDOW OUTPUT 5
  PRINT USING "##.#";twat
  WINDOW OUTPUT 4
  LOCATE 6,61 : PRINT "min. : ";:PRINT USING "##.#";tmin
  LOCATE 7,61 : PRINT "max. : ";:PRINT USING "##.#";tmax
  PSET (x,y)
  i=i+1
  FOR del=1 TO 300:NEXT del
WEND
pressed=DIALOG(1)
IF tp<2 AND pressed =1 THEN
  GOTO dograph
END IF
GOTO freeze

```

```

=====
>>>> Subprograms
=====

```

```

REM Main data acquisition subroutine
SUB putget1 STATIC
SHARED send$,temp
PRINT #1,send$:COUNT=0:s$=""
gh0=TIMER : gh=0
WHILE gh<20
  IGET1:
  gh=TIMER-gh0
  IF LOC(1)=0 THEN GOTO IGET1
  GOTO exwhile
WEND
GOSUB ITIMEOUT
exwhile:
a$=INPUT$(1,#1):IF a$="," THEN a$=CHR$(9)
IF LOC(1) > 0 THEN s$ = a$ + a$ ELSE GOTO IGET2
IF a$ <> CHR$(13) GOTO IGET1
temp=VAL(s$) 'this is the measured value
PRINT #5,s$
PRINT s$
IGET2:
GOSUB DXERROR
COUNT = COUNT + 1:s$ = "":IF LOC(1) > 0 GOTO IGET1
IGETOUT:
EXIT SUB
ITIMEOUT:
PRINT "TIME OUT HAS OCCURED!"
BEEP:BEEP:PRINT"ERROR in data transmission..."
PRINT:PRINT "Please reboot the program"

```

```

RETURN
XERROR:
IF LEFT$(s$,4) <> "9999" THEN RETURN
ERRORNUM$ = LEFT$(RIGHT$(s$,5),3)
BEEP:PRINT "#";ERRORNUM$:XERR=1
RETURN
END SUB
=====
SUB putget STATIC
=====
SHARED send$,temp
putget:
PRINT #1,send$:COUNT=0:s$=""
TIMER ON
ON TIMER (20) GOSUB TIMEOUT
gh0=TIMER : gh=0
WHILE gh<20
GET1:
gh=TIMER-gh0
IF LOC(1)=0 THEN GOTO GET1
GOTO exitwhile
WEND
GOSUB TIMEOUT
exitwhile:
TIMER OFF
FOR ND=1 TO 20:NEXT ND
a$=INPUT$(1,#1):IF a$="," THEN a$=CHR$(9)
IF LOC(1) > 0 THEN s$ = s$ + a$ ELSE GOTO GET2
IF a$ <> CHR$(13) GOTO GET1
temp=VAL(s$) 'this is the measured value
GET2:
GOSUB XERROR
COUNT = COUNT + 1:s$ = "" :IF LOC(1) > 0 GOTO GET1
GETOUT:
EXIT SUB
TIMEOUT:
PRINT "TIME OUT HAS OCCURED!"
BEEP:BEEP:PRINT"ERROR in data transmission..."
PRINT:PRINT "Please reboot the program"
RETURN
XERROR:
IF LEFT$(s$,4) <> "9999" THEN RETURN
ERRORNUM$ = LEFT$(RIGHT$(s$,5),3)
BEEP:PRINT "#";ERRORNUM$:XERR=1
RETURN
END SUB

```

APPENDIX C

SAMPLE HEAT TRANSFER DATA

Table C.1. Typical heat transfer data

Cell #	q (W)	m _g (g/s)	m _w (g/s)	T _{cl} (°C)	T _{co} (°C)	Th,i (°C)	Th,o (°C)	LMTD (°C)	UA (W/K)	Ra*Dhx	Req,Dhx	Nu _{Dhx}	e'
1	850	0.01049	0.00680	10.0	39.9	53.2	34.5	18.3	46.5	4.62E+05	1.73E+08	30.1	0.432
2	540	0.00765	0.00572	12.0	34.6	49.9	30.9	17.1	31.6	1.39E+06	6.59E+08	58.5	0.500
3	879	0.02604	0.00718	15.1	44.4	48.3	39.4	11.2	78.3	5.00E+05	1.41E+08	34.5	0.268
4	789	0.02641	0.00675	12.6	40.6	51.3	43.0	18.9	41.8	2.33E+06	1.09E+09	65.1	0.216
5	488	0.01385	0.00490	8.6	32.4	47.1	36.8	20.7	23.6	3.79E+06	1.62E+09	77.3	0.267
6	818	0.01347	0.00664	12.5	42.0	55.1	39.0	19.0	43.0	1.19E+06	4.45E+08	42.5	0.379
7	376	0.01409	0.00488	14.3	32.7	48.7	41.2	20.9	18.0	8.03E+06	3.66E+09	102.2	0.218
8	453	0.01144	0.00526	15.9	36.5	49.6	38.5	17.4	26.1	3.91E+06	1.52E+09	67.0	0.330
9	792	0.01759	0.00741	16.3	41.8	56.1	44.0	20.2	39.2	1.79E+06	7.29E+08	56.0	0.304
10	702	0.00980	0.00718	17.2	40.6	68.7	49.0	30.0	23.4	8.09E+06	4.47E+09	97.5	0.382
11	1116	0.01445	0.00834	20.3	52.4	77.8	57.3	30.8	36.2	4.56E+06	2.26E+09	68.8	0.356
12	171	0.00680	0.00348	19.7	31.4	34.8	29.0	5.8	29.2	8.31E+05	2.73E+08	38.4	0.382
13	396	0.00771	0.00534	19.0	36.7	44.3	30.7	9.5	41.9	7.14E+05	3.42E+08	49.8	0.539
14	493	0.00515	0.00583	17.6	37.8	49.5	25.5	9.7	50.9	1.98E+05	9.51E+07	29.1	0.753
15	490	0.00464	0.00492	18.1	41.9	60.9	35.5	18.2	26.9	2.05E+06	4.96E+08	53.9	0.593
16	826	0.01264	0.00740	15.6	42.3	49.8	32.3	11.5	71.6	8.96E+04	2.21E+07	14.2	0.511
17	485	0.01338	0.00531	13.5	35.3	49.1	40.9	19.8	24.5	2.67E+06	9.70E+08	63.6	0.230
18	1251	0.01642	0.00811	11.8	48.7	56.9	38.0	15.5	80.7	3.11E+05	9.94E+07	26.4	0.418
19	469	0.00971	0.00467	11.8	35.8	50.7	34.5	18.6	25.2	5.57E+05	1.15E+08	38.2	0.418
20	1186	0.00991	0.00858	15.6	48.7	69.2	38.1	21.4	55.3	8.00E+04	1.90E+07	21.3	0.579
21	777	0.01717	0.00742	18.2	43.3	50.8	38.4	12.8	60.7	5.05E+05	1.13E+08	24.9	0.379
23	552	0.00995	0.00549	13.1	37.1	40.8	25.6	7.2	76.3	1.12E+06	1.65E+08	34.3	0.546
24	1715	0.01703	0.00990	13.8	55.3	60.2	34.7	11.0	156.5	7.02E+05	1.34E+08	33.1	0.550
25	864	0.01022	0.00690	13.9	43.9	48.8	26.1	8.0	107.5	1.05E+05	1.01E+07	15.6	0.649
1+2	535	0.01763	0.00647	20.7	40.5	43.5	35.9*	7.5	71.2	9.98E+04	1.81E+07	29.0	0.333
23+24	1719	0.02977	0.01053	15.6	54.7	56.1	41.4*	8.4	205.6	1.48E+05	1.50E+07	18.9	0.362
23+25	1738	0.02513	0.01052	15.6	55.1	56.6	37.8*	7.6	227.8	4.58E+04	3.61E+06	11.1	0.459
24+25	2281	0.03116	0.01203	15.1	60.4	61.4	42.7*	7.8	293.2	2.30E+04	1.55E+06	7.9	0.403
1+2+22	1249	0.02456	0.00853	13.0	48.0	50.1	36.5*	8.8	141.6	3.44E+03	2.59E+05	4.9	0.367
23+24+25	2258	0.03217	0.01206	16.3	61.1	61.7	44.0*	7.1	318.0	5.89E+03	2.45E+05	5.3	0.39

* - Weighted average

APPENDIX D

GOVERNING EQUATIONS

Equations D.1 to D.4 are the complete Navier-Stokes equations for the steady, constant property, two-dimensional natural convective flow in cylindrical coordinates.

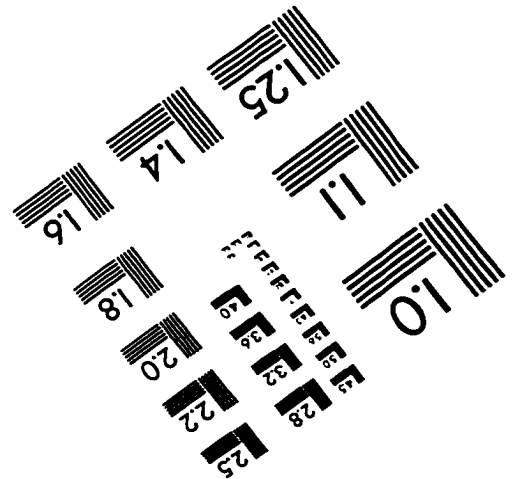
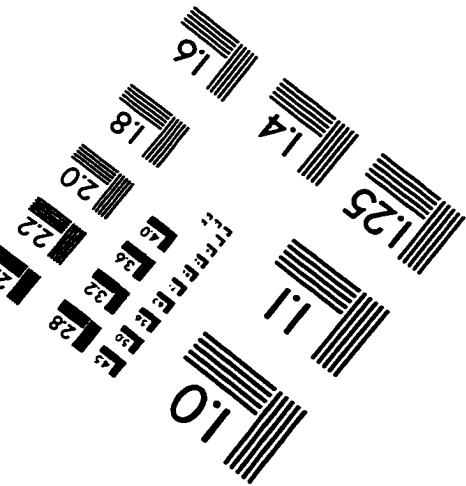
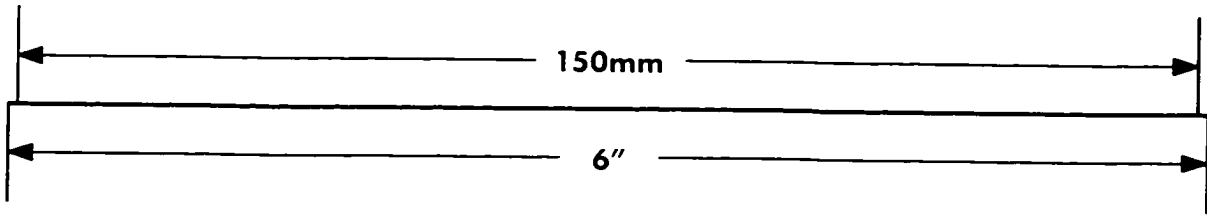
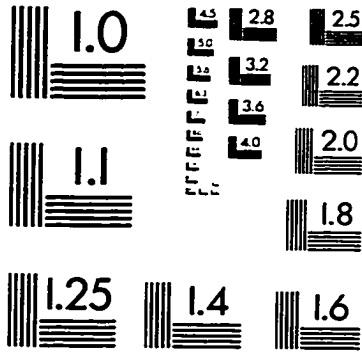
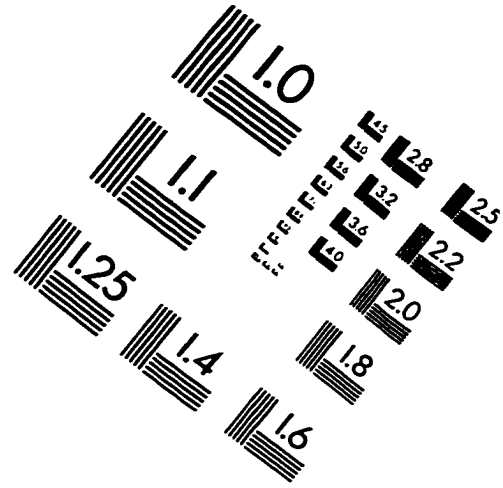
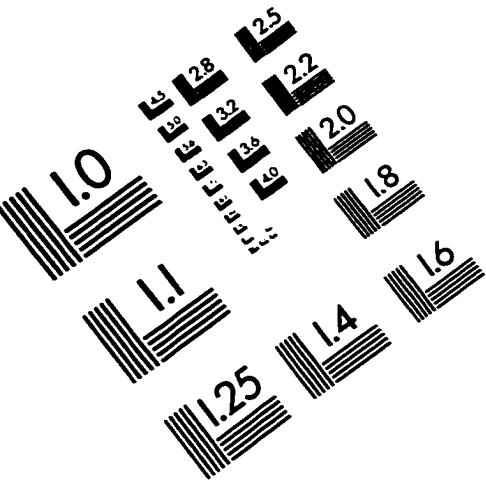
$$\frac{\partial v_z}{\partial z} + \frac{\partial v_r}{\partial r} + \frac{v_r}{r} = 0 \quad \text{D.1}$$

$$\rho \left(\frac{\partial v_z}{\partial t} + v_r \frac{\partial v_z}{\partial r} + v_z \frac{\partial v_z}{\partial z} \right) = -\frac{\partial P}{\partial z} + \mu \left(\frac{\partial^2 v_z}{\partial r^2} + \frac{1}{r} \frac{\partial v_z}{\partial r} + \frac{\partial^2 v_z}{\partial z^2} \right) - \rho g \quad \text{D.2}$$

$$\rho \left(\frac{\partial v_r}{\partial t} + v_r \frac{\partial v_r}{\partial r} + v_z \frac{\partial v_r}{\partial z} \right) = -\frac{\partial P}{\partial r} + \mu \left(\frac{\partial^2 v_r}{\partial r^2} + \frac{1}{r} \frac{\partial v_r}{\partial r} - \frac{v_r}{r^2} + \frac{\partial^2 v_r}{\partial z^2} \right) \quad \text{D.3}$$

$$\rho c_p \left(\frac{\partial T}{\partial t} + v_r \frac{\partial T}{\partial r} + v_z \frac{\partial T}{\partial z} \right) = k \left[\frac{1}{r} \frac{\partial}{\partial r} \left(r \frac{\partial T}{\partial r} \right) + \frac{\partial^2 T}{\partial z^2} \right] \quad \text{D.4}$$

IMAGE EVALUATION TEST TARGET (QA-3)



APPLIED IMAGE, Inc
 1653 East Main Street
 Rochester, NY 14609 USA
 Phone: 716/482-0300
 Fax: 716/288-5989

© 1993, Applied Image, Inc., All Rights Reserved